STUDIES ON FLAGELLAR ROTATION: THE ANGULAR SYMMETRY, THE STALL TORQUE, AND THE PROTON CONSUMPTION OF THE BACTERIAL FLAGELLAR MOTOR

Thesis by

Markus Meister

In Partial Fulfillment of the Requirements

for the Degree of

Doctor of Philosophy

California Institute of Technology

Pasadena, California

1987

(Submitted November 24, 1986)

ACKNOWLEDGEMENTS

My greatest thanks go to Howard, whose interest, guidance, and friendship have accompanied me through all parts of this work. I could not have wished for a better thesis advisor. Howard knows that a young scientist's education must be balanced by life outside the confines of the laboratory, and I thank him for his understanding during the periods where that balance may have tilted away from Caltech. Such troubles could usually be traced to Beth, without whose friendship my tenure as a graduate student might have been somewhat shorter, but so much less enjoyable. Many thanks to all the people in the lab, who have contributed with many fruitful discussions, particularly to Dave Blair, for stimulating my long dormant interest in chemistry, and to David Hitlin, John Hopfield, and Jerry Pine, for serving on my thesis committee. I also wish to thank the secretaries in the Beckman Biology office for their typing support as well as guidance around the, admittedly rare, pitfalls of Caltech's bureaucracy. Finally, I gratefully acknowledge the financial support through Germany's public university system, the scholarships from the "Deutsche Studienstiftung" and the "Stiftung Maximilianeum", as well as the fellowships provided by Caltech.

ABSTRACT

Flagellated bacteria propel themselves through an aqueous medium by rotating their helical flagellar filaments. The torque required for this motion is generated in the flagellar motor, which anchors the filament to the cell wall. The motor measures only about 25 nm in diameter, and electron micrographs of the isolated organelle show several rings arranged on a rod, which is connected to the filament by a curved hook. Flagellar rotation is driven by the protonmotive force across the cytoplasmic membrane. In recent years, a motile strain of Streptococcus has emerged as the organism of choice in studies of the flagellar motor, chiefly because its protonmotive force is easily manipulated. Since this bacterium lacks endogenous energy reserves, it can be starved until no metabolic protonmotive force remains. The gram-positive cell wall leaves the cytoplasmic membrane accessible to ionophores, which facilitates the generation of artificial proton gradients. Flagellar rotation can be visualized by tethering a bacterium to a glass surface by one of its flagellar filaments, which causes the cell body to spin about the point of attachment. Recently it has also become possible to measure the motor's rotation rate in swimming cells. This thesis contains a variety of functional studies as well as some theoretical considerations of torque generation in the flagellar motor.

The rotational angular symmetry of the motor was probed by a study of the angular positions at which it can stop. Only 5 or 6 discrete stopping angles were found. This constraint may result from static interactions between the rod of the motor and components of the cell

wall.

A technique was developed to measure the external torque required to stop flagellar rotation. This stall torque did not depend noticeably on the motor's angular position. It was equal to the running torque measured in a rotating tethered cell. In particular, a decrease in the running torque at very low and very high pH, as well as its saturation at large protonmotive force, were also observed for the stall torque. These results show that the running torque is not limited by the rates of torque-generating processes associated with motor rotation. The apparent saturation of the torque as a function of protonmotive force seems to result from difficulties in generating large potassium diffusion potentials. Similarly, the artificially generated protonmotive force might be affected at extreme values of the pH.

This thesis also reports the first sucessful measurements of the proton flux associated with flagellar rotation. These studies required an investigation of the total proton flux through the cytoplasmic membrane. An unusually large proton conductance was found, ca 10 times higher than the values reported for the membrane of Streptococcus lactis. After energization with an artificial, inwardly directed protonmotive force the rate of proton uptake by the cells decreased by a factor of 10 in 30 to 60 s with roughly exponential time course. Under certain conditions this influx was followed by slow extrusion of protons, part of which could be mediated by passive antiport of protons against other cations. Exchange of H^+ for Na^+ and Li^+ was observed directly. The time course of proton movements accelerated by a factor of 6 as the temperature varied from 16°C to 32°C. The rate of proton uptake was reduced by about 25% through the action of DCCD, an inhibitor

of the proton-translocating ATPase. In D_2O the flux of hydrogen ions was ca. 20% lower than in H_2O.

Only a small fraction of the initial proton influx was associated with flagellar rotation, as determined from measurements on cells whose motors could not turn because their filaments were cross-linked with an antibody. The rotation-dependent component of the proton flux varied proportionally to the speed of the motor, with ca. 1100 protons transferred in one revolution of the filament. These observations support the hypothesis that proton flux and flagellar rotation are tightly coupled by the flagellar motor in a constant stoichiometric ratio. Measurements of the torque acting on the filament suggest that the conversion from electrochemical energy to mechanical work occurs with an efficiency of the order of 5% in swimming cells. At the low speeds of tethered cells the motor generates a larger torque, and the efficiency might be close to unity.

A hypothetical mechanism for torque generation, originally proposed in 1982, is analyzed in detail and compared to other models found in the literature. Its predictions are at odds with the experimental evidence presented in this thesis. However, the model can be altered by the assumption that the conduction of protons through the motor limits its rotation rate at very low torque. In particular, it is suggested that protons may be transferred across the membrane along chains of discrete binding sites. This could account for the strong dependence of the motor's maximal speed on the temperature and the hydrogen isotope.

Table of Contents

General Introduction

Bacteria are the smallest and simplest free-living organisms, consisting of a single cell only a few microns in length. Nevertheless, they are capable of what may be termed behavior, a trait often thought to distinguish higher forms of life from the "bags of chemicals". Bacteria sense the properties of their surroundings, and adjust their bodily functions to the external conditions in many complex ways. In addition, they have the notable ability to move around and to actively seek out regions with a more favorable environment. Meaningful motility requires two distinguishable functions: a means of propulsion and a navigation system for steering. Evolution has solved both these tasks in a manner that is quite foreign to our macroscopic engineering concepts but very effective in the physical world inhabited by these organisms.

This thesis is primarily concerned with the former aspect, namely how bacteria swim, a problem that has attracted far less attention than the question of where they swim. I will give a brief introduction to bacterial motility, but the reader should refer to recent review articles for more detail: the long history of this subject is presented by Weibull (1960) and Berg (1975), while Berg (1985) provides an introduction to the more recent literature; an extensive but not so current review of bacterial motility is given by Macnab (1978); Berg et al. (1982) and Macnab & Aizawa (1984) focus on studies of the flagellar motor; bacterial taxis behavior is reviewed in Parkinson (1981), Hazelbauer & Harayama (1983), and Parkinson & Hazelbauer (1983); genetics and chemistry of the flagellar filament are discussed in Iino

(1977); Burchard (1981) reviews the work on gliding bacteria, which do not employ flagella for motility. I will also give a more extensive account of the recent work in each of the following chapters.

The movements of bacteria had already been observed by the early genius of microscopy, Antony van Leeuwenhoek, who, on August 6, 1676, at 3 o'clock in the afternoon, examined a drop of pepper-water and found

> "...little eels, or worms, lying all huddled up together and wriggling; just as if you saw with the naked eye a whole tubful of very little eels and water, with the eels a-squirming among one another...and I must say, for my part, that no more pleasant sight has ever yet come before my eye than these many thousands of living creatures, seen all alive in a little drop of water, moving among one another, each several creature having its own proper motion..." (Dobell 1960).

Later workers were able to resolve the tail-like appendages called flagella, structures so thin that they appear in a light microscope only when aggregated in large bundles or under very intense illumination. These filaments were often found to be of helical shape, and many theories regarding their function were discussed, including the suggestion that they had no relevance to motility at all. About 15 years ago the prevailing opinion was that bacteria flex their flagella, sending helical waves down their length, much as had been observed in eukaryotic ciliates such as the sperm cell. Viscous drag forces resulting from the motion of this helix through the surrounding fluid would provide the thrust required to propel the bacterial cell. On the basis of the available evidence, Berg and Anderson suggested in 1973 that the flagellar helix might instead be rigid and driven by a rotary

motor at its base. The key to this conclusion was a chance observation by Silverman and Simon (1972) during their studies of a non-motile mutant of Escherichia coli, which grows only incomplete flagellar structures, called polyhooks. When antibodies against the polyhook material were added to the bacterial suspension, they saw pairs of cells attached to each other, executing "violent counter-rotation." Initially some researchers were reluctant to accept that bacteria had developed a rotary joint, which was until then an unknown concept in biology. However, it is now generally accepted that flagellated bacteria rotate their filaments in order to propel themselves through the medium.

Not all organisms use the same hydrodynamic method, although a common principle seems to be the screw: all swimming bacteria (except possibly the cyanobacterium found by Waterbury et al. 1985) show at least one body part with the shape of a helical cylinder. Some of the propulsion schemes are illustrated in Fig. 1. A cell of the species Vibrio (Fig. 1A) has a single helical flagellum which emerges from one end of the roughly cylindrical cell body. Rotation of the flagellum propels the cell forward if the apparent wave travels from the base of the filament to the tip, while the flagellum can pull the cell in the opposite direction when its sense of rotation is reversed. The filaments of this particular organism are covered by a sheath which probably does not rotate relative to the cell body. Spirillum volutans (Fig. 1B) grows two tufts of about 25 flagella at either end. Rotation of the two flagellar bundles causes the helical cell body to revolve about its axis, thus generating the thrust required for movement. The trailing bundle of flagella, whose helicity is opposite to that of the body, also aids in propulsion. Again the direction of swimming reverses

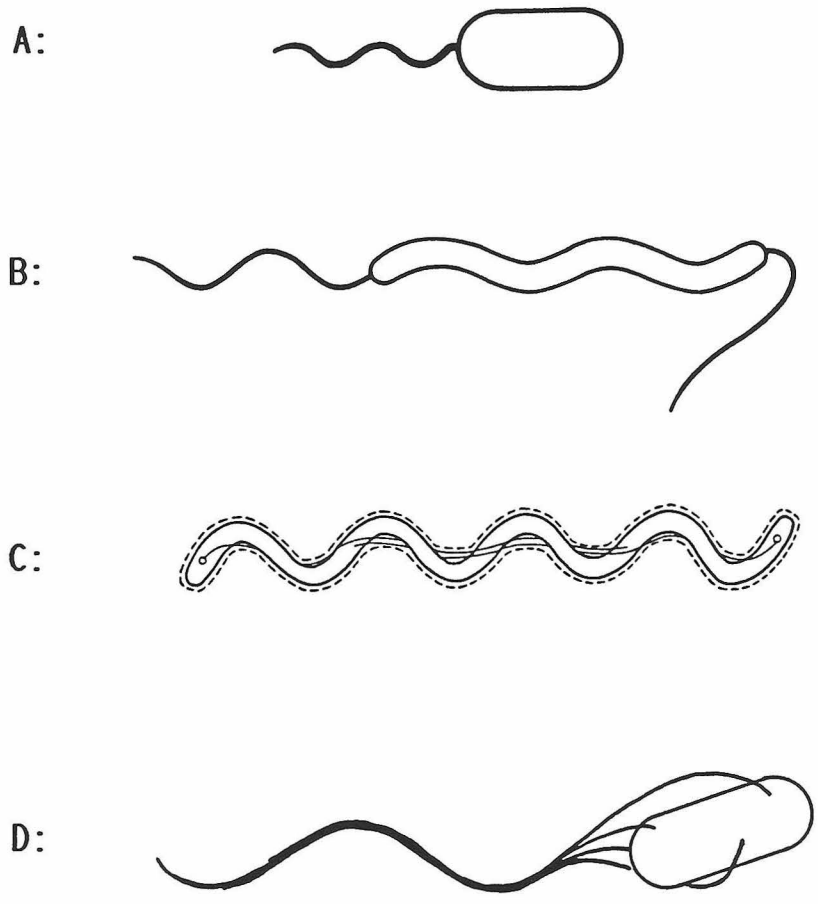

Fig. 1. Modes of propulsion used by various flagellated bacteria. **A:** Vibrio, **B:** Spirillum volutans, **C:** Spirochaeta aurantia, and **D:** Streptococcus V4051.

if both flagellar bundles change their sense of rotation synchronously. These organisms are probably related to the eels wriggling under Leeuwenhoek's microscope. Fig. 1C shows an exotic variant of this scheme employed by Spirochaeta aurantia. This organism has two flagella emerging near the poles that don't protrude into the surrounding fluid but move entirely within the space between the rigid protoplasmic cylinder and an external sheath. Rotation of the filaments causes the skin of this bacterium to revolve about the body, leading to rotation of the body about its helical axis in the medium, which in turn generates propulsive thrust. Finally, the star of this thesis, Streptococcus strain V4051, is shown in Fig. 1D. One to six helical flagella emerge from various points on the cell surface. When they rotate counterclockwise (as observed by somebody standing on the cell body looking down at the spinning flagellum), the filaments join in a single bundle on one side of the cell, pushing the bacterium forward. During clockwise rotation the bundle flies apart, and each filament tugs the cell body in a different direction, which causes it to tumble erratically. When the sense of rotation reverses again, the bundle reforms and the bacterium resumes swimming, although generally in a different direction than before the tumble. Escherichia coli and Salmonella typhimurium, two organisms used extensively for the study of the sensory system, behave in the same fashion.

The early workers of the last century also knew that bacteria respond to a variety of stimuli. Some seek or avoid oxygen, others are attracted by light. A small capillary tube inserted into a suspension of bacteria will attract them if it contains certain sugars or amino acids, while the cells will avoid a capillary filled with a repellent

substance, such as indole. On the microscopic scale one sees that this seemingly directed motion of the bacteria is actually quite erratic. For example, E. coli swims in a gradient of serine, an attractant, in a sequence of fairly straight runs interrupted by tumbles as described above. When the cell happens to be swimming towards higher serine concentrations, the tumbling events are delayed. This lengthens the segments of its three-dimensional random walk so as to carry it in the desired direction, thus leading to a net drift towards the promising capillary tube. What appears to be a rather tedious and wasteful way to navigate may actually be the only solution available to an organism of this size. Because rotational Brownian motion alters its course, a swimming bacterium must reorient itself with respect to the chemical gradient about every 5 s. Berg and Purcell (1977) have shown that it cannot sense the spatial gradient over its body surface while swimming, because the rate at which attractant molecules hit the front half of the cell is much larger than on the back half, even in a medium of homogeneous attractant concentration. Statistical considerations dictate that a temporal comparison of two attractant concentrations along the path of the bacterium requires about 1 s, which is of the order of the mean length of the runs in the random walk.

It is now clear that these bacteria have a set of specialized receptors near their outer surface that senses the external concentrations of chemical attractants and some repellents. A complex biochemical system, whose components have largely been identified, essentially computes the time derivative of this concentration and controls the interval length of clockwise and counterclockwise rotation of the flagellar motor, thus biasing the length of the runs. Other

stimuli, such as pH, oxygen, or light, are probably processed by different pathways. On the scale of the light microscope, the mechanisms of locomotion illustrated in Fig. 1 and their modulation to allow tactic behavior towards external stimuli are fairly well understood. Major questions remain as to the molecular basis of flagellar rotation and its directional control. In the following I will focus on the flagellar motor.

Rotation of the flagellum occurs solely at its base, where it inserts into the cell envelope. The remainder of the flagellum is essentially a rigid helical tube, and, although it can undergo conformational transformations into forms of different torsion and curvature, these processes are only marginally relevant to bacterial swimming. It is an interesting structure, though, about 19 nm in diameter and packed from identical protein subunits that are excreted from the cell through the hollow core of the filament and assemble at the tip. Near the base of the flagellum the protein material changes, and the helical crystal turns into a hook. This element is assumed to play the role of a flexible universal joint that allows the flagellum to bend around the surface of the cell body to join the others in a bundle. The hook then narrows into a shaft, part of the so-called basal body. This structure is visible only in the electron microscope. Several parallel disks are assembled on the shaft. Bacillus subtilis, a gram-positive bacterium, shows only two such rings, while some gram-negative organisms, such as E. coli, have four; the outer two may serve as a bushing to guide the rod through the outer membrane of these cells. The lower pair of rings is presumed to be the actual site of torque generation. They have a diameter of about 22 nm and are separated by

about 3 nm along the motor axis. One of them, the M-ring, is found at the level of the cytoplasmic membrane and might be rigidly connected to the shaft. The S-ring might be attached to the cell wall, thus serving as the stator. A sketch of the basal body, drawn by DePamphilis & Adler (1971a) on the basis of their electron micrographs is shown in Fig. 2.

A genetic analysis of flagellar motility reveals that approximately 35 genes are required for a complete functional motor. Generally three types of mutations are distinguished phenotypically: fla mutants have incomplete flagellar structures or none at all; mot mutants have flagella but don't rotate them; che mutants rotate their motors but cannot reverse them; although motile, these latter strains don't perform chemotaxis. The proteins encoded by these genes range in molecular weight from about 10,000 to 60,000. Not all of them are located in the basal body, in particular none of the mot or che mutations fall into this structure. Clearly the functional motor must have components that are only loosely associated with the basal body and consequently lost during the harsh procedures used in its biochemical isolation. Freeze-fractures of the membrane of Aquaspirillum serpens reveal a ring of transmembrane particles surrounding flagellar insertion sites (Coulton & Murray 1978), and similar structures have been observed more recently in Streptococcus and E. coli (Khan et al. 1986). These may be good candidates for the motA and motB proteins, which are found primarily in the cytoplasmic membrane. Block and Berg (1984) have shown that the motB protein is an essential component of a torque generator that can be added to a pre-assembled motor. Cells of E. coli carrying a defective motB gene have flagella but are non-motile. When the wild-type gene is introduced into these cells and expressed, the motor starts rotating,

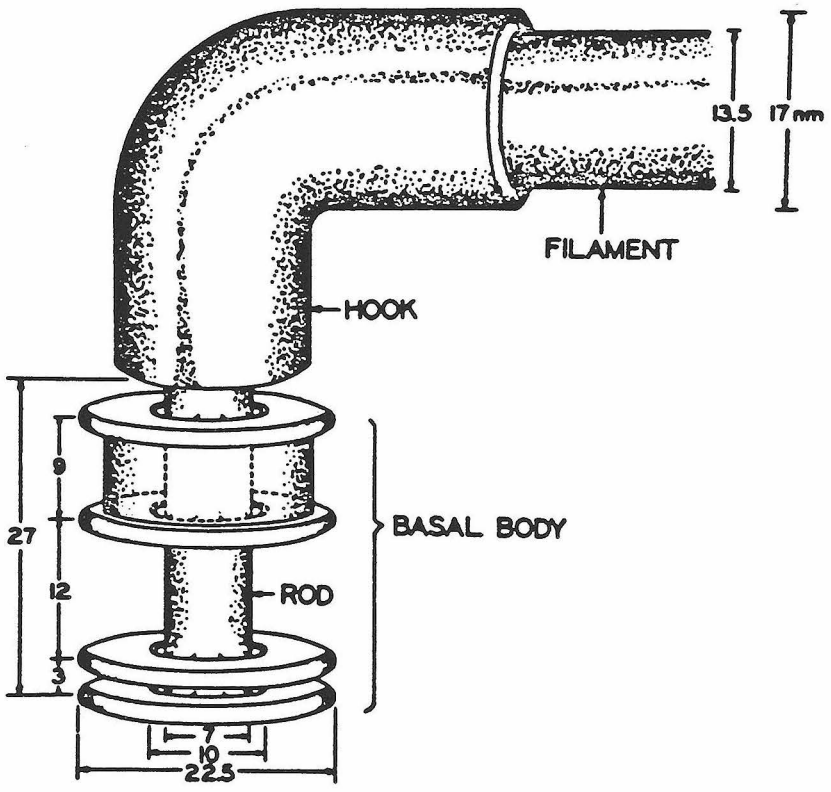

Fig. 2. A drawing of the flagellar basal body based on electron micrographs of isolated flagella. From DePamphilis & Adler (1971a), with permission.

and its torque increases in equal increments, as if several independent torque generators were added sequentially.

The power for flagellar rotation is drawn from the difference in the electrochemical potential of protons across the cytoplasmic membrane, although some species that live in very alkaline environments appear to use sodium ions instead of protons. Most bacterial cells have transport mechanisms that use metabolic energy to extrude hydrogen ions from the cytoplasm into the external medium. This generates both an electrical voltage and a proton concentration difference across the membrane. The free energy stored in this fashion is subsequently used by a variety of molecular mechanisms, for example to pump other ions into or out of the cell, to transport nutrients across the membrane, and, in motile bacteria, to run the flagellar motor. From the researcher's standpoint, this is a very convenient choice, because the proton electrochemical potential is quite amenable to external manipulation. The proton concentration gradient is easily altered by changing the pH of the external medium. The use of membrane-permeant proton carriers even allows some control of the cytoplasmic pH. Manipulation of the electrical component of the proton potential requires a little more care. The membrane conductance to potassium, which is present at relatively high concentrations in the cytoplasm, is increased dramatically by the addition of valinomycin, an antibiotic that carries it across the membrane. Under those conditions, the membrane potential is essentially clamped to the equilibrium potential of K^+. If one now reduces the external potassium concentration, potassium ions will leave the cell, setting up an electrical voltage, negative inside, that can drive protons and thus cause flagellar

rotation. Streptococcus has proven more convenient for such studies than the traditional favorite, E. coli, because these cells can easily be starved until all their internal supplies of nutrients are depleted, making them entirely dependent on the artificially imposed proton potential.

Until recently, the rotation of the flagellum was most commonly analyzed by a method called "tethering". Bacteria are linked to a glass coverslip by their flagella, which are partially removed so that no more than one attaches to the glass surface. The coverslip is placed in a flow chamber, designed to allow exchange of the medium without tearing the cells off the glass surface. Operation of the motor leads to rotation of the cell body, which is easily followed with a light microscope. With these tools, one can observe a single flagellar motor for an arbitrarily long time. One can modulate the free energy available at the input to this molecular machine, the proton electrochemical potential, and monitor its speed of operation with high accuracy. The work performed at the output can be estimated from the frictional forces exerted on the cell body by the surrounding medium. Finally, one can continuously vary many of the environmental parameters, such as the viscosity of the medium, the absolute pH of the medium, or the temperature. Another variable that has been used extensively is the mass of the hydrogen ions: although they rarely encounter this environment in nature, bacteria swim perfectly well in heavy water. By studying the relationships between the variables at the input and output of this molecular motor and their dependence on the environmental parameters, one hopes to learn something about the inner workings of the machine.

When I joined Howard's group, a great deal was already known about the function of the flagellar motor from studies on tethered bacteria. The rotation rate of these cells is inversely proportional to the viscosity of the medium, indicating that the torque generated by the motor is largely independent of its speed over the range from about 0.4 to 8 Hz (Manson et al. 1980). The torque measured in tethered cells also does not depend on the temperature or the hydrogen isotope (Khan and Berg 1983). It increases approximately proportionally to the proton electrochemical potential, once a low threshold value of a few meV is exceeded (Manson et al. 1980; Khan et al. 1985). In E. coli and Bacillus subtilis that threshold appears to be larger, and the torque saturates at large values of the protonmotive force above 80 mV, an effect that is less pronounced in Streptococcus (Khan & Macnab 1980b; Shioi et al. 1980). The reversals in the sense of flagellar rotation initiated by the sensory system don't require a reversal of the proton potential: apparently the motor contains a gear shift. Mutants of Streptococcus in which this switch is defective, rotate exclusively in one direction under the physiological, inwardly directed proton potential but spin in the opposite direction when an artificial, outwardly directed pH-gradient is applied (Khan & Berg 1983).

Howard had also searched for variations in the rotation rate of tethered cells, particularly periodic flutters that might yield some information about the timescale of the torque generating processes. No such high-frequency components were found, but they might have been significantly damped, since the elasticity of the filament and the viscous drag on the cell body act as a low-pass filter (Berg et al. 1982). As a warm-up project Howard suggested that I study the

distribution of the angular positions at which the flagellar motor can stop, since these measurements would not be hampered by the same effects as the above-mentioned dynamical studies. In Chapter 1 I show that the flagellar motor of Streptococcus stops in only five or six discrete positions. This angular dependence may well be related to the structure of the motor's shaft, since both the filament and the hook show a similar symmetry. Section §1.2 contains a number of experimental protocols that were used throughout the work presented in this thesis.

In Chapter 2 I present a technique for measuring the motor's stall torque, the torque one must exert on the shaft to stop its rotation. I discovered this method by chance while playing with cells after an otherwise unsuccessful experiment. One can stall the rotation of a tethered cell by a gentle flow of fluid through the chamber, which orients it downstream from the tethering point. As the flow rate is gradually decreased, the cell body takes on a steeper and steeper inclination with respect to the flow and eventually completes an entire revolution at a fairly well defined flow velocity. I eventually used this method to show that the stall torque is indistinguishable from the running torque measured on tethered cells under a wide range of external conditions. In particular, this significantly altered our interpretation of the motor's behavior at high protonmotive force and at extreme values of pH.

Chapters 3 and 4 are devoted to measurements of the proton flux through the flagellar motor. Such measurements had been attempted previously by Mike Manson and Shahid Khan, since they would effectively complete experimental access to the set of quantities that describe steady state operation of the motor: the driving force at the input,

represented by the proton electrochemical potential, its conjugate velocity, namely the flux of protons, as well as the corresponding quantities at the output, given by the torque and the rotation rate of the motor's shaft. The main technical challenge lay in resolving the proton flux through the motor above the much larger component through other unrelated conductances in the membrane, and most of my experimental work in Howard's laboratory was dedicated to that problem. Chapter 3 describes some general observations on the conductivity of the Streptococcus membrane to protons, made in preparation for the study of motor-related proton fluxes presented in Chapter 4. At the same time, Graeme had developed a technique for the measurement of high flagellar rotation rates in the bundles of swimming bacteria. This method was very useful in the interpretation of the rotation-dependent proton flux and allowed the first direct estimate of the efficiency of energy conversion in the flagellar motor.

In Chapter 5 I will discuss some hypothetical mechanisms for torque generation and eventually propose a model that accounts for the more recent experimental evidence. As in other natural sciences, speculation is an important part of our work. An engineering student faced with a rotating shaft emerging from a black box can immediately determine whether a steam turbine or a combustion engine is driving the axle, for example, by measuring its stall torque. By contrast, we not only get to do the measurements but also have to conceive the machines that the experiments are to distinguish.

CHAPTER ONE : THE FLAGELLAR MOTOR STOPS AT DISCRETE POSITIONS

§1.1 INTRODUCTION

In their studies on isolation and electron microscopy of E. coli basal bodies, DePamphilis and Adler (1971a; 1971b) also tested for angular symmetry of motor components relative to rotation about the motor axis. The face-on image of a dissociated M-ring appeared to have a rotational symmetry of order 16, suggesting that it might be composed of 16 identical subunits arranged at regular azimuthal intervals around the motor axis. Coulton and Murray (1978) inspected freeze-fractured membranes of the polarly flagellated bacterium Aquaspirillum serpens by electron microscopy and found structures that they interpreted as the sites of insertion for flagella. A central plug was surrounded by a circular depression in the convex fracture face of the membrane, approximately equal in diameter to a flagellar basal body. On the circumference of this depression they found a circle of 14 to 16 studs, a few nm in size, which may represent protein macromolecules associated functionally with the basal body. Similar structures have been reported by Khan et al. (1986) in the membranes of E. coli and Streptococcus strain V4051. If the motor were in fact composed of identical parts arranged at a regular angular repeat distance, one would expect the resulting angular symmetry to be of relatively low order: the circumference of the basal body is only about 70 nm, and the motor is known to contain proteins of molecular weight up to 60,000 (Macnab & Aizawa 1984; Aizawa et al. 1985). Even in a very compact configuration these molecules should have a diameter of about 5 nm, such that at most

10 to 20 of them could be arranged on the outer edge of the basal body.

Berg (1974, 1976) and Berg et al. (1982) looked for temporal variations in the speed of tethered cells, which might reveal the underlying symmetry in the structure of the motor. No discrete high-frequency components were detected, but any such variations would have been damped significantly by the elasticity of the flagellar filament, with which the cell is tethered to the glass. Although the speed of the motor may vary considerably, only a fraction of this modulation is apparent in the motion of the cell body, because the motor winds and unwinds the flagellar filament (Berg 1976).

A deenergized motor locks the rotor to the stator in a fixed angular position (Berg 1976). Under these conditions the body of a tethered cell undergoes some Brownian motion but only within the range allowed by the elastic filament. The studies described in this chapter were aimed at the question whether the motor stops in only a finite number of angular positions, and, if so, whether they are spaced at regular angular intervals. I successively energized and deenergized a number of tethered cells, taking micrographs of the cell bodies after they stopped rotating. Their angular positions relative to the glass surface were measured and analyzed by discrete Fourier transform. I found that the stopped Streptococcus motor is limited to discrete angular positions, of which there are 5 or 6 in one revolution.

§1.2 METHODS

The procedures described in parts (a) through (d) apply to all experiments described in this thesis.

a) Reagents.

The following is a list of reagents used for the work presented in this thesis and their suppliers. All other chemicals were of reagent grade, and glass-distilled water was used to prepare their solutions, except where indicated otherwise.

Valinomycin, 2,4-dinitrophenol (DNP), N,N'-dicyclohexylcarbodiimide (DCCD), tannic acid, and poly-L-lysine (MW $\simeq$ 46,000) were obtained from Sigma. Trifluoromethoxycarbonylcyanide phenylhydrazone (FCCP) was purchased from DuPont, N-ethylmaleimide (NEM) from Pierce Chemical Co., and crystal violet from MCB Manufacturing Chemists. Fuming (90%) nitric acid was obtained from Mallinckrodt, Prosil-28 from PCR Research Chemicals, and paraffin oil from the J.T.Baker Chemical Co. Tetraethylenepentamine (tetren) was recrystallized by the method of Reilly & Vavoulis (1959) from a technical grade product supplied by Aldrich.

b) Preparation of cells.

Cells of Streptococcus strains V4051 (wild type) and SM197 (a smooth swimming mutant; Berg et al. 1982) were grown to saturation at 35°C in KTY medium (Harold & Papineau 1972). The inoculum was taken from stocks frozen at -20°C in KTY with 20% glycerol. This first culture was kept in the cold wall (ca 7°C) and used for a month, by which time the cells' viability declined and a fresh monthly culture was

grown from the freezer stock. During the night before an experiment I grew a second culture for 6 to 7 hours from a 1:100 inoculum of the monthly culture in KTY. These cells were diluted once more 1:100 into KTY and grown for 4.5 hours, yielding the experimental culture. At harvest the cell suspension had an optical density of ca 1.1 at 600 nm (Perkin-Elmer 552 spectrophotometer, 10 mm cuvette) and a cell density of ca $4x10^8$ cells/ml, corresponding to late exponential growth phase.

c) Tethering.

Several versions of the original protocol for tethering (Manson et al. 1980) have been used in Howard's laboratory. Here is the one with which I got my best results. The goal in using this technique is to maximize the fraction of cells attached to a coverslip that spin. The more cells one can observe under the same experimental procedure, the better the statistics for a population average of the quantity to be measured. With this protocol I routinely obtained a spinning yield of 50%, making it possible to analyze 80 to 100 spinning cells in a single video field.

The single most important step in tethering is the preparation of the glass surface. I put about 30 or 40 glass coverslips of 12 mm diameter (obtained from Carolina Biologicals or Bellco Glass) in a 30 ml glass beaker, swirled them in acetone, and let them sit for 5 min. Then I poured the acetone off, rinsed them in 95% ethanol in the same manner, and finally washed the ethanol out thoroughly with glass-distilled water. In the following I will refer to glass-distilled water simply as "water". About 20 ml fuming nitric acid were added to the coverslips, the beaker was covered with a small petri dish and placed in a water

(not necessarily glass-distilled) bath, which was then heated to about 70°C in the fume hood. I stirred the coverslips once with a glass rod to ensure that all the surfaces were covered by the acid. Excessive stirring was avoided, since it scratched the glass and produced fines that remained on the surface of the slips. After one hour the bath was allowed to cool, the acid was poured off, and the coverslips were rinsed in the same beaker by swirling them repeatedly with water. At this point a slip that was held at the edge with a clean forceps and rinsed under running water remained covered with a film of water when held vertically, which separated from the glass only gradually and uniformly over the entire surface. The presence of glass fines or other particles was easily detected in this manner. The beaker was covered with parafilm and stored on the shelf. The coverslips could be used for at least 4 weeks.

For each experiment I silanized the coverslips as follows: To avoid repeated contamination of the acid-cleaned batch, all the slips needed for that day were transferred to another clean beaker with water. A glass syringe was filled with 10 ml water to which I added 0.1 ml Prosil-28 (SCM Chemicals). The solution was dispensed through a 3 μm pore size filter (Millipore Filter Corp. SSWP01300) into a disposable polystyrene beaker. This removed the flaky precipitate that appears in Prosil-28, especially after prolonged storage. One by one, the coverslips were picked up at the edge with a forceps, rinsed under running water, submerged in the filtered Prosil-28 solution, and shaken slightly to mix the water layer at the glass surface. After 20 s the slip was removed and rinsed again under running water. This had to be done very thoroughly: when shifted to a pH of 6 or lower, the bodies of

tethered cells tended to attach rigidly to the surface of the coverslip, a problem that was alleviated by extensive rinsing of the slips after the silanizing step. At this point the water formed large drops on the glass surface. These were removed by shaking, not blotting. The slip was ready for use immediately, even when not completely dry, but it could be stored in a covered rack for the day. However, if anything could be seen on the glass surface by holding it against a dark background with bright illumination from the side, then the slip was discarded.

For tethering, Apiezon L grease (Apiezon Products Ltd.) was applied to the edge of one side of the coverslip using a brass ring dedicated to that purpose. A few drops of the cell suspension were deposited within the grease ring, and the slip was covered with a small beaker to avoid evaporation of the water. After 1 to 2 hours, the coverslip was placed in a flow chamber (Berg & Block 1984). For this purpose it was convenient to mount the slip on an elevated support that did not extend beyond the slip's edge. This made it possible to invert the flow chamber directly onto the coverslip without further manipulations.

A few things that did not work: I tried using another silanizing agent, SurfaSil (Pierce Chemical Co.), but with inferior results. Contrary to persistent rumors, baking the silanized slip made no difference. Shearing the cells in a Waring blender did not improve the spinning yield but added a lot of dirt to the suspension, which deposited on the coverslip and might also have had nasty effects on the cells. Tethering worked over a wide range of pH-values, but not at very low ionic strength, where the cells did not attach to the glass as well. I obtained a rather low spinning yield when using SO_4^{2-} as the dominant

anion in the tethering buffer. Addition of 10 to 100 μg/ml bovine serum albumin to the medium alleviated the problem of sticking at low pH, but it had to be added after tethering, or the flagella failed to attach to the glass.

d) Artificial energization.

I will briefly introduce the concepts and notation of artificial energization as used throughout this thesis. When tethered, as described above, and starved in a medium lacking carbon sources, cells of Streptococcus start rotating after a pH-difference or an electrical potential is imposed across the membrane. To attain the former, one merely has to replace the starvation medium in the flow chamber by a buffer of different pH. To generate a diffusion potential, one first exposes the cells to valinomycin, a potassium ionophore (Reed 1979). I used a concentration of 2 to 5 μg/ml for a duration of about 2 min, after which the valinomycin was washed out of the flow chamber again. At this point the conductance of the cytoplasmic membrane to potassium is much larger than to any other ion, and the membrane potential therefore lies close to the potassium equilibrium potential. Thus changes in the external potassium concentration directly affect the electrical potential across the membrane. The protonmotive force is defined as

$$\Delta p = -\frac{kT}{e} \ln(10)\ (pH_i - pH_e) + (\psi_i - \psi_e)$$

where k is Boltzmann's constant, T is the absolute temperature, e is the electronic charge, pH_i and pH_e are the values of the pH in the cytoplasm and the external medium respectively, and $(\psi_i - \psi_e)$ is the electrical voltage applied across the membrane. Note that $-e\Delta p$ is equal to the

difference in the electrochemical potential of protons across the cytoplasmic membrane. In presence of valinomycin one approximates the membrane potential by the potassium equilibrium potential, and thus

$$\Delta p_{nom} = -\frac{kT}{e}\left(\ln(10)\ (pH_i - pH_e) + \ln\left\{\frac{[K^+]_i}{[K^+]_e}\right\}\right)$$

where $[K^+]_i$ and $[K^+]_e$ are the internal and external potassium activities respectively. After several hours of starvation the protonmotive force should be very small, because protons have had ample time to equilibrate. However, the chemical and electrical components need not vanish individually. Streptococcus V4051 starved at 0.2 M external potassium concentration has an internal pH 0.2 units below the external value (Conley & Berg 1984). If cytoplasmic potassium amounts to 0.36 M, as measured in S. lactis by Maloney (1977), then the protonmotive force is, in fact, very close to zero. The nominal protonmotive force after a shift to a different buffer is therefore given by

$$\Delta p_{nom} = -\frac{kT}{e}\left(\ln(10)\ (pH_e^{initial} - pH_e^{final}) + \ln\left\{\frac{[K^+]_e^{initial}}{[K^+]_e^{final}}\right\}\right).$$

The metabolically generated protonmotive force is negative, driving protons into the cell. Streptococcus can also rotate with a positive Δp, but all the experiments discussed in this thesis used a negative protonmotive force, obtained by lowering the external pH or the external potassium concentration. In the latter case, another salt was usually added to the buffer, replacing KCl to keep the ionic strength constant. The effects of this will be discussed in Chapter 3. Some observations indicating that Δp_{nom} represents the true protonmotive force only over a limited range of pH_e and $[K^+]_e$ are presented in Chapters 2 and 4.

e) Experimental protocol.

For the experiments described in this chapter cells were harvested and washed twice with buffer A (0.1 M Na_2HPO_4/NaH_2PO_4, 0.2 M KCl, 0.1 mM EDTA, pH 7.5) by centrifugation at 4000 g for 2 minutes. I then reduced the flagellar filaments to short stubs by shearing the cells (Manson et al. 1980), washed them once more in buffer A and suspended them at a final concentration of ca $2x10^7$ cells/ml for tethering.

Tethered cells in the flow chamber were observed with a Nikon Optiphot microscope (Plan BM 40x objective, Zeiss Optovar). Micrographs of the cells were taken on Polaroid 665 pos./neg. film using a Nikon PFX camera with CF PL 5x projection lens. I replaced the medium in the flow chamber by drawing solutions through polyethylene tubing (0.58 mm I.D.) attached to the inlet and outlet of the chamber with suction provided by a vacuum line; the flow rate was controlled with a needle valve (Berg & Block 1984).

The cells were energized either with an artificial potassium diffusion potential or by adding glucose to the medium. In the former case, I first exposed the starved tethered cells to 2 μg/ml valinomycin in buffer A (added from a solution of 1 mg/ml in methanol) for 2 min. This medium was then replaced by buffer A containing, in addition, 25 mM sodium benzoate and 50 mM methylamine. The cells started spinning after I lowered the external potassium concentration from 0.2 M to 0.05 M, simultaneously adding 0.15 M NaCl to keep the ionic strength constant. About 1 min later, I stopped them again by raising the external potassium concentration back to 0.2 M. In the absence of methylamine and benzoate, the cells often spun slowly in the reverse direction for several minutes following this step. Probably the entry of protons

during the time period at low external potassium concentration had acidified the cytoplasm sufficiently to allow rotation driven by the resulting pH gradient. Weak acids and bases such as benzoate and methylamine are membrane-permeant in their uncharged form and thus can transport protons across the cytoplasmic membrane. Since both agents were added in concentrations comparable to the cytoplasmic buffering capacity (see Chapter 3), they effectively clamped the cytoplasmic pH to the value of the external pH (Repaske & Adler 1981; Kihara & Macnab 1981), thus inhibiting the reverse rotation following a period of artificial energization. After the cells had stopped, I took a micrograph of the field with an exposure time of 10 to 15 s. Then the cells were energized again and the procedure repeated. During the course of the experiment I also took a few long-term exposures of the cells while they were energized, which allowed me to select the spinning cells for later analysis.

In other experiments I induced cell rotation by adding 10^{-5} M glucose to buffer A. To stop rotation, the cells were shifted to buffer A containing, in addition, 0.01 M DNP, a proton conductor that dissipates the protonmotive force. After 20 or 30 successive energizations, the cells usually lost some of their vigor, and I had to increase the glucose concentration to 10^{-4} M.

The choice of the exposure time for the micrographs requires some attention. Even though the motors of deenergized cells appear to be locked in one position, the body of a tethered cell still executes some rotational Brownian motion allowed by the elasticity of the filament that ties it to the coverslip. From the smeared images of deenergized cells on long-term exposures I estimate the angular spread of this

motion at

$$\Delta\theta \simeq 6°,$$

which is about twice the value reported by Berg (1976) for tethered E. coli. Using the estimates for the rotational drag coefficient of a tethered cell derived in Chapter 4, one finds that the time required for the cell body to diffuse across this range is equal to

$$\tau = \frac{(\Delta\theta)^2}{2D} \simeq 0.07 \text{ s}$$

where D is the cell body's rotational diffusion coefficient. If fast film and exposure times of less than 1/15 s are used in these experiments, then the mean angular position of the cell body on the micrograph is not representative of the motor's stopping angle, which will introduce errors of as much as 6°.

f) Measurement of angular positions.

The angular position of each cell selected for analysis was measured relative to a reference line between two points on the coverslip that could be seen in all micrographs. For this purpose I built a small square aluminum table with a plexiglass insert at the center that could be illuminated from below. The negative of the photomicrograph was mounted on a second square plexiglass plate, placed on the table, and oriented by hand until the image of a particular cell was aligned with a line engraved into the bottom plexiglass surface. At this point I measured the angle between the edge of the table and the edge of the negative holder with a universal bevel protractor. The table also provided a mount for a low power dissecting microscope, which facilitated the viewing of rather small images on the micrograph. The

experimental error introduced by this procedure was estimated by repeatedly measuring the angular position of a non-motile cell in various micrographs and found to be 1° to 2°.

g) Data analysis.

For cell number j (j = 1,2,...,m) in a sample of m cells the measurements of part (e) yield a set of n_j stopping angles $\theta_{j,k}$ (k = 1,2,...,n_j). The goal of the analysis is to find periodicities in the distribution function, $p_j(\theta)$ of the stopping angle of cell j. If the cells all have the same motor, then $p_j(\theta)$ should show the same dependence on θ for all j except for a phase angle that is chosen randomly for each cell during tethering. This means that the coefficients $F_j(M)$ in the Fourier series of $p_j(\theta)$,

$$F_j(M) = \frac{1}{n_j} \sum_{k=1}^{n_j} e^{iM\theta_{jk}}$$

have the same modulus for all j, but different phases. One can therefore Fourier analyze the stopping angles independently for each cell and then average the power corresponding to each value of the periodicity, M, over all cells by computing

$$F(M) = \left\{ \frac{\sum_{j=1}^{m} n_j^2 \, F_j(M) \, F_j^*(M)}{\sum_{j=1}^{m} n_j^2} \right\}^{\frac{1}{2}}$$

If all m cells were tethered in phase, one could pool all their stopping angles and analyze the entire set for periodicities, which would improve the resolution by a factor of $\sqrt{m}$. This suggests an alternative analysis, focusing on the difference angle between successive stopping positions,

$$\alpha_{j,k} = \theta_{j,k+1} - \theta_{j,k}.$$

The distribution function $q(\alpha)$ of these angles should be identical for all cells. Furthermore, $-\alpha$ is as likely to occur as $+\alpha$, and therefore the sine component of the Fourier transform vanishes. I therefore computed the cosine transform of the set of difference angles,

$$C(M) = \frac{1}{n} \sum_{j=1}^{m} \sum_{k=1}^{n_j-1} \cos M\alpha_{j,k}$$

where

$$n = \sum_{j=1}^{m} (n_j - 1).$$

In all experiments where I found a distinct periodicity, it could be seen as a peak both in F(M) and in C(M), although the resolution was always better in the cosine transform. To judge the significance of a peak in C(M) I will derive its expectation value and standard deviation under two different assumptions for the distribution function $q(\alpha)$:

1) α is distributed randomly with

$$q(\alpha) = 1/2\pi, \quad 0 \leq \alpha \leq 2\pi,$$

so that

$$\langle \cos M\alpha \rangle = \int_0^{2\pi} q(\alpha) \cos M\alpha \, d\alpha = 0$$

and

$$\langle \cos^2 M\alpha \rangle = \int_0^{2\pi} q(\alpha) \cos^2 M\alpha \, d\alpha = \frac{1}{2}.$$

Thus the mean and standard deviation of the cosine transform are

$$\langle C(M) \rangle = 0$$

and

$$\{\langle C^2(M)\rangle - \langle C(M)\rangle^2\} = \frac{1}{\sqrt{2n}}$$

2. α is distributed normally about the L equidistant angles

$$\alpha_I = 2\pi \frac{I}{L}\ ,\ I = 1,2,\ldots,L$$

with distribution function

$$q(\alpha) = (2\pi\sigma^2)^{-1/2} \frac{1}{L} \sum_{I=0}^{L-1} e^{-(\alpha-\alpha_I)^2/2\sigma^2}\ ,\ -\infty < \alpha < +\infty.$$

The extension of the range of α to $[-\infty,+\infty]$ has a negligible effect as long as $\sigma/2\pi \ll 1$. Then

$$\langle \cos M\alpha\rangle = \begin{cases} e^{-M^2\sigma^2/2}, & M/L \text{ integer} \\ 0, & M/L \text{ not integer} \end{cases}$$

and

$$\langle \cos^2 M\alpha\rangle = \left\langle \frac{1+\cos 2M\alpha}{2} \right\rangle = \begin{cases} \frac{1+e^{-2M^2\sigma^2}}{2}, & 2M/L \text{ integer} \\ \frac{1}{2}, & 2M/L \text{ not integer} \end{cases}$$

so that

$$\langle C(M)\rangle = \begin{cases} e^{-M^2\sigma^2/2}, & M/L \text{ integer} \\ 0, & M/L \text{ not integer} \end{cases}$$

and

$$\{\langle C^2(M)\rangle - \langle C(M)\rangle^2\}^{1/2} = \frac{1}{\sqrt{2n}} \begin{cases} 1-e^{-M^2\sigma^2}, & 2M/L \text{ even integer} \\ (1+e^{-2M^2\sigma^2}), & 2M/L \text{ odd integer} \\ 1, & 2M/L \text{ not integer} \end{cases}$$

Note that for $M\alpha \gg 1$ (large M) the cosine transform approaches that of

a random distribution with vanishing mean and root-mean-square noise $1/\sqrt{2n}$. Also, one can find σ from the primary and secondary maxima:

$$\sigma = \frac{1}{L}\left\{\frac{2}{3}\ln\frac{\langle C(L)\rangle}{\langle C(2L)\rangle}\right\}^{1/2}.$$

§1.3 RESULTS

Fig. 1.1A shows a histogram of the difference angles between successive stopping positions measured on cells of Streptococcus strain V4051 that were energized with a potassium diffusion potential. It contains a total of 516 angles pooled from 16 cells. The corresponding cosine transform, C(M), is plotted in Fig. 1.1B. One finds a very large value at a periodicity, M, of 1, which originates from the large number of difference angles equal or close to zero. These represent cells that stop repeatedly at the same angular position, most likely due to an obstacle on the glass surface. The spectrum also shows a large significant peak extending over periodicities 5 and 6 and another broad peak ranging from M = 10 to M = 12. At very large values of M the spectrum behaves very much like that expected from a uniform distribution of stopping angles, whose root-mean-square amplitude is indicated by the dashed lines.

In a second experiment cells of this strain were metabolizing glucose, and I stopped them with the uncoupler DNP. The resulting distribution of difference angles is given in Fig. 1.2A, including 759 angles from 21 cells. They very clearly cluster around discrete positions, of which four can be seen directly and another one or two may be inferred. The relative paucity of difference angles near 180° is due to an experimental artifact: while medium containing DNP is drawn through the flow chamber, the cell bodies are all aligned with the fluid flow, and the motors of many cells stop turning before the flow ends. When the micrograph is taken, the cell bodies therefore are more likely to be oriented near the direction of fluid flow, leading to an abundance

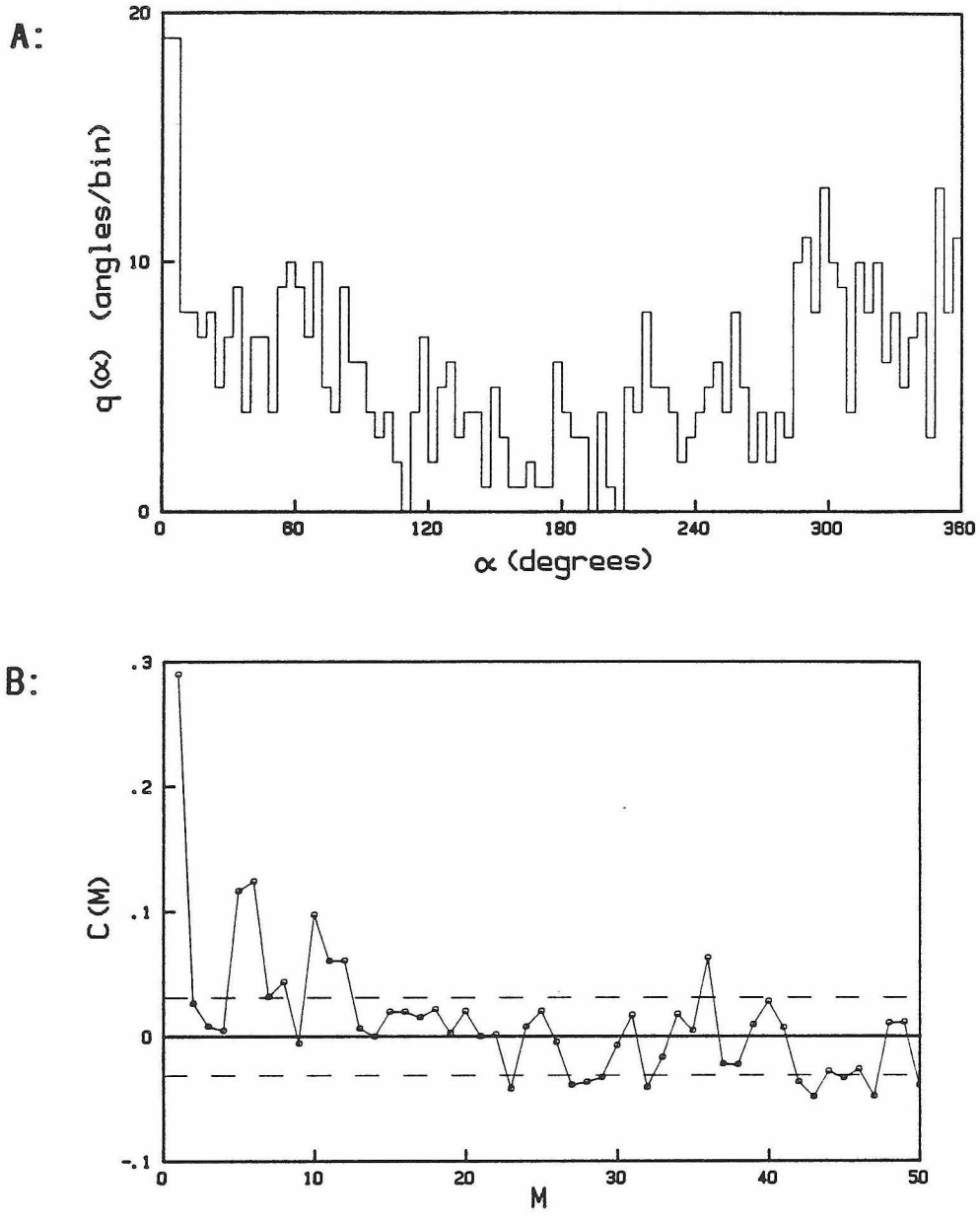

Fig. 1.1. The angular difference, α, between subsequent stopping positions of the cell body of Streptococcus V4051, energized with an artificial membrane potential.

A: Histogram of α. Bin width 4°. 516 difference angles from 16 cells.

B: Cosine transform of the distribution of α. The dashed lines indicate the rms noise expected from a uniform distribution.

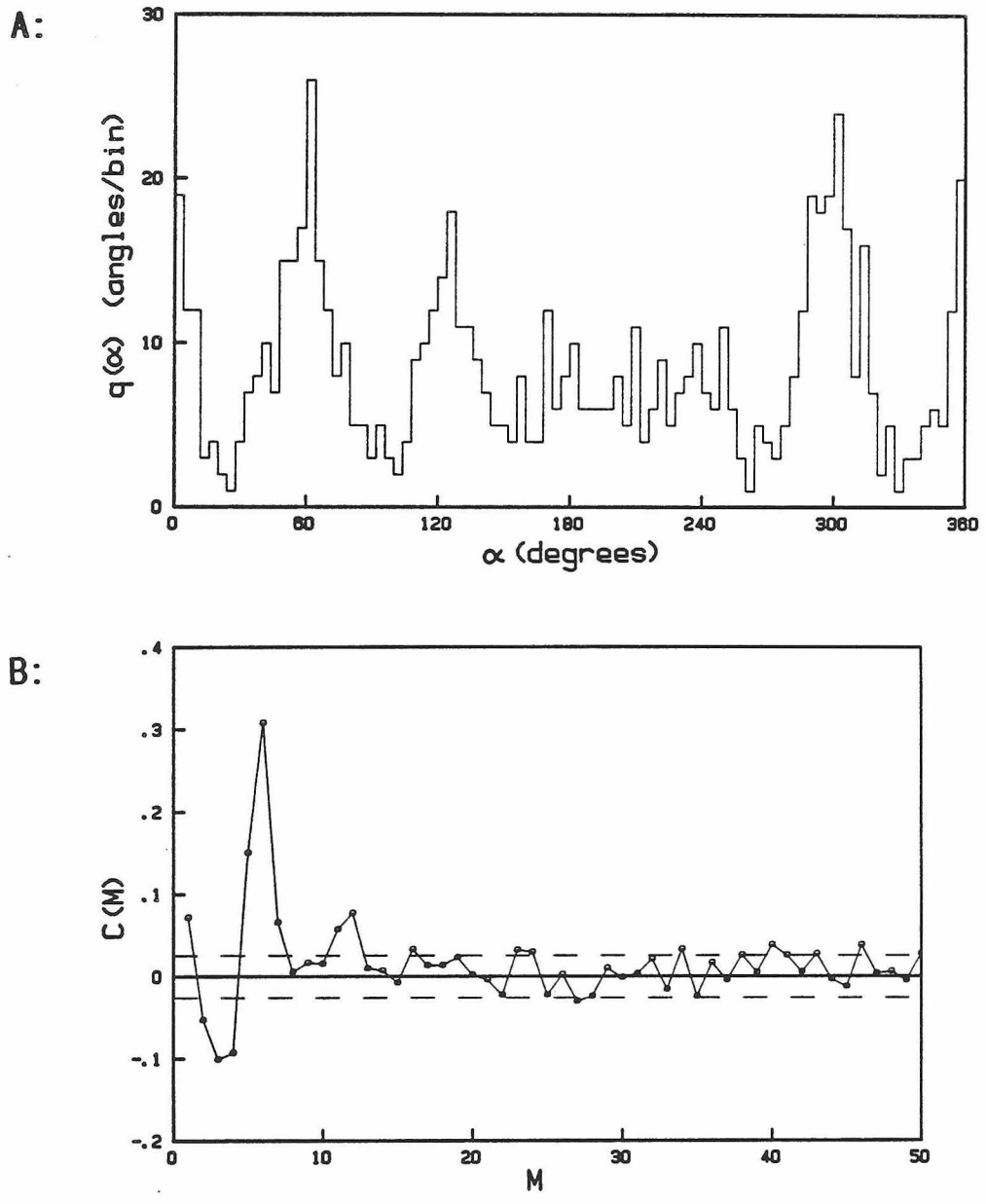

Fig. 1.2. The angular difference, α, between subsequent stopping positions of the cell body of Streptococcus V4051, energized metabolically with glucose and deenergized with DNP.
A: Histogram of α. Bin width 4°. 759 difference angles from 21 cells.
B: Cosine transform of the distribution of α. The dashed lines indicate the rms noise expected from a uniform distribution.

of small absolute difference angles. This property of the distribution causes the large positive value of C(1) and the large negative value of C(3) in the cosine transform, shown in Fig. 1.2B. One also finds a very large peak at M = 5 and M = 6 and another one at M = 10 and M = 11. The value at M = 5 is significantly lower than at M = 6, but it appears that the peak is skewed by the above-mentioned experimental artifact: note that C(4) is still large and negative. During this experiment a substantial number of cells showed several distinct angular positions on the same micrograph. These cells were creeping very slowly (at less than 0.1 Hz) and irregularly during the exposure time. On average they spent more time at some angular positions than at others, producing daisy-like patterns, some of which are pictured in Fig. 1.3. A more extensive analysis revealed that most of the signal in Fig. 1.2B derived from cells that also generated these daisy patterns, but the peak at periodicities 5 and 6 remained significant when only one petal per cell from each micrograph was included in the pool of difference angles.

A similar experiment was performed on cells of the mutant SM197, whose motors turn exclusively counterclockwise. The distribution of 801 difference angles measured on 23 cells is plotted in Fig. 1.4A and shows clear lumps at regularly spaced discrete positions as well as a shortage of difference angles at values around 180°. The cosine transform, Fig. 1.4B, has a very strong peak at periodicities 5 and 6 and a minor peak at M = 11. Fig. 1.5 shows the distribution of the orientation angles of cell bodies in this experiment relative to a common reference on the coverslip. I determined the direction of flow by following the trajectory of two cells that were torn off the slip by the moving medium. That direction is indicated in the figure and coincides roughly

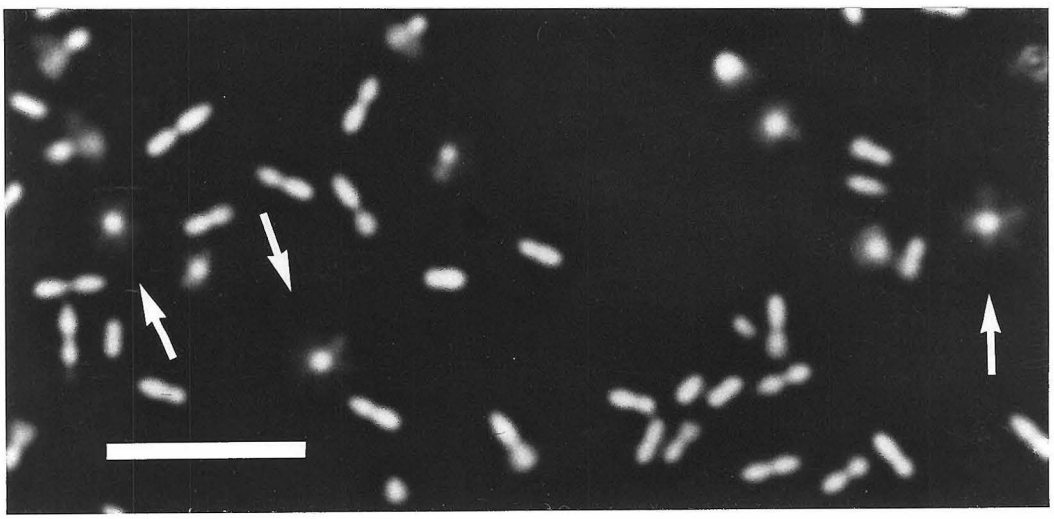

Fig. 1.3. Part of one of the photomicrographs from the experiment of Fig. 1.2. The daisy-like patterns (arrows) are produced by creeping cells. The bar represents 20 μm.

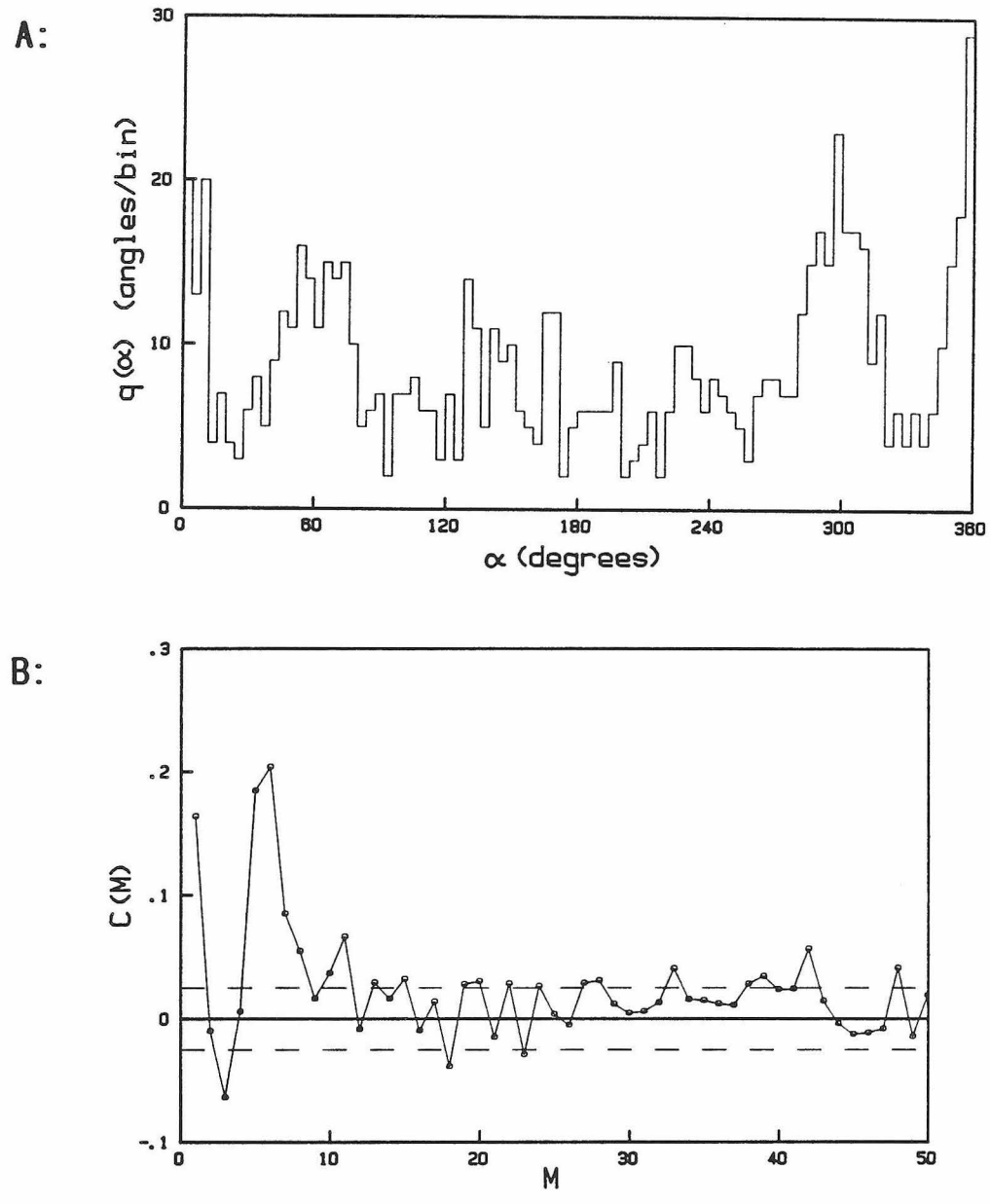

Fig. 1.4. The angular difference, α, between subsequent stopping positions of the cell body of Streptococcus SM197, energized metabolically with glucose and deenergized with DNP.

A: Histogram of α. Bin width 4°. 801 difference angles from 23 cells.

B: Cosine transform of the distribution of α. The dashed lines indicate the rms noise expected from a uniform distribution.

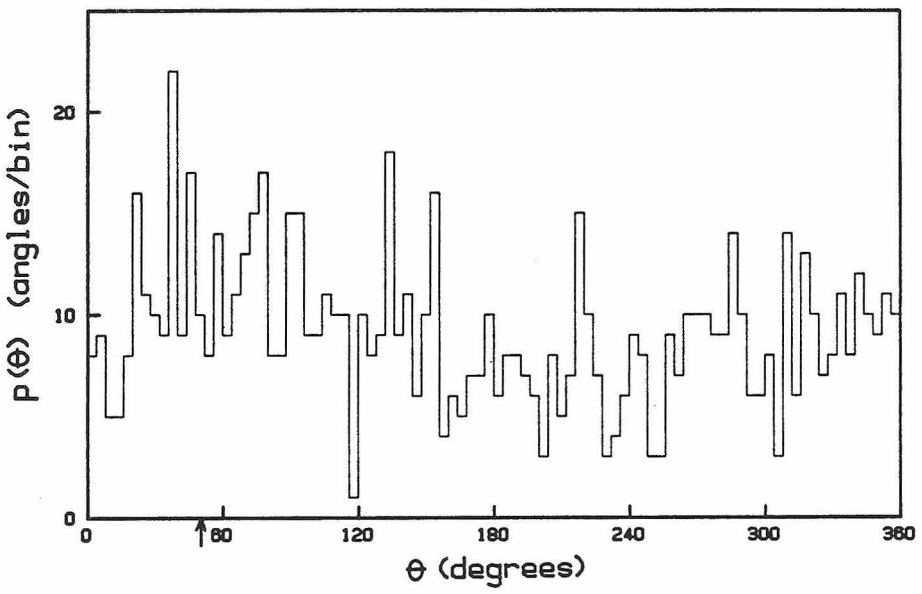

Fig. 1.5. Histogram of the cell body's absolute stopping position, θ, relative to a reference line on the coverslip. Bin width 4°. 824 stopping angles from 23 cells obtained in the experiment of Fig. 1.4. The arrow indicates the direction of fluid flow at the glass surface.

with the broad peak in the distribution of orientation angles, thus confirming the interpretation of the experimental artifact discussed above, which also caused large values of C(1) and C(3) in Fig. 1.4B.

I performed these experiments repeatedly on E. coli strain AW405, tethered with flagellin antibody to glass cleaned with fuming nitric acid (Block et al. 1983). Although it was easy to start and stop the motors many times using DNP, the measurements were hampered by strong interactions between the cell body and the glass surface. Most cells were found in only one or two orientations after the flow had stopped, and often the cells were seen hesitating at those same positions when they were spinning, as if their rotation was obstructed by an obstacle on the coverslip. Several attempts were made to reduce these interactions, including: blending the cells instead of shearing them with syringes, to further shorten the filaments and reduce the possibility of a second one dragging on the glass; treating only the cells with flagellar antibody, which was washed out of the suspension before tethering, such that the glass surface underneath the cell body was not coated with antibody; coating the glass with various proteins (bovine serum albumin, pepsin, protamine); adding mannose to the medium to inhibit the adhesion of mannose-sensitive pili; growing the cells on glucose instead of glycerol to suppress the formation of pili. None of these procedures had any notable effects, except that cell bodies were glued rigidly to the coverslip in the presence of protamine. The irregularities in the motion of tethered E. coli cells make them generally less suitable for studies of motor function than the motile Streptococcus V4051 and the strains derived from it.

§1.4 DISCUSSION

The distribution of stopping angles of the Streptococcus flagellar motor shows large Fourier components at angular periodicities of 5 and 6. In principle the ambiguity in the symmetry could result from an inhomogeneous cell population with some motors having five discrete stopping positions and others six. The Fourier analysis of the stopping angles on a single cell does not provide the resolution required to detect such differences. The experiments on strain SM197 rule out the possibility that the symmetry of the motor depends on its sense of rotation just before it stops.

On the other hand, the stopping angles may not be spaced at absolutely regular intervals, which could explain the broad peak of the cosine transform. Recent studies by Wagenknecht et al. (1981) of the flagellar hook structure in Caulobacter crescentus and Salmonella typhimurium suggest such an interpretation. Monomers of the hook protein assemble in a helical lattice. The generating helix of this lattice shows about 5.5 subunits per turn and a pitch of 2.3 nm. This structure has no defined symmetry relative to rotation about the hook's axis. The only symmetry operation that can image the lattice onto itself is rotation combined with translation parallel to the axis. If the discrete stopping positions were determined by interactions between the hook and another motor component, then the stopping angles would not be evenly spaced, even if the other motor part involved had true azimuthal symmetry. A dramatic feature of the three-dimensional reconstruction of hooks in the above study is the presence of deep, broad helical grooves in the surface of the hook, following the set of

6-start helices. A cross section perpendicular to the axis of the hook shows 5 or 6 dense regions along the periphery (depending on the axial location of the section) separated by angular intervals that vary about a mean of ca. 65 degrees. If the motor's shaft, which forms the proximal extension of the hook, has a similar structure, then its rotation might be constrained by mechanical interaction between these grooves and a single site on the stator or the cell wall. In that case one would expect a cosine transform of the stopping angle distribution to show the peak extending over periodicities 5 and 6 that I have observed. The relevant sites on the stator cannot have true azimuthal symmetry of order greater than one, otherwise the first peak in C(M) would appear at higher multiples of 5 and 6.

In summary, it appears most likely that the discrete stopping angles result from a static interaction between the surface of the shaft and parts of the stator or the cell wall, although this interpretation rests on the assumption that the shaft of Streptococcus is similar in structure to the hook of C. crescentus. The analysis offers no insight regarding the symmetry of the torque-generating machinery, but it points out an interesting problem in matching any such azimuthal symmetry to the helical symmetry of the flagellum. If the grooves in the surface of the hook are of structural importance in the connection between hook and M-ring, one might expect the latter to have a rotational symmetry of order 6.

CHAPTER TWO : THE STALL TORQUE OF THE BACTERIAL FLAGELLAR MOTOR

§2.1 INTRODUCTION

Until now measurements of the torque generated by the flagellar motor have relied on the observation of spinning flagella or tethered cell bodies and the calculation of the viscous drag associated with that rotation. Manson et al. (1980) varied the rotation rate of glycolyzing tethered cells by changing the viscosity of the medium and found that the motor torque was independent of speed over the range from 0.4 to 8 Hz. At the much higher flagellar rotation rates seen in swimming cells the torque is considerably lower (Lowe et al. 1986; Chapter 4 of this thesis). In this chapter I will present a technique for measuring the motor's stall torque, that is, the external torque on the motor's shaft required to stop its rotation. These studies extend the experimentally accessible range of the torque-speed relationship down to 0 Hz.

The method relies on the fact that tethered cells spin about an axis that does not pass through the center of the cell body. One can therefore exert a torque on the cell body by flowing fluid past these cells. The cell then rotates more slowly during the half-revolution where it works against the flow and more rapidly on the half-revolution where it works with the flow. As one gradually increases the flow rate, a point is reached where the cell stops rotating, and the long axis of the cell body remains pointed approximately at a right angle to the flow. At even higher flow rates the cell body is oriented further and further downstream. The torque exerted on the cell body by the flow can

be calculated from the flow velocity, the translational drag coefficient of the cell body, and its angle of inclination relative to the direction of flow. This torque is equal and opposite to the stall torque generated by the flagellar motor. When computed in this way, the stall torque is found to be similar to the torque determined from the rotation of tethered cells. Due to systematic errors, its absolute value is subject to considerable uncertainty, while relative changes in the stall torque generated by any given cell can be determined quite accurately. Therefore, most of my studies involved comparing the torque measured on a particular motor to the value found for that same motor under a different set of conditions. For example, I found that the stall torque does not depend noticeably on the rotation angle of the flagellar filament relative to the cell body.

I then applied this method extensively to test the hypothesis that the motor torque in a tethered cell might be strongly dependent on its speed under certain environmental conditions. This suspicion originated from observations that the swimming speed of Bacillus subtilis drops dramatically at values of the external pH below 6 or above 8.5, and that it saturates at large protonmotive force, remaining approximately constant at values above -80 mV (Shioi et al. 1980). Shahid Khan found similar effects of extreme pH and large Δp on the speed of tethered artificially energized Streptococcus (unpublished). These results were in contradiction with the simple picture put forward by Manson et al. (1980) to explain what was known about motor physiology at the time. In this view, the torque measured in tethered cells is strictly proportional to the protonmotive force, because a constant number of protons carries the motor through each revolution, and torque generation

in tethered cells occurs very near thermodynamic equilibrium and thus at an efficiency close to one. Why, then, does the torque drop below its expected value at extreme pH or very high protonmotive force? A possible explanation might be that, although the motor does couple proton flow and rotation of the flagellum with a constant stoichiometry, it does not operate reversibly under those extreme conditions. For example, if proton conduction in the motor occurs along chains of proton-accepting sites, one expects the rate of transfer to depend on the pH of the medium. If the absolute proton concentration is very different from the dissociation constant of the sites, a net flow of protons leads to considerable dissipation along the conducting chain. At high protonmotive force the torque of the motor might be limited for similar reasons. The finite mobility of mechanical components of the torque generating machinery could also be limiting the torque of a running motor (Berg and Khan 1983; see also §5.3). However, none of these processes would affect the stall torque. In a tightly coupled, stalled motor there is no net transfer of protons, no net movement of mechanical parts, and therefore no dissipation of free energy. In fact, a mechanism that transfers a constant number of protons for each revolution of the rotor is by necessity reversible at very low speeds: if the free energy loss of protons translocated during infinitesimally slow rotation were larger than the mechanical work performed at the output, then one could pump protons with efficiency greater than one by driving the motor externally. Therefore, such a motor generates a stall torque

$$(2.1) \qquad N_S = \frac{(-e\Delta p)\ S}{2\pi}$$

where S is the number of protons transferred across the membrane per

revolution. So the hypothesis that the motor is tightly coupled but operates far from thermodynamic equilibrium under extreme conditions predicts that the stall torque remains strictly proportional to Δp and independent of pH, even when the running torque drops significantly below this value. The experiments that I will present here clearly contradict this prediction, and I will discuss the resulting dilemma at the end of the chapter.

§2.2 METHODS

a) Hydrodynamics.

Measurements of the motor torque are greatly facilitated by the fact that all fluid flows occur at low Reynolds number. Inertial forces within the fluid in the flow chamber are negligible and thus the Navier-Stokes equation is linear in the velocity:

$$\eta \, \Delta\vec{v} + \vec{\nabla}p = 0$$

where η is the dynamic viscosity, $\vec{v}$ is the fluid velocity, and p is the pressure, excluding the hydrostatic component. Thus the flow velocity at any point in the flow chamber is proportional to the pressure drop from inlet to outlet. Similarly, the force and torque on a stationary cell body tethered in this flow chamber are proportional to the pressure drop. Furthermore one can use the method of linear superposition of flow fields to determine the torque on the cell body as a function of its orientation relative to the flow. Fig. 2.1 illustrates the body of a tethered, energized cell, which I will approximate by a cylinder, stalled by the flow of the surrounding fluid. The cell body is free to rotate about an axis orthogonal to the coverslip that intersects the body's symmetry axis at a right angle. If one temporarily ignores the proximity of the coverslip and other surfaces of the flow chamber, then the boundary conditions are that the velocity, $\vec{v}$, vanish on the cell surface and that $\vec{v}$ be equal to $\vec{v}_0$ at infinity. Then one can linearly decompose the flow into one component whose homogeneous flow velocity at infinity is parallel to the body axis and of magnitude

$$v_0^{\parallel} = v_0 \cos\theta .$$

and another component whose flow velocity at infinity is perpendicular

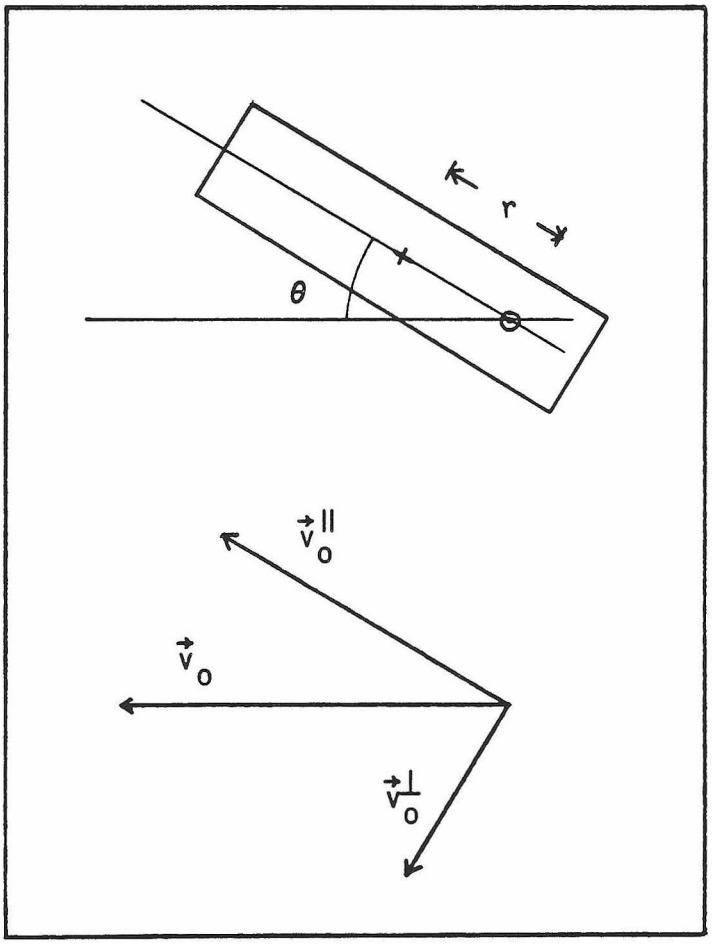

Fig. 2.1. Illustration of an energized tethered cell, stalled because the surrounding fluid flows at a velocity $\vec{v}_0$ relative to the coverslip.

to the body axis and of magnitude

$$v_0^{\perp} = v_0 \sin\theta$$

The parallel component exerts no torque on the cell body, while the perpendicular flow generates a torque

$$N_S = c_T^{\perp} v_0 \, r \sin\theta$$

where $c_T^{\perp}$ is the frictional drag coefficient for translation perpendicular to the body axis, r is the distance from the rotation axis to the center of the cell body, and θ is the angle between the long axis of the cell and the direction of flow at infinity. This treatment applies rigorously even when additional boundary surfaces are introduced. For example, one may require $\vec{v}$ to vanish on two parallel planes representing the top and bottom coverslips of the flow chamber. As long as the cell's rotation axis is orthogonal to these planes, the geometry of the entire boundary surface is independent of the angle θ, and therefore linear decomposition of the flow field is possible. Furthermore there are no restrictions on the shape of the cell body: it need not have a symmetry axis or even a center of hydrodynamic stress and may rotate about any axis.

To compute the torque exerted on a rotating cell by a medium that is stationary at infinity, one can again use linear superposition. Rotation of the cylinder about an arbitrary axis can be decomposed into translation of the cylinder and rotation about its center. Both translation and rotation can be further decomposed into their vector components along and transverse to the cylinder axis. The resulting forces and torques are computed using the four drag coefficients corresponding to these motions and added vectorially to yield the total force and torque about the center acting on the cylinder. Finally the

torque along the original axis of rotation is computed from these quantities. Again this treatment is not limited to a particular shape of the cell body. A more general discussion of these methods is found in Happel and Brenner (1983). Under the above assumptions the torque generated by the motor of a rotating tethered cell is

$$N_R = (c_R^{\perp} + r^2 c_T^{\perp}) \frac{d\theta}{dt} = (c_R^{\perp} + r^2 c_T^{\perp}) 2\pi f$$

where f is the rotation rate of the cell body and $c_R^{\perp}$ is the frictional drag coefficient corresponding to rotation about an axis through the center of the cylinder and perpendicular to its symmetry axis.

Tirado and de la Torre (1979, 1980) give numerical estimates derived from a spherical bead model of the principal drag coefficients for a cylinder: $c_T^{\perp}$, $c_R^{\perp}$, as well as $c_T^{\parallel}$ for translation along the cylinder axis, and $c_R^{\parallel}$ for rotation about the cylinder axis. (Note that the formula for $c_R^{\parallel}$ is misquoted in the review of de la Torre and Bloomfield (1981); the value given is 4 times too small.) I used these formulae in computing the stall torque and the running torque of the motor driving a tethered cell. In order to calculate the absolute torque acting on the body of a tethered cell I measured the dimensions of its image on a photomicrograph (Polaroid 665 pos./neg. film). The distance, r, between the rotation axis and the center of the cell body was determined from the cell's length and the diameter of the bright disk it produced on a long-term exposure taken while it was spinning. The viscosity of water was taken from the Gmelin Handbook of Inorganic Chemistry (1963). In calculating the torque on a rotating cell I ignored the proximity of the coverslip. This seems justified by the work of Jeffery (1915), who computed the drag coefficient of a sphere rotating near a solid plane wall about an axis perpendicular to the wall and found that it increases

only by 6% as the sphere approaches from infinity to a distance of 1/3 of the radius and by 17% at a distance of 1/50 of the radius.

The no-slip boundary condition at the glass surface is more relevant to calculation of the stall torque. Since the cell is about one μm wide and only one or two μm away from the coverslip, the flow velocity changes appreciably over the dimensions of the cell body. Nevertheless I applied the treatment for a cylinder in a homogeneous flow field. For the flow velocity at infinity, v_0, I chose the average value at the location of the cell bodies, determined by measuring the velocity of originally tethered cells that are carried away by the flow during the first 0.1 s after they are torn off the glass.

b) Generation of flows.

I used three different methods for generating the flow of fluid required to stall tethered cells. In the first and simplest version, the flow was driven by hydrostatic pressure, which I adjusted manually. The medium flowed from a reservoir kept at constant level through polyethylene tubing into the flow chamber and from its outlet into a beaker with medium at a variable level below the inlet reservoir. For fast replacement of medium in the chamber, its outlet could also be connected to a vacuum line using a three-way valve. With this setup I usually chose one cell in the microscope field and adjusted the level of the outlet beaker such that the cell was just able to complete a revolution by turning through the opposing flow. This flow rate was fairly well defined, and I marked the corresponding beaker level on a vertical strip chart. The level leading to zero flow was easily determined by observing some freely suspended cells in the chamber and

adjusting the beaker until they stopped moving. Finally, the flow rate was measured as a function of the level difference between inlet and outlet by weighing one of the beakers after a given period of flow. This flow rate was found to be proportional to the pressure drop across the whole line to within the accuracy of the measurements (ca 1%), which confirms the assumption that nonlinear velocity terms are negligible in the equations governing the flow through the flow chamber and the tubing. With this technique the minimal flow required to stall rotation, corresponding to an inclination angle $\theta = 90°$, could be determined quite accurately. However, I could only observe one cell at a time, a serious disadvantage when averages over a large number of cells are required.

In Mark II the flow was again driven by hydrostatic pressure but the outlet beaker was mounted on a mechanical elevator. This device was designed by Howard and built from the remains of an old fraction collector. It raised or lowered the platform with the beaker through a range of 50 cm at a rate chosen by a gear box connected to the electrical motor. I generally started at the lowest level, corresponding to the highest flow rate with many cells stalled. When the elevator started raising the beaker, a time display on the video recording of the microscope field (Ishihara et al. 1983) changed color. As the flow rate gradually decreased, more and more cells started spinning. At the end of the sweep the time display reverted to the original color. These experiments were analyzed off-line during play-back of the video tape. For each cell I determined the time at which it first turned through $\theta = 90°$ to complete a revolution. The corresponding flow rate was obtained from calibrations of beaker level

as a function of sweep time and flow rate as a function of level difference. This method had the great advantage that the stall torque could be measured for many cells, generally 10 to 20, in a single sweep lasting only 25 s. However, the maximal pressure drop available between the microscope stage and the floor was not sufficient to stall all the cells, even when wide tubing of 1.19 mm internal diameter was used. Particularly the small and fast spinning cells were left out of the sample, which was unfortunate in experiments designed to test for a drop in torque with increasing speed. Another disadvantage was that obstructing particles could become lodged in the tubing or the flow chamber, which changed the resistance of the line. To check for this I had to measure the flow rate both before and after each experiment.

Therefore, in the third version of the apparatus, the flow rate was controlled directly by drawing the fluid through the chamber with a peristaltic pump (Gilson Minipuls 2). I modified its electronics such that the rotation rate of the roller head was controlled by an external voltage. This signal was provided by a circuit that generated a linear voltage ramp between an initial and a final level. Again the duration of the sweep was indicated on the video time display. The periodic component of the pump rate, due to individual rollers compressing the tubing, was removed with a surge filter, consisting of a small volume of air, typically 0.4 cm^3, in the line between the pump and the flow chamber (Block et al. 1983). The presence of this filter complicates the computation of the flow rate at a given time during the sweep. The volume flow rate through the chamber, j(t), is given by

$$\frac{dj}{dt}\,\frac{\frac{RV}{P}}{\{1-\frac{R}{P}j(t)\}^2} + j(t) = i(t)$$

where i(t) is the volume pump rate, R is the flow resistance of the line upstream of the surge filter, V is the volume of air in the filter, and p is the atmospheric pressure. I determined the filter time constant, p/RV, by following the movement of suspended latex beads (1.3 μm diameter) through the flow chamber after the pump was turned off. At late times after the shut-off their velocity decreased exponentially with a 1/e-decay time of p/RV. The filter volume V was chosen to yield a filter time constant much greater than the surge period. For each sweep I then solved the above differential equation for j(t) numerically, omitting the surge component in the pump rate, i(t). The slowly varying part of i(t) was known from calibrations against the pump controller voltage.

c) Experimental procedure and data analysis.

Cells of Streptococcus strain SM197 and in one case SM29 were grown, washed, and tethered as described in Chapter 1. Both these strains are mutants whose flagellar motors don't reverse (Berg et al. 1982), which is essential for the stall torque measurements. For artificial energization with an electrical membrane potential the cells were first exposed to 2 μg/ml valinomycin for 2 . Then the potassium in buffer A was partly replaced by sodium. In experiments where the cytoplasmic pH was clamped to the external pH I added 50 mM methylamine (pK 10.66) to the buffer at pH-values above 7.5 and 50 mM sodium benzoate (pK 4.19) at pH-values below 7.5. Since weak acids and bases can permeate the membrane in the uncharged form, and they are added in concentrations comparable to the cytoplasmic buffering capacity (see Chapter 3), this procedure effectively clamps the internal pH to the

external value (Repaske & Adler 1981; Kihara & Macnab 1981). The cells were observed under inverse phase contrast with a Nikon Optiphot microscope (Plan BM 40x objective, Zeiss optovar) and recorded on video tape (Ikegami ITC-47 camera, Panasonic NV-8950 recorder). Most stall torque measurements were obtained using the mechanical elevator or the peristaltic pump. The cells were first energized, either artificially or by addition of 0.01 M glucose to the medium, and observed while spinning. Then the flow was started at the high level, corresponding to the bottom position of the elevator or fast rotation of the peristaltic pump, which stalled most of the cells. When using the pump I had to wait for a few filter time constants to allow the flow rate through the chamber to reach its steady-state value. Then the ramp was initiated and the flow rate decreased gradually. The inclination angles of the tethered cells increased, and one by one they started spinning. At the end of the sweep I turned the flow off and observed the cells spinning for another few seconds. The entire period of flow typically lasted 30 s.

For studies of the stall torque as a function of the motor rotation angle I mounted a Polaroid camera (Nikon PFX with CF PL 5x projection lens) on the microscope and used its focusing telescope and a 16 mm/1:1.6 TV lens to simultaneously image the field onto the video camera. In these experiments I took a micrograph of the field (Polaroid 665 pos./neg. film, 5 s to 10 s exposure) during the initial period of constant flow before initiating the ramp. After the flow had ended, the measurement was repeated at a different initial flow rate. To determine the orientation of the flow field I deenergized the cells at the end of the experiment by adding 0.01 M 2,4-dinitrophenol (DNP) to the medium

and took another micrograph at moderate flow rate. Under these conditions the flagellar motor generates no torque, and the cell bodies align themselves with the flow. For each cell I used this orientation as a reference in computing the inclination angle, θ. The angles of all cells were measured on the Polaroid negatives as described in Chapter 1. During play-back of the video tape I determined at what time during the ramp each cell passed through $\theta = 90°$ to complete the first revolution. The corresponding flow rate was taken as a measure of the stall torque. In analyzing the dependence of the torque on the rotation angle I also computed the stall torque from the inclination angle, θ, and the flow rate during the Polaroid exposure. The average of the cell rotation rates before and after the flow ramp was used as a measure of the running torque.

§2.3 RESULTS

a) Comparison of stall torque and running torque.

Determination of the absolute value of the stall torque by the methods outlined in §2.2 are rather unreliable. The experimental results shown in Fig. 2.2 serve as an illustration of this. I computed the stall torque, N_S, and the running torque, N_R, for 17 glycolyzing cells on the same coverslip. The plot shows the ratio of N_R to N_S as a function of the speed of that cell. If stall torque and running torque were equal and the latter was independent of the rotation speed, this ratio should be equal to one for all speeds. It does not show a correlation with speed, but the scatter is considerable, and on average the running torque is 3.5 times larger than the stall torque. This is most likely due to systematic errors involved in calculating the torque. In particular, the stall torque is very sensitive to the measurement of cell sizes: it is directly proportional to the distance between the cell center and the rotation axis, r, which is obtained as the difference between two larger quantities, namely the length of the cell and the diameter of the circle it sweeps out during its rotation. The computed stall torque is also proportional to the flow velocity at the location of the tethered cell. The flow velocity decreases sharply as one approaches the coverslip and may not be estimated appropriately by the method described in §2.2.a. Finally, there are uncertainties related to evaluation of the drag coefficients: if one approximates the cells as ellipsoids with drag coefficients as given by Perrin (1934, 1936), the average ratio N_R/N_S drops to 2.4. Generally I trust the estimate of the running torque more than that of the stall torque; the average running

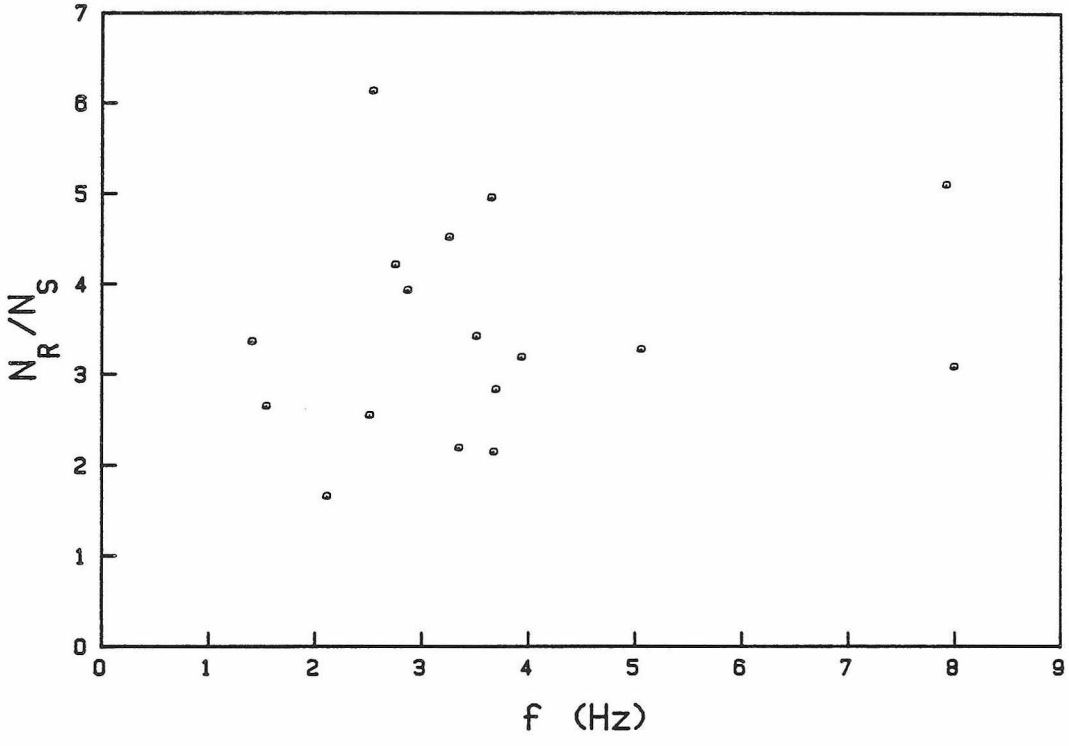

Fig. 2.2. Comparison of running torque and stall torque. The ratio of the running torque to the stall torque of glycolyzing, tethered cells is plotted against their rotation rate in absence of a fluid flow.

torque and its standard deviation in this sample were $(8.5 \pm 2.6)\times10^{-12}$ dyn cm.

b) Dependence of the stall torque on the rotor angle.

None of the above-mentioned systematic errors affect a measurement of the relative change in the stall torque of a given cell when it is energized under two different conditions. As outlined in §2.2.a, the stall torque is strictly proportional to the pressure difference across the flow chamber, as long as the geometrical configuration of the cell and other boundaries is the same in the two measurements. Partly in order to test the assumption of invariant tethering geometry and the validity of the conclusions I drew from it, I measured the stall torque of glycolyzing cells at various flow rates and therefore varying inclination angles, θ, of the cell body relative to the flow. Fig. 2.3 shows a plot of $v_\theta \sin\theta / v_S$ as a function of θ, where v_θ is the flow rate required to stall a particular cell at an inclination angle θ, and v_S is the minimal flow rate required to stall that cell. The graph contains data from 21 cells with 1 to 6 measurements per cell. If the hydrodynamic treatment illustrated in Fig. 2.1 applied exactly and the stall torque was independent of θ, this ratio should be identical to one. Instead one finds that it shows considerable scatter and is somewhat larger than unity at small angles, which correspond to high flow rates. A possible explanation is that the elastic filament, by which the cell is tethered, bends somewhat at high flow rates, bringing the cell body closer to the coverslip, where the flow velocity and therefore the drag are smaller. In all subsequent studies I determined the stall torque by the lowest flow rate, v_S, required to stall the cell

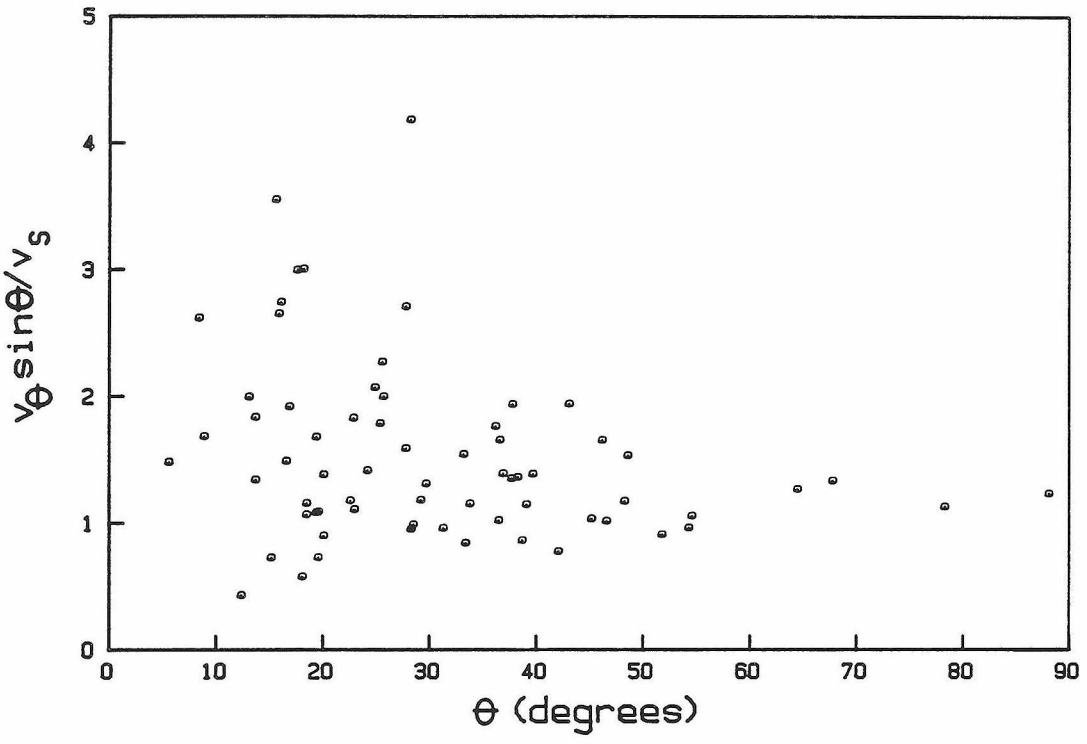

Fig. 2.3. Dependence of the stall torque on the stall angle relative to the direction of fluid flow, θ. The torque required to stall a cell at angle θ is divided by the torque required with the cell body at a right angle relative to the flow. That ratio is plotted as a function of θ. Data from 21 glycolyzing cells; 1 to 6 measurements per cell.

at θ = 90°, thereby minimizing such changes in the tethering geometry.

What do these measurements say about a possible dependence of the torque generated by the motor on the angular position of the rotor relative to the stator? If the interactions that give rise to the discrete stopping angles found in Chapter 1 also occur in energized cells, one might expect the stall torque to show a periodic dependence on the rotor angle. The data of Fig. 2.3 cannot reveal such a periodic modulation, because all the motors are tethered at random orientations relative to the flow. In order to detect such effects one would have to study a single cell very extensively. The resolution of torque modulations with rotor angle is also hampered by the elasticity of the flagellar filament that anchors the rotor to the glass. Since this effect may be relevant to further studies of the torque's angular dependence currently planned in Howard's group, I will present a detailed analysis.

Treating the flagellum as a torsion wire whose twist is proportional to torque, Berg (1976) estimated that it winds up by ca 70° in a spinning cell of E. coli. The torsional constant can be estimated from the extent of rotational Brownian motion exhibited by the cell body when the motor is deenergized and locked in position. During the experiments described in the previous chapter I found that tethered cells of Streptococcus wander somewhat further than the 3° that Howard reported for E. coli: the smear on long-term photographic exposures of stopped cells typically shows an angular width, $\Delta\theta$, of ca 6°. I therefore estimate the twist in the flagellum, β_0, at a motor torque, N, of 10^{-11} dyn cm as

$$\beta_0 = \frac{N(\Delta\theta)^2}{kT}$$

(see Berg 1976). If the motor torque were independent of the rotor angle, then the twist would remain unchanged as θ varies with different flow rates during a stall torque measurement. In that case the motion of the cell body relative to the coverslip directly reflects motion of the rotor relative to the stator. If, however, the motor's torque depends on the rotor position, then the filament will twist and untwist as θ is varied. This leads to a smoothing of the torque modulation as well as a change in the average torque.

Consider for the moment a stationary energized cell in a stationary medium. In a thought experiment we can hold the cell body at a fixed angle θ (referenced to the direction of fluid flow during the stall torque measurement) with a very tiny torque wrench and measure the torque required to keep it there. Let α be the angle of the rotor relative to the stator (referenced, say, to the position at which the torque is smallest). The twist angle of the filament is denoted by β (referenced to the relaxed state), and the value of θ obtained when both α and β vanish is called ϕ. This latter phase angle is different for every cell, chosen at random when the cells tether. Furthermore, $N(\theta)$ denotes the torque indicated on the torque wrench, $N_{fil}(\beta)$ is the torque acting in the filament, and $N_{mot}(\alpha)$ is the torque exerted by the motor on its shaft. The problem is to determine $N(\theta)$ given the values of θ and ϕ. The rotor will adjust itself with respect to the stator until it reaches an angle, α, with corresponding flagellar twist, $\beta = \alpha + \phi - \theta$, such that $N_{fil}(\beta) = N_{mot}(\alpha) = N(\theta)$. This process is illustrated in Fig. 2.4A. The horizontal axis is α, the motor-specific coordinate. The

Fig. 2.4. Illustrations regarding the angular dependence of the stall torque.

A: The torque generated by the motor, N_{mot}, is shown as a saw-tooth shaped function of the angle between rotor and stator, α. The torque in the twisted elastic filament is a linear function of α, whose intercept depends on the angle, θ, of the cell body relative to a reference on the tethering surface.

B: The motor torque, N, as a function of θ, obtained from the intersection of the two functions N_{mot} and N_{fil} in (A).

C: The motor torque, N, and the torque exerted on the cell body by the flowing medium, N_{fluid}, as a function of the angle, θ, between the cell body and the direction of fluid flow.

A:

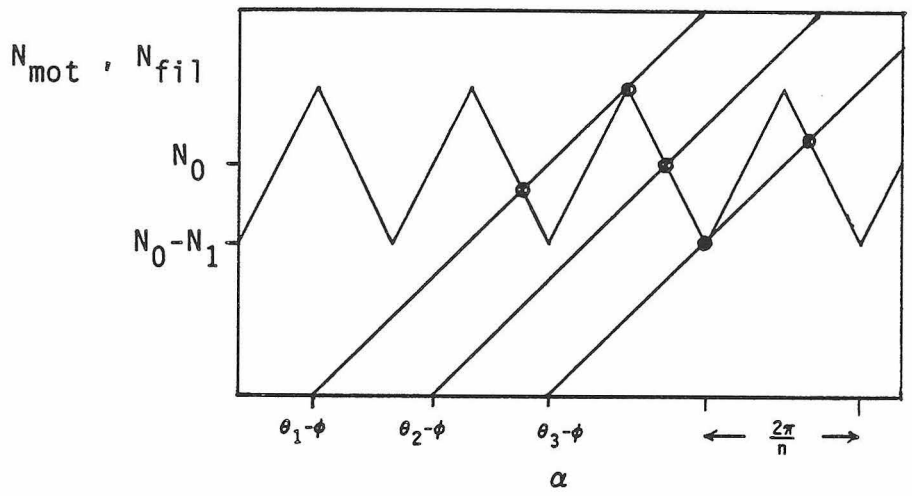
N_{mot} , N_{fil}
N_0
N_0-N_1
$\theta_1-\phi$
$\theta_2-\phi$
$\theta_3-\phi$
$\frac{2\pi}{n}$
α

B:

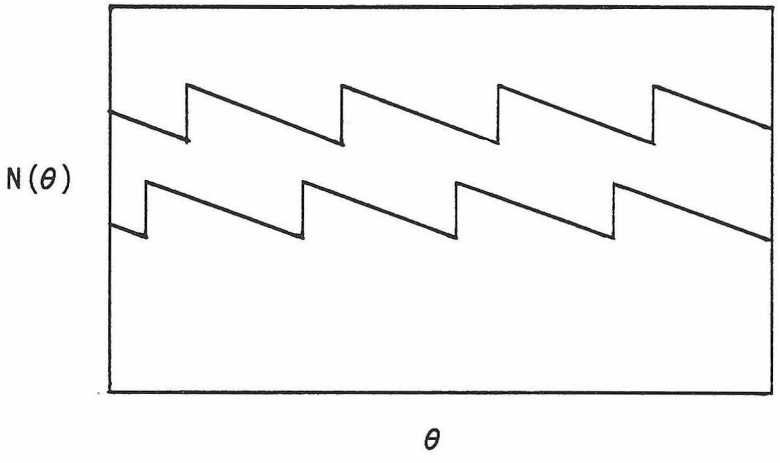
$N(\theta)$
θ

C:

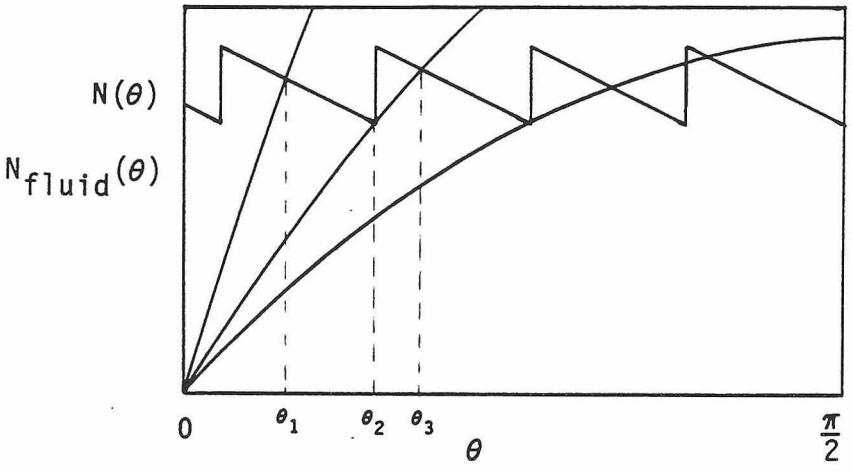
$N(\theta)$
$N_{fluid}(\theta)$
0
θ_1
θ_2
θ_3
θ
$\frac{\pi}{2}$

jagged curve shows the torque generated by the motor, $N_{mot}(\alpha)$, as a function of this angle: for simplicity I used a sawtooth modulation of amplitude N_1 about a mean value N_0 with n periods in a full revolution. The straight line shows how the torque in the filament, N_{fil}, depends on α:

$$N_{fil}(\alpha) = B\beta = B(\alpha-\theta+\phi)$$

where B is the filament's torsion constant. Since N_{mot} must be equal to N_{fil}, the correct value of α and the corresponding torque are given by the intersection of the two curves. Changing the angle of the cell body, θ, corresponds to moving the line for N_{fil} horizontally. For a very stiff filament ($B = \infty$) one sees that $N(\theta) = N_{mot}(\alpha+\phi)$, as expected, since the motion of the cell body directly corresponds to the rotation of the rotor relative to the stator. For finite but large B the torque $N(\theta)$ retains the full modulation of $N_{mot}(\alpha)$ but the shape of the periodic variations changes: the positive slope becomes steeper and the negative slope shallower. A qualitative change occurs when B is smaller than the maximal derivative of $N_{mot}(\alpha)$, which is the case shown in Fig. 2.4A. Now there may be several values of α (always an odd number) at which N_{fil} and N_{mot} intersect. Of these only the odd ones are stable. Which one of these is actually chosen depends on the history of the approach to the current angle θ. For example, if θ is continuously increased from θ_2 one finds that the torque, $N(\theta)$, changes gradually from θ_2 to θ_3. At this point the motor suddenly increases the filament twist and the torque jumps to a higher value. As θ is increased further, the torque drops gradually once more; this dependence is plotted in the lower curve of Fig. 2.4B. In practice, of course, there is no discontuous change in the torque, but the time required to move

the rotor and parts of the filament to their new position is very short compared to, for example, the period of revolution of a spinning cell or the time scale on which the flow velocity changes in a stall torque measurement. If, on the other hand, θ is varied in the opposite direction, then it increases gradually from θ_2 until θ_1, drops discontinuously, and then increases gradually again. The resulting form of $N(\theta)$ is shown in the upper curve of Fig. 2.4B. One sees that the average value of $N(\theta)$ is smaller than N_0 when θ is increased, working with the motor, while the average torque is larger than N_0 when θ is decreased, working against the motor. But the work per revolution performed by the motor is equal to N_0. Where does the remaining energy go? It turns into heat every time the rotor and the attached flagellum click into a new position. It is also apparent that the modulation of the torque is smaller than the modulation in $N_{mot}(\alpha)$. In fact, for a given torsional constant of the filament, B, the maximal peak-to-peak modulation one can observe in $N(\theta)$ is equal to $B2\pi/n$. These results are valid for any shape of the modulations in $N_{mot}(\alpha)$.

Now let us consider what happens when we disconnect the torque wrench from the cell and let it spin freely. If the filament is weak, then the torque shows discontinuous changes as a function of angle, and, as suggested above, the time required for the corresponding clicks of the rotor may be ignored. The torque $N(\theta)$ is balanced by the viscous drag due to the instantaneous rotation rate of the cell, $f(\theta)$. Since θ varies in the direction of positive torque, the lower curve of Fig. 2.4B applies. So in addition to the mechanical work required to rotate the cell the motor also performs work that dissipates in the clicking motion of the rotor and filament and is never apparent to the outside observer.

This does not occur if the filament is stiff enough, as discussed earlier. For a stiff filament the relative modulation in the rotation rate, $\Delta f/f$, is equal to the relative modulation, $\Delta N/N$, in the motor torque, $N_{mot}(\alpha)$. For a weak filament, however, it cannot exceed

$$(\Delta f/f)_{max} = \frac{2\pi}{n\beta_0}$$

where β_0 is the average twist in the filament.

Berg (1976) presented a different analysis of how variations in the behavior of the motor are smoothed by the elastic filament. In that treatment it was assumed that the speed of the rotor is determined by the motor machinery independent of the torque acting on the rotor, and that the speed varies as an explicit function of time, much as in a stepping motor. From more recent experimental work we know that the mean speed (averaged over one revolution) of a tethered cell varies greatly when the viscosity of the medium is changed, while the mean torque remains the same. I therefore believe that the present analysis, which assumes that the motor determines torque as an explicit function of the rotor angle but independently of speed, is more appropriate in the case of tethered cells. Of course, a complete description valid at all speeds would require knowledge of the torque, $N(\theta,\dot{\theta})$, as a function of both rotor angle and rotor speed.

During a stall torque measurement the torque $N(\theta)$ must balance the torque exerted on the cell body by the medium,

$$N_{fluid}(\theta) = v_0 \, c_T^{\perp} \, r \sin\theta = N(\theta).$$

As illustrated in Fig. 2.4C, the intersection of $N_{fluid}(\theta)$ and $N(\theta)$ occurs at a small angle θ_1 when the flow rate is large. As the flow rate is lowered, the angle increases gradually until θ_2 from where it

jumps discontinuously to θ_3. These jumps are less sudden than the ones considered earlier, since now the entire cell body must move to the new position. The net torque it has available for this motion is of the order of the modulations in $N(\theta)$ and therefore the rotation can occur no faster than that of a freely spinning cell. Nevertheless, these events should be clearly distinguishable from the very slow rise in θ as the flow rate is decreased. During my analysis of about 10^3 cells I have never seen such jumps and therefore the modulations in $N(\theta)$ cannot be very large. Assuming the sawtooth dependence of $N_{mot}(\alpha)$ shown in Fig. 2.4A, one can compute the maximal modulation ratio, $(N_1/N_0)_{max}$, that never produces jumps larger than a given threshold, θ_0:

$$(N_1/N_0)_{max} = \begin{cases} 1 & , \text{ if } (1+a) < b \\ \dfrac{1}{a+b(1-a)/(1+a)} & , \text{ if } b < (1+a) < 2b \\ c\{-1\pm(1+1/bc^2)^{1/2}\} & , \text{ if } 2b < (1+a) \end{cases}$$

where

$$a = 1 + \frac{(4-\theta_0 2n/\pi)\ \cos\theta_0}{1-\cos\theta_0},$$

$$b = \beta_0 \frac{2n}{\pi}$$

$$c = \frac{a/b-1}{2}$$

and the sign of the square root is chosen equal to the sign of c. The algebra is straightforward but tedious and left as an exercise to the reader. Assuming a resolution of jump angles of $\theta_0 = 25°$, a periodicity of n = 6, and a filament twist of $\beta_0 = 180°$, I compute a maximal ratio N_1/N_0 of 0.08. I therefore conclude that the rotation barriers which determine the discrete stopping angles found in Chapter 1 cause a peak-to-peak modulation in the motor torque of at most 16% of the mean.

However, this does not imply that they have disappeared in an energized motor. The piecewise parabolic potential corresponding to the sawtooth-like torque variations has wells of depth

$$\Delta E = N_1 \frac{\pi}{2n} \leq 2 \times 10^{-13} \text{ erg},$$

which is still much larger than kT and therefore sufficient to lock the deenergized motor.

The upper bound on the torque modulation quoted above is relatively sensitive to the estimate of the twist angle β_0. For example, if the filament is wound up by an entire turn, $\beta_0 = 360°$, then the ratio N_1/N_0 may be as large as 0.66. Clearly experiments of this sort should be performed on cells with stiff tethers, for example hook mutants of E. coli. But instead of searching for angular variations in $N(\theta)$ one could try to measure the difference in the torque observed when θ is varied in opposite directions. As seen from Fig. 2.4B, this effect of the torque modulations is actually more pronounced the smaller the stiffness of the flagellum. Such experiments could be performed by repeatedly increasing and decreasing the flow of fluid past a stalled cell, thus varying θ between 0° and 90°.

c) Dependence of the stall torque on pH.

Fig. 2.5A shows the results of an experiment in which cells were energized by a potassium diffusion potential of nominally -77 mV at various values of the pH. The stall torque and running torque were first measured in buffer A with 10 mM KCl and 190 mM NaCl at pH 7.5. The cells were brought back to 0.2 M K^+ and then shifted to buffer A containing additionally 50 mM sodium benzoate at pH-values 7.5, 7.0, or 6.5. After 30 min in this medium, which allowed for adequate

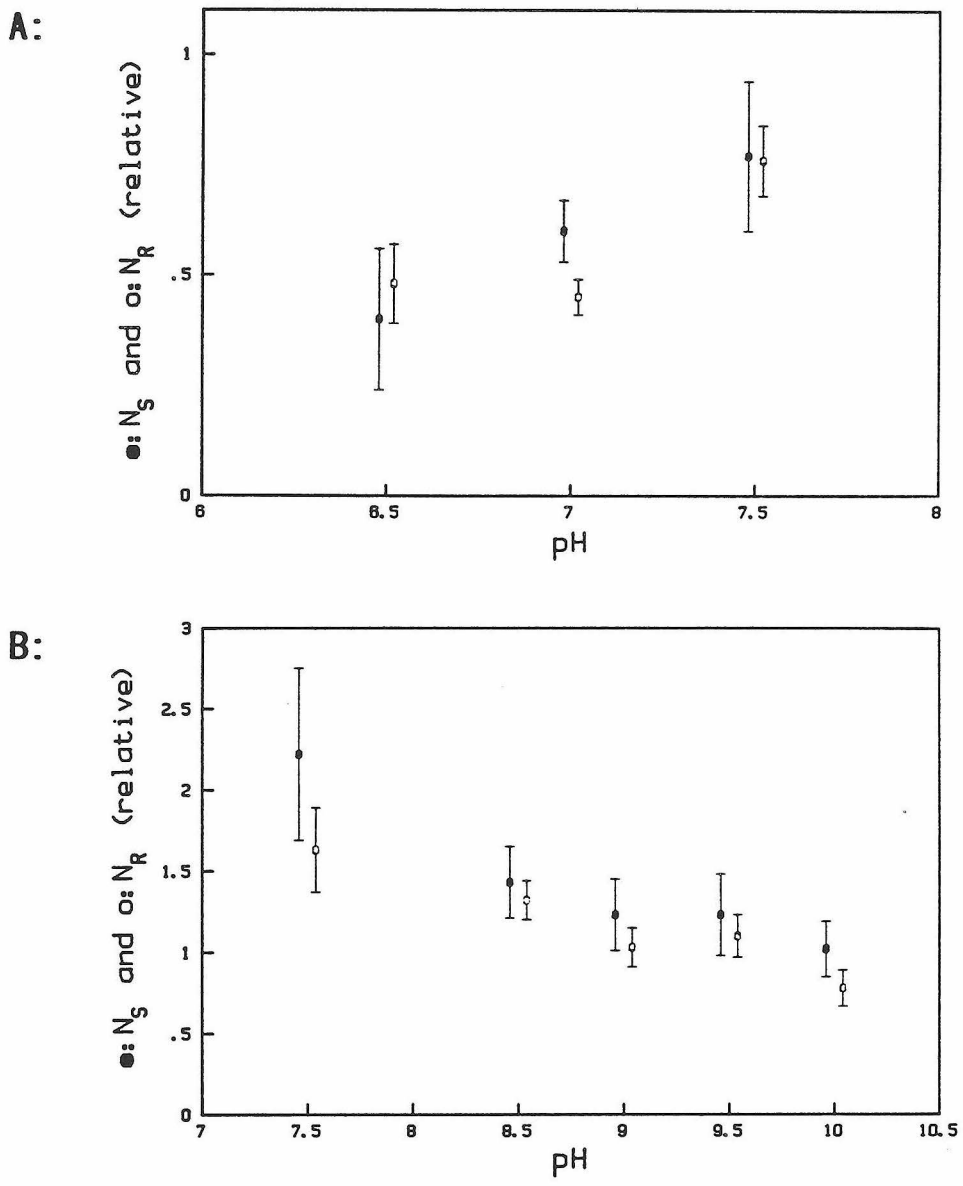

Fig. 2.5. Dependence of the stall torque (closed symbols) and the running torque (open symbols) on the absolute pH.

A: Second energization at acidic pH with 50 mM sodium benzoate present. Torque ratios averaged over 5 to 11 cells.

B: Second energization at alkaline pH with 50 mM methylamine present. Torque ratios averaged over 11 to 15 cells.

equilibration of the pH-gradient, the cells were energized again by a shift to low external potassium concentration, and I measured stall torque and running torque as before. For each cell I divided these torques by the respective values obtained during the first energization. The means and standard errors of these ratios are shown in Fig. 2.5A. At pH 7.5 the cells rotate slower after benzoate is added to the buffer, and the stall torque decreases as well. Both running torque and stall torque drop further as the pH is decreased and seem to vary identically to within the experimental resolution. Note that every pair of data points (N_S,N_R) is derived from a different sample of cells on a different coverslip. The average rotation rate of the cells during the first energization (corresponding to a relative running torque of 1.0 in Fig. 2.5A) was 2.5 Hz.

I performed a similar experiment at alkaline pH-values, where 50 mM methylamine was used to clamp the pH. The results are plotted in Fig. 2.5B. At pH 7.5 the torque is almost twice as large after addition of methylamine. It drops as the pH is increased, and again the stall torque and running torque are statistically indistinguishable. Here cells spun at an average of 1.9 Hz during the first energization.

d) Dependence of the stall torque on the protonmotive force.

To test whether the stall torque shows the same saturation at large Δp that we had observed for the speed of tethered cells I generated a large protonmotive force in several different ways. In one experiment cells were energized repeatedly with a varying potassium diffusion potential. After starvation in 0.2 M K^+ I shifted them to 10 mM K^+, 1 mM K^+, 0.1 mM K^+, and again to 10 mM K^+, measuring both running torque

and stall torque each time. Note that no benzoate or methylamine was present in these studies. Between energizations the cells were kept at 0.2 M K^+ for 10 min. At the end of the experiment I added 10 mM glucose to the buffer and measured the torques after the cells had begun glycolyzing. Fig. 2.6 shows the torques as a function of the nominal artificial Δp and in glucose. For each cell the torque is divided by its value during the first energization and the average ratios are plotted. The stall torque and running torque vary in exactly the same manner and are seen to saturate at large potassium dilution ratios. After addition of glucose the torque is ca 1.6 times larger than at a nominal membrane potential of -195 mV, where the cells rotated at an average rate of 3.9 Hz.

In another experiment I varied the protonmotive force by changing the external pH while cells were glycolyzing. I first measured running torque and stall torque at pH 7.5, then the cells were brought to a different pH and I measured the torques again within 60 s of the shift. Stall torque and running torque are plotted in Fig. 2.7, referenced to the values at pH 7.5, and are found to depend on pH in the same way. The torque increases slightly at pH 6.5, then drops off as the pH is decreased further. On the alkaline side the torque drops with increasing pH and extrapolates to zero at about pH 10.5. These cells were not treated with valinomycin, and at pH 7.5 they rotated at an average rate of 5.4 Hz.

A third indication that stall torque and running torque vary proportionally even at high Δp is given by observations on glycolyzing cells whose protonmotive force was reduced by addition of DNP. Fig. 2.8 shows measurements obtained from a single cell of SM29 using manually

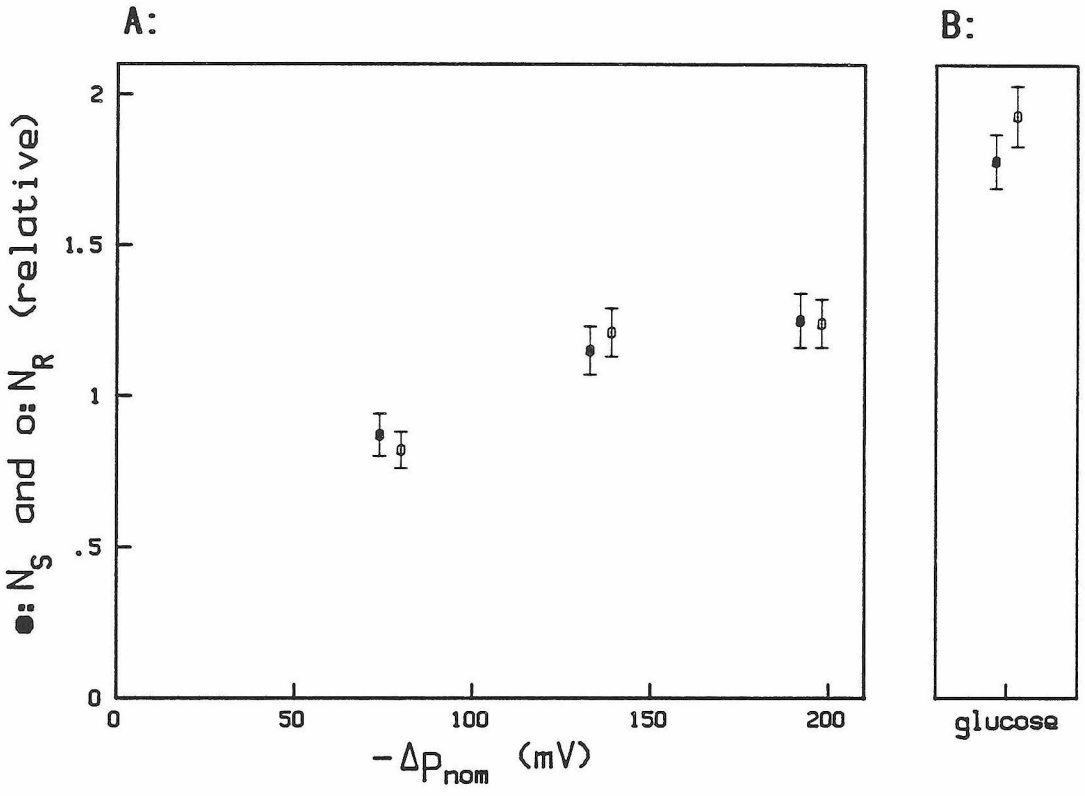

Fig. 2.6. Dependence of the stall torque (closed symbols) and the running torque (open symbols) on the protonmotive force. Torque ratios averaged over 25 cells.

A: Cells energized with a potassium diffusion potential.

B: Same sample of cells glycolyzing after exposure to valinomycin.

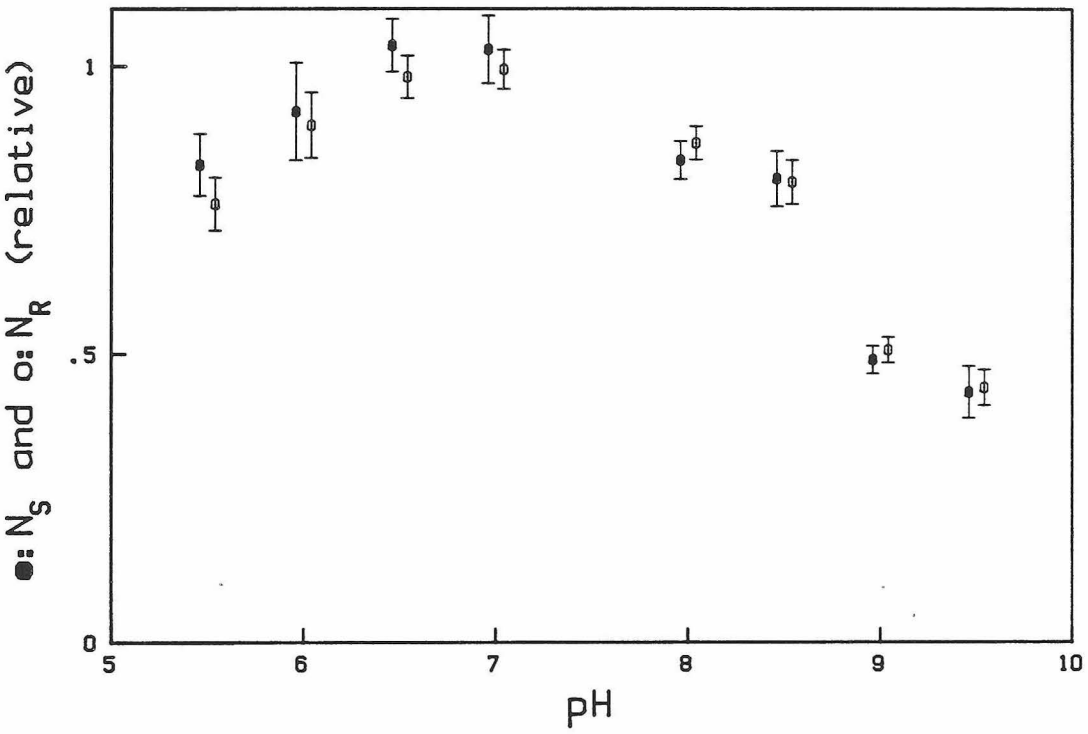

Fig. 2.7. Dependence of the stall torque (closed symbols) and the running torque (open symbols) of glycolyzing cells on the external pH. Torque ratios averaged over 36 cells.

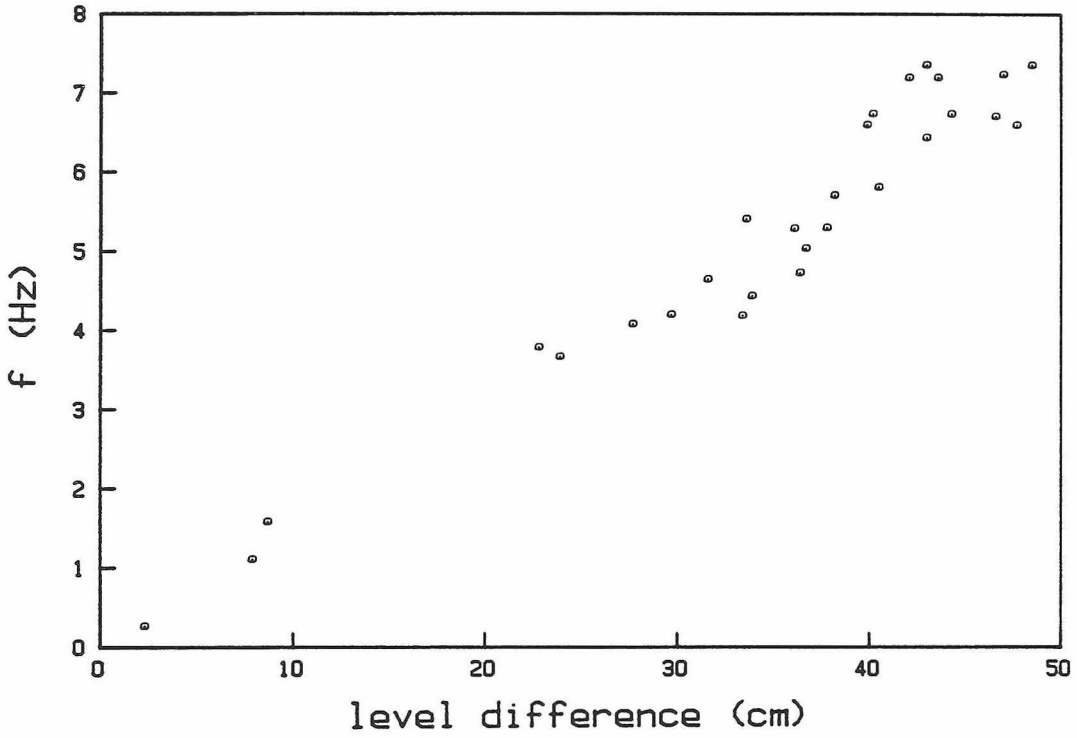

Fig. 2.8. Rotation rate of a tethered cell plotted against the level difference between inlet and outlet of the flow chamber required to stall rotation. Measurements were taken on a single glycolyzing cell, whose protonmotive force was gradually reduced with DNP.

controlled hydrostatic pressure to drive the flow. The rotation rate of the cell body is plotted against the level difference between inlet and outlet of the flow chamber required to stall rotation. The speed dropped gradually after addition of 1 mM and then 5 mM DNP to the buffer, and the stall torque remained proportional to the running torque to within the scatter of the measurements.

§2.4 DISCUSSION

I have shown here that the stall torque of the flagellar motor varies proportionally to the torque generated in a spinning tethered cell under a large variety of conditions. These include artificial energization with a varying membrane potential, energization with a membrane potential at varying pH, and changes in the protonmotive force of metabolizing cells via shifts in the external pH or through the action of an uncoupler. Apparently the stall torque is related to the torque generated at the speeds of tethered cells (about 1 to 6 Hz in the experiments described here) by a constant factor. Direct calculation of the absolute torques does not provide a reliable estimate of this factor. Since there is no measurable change in the torque driving tethered cells over speeds from 0.4 to 8 Hz (Manson et al. 1980), I expect no dramatic changes from 0.4 Hz to 0 Hz. Therefore I suggest that the stall torque is equal to the tethered cell running torque to within a few percent. Lowe et al. (1986), who measured the motor torque at low speeds in tethered cells and at high speeds up to 100 Hz in swimming cells, found that the torque decreases linearly with increasing speed. If that linear relationship is extrapolated to zero speed, one predicts that the torque should drop by only 10% over the range from stall to a speed of 10 Hz, clearly in agreement with the above results.

What do these measurements tell us about the question of coupling in the torque generating mechanism? As mentioned earlier (eqn. (2.1)), a motor that tightly locks motion of protons to revolutions of the rotor must show a stall torque, N_S, that is strictly proportional to the protonmotive force. But experimentally N_S varies strongly with pH at

nominally constant protonmotive force and does not increase proportionally to Δp at values larger than -80 mV. Only two interpretations remain: either the motor is not tightly coupled, or the real protonmotive force, Δp, is not equal to the value calculated from the Nernst equation, Δp_{nom} (see §1.2.d). I believe that the latter of these is more likely, for the following reasons: Aside from threshold effects at very low protonmotive force, the rotation rate of starved tethered cells is found to be proportional to the applied potassium diffusion potential up to values of $\Delta p_{nom} \simeq$ -80 mV (Manson et al. 1980; Khan et al. 1985). In this regime, the true membrane potential is close to its nominal value (Conley & Berg 1984). Fig. 2.6 shows that at larger potassium dilutions the rotation rate saturates as a function of Δp_{nom}. At a nominal protonmotive force of -195 mV the cells spin only 0.64 times as fast as when they are glycolyzing at the end of the experiment. Since the membranes of these cells contained valinomycin, I compared the rotation speeds of glycolyzing cells before and after exposure to valinomycin in a separate experiment and found that cells slow down by a factor of 0.74 on addition of the ionophore. Therefore glycolyzing cells without valinomycin spin 2.1 times faster than artificially energized cells at a nominal protonmotive force of -195 mV. We have not determined the Δp in glycolyzing cells of our Streptococcus strain by direct measurement, but values in other fermenting bacteria range from -80 mV to -170 mV (Kashket 1981, 1985b; Harold & Kakinuma 1984) with an average of -150 mV reported in glycolyzing S. lactis. It therefore seems very likely that the real protonmotive force is much smaller than its nominal value in the regime where the torque levels off. In fact, if one assumes that the speed of tethered cells is

strictly proportional to Δp over the entire physiological range of the protonmotive force, and that Δp is equal to Δp_{nom} for the first data point in Fig. 2.6 (-77 mV) but saturates at higher values of Δp_{nom}, then one obtains an estimate of -200 mV for the protonmotive force in glycolyzing cells, which is reasonably close to the reported values mentioned above. I will return to this question in §4.3.b and discuss some more observations suggesting that the generation of an artificial membrane potential becomes inefficient at external potassium concentrations much below 10 mM.

In the experiments of Fig. 2.7 we don't know exactly what the protonmotive force is, either. The interpretation of a similar study given by Manson et al. (1980), namely that the pH-gradient after the shift simply adds to the constant metabolically generated Δp, is at least doubtful. Shioi et al. (1980) measured the protonmotive force in glycolyzing Bacillus subtilis as a function of the external pH and found it to vary relatively little over the range from pH 4.5 to pH 8.5, although its composition changes. The cells' internal pH remains approximately constant, but the electrical membrane potential decreases at low values of the external pH. Apparently the ATP-driven proton pump can work as well against an electrical potential difference as against a proton concentration gradient. Since only very few elementary charges need to be transferred across the membrane to significantly change the electrical potential, I expect that the new steady state should establish itself almost immediately following the pH-shift, certainly before tethered cell rotation can be observed. Therefore I suggest that the experiments of Manson et al. (1980) as well as those of Fig. 2.7 probed the pH-dependence of the proton pump in Streptococcus rather than

the Δp-dependence of the motor torque. Similarly, the fact that the torque in artificially energized cells drops at extreme values of the pH (Fig. 2.5) may actually reflect difficulties in generating a potassium diffusion potential under those circumstances. On the other hand, direct damage to the motor is also a possibility. For example, the loss of individual torque generators of the type proposed in the hypothetical mechanism of Berg and Khan (1983) would lead to a parallel drop in the stall torque and the running torque. A puzzling observation in these experiments, which I have seen again repeatedly, is that the torque increases on addition of methylamine to the buffers and decreases in a medium containing benzoate. Note that the cells are starved in each new medium for 30 min before energization, which should allow ample time for the permeant ions to equilibrate across the membrane. The presence of a proton conductor would avoid the build-up of an opposing pH-gradient as protons are driven into the cell by the electrical membrane potential. As I will show in Chapter 3, this may enhance the protonmotive force significantly, suggesting a role for methylamine in equilibrating the internal and external proton concentrations. But why does benzoate, which is also membrane-permeant, decrease the motor speed?

In Chapter 4 I will present direct evidence that the flow of protons is tightly coupled to the revolutions of the motor. I will also discuss the problems involved in generating and measuring a protonmotive force more extensively. A direct determination of Δp would clearly be very useful in discussing some of the results reported here, and the need will become more obvious in the following chapters of this thesis. Clearly this problem should be high on the list of projects that Howard will distribute to his eager graduate students next year.

Finally I would like to suggest another experiment involving measurements of the motor's stall torque: a study of its temperature dependence. In fact, this may be the only case in which the stall torque deviates from the torque measured in spinning cells. As shown in Fig. 4.12B of Chapter 4, the torque developed in tethered cells changes only little with temperature. But the speed of the motors in swimming cells, which run at almost vanishing torque, drops significantly as the temperature is decreased. If the linearity of the torque-speed relationship mentioned earlier still holds at low temperatures, then at 10°C the stall torque may be 15% to 20% larger than the running torque in the average tethered cell. This difference should be measurable by the techniques I used and a preliminary analysis of spinning glycolyzing cells suggests that it exists. The torque of these motors changes as the temperature is varied, probably because of effects on the cell's metabolism or the ATPase. But the smaller and therefore faster cells in the sample seemed to slow down by a larger factor as I decreased the temperature.

CHAPTER THREE : THE PROTON FLUX THROUGH THE MEMBRANE OF STREPTOCOCCUS

§3.1 INTRODUCTION

The source of energy for motility in Streptococcus and many other bacteria is a difference in the electrochemical potential of protons across the cytoplasmic membrane (see Hirota et al. 1981 for a flagellar motor driven by a sodium electrochemical potential). Bacteria generate this proton gradient by extruding protons either in the course of oxidative phosphorylation or, under anaerobic conditions, with the use of a proton pumping ATPase. Membrane agents that dissipate the proton potential gradient stop flagellar motility in metabolizing cells (Larsen et al. 1974; Skulachev 1975; Belyakova et al. 1976). When cells are depleted of internal and external energy sources, artificial generation of either an electrical potential or a proton chemical potential across the membrane is sufficient to induce motility (Manson et al. 1977; Matsuura et al. 1977, 1979; Shioi et al. 1980; Khan & Macnab 1980b; Eisenbach & Adler 1981; Ravid & Eisenbach 1984). These results don't exclude the existence of another intermediate form of energy, which is generated from the proton electrochemical potential and subsequently converted to mechanical work by the motor. However, it has been shown that none of the common ions other than H^+ or OH^- are required in the external medium; in fact, E. coli swims happily in distilled water (Manson et al. 1977; Glagolev & Skulachev 1978; Matsuura et al. 1979; Khan & Macnab 1980a). Cell envelopes of S. typhimurium whose cytoplasm was replaced by buffer of known composition also exhibit flagellar

rotation in response to an artificially imposed proton gradient, indicating that none of the cytoplasmic components are required either (Ravid & Eisenbach 1984). No other form of energy available to the bacterial system seems to be involved in motility, and it is therefore commonly assumed that the proton electrochemical potential directly drives the flagellar motor.

Since free energy can be drawn from the proton potential difference only by transfer of protons between the external medium and the cytoplasm, the mechanism of flagellar rotation must involve movement of protons. Chapters 3 and 4 describe direct measurements of transmembrane proton fluxes coupled to rotation of the flagellar motor. (I should note that no experimental evidence is available indicating whether protons or hydroxyl ions are driving the motor. The two alternatives are indistinguishable by the methods used here or in any previous observation of flagellar motility. I will speak of "proton flux" to denote the net transfer of protons, some or all of which may in fact be flux of hydroxyl ions in the opposite direction.) Aside from providing another piece of evidence that the proton electrochemical potential immediately powers flagellar rotation, these measurements complete the set of quantities required to describe the steady state operation of the motor. With the knowledge of force and flow at the input (proton electrochemical potential and proton flux) as well as at the output (torque and angular velocity of the rotor) one can estimate the efficiency of energy conversion and the degree of coupling between proton flux and motor rotation. These results allow more stringent tests of proposed models for the mechanism of rotation, as discussed in Chapter 5.

Several powerful techniques have become available recently that allow the study of a particular membrane-bound ionic conductor independently of all the other conductance mechanisms present in the membrane. Reconstitution experiments involve the isolation and purification of the protein and its insertion into an empty artificial membrane separating two easily accessible compartments (Miller 1983; Miller 1984). Alternatively one can use patch electrodes to study the conductor in its native membrane (Sakmann & Neher 1984). The approach here is to limit the measurement of ionic current to a very small area of the membrane which can be chosen, by trial and error, to contain only or predominantly the conductor of interest. Neither of these methods appears to be useful for measuring the flux through the flagellar motor. Even if it proved possible to isolate intact and functional motors and insert them in an artificial membrane, they would lack the solid support required to anchor the stator, which is normally provided by the bacterial cell wall. Another stumbling block is the need to visualize flagellar rotation so that its torque and speed can be estimated.

I measured the flux of protons coupled to rotation of the motor in intact swimming bacteria. Starved cells were energized with an artificial proton potential large enough to induce swimming. The movement of protons into the cytoplasm was deduced from the rise in the pH of the weakly buffered external medium. By comparing the rate of proton uptake to the value obtained when motor rotation is stopped by cross-linking the flagellar filaments with antibody, I calculated the flux of protons linked to operation of the motor. Under physiological conditions the flux of protons required energetically to power flagellar motility is a small fraction of the total flux across the bacterial

membrane. The proton electrochemical potential serves as energy source for a large number of other membrane mechanisms such as ion pumping, transport of metabolites, and generation of ATP from ADP (Kashket & Wilson 1973; Maloney 1982; Harold & Kakinuma 1984). The presence of these large unrelated fluxes impedes the resolution of the motor flux which is given by the difference between two measurements of the total transmembrane proton flux. I therefore spent much time searching for conditions under which the total proton flux is small. The resulting observations on the general conductance of the Streptococcus membrane to protons are presented in this chapter.

A proton chemical potential is easily imposed across the membrane of starved cells by changing the pH of the external medium. As described in §1.2.d, the generation of an electrical membrane potential requires a large reduction of the external potassium concentration. To maintain the ionic strength, potassium is usually replaced by some other ion, typically sodium. The consequences of generating concentration gradients of these other ions have traditionally been ignored in studies of flagellar motility. I have found that they have important effects on the transmembrane proton flux. In particular there seems to be a membrane mechanism for direct exchange of Na^+ or Li^+ for protons. The membrane also has a significant conductivity to Mg^{2+} ions and a small but measurable conductivity to $choline^+$. In addition, I studied the effects of substituting deuterium ions for protons, the dependence of the proton conductivity on temperature, and the action of several membrane agents known to block some of the proton conductors unrelated to flagellar rotation. All these experiments eventually led to the choice of conditions for the measurement of motor fluxes. However, they

also raise some interesting questions, which might be answered by a more comprehensive approach to the ionic conduction mechanisms in the Streptococcus membrane.

§3.2 THERMODYNAMIC DESCRIPTION OF IONIC FLOWS

In the framework of thermodynamics one can treat the bacterial cell as a system in contact with a heat bath at constant temperature and able to exchange particles with the external medium. Furthermore, the internal energy of the system is given by the membrane potential and the total charge in the cell. Classical thermodynamics can only tell us that if we starve the cell long enough, it will settle in the state of highest entropy, where all flows across the membrane as well as those associated with internal chemical reactions vanish. If thermodynamic equilibrium is perturbed, for example by changing the external ionic concentrations, a net flow of the various ions results. A few general statements can be made about the relationships among these flows if they are steady and their magnitude depends linearly on the driving forces. This assumption of linearity is generally justified for small deviations from equilibrium. In our case, a further complication is introduced by the fact that the membrane potential, the internal ionic concentrations and the magnitude of the flows change significantly over the time of observation. In spite of all these restrictions on the validity of the linearized formalism I will present it for the following reasons: It will allow me to introduce the concepts and notation I will use in discussing my experiments. Also, a few predictions are possible due to the particular nature of the bacterial membrane system that hold even outside the linear regime. Finally, it will be interesting to see which of the experimental observations can be explained with this formalism and where the assumptions made in its derivation break down.

The following treatment of the time-dependent decay of deviations

from thermodynamic equilibrium applies to any isothermal system. I will outline its regime of validity in part (a), discuss the time-dependent solution in part (b), and specialize to the bacterial cell in part (c).

a) Regime of validity.

Consider a system at constant temperature T, whose state is defined by m independent extensive variables n_i (e.g., the number of particles of species i found in a bacterial cell). Define flows

$$J_i = \frac{dn_i}{dt}$$

and forces

$$X_i = \frac{\partial S}{\partial n_i}$$

where $S(n_1,\ldots,n_m)$ is the entropy of the system. At thermodynamic equilibrium all flows vanish. Also, since

$$0 = T\,dS = T \sum_i X_i\,dn_i$$

all forces vanish. When finite forces are imposed, the resulting flows can be expanded about the point of thermodynamic equilibrium as

$$J_i(X_1,\ldots,X_m) = \sum_i L_{ik} X_k + \sum_i \sum_k A_{ikl} X_k X_l + \ldots$$

One can show from the principle of microreversibility in statistical mechanics that

$$L_{ik} = L_{ki} ,$$

which are known as Onsager's reciprocity relations (Onsager 1931a, 1931b; Casimir 1945). The conductance matrix $[L_{ik}]$ is positive definite, since the rate of entropy production

$$\frac{dS}{dt} = \sum_i X_i J_i = \sum_i \sum_k X_i L_{ik} X_k + \ldots$$

is positive. In the following discussion I will use the term "linear regime" to designate the domain where terms of higher than first order in the driving forces are negligible in the above expansion of the flows.

How far this regime extends from thermodynamic equilibrium generally depends on the detailed statistical mechanics of the system. There are some heuristic rules indicating when the assumptions of linear force-flow relationships are justified. If a flow consists of statistically independent processes (e.g., single molecular reactions, passage of single particles through a membrane), then a sufficient condition for linear behavior is that the change in free energy associated with an individual elementary process at steady state flow levels is small compared to kT, where k is Boltzmann's constant and T is the temperature. This is not a necessary condition, and some phenomena, such as diffusion, heat conduction, electrical conduction, show linear force-flow relationships that satisfy Onsager's relations over a much wider range. In many cases the underlying reason is that the elementary process (e.g., diffusion of a solute molecule through a layer of solvent) is really a sequence of many identical reactions (e.g., collisions with many solvent molecules during diffusion), and the free energy change associated with each of these reactions is much smaller than kT.

The following treatment of time-dependent changes makes one further assumption. The change in the driving forces is presumed to be so slow that the resulting flows are essentially equal to their steady-state

value. In the above context this means that the time scales on which the driving forces change should be large compared to the time required for an elementary process.

b) Time-dependent approach to equilibrium.

A deviation from thermodynamic equilibrium in the form of non-vanishing initial driving forces, X_i, results in flows, J_k, and a corresponding change of the state variables, n_k. This, in turn, leads to a change in the driving forces. By linearizing all these relationships about the point of thermodynamic equilibrium one obtains a system of m coupled, first-order, homogeneous differential equations. I will use vector notation, where $\vec{X}$ is a column vector, $\vec{X}^T = (X_1,\ldots,X_m)$ is its transpose, $\mathbf{L} = [L_{ik}]$ is an (mxm) matrix, and det(**L**) is its determinant. Define

$$M_{ik} = \frac{\partial X_i}{\partial n_k}$$

The matrix $\mathbf{M} = [M_{ik}]$ is symmetric and negative definite, as seen from an expansion of the entropy about thermodynamic equilibrium

$$dS = \sum_i \frac{\partial S}{\partial n_i}\, dn_i + \sum_i \sum_k \frac{1}{2} \frac{\partial^2 S}{\partial n_i \partial n_k}\, dn_i\, dn_k + \ldots$$

$$= \frac{1}{2}\, (d\vec{n})^T\, \mathbf{M}\, (d\vec{n}) + \ldots$$

Then

$$\dot{\vec{X}} = \frac{d\vec{X}}{dt} = \mathbf{M}\, \frac{d\vec{n}}{dt} = \mathbf{M}\, \vec{J} = \mathbf{M}\, \mathbf{L}\, \vec{X}$$

Since **L** is symmetric and positive definite, $\mathbf{L}^{1/2}$ exists with

$$\mathbf{L}^{1/2}\, \mathbf{L}^{1/2} = \mathbf{L}\ ,\ \mathbf{L}^{1/2} = (\mathbf{L}^{1/2})^T\ ,\ \det(\mathbf{L}) \neq 0$$

Therefore one can transform the driving forces according to

$$\vec{Y} = L^{1/2}\,\vec{X}$$

and the new forces obey

$$\dot{\vec{Y}} = L^{1/2}\,M\,L^{1/2}\,\vec{Y} \tag{3.1}$$

The matrix $L^{1/2}ML^{1/2}$ is symmetric, all its eigenvalues $\lambda_1,\ldots,\lambda_m$ are negative, and the corresponding eigenvectors $\vec{e}_1,\ldots,\vec{e}_m$ can be chosen orthonormal. The solution to (3.1) corresponding to initial conditions $\vec{Y}(0)$ is therefore given by

$$\vec{Y}(t) = \sum_i \{\vec{e}_i^{\,T}\,\vec{Y}(0)\}\,\vec{e}_i\,e^{\lambda_i t} \tag{3.2}$$

Since the forces X_i are linear functions of the Y_k, each driving force is a sum of at most m decaying exponentials, as pointed out by Meixner (1949).

By multiplying (3.2) with the initial forces one obtains

$$\vec{X}^T(0)\,\vec{J}(t) = \vec{Y}^T(0)\,\vec{Y}(t) = \sum_i \{\vec{e}_i^{\,T}\,\vec{Y}(0)\}^2\,e^{\lambda_i t} \tag{3.3}$$

Therefore the projection of the flux vector, $\vec{J}(t)$, on the initial force vector, $\vec{X}(0)$, is always positive and decreases monotonically with time. In particular, if the initial conditions consist of only one driving force (e.g the proton electrochemical potential), then the conjugate flow (e.g. proton flux) never changes sign during the relaxation to equilibrium.

c) Application to ionic flows through the membrane of Streptococcus.

To describe this system one can choose as state variables, n_i, the number of particles of species i inside the cell. The corresponding driving forces are

$$X_i = -\frac{1}{T}(\mu_i + ez_i\psi)$$

Here μ_i is the chemical potential of species i inside relative to outside the cell, given by

$$\mu_i = kT \ln\left\{\frac{\gamma_i \frac{n_i}{v}}{N_A[i]_e}\right\}$$

where γ_i is the activity coefficient of species i in the cytoplasm, v is the volume of the cell, N_A is Avogadro's number, and $[i]_e$ is the external activity of species i. ψ is the electrical potential of the cytoplasm relative to the external medium, also called the membrane potential, and ez_i is the charge carried by a particle of species i. The quantity $(\mu_i + ez_i\psi)$ is the electrochemical potential of species i, and, in the case of protons

$$\Delta p = -\left(\frac{\mu_H}{e} + \psi\right)$$

is called the protonmotive force. Note that the differences in the chemical potential and in the electrical potential across the membrane are usually denoted by $\Delta\mu_i$ and $\Delta\psi$ in the literature. Here I have defined both these potentials as vanishing in the external medium, and I will therefore omit the "Δ".

The state variables may not be independent, for example, if two non-permeant species are coupled by a chemical reaction $i \longleftrightarrow k$. In such cases one can reduce the number of variables by the number of constraints imposed on the system. For example, one would introduce a single variable $n_j = n_i - n_k$ driven by $X_j = -1/T(\mu_i - \mu_k)$. The requirement that the variables be independent is equivalent to demanding that the

conductance matrix **L** be regular.

With these definitions one obtains

$$\frac{\partial}{\partial n_k} \mu_i = \delta_{ik} \frac{kT}{n_i}$$

where δ_{ik} is the Kronecker delta.

Furthermore

$$\frac{\partial}{\partial n_k} \psi = \frac{ez_k}{C}$$

where C is the capacitance of the membrane. So

$$M_{ik} = \frac{\partial X_i}{\partial n_k} = -\frac{1}{T}\left(\frac{\partial}{\partial n_k}\mu_i + ez_i \frac{\partial}{\partial n_k}\psi\right)$$

$$M_{ik} = -k\left(\frac{\delta_{ik}}{n_i} + \frac{e^2 z_i z_k}{C\ kT}\right) \qquad (3.4)$$

The ratio of the second to the first term is very large under our conditions: for an ion of valence one at a concentration of 0.1 M in a spherical cell of 1 μm radius with a specific membrane capacitance of 1 $\mu F/cm^2$ one obtains

$$\frac{e^2 z^2 n}{CkT} \simeq 10^4$$

Correspondingly, $\vec{X} = \mathbf{M}\vec{J}$ is large if $\vec{J}$ is proportional to $\vec{z}$ and 10^4 times smaller if $\vec{J}$ is orthogonal to $\vec{z}$. Since the total current into the cell, I, is given by $I = e\,\vec{z}^T\vec{J}$, the latter condition corresponds to flow vectors that carry no net charge into the cell. This has a simple interpretation: the number of charges that need to enter the cell in order to establish a membrane potential of the order of kT/ze is 10^4 times smaller than the number of ions of that species in the cell. Therefore the approach to equilibrium occurs on two very different time

scales. Following a change in the chemical potentials at time zero, a net current into the cell charges up the membrane capacitance. This process is complete after a time t_1. From then on the membrane potential changes only very slowly on a time scale $t_2 = 10^4 t_1$, which is determined by the changes in the ionic concentrations due to the ionic flows. Over this period the total current into the cell is comparatively very small. Since we can only observe changes on the time scale t_2, one can approximate the system as being subject to the constraint that the total current into the cell vanish

$$\vec{z}^T \vec{J} = 0$$

This constraint is sometimes referred to as "charge balance". Since the n_i now are no longer independent variables, the matrices **M** and **L** are singular. One can transform to a set of (m-1) independent variables and apply the previous analysis. One concludes that, if at least one of the m species determining the state of the system is charged, then any flow can reverse at most (m-2) times on time scales much greater than t_1. As all preceding statements, this is only true in the linear regime. In the special case of m=2, however, it generalizes to situations arbitrarily far from equilibrium:

If the state of the cell is determined by the concentrations of two species, at least one of which is charged, then neither flow can reverse on time scales much greater than t_1. Otherwise there would be two distinct points in time before and after the reversal where the cell contains the same number of particles of species 1 and therefore, due to charge balance, also the same number of particles of species 2. The fact that the flow is positive at one and negative at the other point in time contradicts the assumption that the state of the system is

determined by the cell content of species 1 and 2.

§3.3 MATERIALS AND METHODS

a) Buffers.

2[N-morpholino]ethanesulfonic Acid (MES, pK=6.1) and tris[hydroxymethyl]methylaminopropane sulfonic acid (TAPS, pK=8.4) were used as buffering species at three different strengths:

B = 10 mM MES, 10 mM TAPS

C = 1 mM MES, 1 mM TAPS

D = 0.1 mM MES, 0.1 mM TAPS.

In addition, all buffers contained salt at 0.2 M ionic strength, unless indicated otherwise, and 0.1 mM Tetren, which chelates many heavy metals, but not Mg^{2+} or Ca^{2+}. Throughout the following sections the ionic composition and pH of a buffer will be identified in the form [salt pH], for example [$MgCl_2$ 7.5] means 0.067 M $MgCl_2$ (0.2 M ionic strength) at pH 7.5. In buffers prepared with D_2O the pD was determined by adding 0.4 to the reading obtained with a glass combination pH electrode (Gandour & Schowen 1978). All buffers were titrated to the right pH using dilute KOH. The strength of buffer D was sometimes increased to 0.2 mM MES, 0.2 mM TAPS, when I worked with very dense final cell suspensions.

b) Preparation of cells.

Cells of Streptococcus strain SM197, a smooth swimming mutant (Berg at al. 1982), were grown as described in §1.2.b. Cells were harvested and washed twice with buffer B [KCl 7.5 or 8.5] by centrifugation at 4000 g for 2 minutes. To avoid breakage of flagellar filaments and consequent deterioration of swimming motility, some care was taken in

resuspending pelleted cells. However, the flagella appear to be more robust than those of E. coli, and I found gentle pipetting through a Pasteur pipette to be acceptable. Subsequently, the cells were exposed to valinomycin at 5 μg/ml final concentration, added to buffer B from a 1 mg/ml solution in methanol. After 2 minutes, cells intended for flux measurements were washed twice in buffer C [KCl 7.5 or 8.5]. The final suspension had a cell density of $2x10^{10}$ to $4x10^{10}$ cells/ml.

For measurements of intracellular buffering capacity cells were washed twice in 0.2 M KCl and suspended at a final density of 10^{10} cells/ml.

Cells used in tethering experiments were sheared (Manson et al. 1980), washed once in buffer B [KCl 7.5 or 8.5] and suspended at a final concentration of ca $2x10^{7}$ cells/ml.

c) Flux measurements.

2 ml of buffer C were stirred vigorously in a glass vial which was mounted in a thermostatted aluminum block. Unless indicated otherwise in the text, the temperature of the block was controlled at 23.9°C. A combination pH electrode (Radiometer GK2321C) was inserted in the solution. A 5 mm thick layer of paraffin oil floating on top of the buffer effectively inhibited exchange of CO_2 with the air which caused significant pH drifts. In some experiments 50 μg/ml carbonic anhydrase was added to buffer C. This enzyme accelerated the reaction $H_2O+CO_2 \longleftrightarrow H_2CO_3$ and thus suppressed pH overshoots, particularly following addition of very basic solutions that had accumulated large amounts of CO_3^{2-} through uptake of CO_2 from the air.

The electrode potential was measured with a pH meter (Radiometer

PHM26) whose output signal (10mV/pH) was displayed on a chart recorder (Houston Instruments D-5000). This signal was also amplified and recorded by an Apple II microcomputer via a 12 bit A/D converter (Metrabyte APM-08).

The flux measurement was initiated at t = 0 s by addition of 20 to 50 μl of the concentrated cell stock to the stirred buffer. The change in the pH gradient across the membrane is determined by the pH difference between buffer C and buffer D, while the change in the membrane potential results primarily from the dilution of potassium ions in going from buffer C to the final suspension. Mixing was complete to 90% at t = 4 s, as judged from the pH change following addition of acid or base to buffer alone. Following addition of cells to buffer D, I observed a rapid pH shift of up to 0.1 units during mixing. This initial shift is related to movement of protons within the external medium, due to a difference in the pH of buffers C and D or a difference in their ionic compositions, which can alter the dissociation constants of proton binding sites on the outer cell surface. To offset this shift, small amounts of dilute HCl or KOH were drawn into the tip of a Gilson Pipetman along with cells from the concentrated stock, but separated from them by an air bubble. Then both were dispensed simultaneously into the final buffer.

After the mixing time, changes in the external pH are related to movement of protons across the membrane. In a typical experiment at large protonmotive force (1:40 dilution from buffer C [KCl 8.5] into D [$MgCl_2$ 6.5]) and a cell density of 10^9/ml, proton uptake by the cells led to a rise in the external pH of ca. 0.7 units which was complete after about 3 minutes. At the end of the experiment, the suspension was

titrated back to the initial pH by adding 20 μl aliquots of 0.001 N HCl. The initial rapid pH drop following addition of acid reflects the buffering capacity of the external medium which was later used to compute the observed proton flux. Under these conditions the cells contributed ca. 20% to 30% of the external buffering capacity. Fig. 3.1 shows a plot of the pH of the cell suspension as a function of time after energization. In this particular experiment 50 μl cells in buffer C [KCl 8.62] were diluted into 2 ml buffer D [$MgCl_2$ 6.5]. This figure also illustrates the motivation for using MES and TAPS as buffering species. Most flux experiments, particularly those designed to measure motor-related fluxes, required a shift from pH 8.5 to pH 6.5. Thus the concentrated cell stock is kept at a pH close to the pK_D of TAPS, where the small remanent proton efflux described below causes only small drifts in the pH. The pH of the final medium is close to the pK_D of MES, which minimizes the shift in pH due to the addition of cells on dilution. As protons are taken up by the cells, the pH of the medium rises. Consequently its buffering capacity decreases, as can be seen from the titration in Fig. 3.1. This improves the resolution of small proton fluxes at late times after energization.

Finally, the optical density of the suspension was measured at a wavelength of 600 nm (see §1.2.b). The ratio of cell number density to optical density was determined for each culture using a Petroff-Hausser bacteria counter. It varied considerably among cultures (mean 3.68×10^8, standard deviation 0.67×10^8 cells/ml/OD_{600}), probably due to differences in cell size and shape.

The pH of the concentrated cell stock dropped slowly with time at a rate of 0.01 units/min, corresponding to proton efflux of ca.

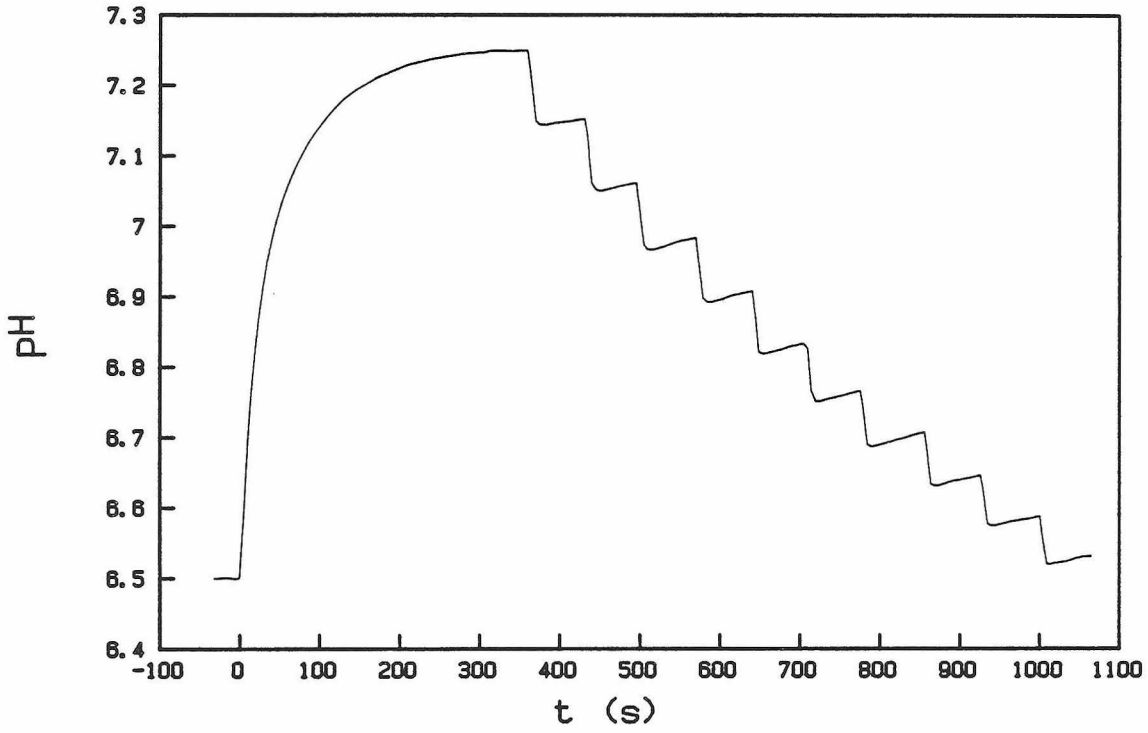

Fig. 3.1. Raw data obtained during a flux measurement: the pH of the cell suspension as a function of the time after dilution. The gradual rise is due to proton uptake by the cells, the stepwise decrease results from titration of the suspension with HCl.

$6x10^3$ H^+/cell/s. This may reflect extrusion of protons or lactate due to a small remanent metabolic rate. To keep the pH of this suspension stable, dilute KOH was added by gravity feed through a long thin piece of polyvinyl tubing at a rate of ca 0.2 μl/min. Later I found that keeping the cell stock on ice instead of at room temperature significantly reduces the pH drift. Under these conditions the membrane proton conductance and the cells' swimming motility also show less variation from sample to sample.

An alternative method of energizing cells is to suspend cells that have not been exposed to valinomycin in a weak buffer (Maloney 1977; Manson et al. 1980). A pH gradient can then be imposed by addition of acid or base to this suspension. If the potassium concentration is lower in buffer D than in buffer C, then addition of valinomycin leads to establishment of a negative membrane potential. One advantage of this method is that the cell density during the flux measurement is not limited by the dilution ratio required for the desired potassium diffusion potential. I chose not to use this technique because the flux measurement is perturbed for up to 20 or 30 seconds following shifts in external pH by a unit or more, due to the finite response time of the pH electrode. In addition, cells suspended in buffer D at low potassium concentration show a slow uptake of protons even before exposure to valinomycin due to the finite conductivity of the membrane to potassium ions. This introduces additional uncertainty about the value of the protonmotive force.

For analysis of these measurements the titration of the sample was used to compute the external buffering capacity

$$B_e = \frac{H/N_C}{pH_0 - pH_1}$$

where H is the number of protons added, N_C is the number of cells in the suspension, pH_0 is the external pH before addition, and pH_1 is the pH measured just after mixing (see also §3.3.d below). B_e as a function of $(pH_0+pH_1)/2$ was interpolated with a quadratic polynomial. The membrane proton flux per cell, $J_H(t)$, following energization was computed as

$$J_H(t) = B_e(pH) \frac{dpH}{dt}$$

After the first 8 to 10 seconds, during which mixing effects and the slow electrode response affect the measurement, one finds that this flux decays approximately exponentially, as illustrated by the semilogarithmic plot in Fig. 3.2B. A linear least-squares fit to the logarithm of $J_H(t)$ was computed, weighted such as to approximate an exponential fit to $J_H(t)$. The initial flux, $J_H(0)$ was estimated by extrapolation to t = 0 s from the interval between 15 s and 25 s. The time during which the flux decays to 1/10 of its initial value was obtained from the slope of this fit. The uncertainty in the value of $J_H(0)$ as well as the decay time $t_{1/10}$ was estimated from the variance of the data points about the exponential fit. Under optimal conditions the values of $J_H(0)$ and $t_{1/10}$ were reproducible in samples from the same concentrated suspension to within 2%. This is comparable to the uncertainty in the estimates of these quantities in each individual sample.

d) Cytoplasmic buffering capacity.

Measurements of cytoplasmic buffering capacity were performed using

a variation of the method of small acid pulses described previously (Mitchell & Moyle 1967; Scholes & Mitchell 1970; Maloney 1979). A small amount of acid is added to a bacterial suspension containing no proton buffering species other than the cells. This causes a rapid drop in the pH of the extracellular medium by about 0.1 units from its initial value pH_0 to pH_1, which is complete after the time required for mixing. This initial pH change corresponds to rapid titration of the proton accepting groups on the cell's external surface, e.g., the porous cell wall. Subsequently, the pH rises slowly with an approximately exponential time course and finally settles at a value pH_2. This phase corresponds to slow movement of protons across the membrane and titration of the cytoplasm. The process reaches equilibrium when the internal and external proton activities are equal. The magnitude of the initial fast pH change, (pH_0-pH_1), is used to calculate the external buffering capacity, B_e. The total pH change from before dilution to the equilibrium value, (pH_0-pH_2), indicates the combined buffering capacity of cytoplasm and external medium, B_t, and the time course of the slow rise in pH allows calculation of the membrane's conductivity to protons, c_m.

I used the same apparatus as described in §3.3.c. The cell suspension was brought to pH 9.1 by addition of KOH. After the pH had stabilized, it was titrated back to 6.6 by addition of 10 μl aliquots of HCl at intervals of several minutes, allowing the pH to stabilize before each addition. Finally, the suspension was brought back to high pH and a few measurements were repeated to control for changes that might have occurred over the course of the experiment.

Analysis of these experiments proceeded in a fashion similar to

that presented by Maloney (1979). After approximately 100 s the extracellular pH had settled to a constant value, sometimes it showed a small but constant drift. A linear least squares fit was performed to the pH time course over the interval from t = 100 s to t = 150 s. The extrapolation of this fit to t = 0 s was taken as the value of pH_2. The difference between the pH time course and this linear fit was interpolated by an exponential over the interval from t = 10 s to t = 25 s. The value of this function at t = 0 s was taken to be (pH_1-pH_2). Finally, using the decay time of this exponential, $t_{1/10}$, the number of protons added, H, and the number of cells contained in the suspension, N_C, one computes the buffering capacities and the membrane conductivity as

$$B_e = \frac{H/N_C}{pH_0-pH_1} \quad ,$$

$$B_t = \frac{H/N_C}{pH_0-pH_2} \quad ,$$

$$c_m = B_e \frac{\ln 10}{t_{1/10}} \frac{pH_2-pH_1}{pH_0-pH_1} \quad .$$

e) Tethered cell rotation.

Cells were tethered to a coverslip which was subsequently mounted in a flow cell as described in §1.2.c. Rotation of cells was observed with phase contrast optics (Nikon S-Ke microscope equipped with a thermostatted stage, Nikon Plan 40 BM objective, and Zeiss optovar) and recorded on video tape (Ikegami ITC-47 camera, Panasonic NV-8950 recorder). Tethering buffer B was first replaced by buffer C. A few minutes later, cells were energized by a shift to buffer D. In

experiments designed to compare the time course of proton flux and motor rotation, the gradual rise in the external pH during flux measurements had to be taken into account. Therefore, cells were energized in suspension, as described for the flux measurements, and the suspension was drawn into the flow cell immediately following mixing. Thus, the cells tethered to the coverslips experienced the same changes in pH and ionic concentrations as those in suspension. In some experiments I did not expose cells to valinomycin until just prior to energization in the flow cell. No significant differences resulted from using this procedure.

I measured the rotation rates of tethered cells during playback of the video tape using a system linked to an Apple II computer that times intervals between transitions of the video image over a cursor (Khan et al. 1985). When the flow cell was filled with a cell suspension, the poor image contrast precluded use of this technique and rotation periods were counted by eye.

§3.4 EXPERIMENTAL RESULTS

a) General time course of proton movements following energization.

After several hours of starvation the cell is probably close to thermodynamic equilibrium, such that the driving forces for all membrane fluxes or relevant intracellular reactions are very small. This does not require that the electrical membrane potential and the chemical potentials vanish individually. In fact there is evidence that starved cells show a small negative membrane potential, as discussed in more detail in part (f) of this section.

When cells that have been exposed to valinomycin are diluted from the starvation buffer containing 0.2 M KCl into a medium with low potassium concentration, K^+ ions rapidly leave the cell, establishing a negative membrane potential that drives protons into the cell. As a result the cytoplasm gradually acidifies and a chemical potential builds up that opposes the electrical component of the proton driving force. At the same time the chemical potential of K^+ drops as potassium ions leave the cell. If the valinomycin conductance greatly exceeds the other ionic conductances, the electrical membrane potential is equal and opposite to the K^+ chemical potential and consequently rises in this process. Both these effects lead to a gradual decay of the proton driving force and as a result the rate of proton uptake decreases. Fig. 3.2A shows the number of protons that have entered the cell, n_H, as a function of time after a 1:40 dilution of cells from [KCl 7.5] into [$MgCl_2$ 7.5]. The rate of proton uptake decreases gradually, then it changes sign and a comparatively small but steady efflux of protons is seen at times greater than 5 min after energization. Fig. 3.2B shows

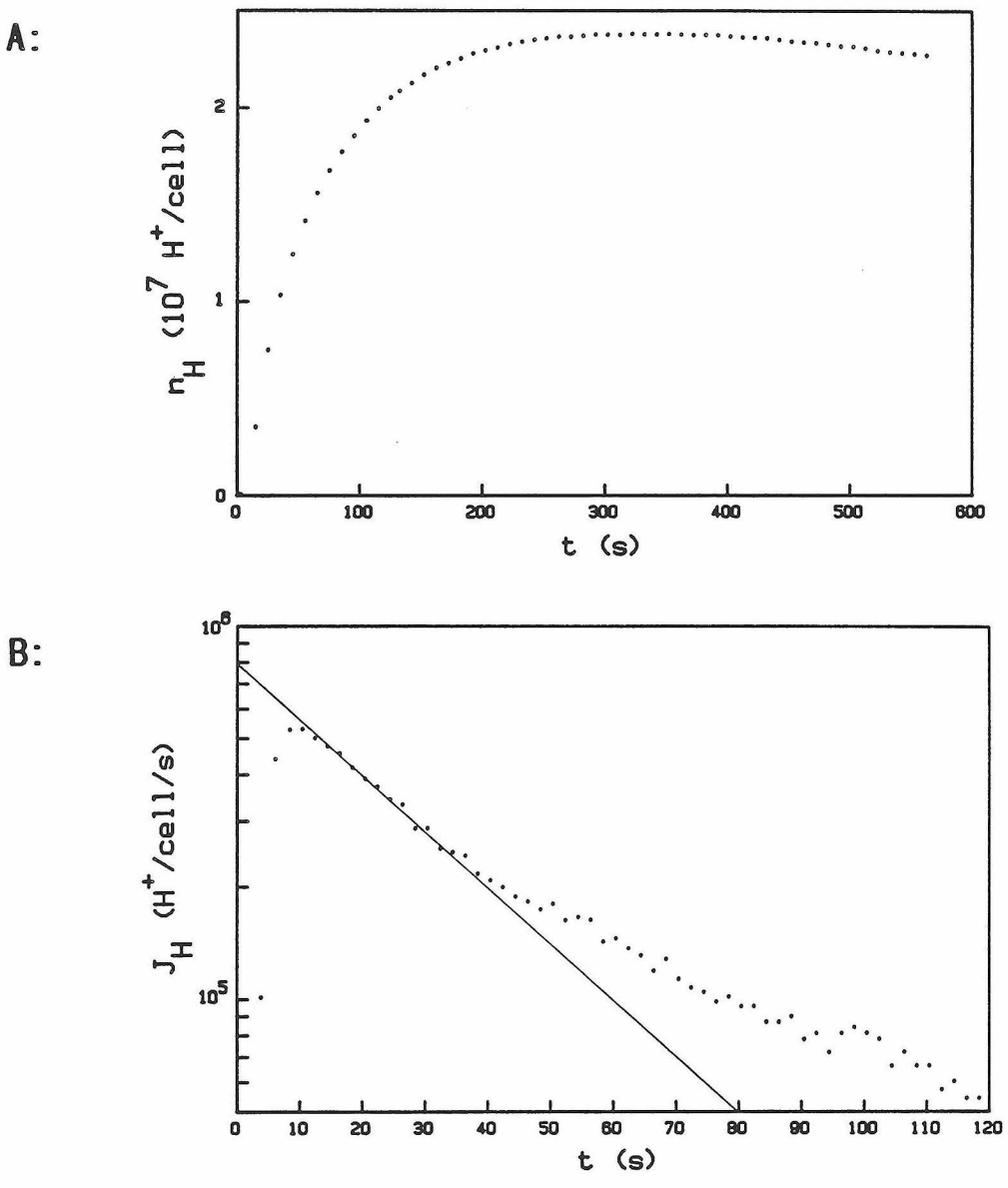

Fig. 3.2. Proton uptake after energization with a potassium diffusion potential.

A: The number of protons that have entered the cell as a function of time after dilution.

B: The proton flux as a function of time after dilution. Note the logarithmic flux scale. The line is a least squares fit to the interval from 15 s to 25 s after dilution.

the rate of proton uptake, $J_H = dn_H/dt$, over the first two minutes. Note that J_H is plotted on a logarithmic scale. Due to mixing effects J_H can not be determined accurately during the first 8 to 10 seconds. Over the following 30 seconds it decays approximately exponentially with time, and a linear least-squares fit to the logarithm of J_H over the interval from 15 to 25 seconds is shown in the figure. This fit provides an estimate of the initial flux, $J_H(0)$, as well as the time over which the flux decays to 1/10 of its initial value, $t_{1/10}$. In this particular experiment $J_H(0) = (8.0 \pm 0.3)\times10^6$ H^+/s and $t_{1/10} = (67 \pm 4)$ s.

When cells are diluted into a medium of lower pH without changing the external potassium concentration, the initial proton driving force is provided by the negative chemical potential. As the cytoplasm acidifies the proton chemical potential increases. Furthermore, the concomitant efflux of K^+ gradually lowers the intracellular potassium concentration and thus leads to a positive membrane potential. Again, the proton driving force and therefore also the proton influx decrease with time. The proton uptake following dilution of cells from [KCl 7.5] into [KCl 6.5] is shown in Fig. 3.3A. Note that the proton flux never reverses. Fig. 3.3B is a semilogarithmic plot of $J_H(t)$, again showing the linear fit over the interval from 15 to 25 s. Here $J_H(0) = (8.3 \pm 0.4)\times10^5$ H^+/s and $t_{1/10} = (29 \pm 1)$ s.

b) The early proton flux : effects of ionophores and dependence on the initial driving force.

To justify the interpretations of the early proton influx given in part (a) one must show that the conductance of valinomycin is in fact

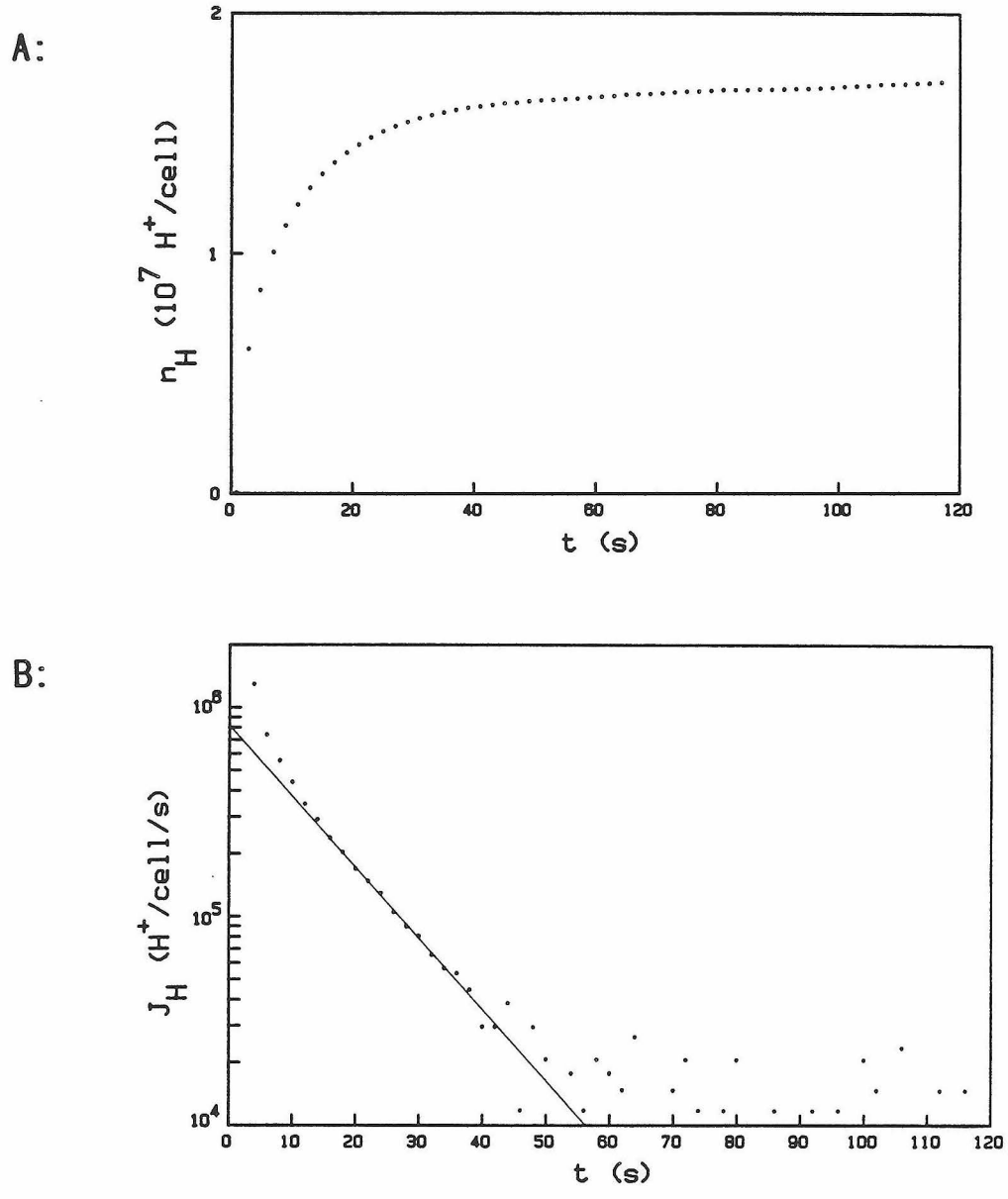

Fig. 3.3. Proton uptake after energization with a pH-gradient. **A:** The number of protons that have entered the cell as a function of time after dilution.

B: The proton flux as a function of time after dilution. Note the logarithmic flux scale. The line is a least squares fit to the interval from 15 s to 25 s after dilution.

large enough to effectively clamp the membrane potential to the equilibrium potential of potassium. When cells were diluted 1:40 from [KCl 7.5] into [$MgCl_2$ 7.5] before exposure to valinomycin I measured a small proton influx of ca $6x10^4$ H^+/cell/s. When valinomycin was added to this suspension at 10 μg/ml, the proton flux increased by a factor of 30 within a few seconds. In another experiment I saw a somewhat larger flux in the absence of valinomycin, and addition of the ionophore increased the flux by a factor of 12. This shows that valinomycin is required to establish a sizeable electrical potential following a shift in the potassium chemical potential.

The initial rate of proton uptake after cells were diluted from [KCl 9.5] into [KCl 6.0] was only about twice as large in cells that had been pretreated with valinomycin as the value measured in the absence of the ionophore. This means that even before exposure of the membrane to valinomycin there is a significant conductance to potassium or other ions that keeps the membrane potential low and thus allows uptake of protons driven by a pH-gradient.

If cells are treated both with valinomycin and the proton conductor FCCP (10 μg/ml) and then diluted from [KCl 7.5] to [$MgCl_2$ 7.5] containing FCCP, one measures an initial proton flux that is ca 40 times larger than the value obtained in absence of FCCP. This suggests that the conductance of valinomycin to K^+ is so large that it does not limit the flux of H^+ in absence of FCCP, and the membrane potential, ψ, in fact lies very close to $-\mu_K$.

Another indication that the valinomycin conductance is not limiting the size of the membrane potential comes from the measurements of ψ reported by Conley and Berg (1984). They deduced the membrane potential

from the uptake of rubidium after cells of Streptococcus V4051 were diluted 1:20 into potassium-free buffer containing trace amounts of ^{86}Rb. Rubidium is transported across the membrane primarily by valinomycin, which has similar affinities to Rb^+ and K^+. Therefore the characteristic time required for equilibration of the two ions is the same. But the two ions flow in opposite directions: K^+ leaves the cell, while Rb^+ enters the cell. If the conductance to valinomycin were limiting the equilibration of the two ions over the time required to assay the cells' content of ^{86}Rb, typically 20 s, one would expect the ratio of internal to external rubidium to be smaller than the corresponding ratio for potassium. Instead, one finds that the distribution ratios of both ions agree to within the resolution of the technique.

Fig. 3.4 shows the results of an experiment in which cells were diluted from [KCl 7.5] into [$MgCl_2$ 7.5] by varying ratios. A plot of the initial proton flux, $J_H(0)$, as a function of the change in the K^+ chemical potential, $\Delta\mu_K$, shows that they are approximately proportional with

$$J_H(0) = \frac{\Delta\mu_K}{kT} \times (2.0 \pm 0.2)\times 10^5 \ H^+/\text{cell/s}.$$

The early proton flux induced by a change in μ_H is also approximately proportional to $\Delta\mu_H$, but the ratio is larger:

$$J_H(0) = \frac{\Delta\mu_H}{kT} \times (-4.6 \pm 0.4)\times 10^5 \ H^+/\text{cell/s}.$$

c) The late proton flux : effects of various cations.

The most intriguing property of the proton flux at late times is

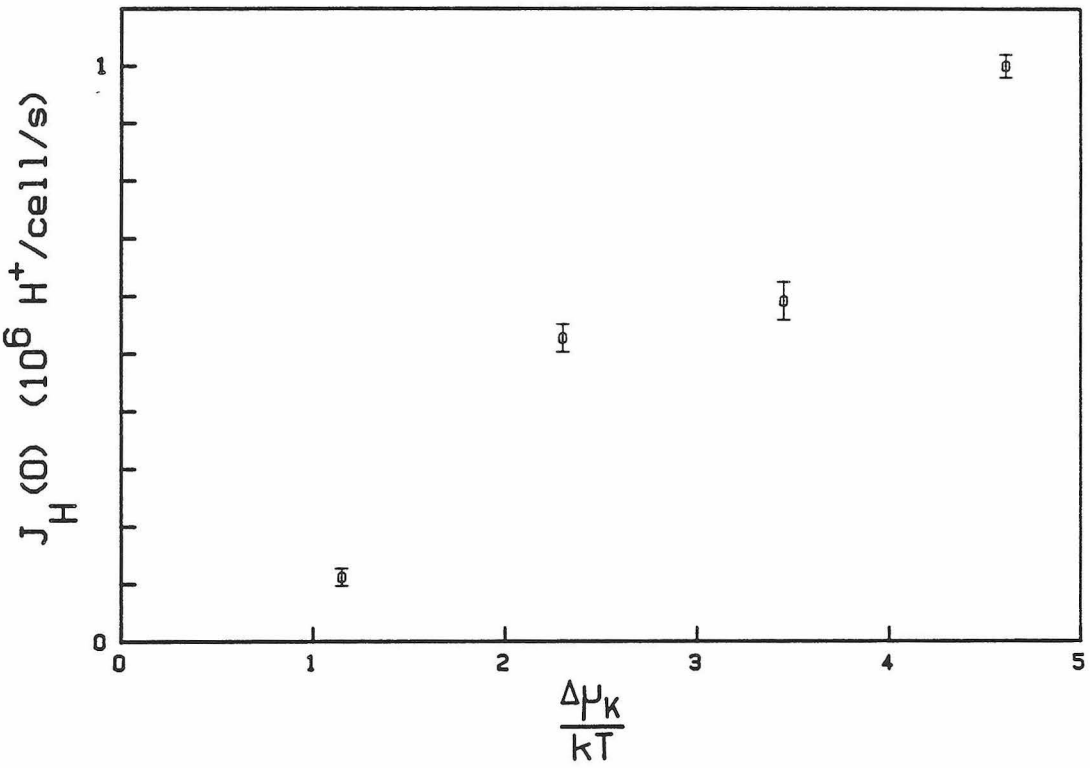

Fig. 3.4. The initial proton flux as a function of the nominal potassium diffusion potential.

that it can change sign. Due to the requirement of vanishing total current this cannot be explained by consideration of H^+ and K^+ alone, as indicated in §3.2.c. One needs to invoke at least one other species. Note, however, that this species need not be charged or even permeate the membrane. For example, protons driven by the membrane potential could pass through a membrane-bound ATPase during the early phase of the flux, converting intracellular ADP to ATP. At late times, when the proton driving force has decayed, the ATPase may be working in the opposite direction, using the chemical potential of ATP to pump protons out of the cell (Maloney 1977).

In principle, the late proton efflux could also be driven by the change in concentration of whatever cation is used to substitute for potassium in the final buffer. To test for this possibility I compared the effects of various cations in the final buffer. Figs. 3.5A, B, and C show the proton uptake as a function of time after dilution of cells from KCl into NaCl, $MgCl_2$, and choline Cl respectively, all at pH 7.5. In the experiment shown in Fig. 3.5D the cells were diluted from KCl into a buffer containing no salts. This changes the ionic strength considerably but also avoids introduction of another species. The rate of efflux at late times decreases in the order Na^+, Mg^{++}, choline$^+$, no cation. Only a very small efflux of at most -3.4×10^3 H^+/cell/s is seen in choline Cl. When the final buffer contains no salt, the proton flux never changes sign. This is in agreement with the prediction made in §3.2.c, which relies on the assumption that K^+ and H^+ are the only species involved in the process. Apparently neither Cl^-, which experiences a large driving force in this experiment, nor some intracellular species, such as ATP, are involved in producing the late

Fig. 3.5. The proton uptake as a function of time after energization with a potassium diffusion potential. Potassium chloride was substituted in the energization buffer by **A:** sodium chloride; **B:** magnesium chloride; **C:** choline chloride; **D:** no salt.

A:

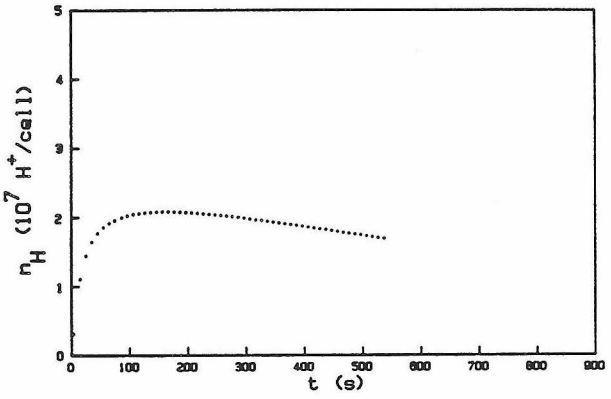

B:

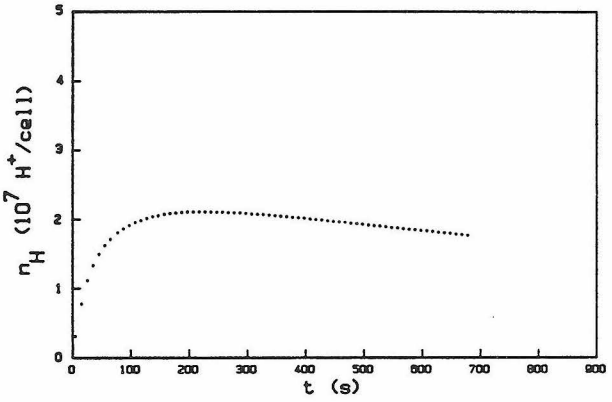

C:

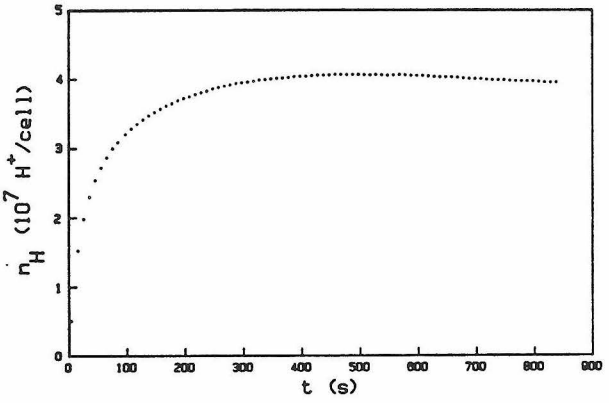

D:

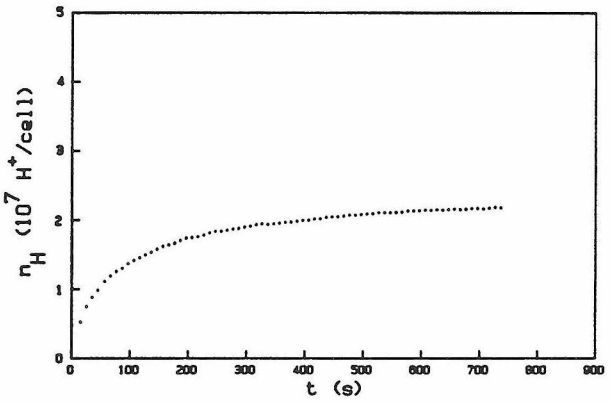

efflux.

Although these experiments indicate that the change in chemical potential of external cations other than K^+ does affect proton movements, they do not point towards a specific mechanism. One can imagine two alternatives:

The late proton flux could be driven by the electrical membrane potential, which is kept above the proton and potassium equilibrium potentials due to a nonzero membrane conductance to the external cation. In the linear domain this would result from a non-vanishing diagonal component for this cation in the conductance tensor **L**.

Alternatively the proton efflux may be due to an exchange mechanism that, for example, couples the inward movement of one Na^+ ion to the extrusion of one H^+. This mechanism would be driven by $(\mu_{Na}-\mu_H)$ and corresponds to an off-diagonal term in the conductance tensor **L** coupling Na^+ and H^+.

To distinguish among these two possibilities I repeated the experiment in presence of FCCP. This ionophore conducts H^+ in response to both a membrane potential and a proton chemical potential but should not affect the performance of any antiport mechanism. It dramatically increases the diagonal component L_{HH} of the conductance tensor but leaves the off-diagonal components unchanged. Figs. 3.6A to D show the results of these experiments. The rate of efflux increases dramatically in presence of FCCP. Only in the case where no external cation is added the proton flux still does not change sign.

These experiments indicate that the membrane does have a finite conductance to the cations Na^+, Mg^{++}, and $choline^+$, and that the magnitudes of the conductance decrease in that order.

Fig. 3.6. The proton uptake as a function of time after energization with a potassium diffusion potential in presence of FCCP. Potassium chloride was substituted in the energization buffer by **A:** sodium chloride; **B:** magnesium chloride; **C:** choline chloride; **D:** no salt.

A:

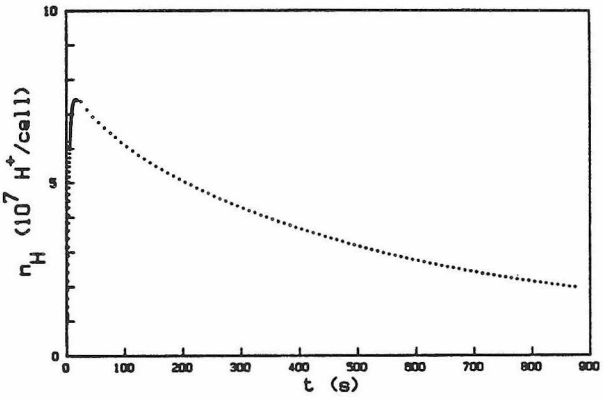
10
5
0
n_H (10^7 H^+/cell)
0
100
200
300
400
500
600
700
800
900
t (s)

B:

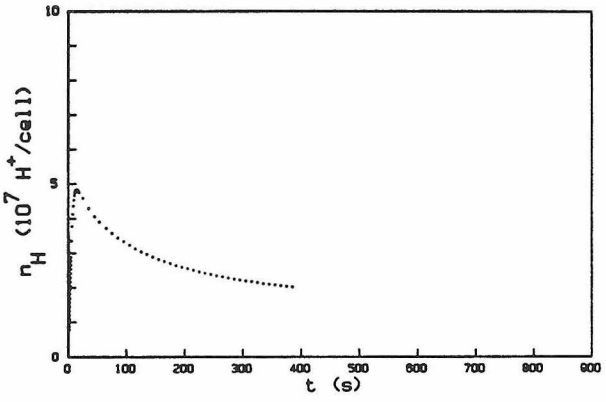
10
5
0
n_H (10^7 H^+/cell)
0
100
200
300
400
500
600
700
800
900
t (s)

C:

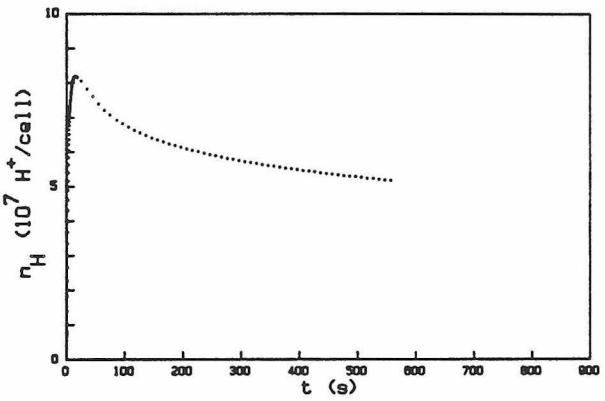
10
5
0
n_H (10^7 H^+/cell)
0
100
200
300
400
500
600
700
800
900
t (s)

D:

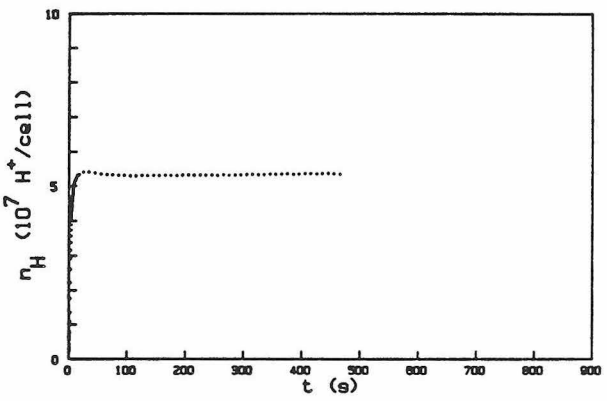
10
5
0
n_H (10^7 H^+/cell)
0
100
200
300
400
500
600
700
800
900
t (s)

d) Na^+/H^+ antiport.

The experiments described in (c) do not rule out the possibility that part of the efflux is due to a direct exchange mechanism. To test for such effects I measured the proton flux under conditions where the initial driving force affected only cations other than H^+ or K^+. Since choline$^+$ seems to participate least in the process of H^+ extrusion at late times, it was chosen as a reference. Fig. 3.7A shows the proton uptake after cells starved in [0.2 M KCl + 0.2 M choline Cl] are diluted into [0.2 M KCl + 0.2 M NaCl] at pH 7.5. Following dilution protons leave the cell at an initial rate of approximately 10^6 H^+/cell/s and the proton movement is 90% complete after ca 70 s. If cells are diluted from [0.2 M KCl + 0.2 M NaCl] into [0.2 M KCl + 0.2M choline Cl] one finds that protons enter the cells with a similar time course, as seen in Fig. 3.7B. When 0.2 M NaCl is added to the suspension after the flux has decayed, protons are extruded again. In principle these fluxes could be driven either by a membrane potential or directly by the Na^+ chemical potential via an antiport mechanism. To determine the origin of these proton movements I observed the behavior of tethered cells. The motor of Streptococcus mutant SM197 spins exclusively counterclockwise when protons flow through it into the cytoplasm and clockwise when they move in the opposite direction. One finds that cells starved in [0.2 M KCl + 0.2 M choline Cl] spin counterclockwise when the external choline Cl is replaced by NaCl. They spin slower when the external Na^+ concentration is decreased. Addition of valinomycin leads to a small increase in rotation speed. If the resulting H^+ efflux (Fig. 3.7A) were due to a positive membrane potential, protons would be expected to pass through the motor in the same direction, leading to clockwise rotation.

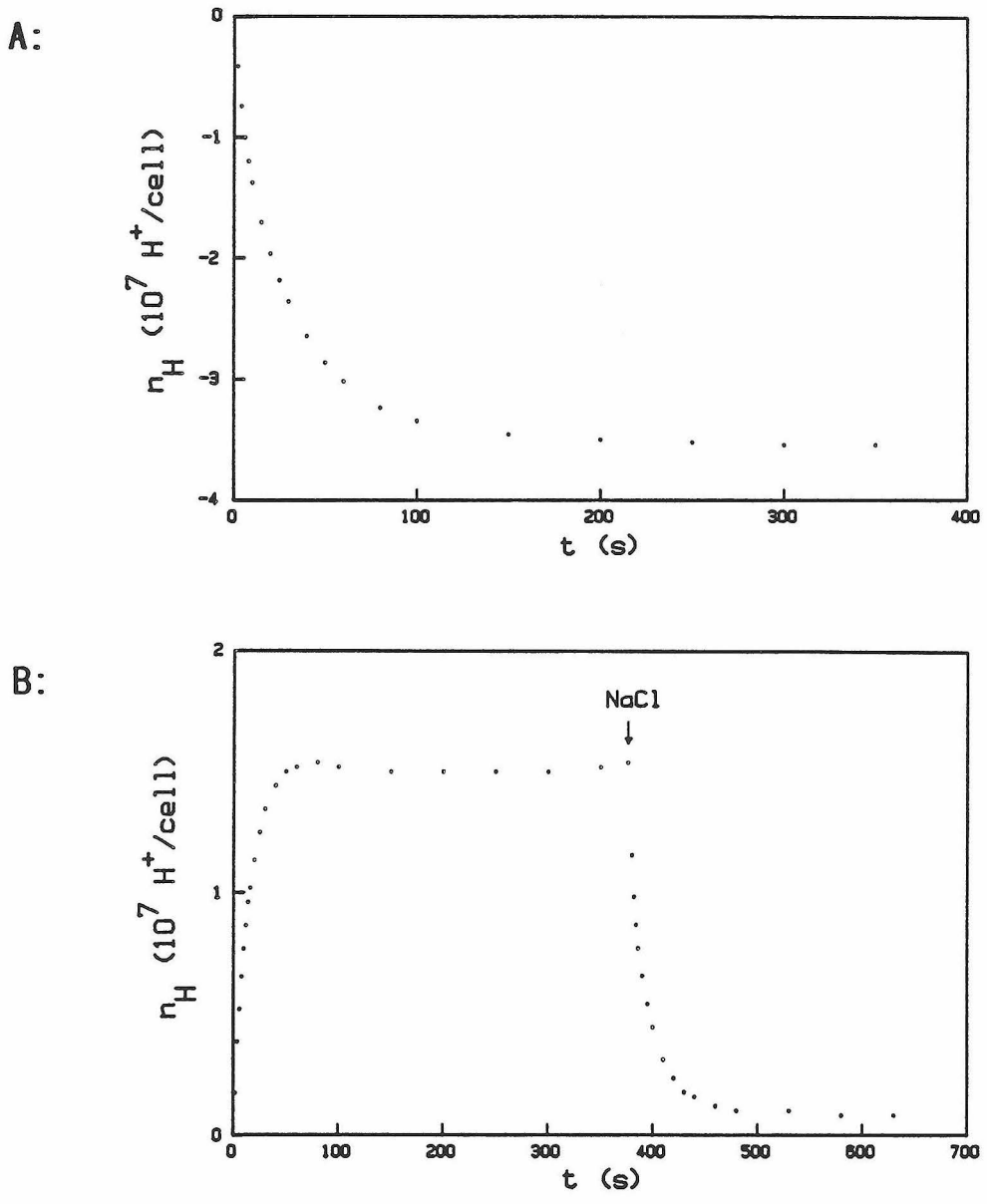

Fig. 3.7. Proton movements resulting from changes in the external sodium concentration.

A: Proton uptake as a function of time after external choline is replaced by sodium. Note that protons leave the cell.

B: Proton uptake as a function of time after external sodium is replaced by choline. The arrow indicates addition of sodium to the level present prior to dilution.

Addition of valinomycin should lower the membrane potential and slow rotation of the motor. Furthermore, one finds that the cells don't start spinning immediately as would be expected if they ran on a membrane potential which is established within milliseconds. Rather the rate of rotation follows approximately the time course of total proton movement, increasing gradually over 1 to 2 min. This strongly indicates that the motor is driven by a proton chemical potential generated by proton extrusion via a Na^+/H^+ antiport mechanism. Rotation stops within seconds after addition of nigericin (an electroneutral K^+/H^+ exchanger) or 2,4-dinitrophenol (a proton conductor), eliminating the possibility that the motor is driven directly by sodium ions. If the external Na^+ concentration is decreased, as in the experiments of Fig. 3.7B, the motors rotate clockwise, and the rate of rotation again follows the time course of proton uptake.

These experiments were repeated with LiCl instead of NaCl, which led to very similar observations. I conclude that the membrane contains enzymes that mediate the exchange of Na^+ or Li^+ for H^+ (see also §4.3.c).

e) Intracellular and extracellular buffering capacity, and the membrane conductance to small pH shifts.

Knowledge of the buffering capacity of the cytoplasm is necessary in order to compute the time course of the proton electrochemical potential presented in part (f). These measurements were performed by slow titration of a cell suspension in 0.2 M KCl with aliquots of dilute HCl leading to pH-shifts of 0.1 to 0.2 units as described in §3.3.d. Fig. 3.8A shows a plot of the total buffering capacity, B_t, and the

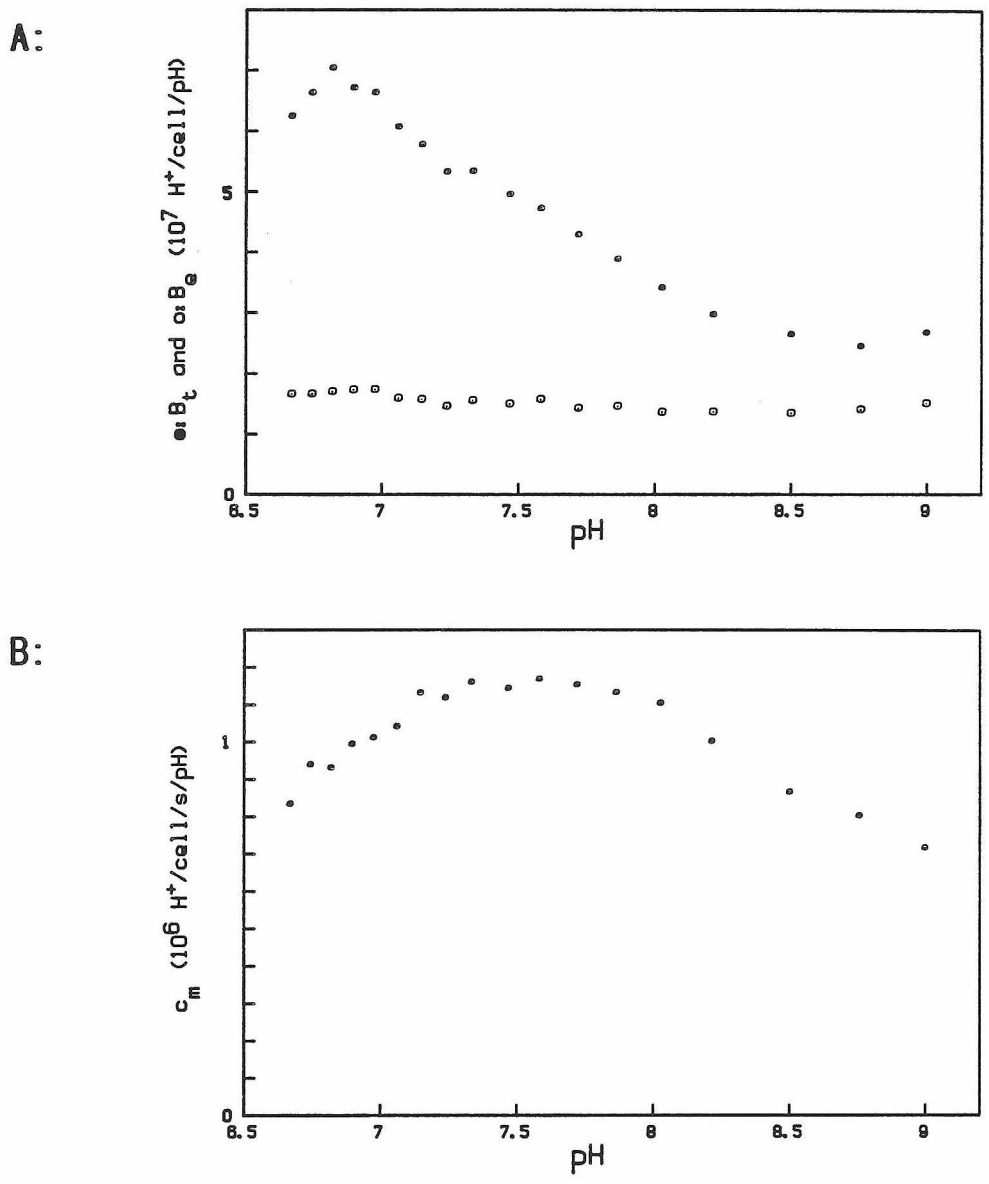

Fig. 3.8. Titration of cells suspended in 0.2 M KCl with small acid pulses.

A: The external buffering capacity (open symbols) and the total buffering capacity, including contributions from the cytoplasm, (closed symbols) as a function of the external pH.

B: The membrane conductance as a function of the external pH.

external buffering capacity, B_e, as a function of pH. The internal buffering capacity, B_i, is given by the difference, $B_i = B_t - B_e$. B_i is seen to depend approximately linearly on the external pH over the range from 6.8 to 8.2:

$$B_i = [3.4 - 2.8 \times (pH_e - 7.5)] \times 10^7 \ H^+/cell/pH.$$

At pH 7.5 this corresponds to a cytoplasmic buffering power of 0.067 M, in agreement with values ranging from 0.062 M to 0.100 M measured by F. M. Harold and M. D. Manson (unpublished).

The time it takes for the external pH to settle after addition of acid allows an estimate of the membrane proton conductance, c_m. A plot of c_m as a function of external pH is shown in Fig. 3.8B. The conductance is maximal near pH 7.5 with a value of ca 1.2×10^6 H^+/cell/s/pH and drops slightly at higher and lower values of pH_e. I also measured c_m in presence of magnesium with cells suspended in 0.2 M KCl + 0.067 M $MgCl_2$. Under these conditions the conductance was only 7×10^5 H^+/cell/s/pH at pH 7.5 and increased slightly to 9×10^5 H^+/cell/s/pH at pH 6.5.

f) Time course of tethered cell rotation rate, proton flux, and proton electrochemical potential.

The rotation rate of tethered cells is known to be proportional to the protonmotive force for values up to at least -80 mV (Manson et al. 1980, Khan et al. 1985). In the regime where flows and forces are related linearly the proton flux is proportional to the proton driving force, if the off-diagonal coefficients in the conductance matrix are negligible. Under these assumptions one would expect proton flux and motor rotation to follow a similar time course after energization. The

experiments described in this section indicate that the proton flux decays much faster than the motor rotation speed and, in fact, can change sign while the motor keeps spinning in the same direction. Fig. 3.9A shows the rotation rate of tethered cells as a function of time after cells are diluted 1:40 from [KCl 8.5] to [$MgCl_2$ 6.5]. In order to correctly reproduce time-dependent changes in the pH of the weakly buffered external medium the cells tethered to a coverslip were energized with a cell suspension identical to the one used for flux measurements, as described in §3.3.e. In analyzing this experiment I followed all cells that were rotating at 30 s after energization for a period of 5 min. At intervals of 30 s I measured each cell's rotation rate and divided it by the speed at 30 s. Finally I averaged these ratios over the set of cells.

The rate of proton uptake under the same conditions is plotted against time in Fig. 3.9B. The flux is 2.0×10^6 H^+/cell/s immediately following dilution and drops to 1/10 of that value in 46 s.

Fig. 3.9C is a graph of the estimated electrochemical potential of protons, $-e\Delta p = \mu_H + e\psi$, as a function of time. Before dilution it is assumed that $\Delta p = 0$, since the system has equilibrated at constant pH and ionic composition for several hours. However, the electrical and chemical components don't necessarily vanish individually. When the internal pH, pH_i, of cells starved in 0.2M KCl at pH 7.5 was measured by ^{31}P-NMR it was found to be 0.2 units below the external pH, pH_e (Conley & Berg 1984). If all ionic species are at equilibrium under these conditions, then $\mu_H + e\psi = \mu_K + \psi = 0$. Therefore

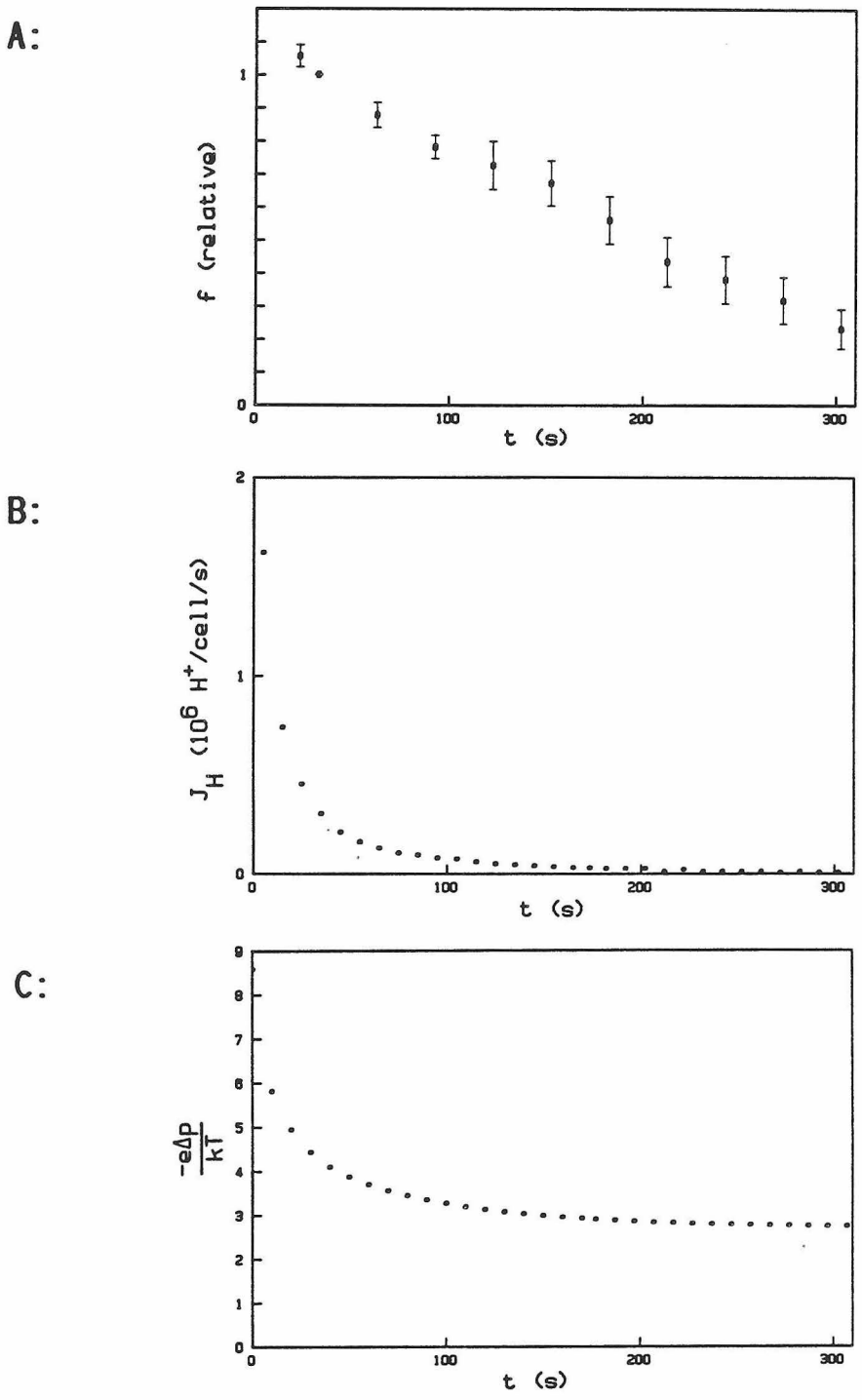

Fig. 3.9. The time course of **A:** tethered cell rotation rate, **B:** membrane proton flux, and **C:** protonmotive force following energization with a combined potassium diffusion potential and pH-gradient.

$$pH_i = pH_e - 0.2$$

$$e\psi = -kT \ln(10) \times 0.2 = -13 \text{ meV}$$

$$[K^+]_i = [K^+]_e \, e^{-e\psi/kT} = 0.32 \text{ M}$$

This estimate of the internal K^+ activity, $[K^+]_i$, agrees well with values measured on Streptococcus lactis by other means (Maloney 1977). Following energization, the inward proton flux lowers the cytoplasmic pH according to

$$n_H(t) = \int_{pH_i(0)}^{pH_i(t)} -B_i(pH_i') \, dpH_i'$$

where

$$B_i(pH_i) = -\frac{dn_H}{dpH_i}$$

is the cytoplasmic buffering capacity, and $n_H(t)$ is the number of protons that have entered the cell since the time of dilution. As protons flow into the cell, the pH of the weakly buffered external medium, pH_e, rises. This quantity is measured directly, and the record of pH_e in this experiment is shown in Fig. 3.1.

In computing the electrical potential I will ignore contributions from all ions except K^+ and H^+. Furthermore I will approximate the electrical potential as being equal and opposite to the K^+ chemical potential, which seems appropriate in light of the large conductivity of valinomycin demonstrated in the experiments described in (b). I also assume that there is no potassium buffering in the cytoplasm, such that the 0.32 M K^+ present in the cell originally represents all the potassium available to ionic flows. Note that all these assumptions tend to overestimate the change in $e\psi$ due to movement of K^+.

Nevertheless, the contribution of $e\psi$ to time dependent changes in $e\Delta p$ will turn out to be quite small. The total current into the cell vanishes, therefore

$$[K^+]_i(t) = [K^+]_i(0) - \frac{1}{N_A}\frac{n_H(t)}{v}$$

where v is the volume of intracellular water per cell, equal to approximately 0.84 μm^3 (Manson et al. 1980), and N_A is Avogadro's number. The external K^+ concentration, $[K^+]_e$, does not change significantly in the course of the experiment. In summary, the proton electrochemical potential is given by

$$-e\Delta p(t) = \mu_H(t) + e\psi(t)$$

$$\mu_H(t) = kT \ln(10)\ (pH_e(t) - pH_i(t))$$

$$e\psi(t) = -\ kT \ln \frac{[K^+]_i(0) - \frac{1}{N_A}\frac{n_H(t)}{v}}{[K^+]_e}$$

Fig. 3.9C shows that the proton potential drops from its initial value of 220 meV to 1/2 of that in 36 s and settles at about 1/3 of the initial value. At this point μ_H is positive with the cytoplasmic pH ca 0.5 units lower than the external pH, but the electrical potential is almost unchanged, leaving the protonmotive force directed inward.

There is a clear difference between the time courses of the proton flux and of tethered cell rotation. Proton influx decays rapidly and with approximately exponential behavior, while the rotation speed of tethered cells decreases nearly linearly with time and has dropped only by 10% when the influx is already reduced by 90%. In addition, a sizeable proton potential seems to remain at late times, when there is no measurable proton flux. In some experiments I have seen the flux of

protons reverse, while tethered cells kept spinning counterclockwise, corresponding to protons entering through the motor. The origins of these discrepancies are not well understood and some speculations are presented in §3.5. These findings critically affected the choice of experimental method in measuring rotation-dependent fluxes.

g) Effects of temperature on the proton flux.

The studies described here concern the dependence of the membrane proton conductance on temperature. Fig. 3.10A shows the initial rate of proton uptake, $J_H(0)$, as a function of temperature in experiments where cells are diluted 1:40 from [KCl 8.5] into [$MgCl_2$ 6.5]. The initial proton flux increases by a factor of 6 from 16°C to 32°C. A plot of the initial decay time $t_{1/10}$ as a function of temperature is given in Fig. 3.10B.

The time course of proton uptake at temperatures of 15.9°C, 24.3°C, and 32.7°C is shown in Figs. 3.11A, B, and C. A rise in temperature clearly increases both the initial rate of proton influx and the rate of efflux at late times. Qualitatively this mimicks the action of FCCP, which increases the component of proton flux driven by μ_H and $e\psi$. Of course, this does not exclude that the temperature also affects other ionic conductances, as well as off-diagonal terms in the conduction tensor.

Temperature may affect the initial proton flux differently depending on the composition of the driving force. In one experiment where cells were diluted 1:100 from [KCl 7.5] to [$MgCl_2$ 7.5] the dependence of the initial flux on temperature was steeper at higher temperatures.

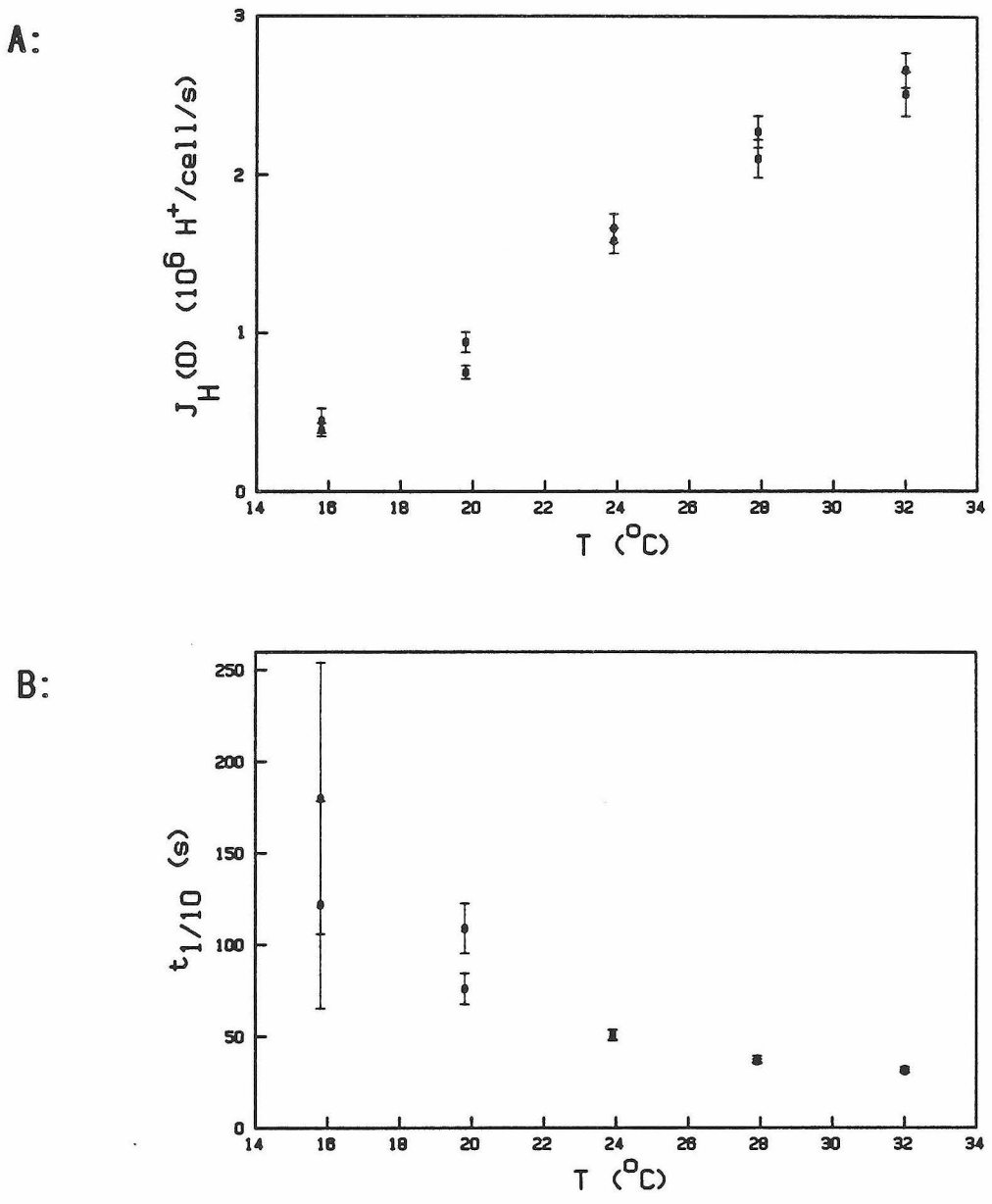

Fig. 3.10. Dependence of the proton flux on temperature.

A: The initial proton flux as a function of temperature.

B: The 1/10 decay time of the proton flux as a function of temperature.

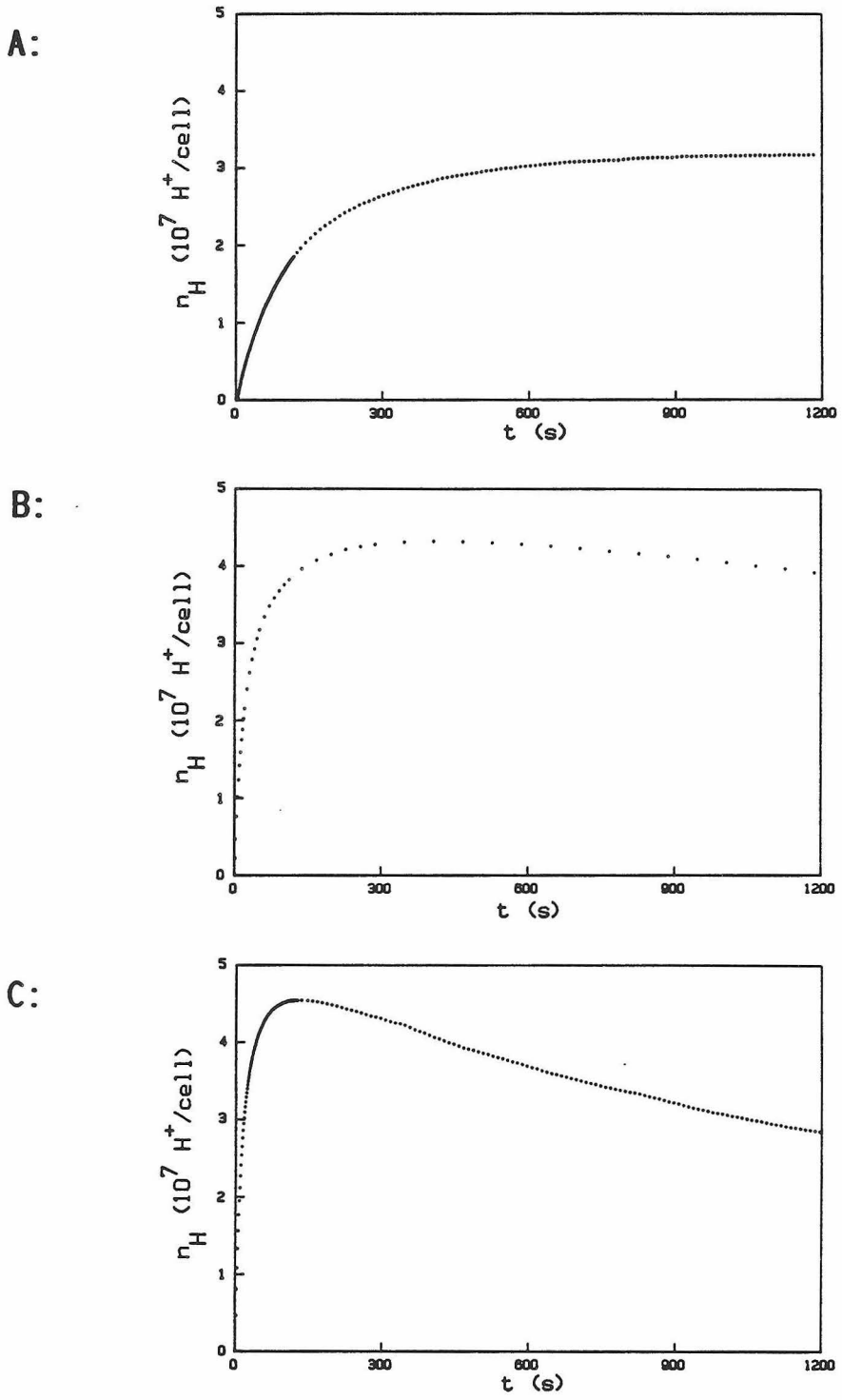

Fig. 3.11. The proton uptake as a function of time after energization at various temperatures; **A:** T = 15.9°C, **B:** T = 24.3°C, **C:** T = 32.7°C.

h) Isotope effects on the proton flux.

The flagellar motor has been shown to generate the same torque in D_2O as in H_2O when running at the speed of a tethered cell (Khan & Berg 1983). In the hope of being able to suppress much of the initial proton flux without interfering substantially with motor rotation I studied the effects of substituting deuterium for hydrogen. Cells were diluted 1:40 from [KCl 8.5] into [$MgCl_2$ 6.5], prepared with H_2O, or into [$MgCl_2$ pD 7.0], prepared with D_2O. In the latter case the intracellular water rapidly exchanges with the extracellular medium (Finkelstein 1984), replacing virtually all of the cytoplasmic H_2O by D_2O. As a result the dissociation constants of the intracellular titratable groups change and the cytoplasmic pD is found to be about 0.5 units higher than the pH was before the isotope substitution (Khan & Berg 1983; G.Lowe unpublished). Since the exchange of water across the membrane is much more rapid than that of any ionic species, the procedure I used for energization in heavy water should be equivalent to diluting cells from [KCl pD 9.0] into [$MgCl_2$ pD 7.0]. In three experiments the initial flux in H_2O was found as $(1.87 \pm 0.16)\times10^6$ H^+/cell/s with an initial decay time of (41.0 ± 0.6) s. The flux in D_2O was lower by a factor of 0.80 ± 0.05 and decayed more slowly. Its decay time was larger than in H_2O by a factor of 1.11 ± 0.07. Apparently the membrane conductance to deuterons is somewhat smaller than to protons, but the effect is not very dramatic.

i) Miscellaneous factors affecting the proton flux.

This section describes a few more observations resulting from my desperate attempts to reduce the initial rate of proton influx in order to better resolve its rotation-dependent component.

1. DCCD.

The membrane of Streptococcus faecalis is known to contain an H^+-ATPase that can be driven by a large proton electrochemical potential (Maloney et al. 1974; Maloney 1977; Harold & Kakinuma 1984). This enzyme is strongly inhibited by DCCD, which binds covalently to the F_o subunit, known to be a proton channel, and blocks its conduction to protons (Maloney 1977, 1979). Starved cells were incubated for 30 min with 0.2 mM DCCD, taken from a stock at 10 mM in methanol. After a 1:100 dilution from [KCl 7.5] into [$MgCl_2$ 7.5] the initial rate of proton uptake by DCCD-treated cells was found to be approximately 75% of that seen in cells treated with methanol alone. An effect of similar magnitude was observed after a shift from [KCl 7.5] to [$MgCl_2$ 6.5]. The initial influx of hydrogen ions was followed by proton extrusion with a time course very similar to that reported in §3.4.c. Apparently, the late proton efflux is not driven by the H^+-ATPase using ATP generated during the initial phase of proton influx. The addition of 2% methanol to starved cells was later found not to affect the proton flux at all.

2. NEM.

N-ethylmaleimide (NEM) is an uncharged sulfhydryl reagent that inhibits lactose transport in E. coli membrane vesicles (Fox & Kennedy 1965; Cohn et al. 1981). It has been shown not to interfere with rotation of the flagellar motor in artificially energized cells (Conley & Berg 1984). In the hope of jamming some of the unknown proton translocating mechanisms in the cytoplasmic membrane I added 5 mM NEM from a stock of 0.5 M in methanol to starved cells in [KCl 7.5]. The pH of the concentrated suspension dropped gradually by 0.1 units over 15 min. When these cells were diluted 1:50 into [$MgCl_2$ 7.5], the initial

proton flux was approximately 30% higher than that seen in cells treated with methanol only. I saw no significant effect of NEM treatment on the initial flux when cells were diluted from [KCl 7.5] to [KCl 6.5].

3. Substitution of chloride by methanesulfonate.

Several authors have reported a small but measurable conductance to Cl^- ions in the cytoplasmic membrane of E. coli (Flagg & Wilson 1977; Maloney 1978). Even though the chloride chemical potential does not change significantly on energization, I wanted to test for involvement of Cl^- in generation of the proton flux by replacing it with $CH_3SO_3^-$, a relatively impermeant anion (Kometani & Kasai 1978). When the Cl^- driving force alone was changed by diluting cells starved in [KCH_3SO_3 7.5] into [KCl 7.5] or vice versa, no proton movement was detected. Note that these cells were treated with valinomycin, so the result of these measurements merely indicates that the conductance to K^+, mediated by valinomycin, is much larger than the Cl^- conductance, thus keeping the membrane potential close to the potassium equilibrium potential. Also, any transport of protons coupled directly to the chloride driving force, for example in the form of HCl symport, seems to be weak in comparison to the membrane's total proton conductance. In other experiments I energized cells by a 1:25 dilution from [KCH_3SO_3 7.5] into [$Mg(CH_3SO_3)_2$ 7.5] and compared the resulting proton flux to that obtained after diluting cells starved in [KCl 7.5] into [$MgCl_2$ 7.5]. The measurement was perturbed by an exceptionally large fast pH shift associated with dilution as described in §3.3.d. However, for times grater than 30 s the fluxes in the two cases were virtually identical. I conclude that, under the conditions I used, any membrane conductance to Cl^- does not play an important role in determining the flux of

protons.

4. Growth stage.

To determine whether the proton flux depends on the culture density at which cells are harvested I prepared two cultures: one grew for 3 hours to an OD_{600} of 0.17, corresponding to approximately $0.63x10^8$ cells/ml, another grew for 4.5 hours to an OD_{600} of 1.5, containing approximately $5.5x10^8$ cells/ml. After harvest cells were treated identically and starved at the same final density in [KCl 7.5]. A 1:100 dilution into [$MgCl_2$ 7.5] led to very different time courses of the proton flux in cells of the two cultures, as shown in Figs. 3.12A and B. At 15 s after energization the rate of proton uptake was very similar in the two experiments. In cells grown to high density (Fig. 3.12A) it then decayed exponentially with a time constant, $t_{1/10}$, of 34 s, eventually changing sign after 1.5 to 2 min. By contrast, the proton influx soon leveled off in cells grown to low density (Fig. 3.12B) and remained at much higher values, reversing only after approximately 5 min. This experiment emphasizes the need to control growth conditions to ensure reproducible results. Most experiments discussed in this and the following chapter used cells grown to an OD_{600} of approximately 1.0.

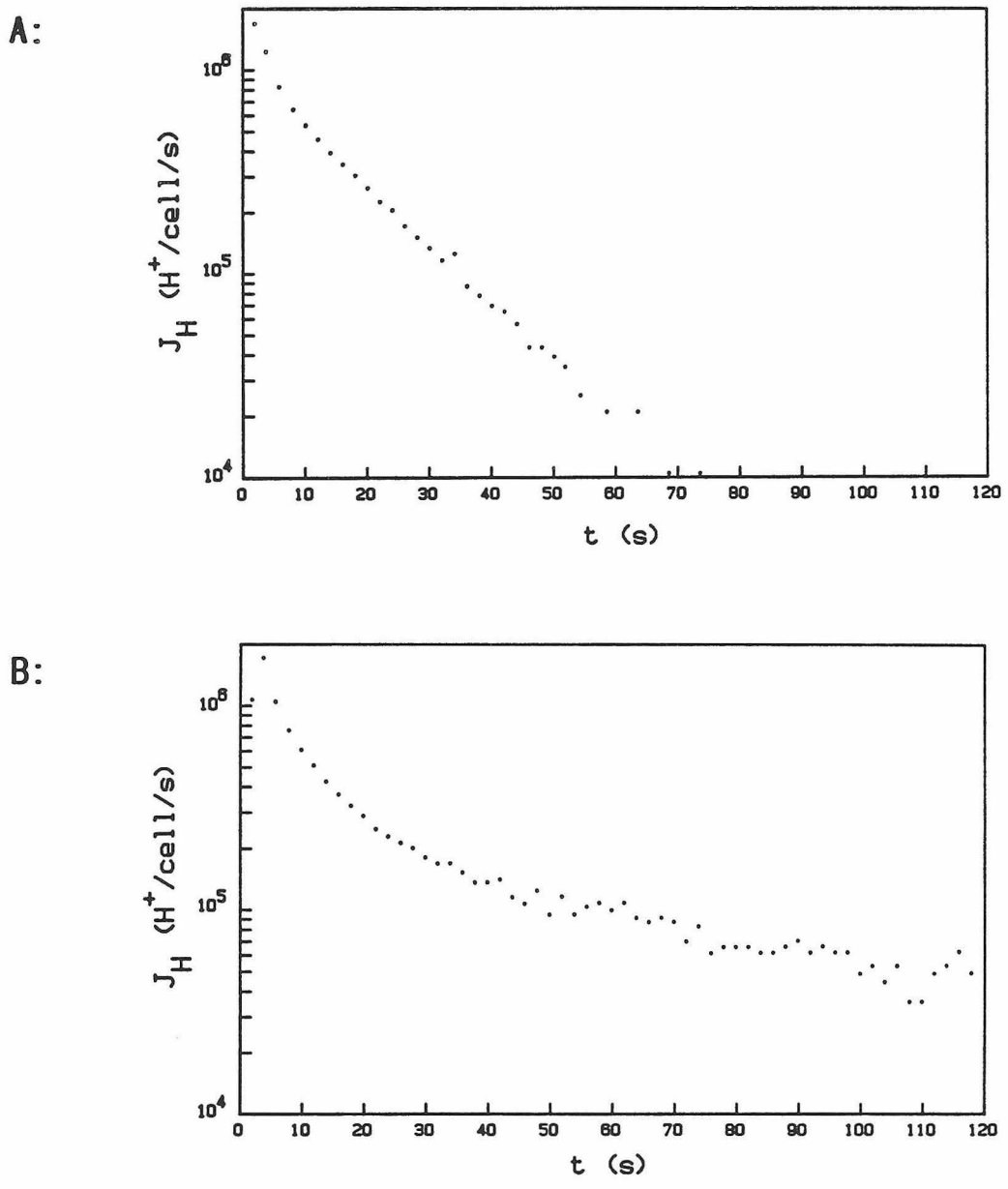

Fig. 3.12. Effects of the growth conditions. The proton flux as a function of time after energization in cells that were grown to a density of **A:** 5.5×10^8 cells/ml and **B:** 0.63×10^8 cells/ml.

§3.5 DISCUSSION

I will not attempt an exhaustive review of the vast literature on membrane transport involving protons. Since this study was limited to the transport of protons alone, it can not reveal the nature and function of the relevant conduction mechanisms, which may well involve movement of other ionic species. I will therefore simply present a summary of the phenomenological observations of the proton flux and indicate how some of them may be understood in terms of molecular mechanisms known to exist in bacterial membranes. Most qualitative features of the proton flux time course can be accommodated within the linear formalism outlined in §3.2. However, it will be seen that this leads to some assumptions that are quantitatively unlikely. Particularly, the discrepancy between the time course of proton uptake and that of flagellar rotation remains unexplained.

Following a pH-shift of the external medium the proton flux decays approximately exponentially and never reverses (Fig. 3.3). This is in accordance with the result of §3.2.b that the component of the flow conjugate to the initial driving force is positive and decays monotonically, if flows and forces are related linearly. But the chemical potential under these conditions is large (ca 4.6 kT) and linearity is therefore not guaranteed. However, the observation might also be explained if H^+ and K^+ are the only permeating species in these experiments. The requirement for charge balance would ensure that neither flow can change sign during the approach to equilibrium, as outlined in §3.2.c. It would be interesting to test whether the proton flux after a pH-shift remains monophasic when a third permeating

species, such as Mg^{2+}, is included in the medium.

When proton flux is initiated by a change in the chemical potential of potassium, a reversal of the direction of proton flux is observed at late times (Fig. 3.2). This may be understood if one assumes that the membrane has a finite conductance to the cations used to substitute for potassium in the energization buffer: sodium, magnesium, and, to a smaller extent, choline. The following analogy may make this interpretation more intuitive. If the conductance tensor **L** is diagonal and all permeating species are charged, then the linearized membrane-ion system is equivalent to the resistor-capacitor network drawn in Fig. 3.13A. The capacitor C_i represents the number of ions of species i in the cell, U_i their chemical potential, a current I_i corresponds to ions flowing into the cell, which is at a potential V relative to the external medium. As outlined in §3.2, the membrane capacitance, C, is so small compared to the C_i that it may be omitted. The detailed correspondence is:

RC network (Fig. 3.13A)	Membrane system
V	ψ
C	C
R_i	T/L_{ii}
U_i	$-\mu_i/ez_i$
I_i	ez_iJ_i
C_i	$n_i(ez_i)^2/kT$

The initial driving forces after dilution of cells from KCl into $MgCl_2$ correspond to a negative voltage U_K, a positive U_{Mg}, and vanishing U_H. By building this circuit and recording U_H with a storage oscilloscope one can easily verify that the current I_H is biphasic if R_KC_K is chosen

A:

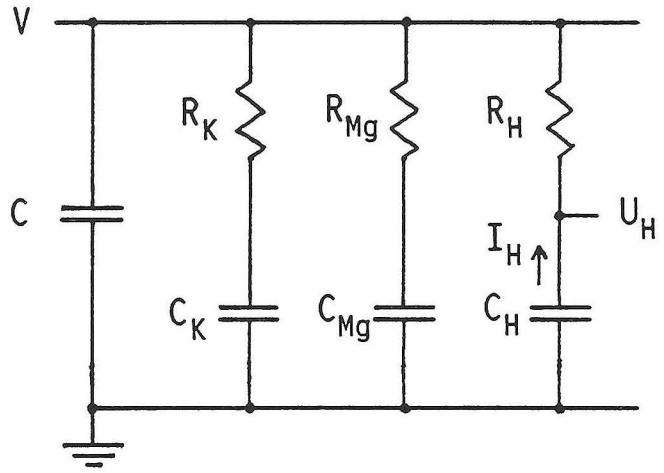

B:

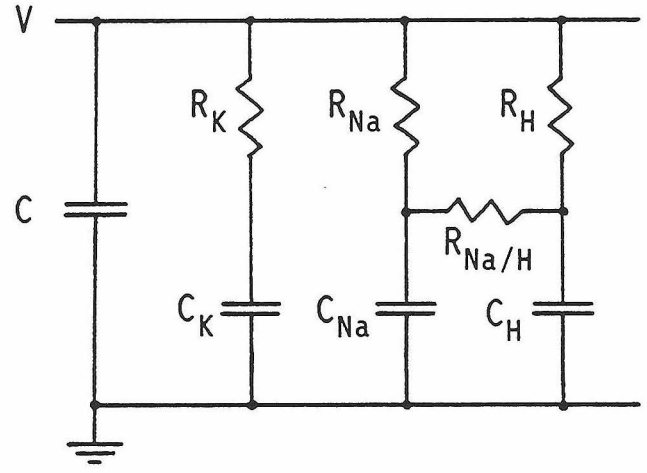

Fig. 3.13. Resistor-capacitor networks that simulate the linearized membrane-ion system.

A: Conductance tensor diagonal.

B: Off-diagonal elements, resulting from electroneutral sodium/proton antiport, included.

much smaller than $R_{Mg}C_{Mg}$, and further tuning of the individual parameters leads to time courses very similar to those observed for the proton flux. Some bacterial membranes do, in fact, have a finite conductance to Mg^{2+} (Willecke et al. 1973). Similarly, a passive permeability to Na^+ has been suggested in Streptococcus lactis (Maloney 1977). Other bacteria are known to use the flow of sodium ions in a variety of membrane-bound mechanisms (Lanyi 1979). Choline, on the other hand, is generally regarded as an impermeant cation, which may explain the relatively small efflux seen at late times after dilution into a choline buffer. However, this hypothesis, namely that protons are extruded at late times due to a positive protonmotive force generated by a cation other than H^+ or K^+, contradicts the observation that the flagellar motors continue rotating in the direction corresponding to inward proton flux. On the other hand, direct exchange of protons for the cation (Na^+, Mg^{2+}, $choline^+$) might lead to a net proton efflux, even in presence of an inwardly directed protonmotive force.

One can verify this using the resistor-capacitor network pictured in Fig. 3.13B. This extension of the analogy to the membrane-ion system now includes off-diagonal elements of the conductance tensor, if they result from electroneutral ion exchange. For example, 1:1 antiport of sodium ions for protons is represented by the additional resistor $R_{Na/H}$. This model also shows how protons can be driven by changes in the external sodium concentration alone. Dilution of cells from choline Cl into NaCl corresponds to a positive U_{Na} (choline has been omitted from the diagram because its conductance is comparatively small). One finds that significant movement of protons results if R_{Na} is not much smaller

than $R_{Na/H}$, even though the small value of R_K (representing valinomycin) holds the membrane potential close to zero. The observations of proton fluxes coupled to a sodium driving force (Fig. 3.7) point towards such a configuration. This does not come as a surprise since Na^+/H^+ exchange mechanisms are well known to exist in the membrane of E. coli (Harold & Altendorf 1974). They have been suggested in Streptococcus lactis (Maloney 1977) and Streptococcus faecalis (Heefner and Harold, 1980). Previous observations on tethered Streptococcus V4051 and SM197 have also indicated Na^+/H^+ antiport (Manson et al. 1980, S. Khan unpublished). Krulwich (1983) reviews recent work on sodium/proton antiporters in other bacteria.

The approximate proportionality of the initial proton flux and the initial potassium chemical potential (Fig. 3.4) is explicitly predicted by the linear formalism. On the other hand, it is harder to explain why the proton flux is lower than when an equivalent proton chemical potential is used. Thermodynamically the membrane potential and the proton chemical potential contribute equally to the proton driving force. One would therefore have to argue that the conductance of valinomycin to K^+ is finite and the electrical potential therefore somewhat lower than the potassium chemical potential. Within the linearized approximation, this is not sufficient: as can be seen from Fig. 3.13A, a significant membrane resistance to potassium, R_K, has the same effect on the proton current driven by U_H as driven by U_K unless a third charged permeating species is invoked, whose chemical potential is close to zero.

This construction seems somewhat contrived and it is tempting to leave the constraint of linear force-flow relationships behind and enter

the regime far from equilibrium, where there are no such rules. One can easily imagine transport mechanisms whose rate of operation is limited by proton binding and unbinding events at either side of the membrane. If, for example, the pK_D of the binding site is 8.5 at the cytoplasmic side and 6.5 at the external side of the membrane, such a mechanism would operate fast in response to a pH-shift from pH 8.5 to 6.5 but slowly in response to a potassium dilution at pH 7.5 (see Tanford 1983 for examples of such mechanisms). One could test this hypothesis by performing both experiments over a range of external pH values. Another likely possibility is that Mg^{2+} modulates the conductivity of the membrane to protons. The discrepancy between the fluxes initiated by μ_H and μ_K is largest when Mg^{2+} is used to replace K^+ in the latter case. Titration of cell samples in the course of measurements of the intracellular buffering capacity also showed a lower conductance to small pH-shifts in the presence of $MgCl_2$.

The direct cation/proton exchange mechanisms considered above can, in principle, accomodate the observation of proton efflux without a reversal in the sense of flagellar rotation. However, the drastic difference between the time course of the proton flux and that of tethered cell rotation (Fig. 3.9) is still not explained satisfactorily. While the magnitude of the late proton efflux depended on the cationic composition of the external medium, the initial rapid decay of the proton influx was altered significantly only by lowering the temperature. At room temperature, the 1/10 decay time of the proton flux ranged from about 30 s to 60 s in all experiments described in this chapter, while the rotation rate of tethered cells drops only by 20% during the first minute (Fig. 3.9A). In principle, the cell population

might be drastically inhomogeneous: the majority of cells could have membranes with a very high proton conductance, accounting for the bulk of the initial proton flux. When tethered, these cells might never spin during the period of observation, and therefore they would be excluded from the sample of motor rotation rates. This interpretation still cannot account for the discrepancy between the proton flux and the protonmotive force, as calculated from the movement of hydrogen and potassium ions (Fig. 3.9C). During the experiments reported in Chapter 4, I noted that more than 80% of the cells swim when energized artificially as in Fig. 3.9, which also argues against this hypothesis. Alternatively, the rapid decay of the initial flux might be caused by a time-dependent change in the membrane conductance. One would have to postulate that the membrane conductivity to protons decreases following energization on a time scale of about 30 s, irrespective of the composition of the external medium or the nature of the initial protonmotive force. An observation speaking against such a time-dependent conductance is that the flux decays faster when its absolute value is large. This correlation between the initial rate of proton uptake and the decay time is particularly evident in the studies of the temperature dependence (Fig. 3.10) and the effects of the proton ionophore FCCP (Figs. 3.5 and 3.6). It suggests that the time dependence of the proton flux is mainly due to a decrease in the driving force, which occurs more rapidly when the proton influx is large. The drastic acceleration of the early flux by FCCP also speaks against the suggestion that the early time course may reflect a slow titration of the external cell surface and not involve transmembrane flows at all. I also repeated these experiments with cells that had been disrupted by

passage through a french press: the cytoplasmic contents and the cell envelope fragments were titrated within the mixing time of the sample, and no further pH-change was observed after about 10 s. Lysing the cells in 10% n-butanol prior to dilution in the energization buffer led to the same rapid titration.

The membrane proton conductance of this Streptococcus, as determined from the initial proton influx following energization, seems rather large when compared to other biological membranes. It is convenient to express the conductance normalized to the membrane area. Treating the cell as a cylinder of length 3.3 μm and width 1.3 μm one obtains a value of 20.3 $\mu S/cm^2$ for the conductance, c_m, measured with small pH-shifts of ca 0.1 units at 24°C. The average conductance measured with large pH-shifts is 17.9 $\mu S/cm^2$ and that obtained using the membrane potential alone is 7.8 $\mu S/cm^2$. The corresponding values measured by Maloney (1982) on S. lactis are 1.60 $\mu S/cm^2$, 1.37 $\mu S/cm^2$, and 0.96 $\mu S/cm^2$, smaller by a factor of 11 on average. Scholes and Mitchell (1970) obtained a value of 0.47 $\mu S/cm^2$ from titrations of M. denitrificans, which increased to 17.4 $\mu S/cm^2$ in presence of 2 μM FCCP. Mitchell and Moyle (1967) found a very similar conductance of 0.45 $\mu S/cm^2$ for the cristae mambrane of rat liver mitochondria. In my efforts to reduce the membrane proton conductance of our Streptococcus strain I had pinned great hopes on the action of DCCD. Maloney (1977) saw a sharp increase in the proton flux through the membrane of S. lactis at a protonmotive force above 175 mV, which could be suppressed by DCCD. This increase in the proton conductance is attributed to the onset of ATP synthesis by a membrane-bound ATPase. The H^+-ATPase of S. lactis is also assumed to dissociate at pH values below 5.0, leading to

a very large DCCD-sensitive proton conductance mediated by the unattached F_o-segment. In my experiments I saw no dramatic effect of DCCD on the proton flux, probably because I never reached the large threshold potential for ATP synthesis, and the external pH was always kept above pH 6.

The large membrane conductance to protons is a serious obstacle to the measurements of rotation-dependent proton fluxes presented in the following chapter. In that context it is worth noting that B. subtilis can also be starved, swims in response to an artificial proton gradient, and shows a considerably smaller proton flux of 1.2×10^5 H^+/cell/s/pH (Matsuura et al. 1979). This bacterium may be an alternate candidate for those measurements.

CHAPTER FOUR : THE FLUX OF PROTONS THROUGH THE FLAGELLAR MOTOR

§4.1 INTRODUCTION

In this chapter I will present my measurements of the flux of protons coupled to rotation of the flagellar motor in Streptococcus SM197. The approach is to measure the total flux of protons through the membrane once when cells are swimming and again when rotation of the motor is stopped by cross-linking the flagella with an antibody raised against flagellar filaments. The flux coupled to rotation is given by the difference between the two values obtained. This does not necessarily represent the entire flux of protons through the motor, since significant uncoupled proton translocation may be taking place even when the motor is stalled. I studied the dependence of the coupled proton flux on three parameters: the time after energization, the temperature, and substitution of ^{2}H for ^{1}H in the external medium. The motor rotation frequency in swimming cells as well as the rotation rate of tethered cells were measured under the same conditions. Together, these experiments allow conclusions both about the stoichiometry of protons to flagellar revolutions and the efficiency of energy conversion in the motor.

These are by far the most illusive experiments I have done to date. In fact, I stumbled upon the successful technique only after a year and completed the measurements in the following two months. Prior to then my approach was to divide a concentrated stock of cells into two batches: one was treated with anti-filament antibodies, the other was

not. Then I took samples from either batch in an alternating sequence and diluted them into energization buffer, measuring the proton flux over the first two minutes as described in Chapter 3. For each sample I determined the initial rate of proton uptake and searched for a systematic difference between treated and untreated cells. Since the effect never materialized, I got a lot of practice in doing this: eventually I could reproduce the initial proton flux to within two or three percent in a series of seven successive samples, an accuracy equal to the uncertainty associated with each individual value. Apparently the flux through other conductances immediately following energization completely swamped the motor flux. When I had quantitatively compared the time course of the proton flux with that of the tethered cell rotation rate (Chapter 3, Fig. 3.9), it was clear that the ratio of motility to total proton flux became more and more favorable at late times after energization. I then looked at my old results again, comparing the magnitude of the proton flux at 60 s after dilution, a time domain to which I had never paid much attention. In fact, the flux after 1 min was systematically lower in samples whose cells had been pretreated with flagellar antibody, although that interpretation required some faith, since the scatter was still quite large. Next I tried adding antibody to the final cell suspension during the flux measurement at about 30 s after dilution. The cells stopped swimming and agglutinated within a few seconds after antibody addition. Simultaneously I saw a clear drop in the proton flux by about 20% of its value before addition. By this time I had become quite skeptical of apparent successes, but the series of tests described in §4.4 convinced me that I was observing an effect associated with rotation of the motor.

The decisive advantages of this technique are that the measurements on cells with and without antibody are performed at a time when the total proton flux is small, on the same set of cells, and within about 5 s of each other. In hindsight I wish I had started out from the beginning with this idea, in which case most of the measurements in Chapter 3 would never have been made. On the other hand, I am glad that I eventually did find the appropriate trick for measuring the flux through the motor, which by itself is so much more exciting than the remaining 99% of the membrane proton flux.

In §4.3 I have collected a number of observations on flagellar motility that motivated my choice of experimental conditions in these experiments. The final combination of buffers and ions and the composition of the artificial protonmotive force should be appropriate for most studies on our Streptococcus strain.

§4.2 METHODS

a) Nomenclature.

The buffers in the flux measurements were the same as those of Chapter 3, and I will use the same notation to refer to them. During the preliminary experiments presented in the following section a number of different buffers and ionic species were used, which are given in the text for each individual case. The proton flux through the membrane and its time integral were denoted by J_H and n_H respectively in Chapter 3, but I will call them J and n in this chapter.

b) Flagellar antibody.

The antibody was raised in 1977 by Jon Izant in Howard's lab at the University of Colorado by injecting rabbits with Streptococcus flagellin in the presence of Freund's complete adjuvant. The antigen was obtained by blending cells of strain V4051 in a homogenizer, removing the cell bodies by centrifugation (4000g, 2 min), and pelleting the flagella (125000g, 15 min). The IgG-fraction of the immune serum was purified by ammonium sulfate fractionation (0-50%) and chromatography on a DEAE-cellulose column and stored in 0.1 M potassium phosphate at pH 7.5 and -20°C. I dialyzed this sample against a solution of 0.067 M $MgCl_2$, 0.1 mM tetren at pH 7. A 50-fold dilution of this stock into a suspension of cells of SM197 in KTY stopped all swimming by the time motility could be monitored, ca 7 s after onset of mixing. Inspection of samples during flux experiments, just after the addition of antibody at this concentration, showed 90% to 95% of the cells agglutinated in large clumps, and at the edge of these clumps a few cell bodies could be

observed spinning. A few single cells still jiggled or tumbled. Cross-linking of flagellar filaments by this method worked well at pH-values between 6 and 10.

c) Rotation-dependent flux.

Measurements of proton uptake were performed with the apparatus and protocol described in Chapter 3. Unless noted otherwise in the text, cells were energized by adding 50 μl of the concentrated cell stock in buffer C [KCl 8.5] into 2 ml of buffer D [$MgCl_2$ 6.5]. Simultaneous addition of approximately 20 μl of 0.005 N HCl suppressed most of the positive pH-shift associated with dilution. At 30 s to 35 s after dilution a small volume of antibody stock, typically 20 μl, was added to the suspension. Since the antibody solution contained no buffering species other than the protein itself, this did not perturb the absolute pH of the sample. However, when motile cells of SM197 were used, the rate of proton uptake decreased rapidly over a period of a few seconds, the time required for complete mixing of the sample, and then resumed the slow, approximately exponential decay seen before antibody addition. After ca. 2 min the cell suspension was titrated back to the initial pH with 20 μl aliquots of 0.001 N HCl. Before determining the OD_{600} the samples were agitated vigorously (Vortex-Genie, Model K-550-G, Scientific Instruments Inc.) in order to break up clumps of agglutinated cells which perturbed the cell density measurement.

Fig. 4.1A shows a semilogarithmic plot of the proton flux as a function of time in cells of SM197. During the first 30 s the flux decays from $2x10^6$ H^+/cell/s to $4x10^5$ H^+/cell/s. It drops to $2.5x10^5$ H^+/cell/s within 4 s after addition of antibody, then continues to decay

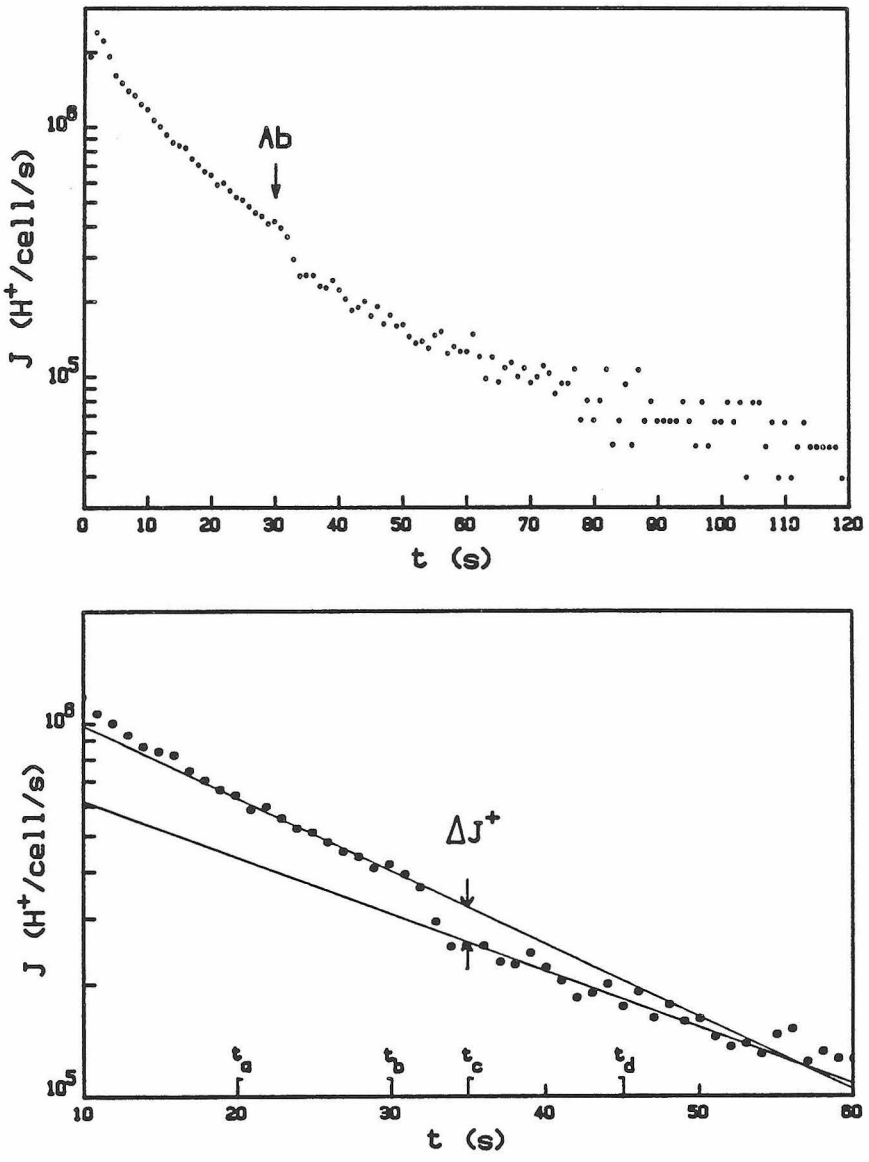

Fig. 4.1. Measurement of the rotation-dependent flux.

A: The proton flux as a function of time after energization. The arrow indicates the time at which flagellar antibody was added to the sample. **B:** The data of (A) replotted on a larger scale. The two lines are least-squares fits over the intervals $[t_a, t_b]$ and $[t_c, t_d]$. The arrows indicate the rotation-dependent flux, $\Delta J^+(t_c)$.

slowly with a time constant, $t_{1/10}$, of 64 s. The analysis of such experiments is illustrated in Fig. 4.1B. Two linear least-squares fits are made to the data points of Fig. 4.1A, weighted such as to approximate exponential fits to J(t). One fitting function, $j_1^+(t)$, extends from t_a, ca 10 s before addition of antibody, to the time of addition, t_b. This fit is used to extrapolate the time course that the flux would have taken if no antibody had been added to the sample. The other linear fit, $j_2^+(t)$, extends from t_c, 4 or 5 s after addition of antibody, to t_d, ca 10 s later, and interpolates the behavior after mixing is complete. The difference between these two functions is computed at time t_c,

$$\Delta J^+(t_c) = j_1^+(t) - j_2^+(t)$$

which for simplicity is defined positive when the flux after addition of antibody is lower than before. This value requires a significant correction to yield the instantaneous change in flux due to addition of antibody. The two linear fits cover a range of 25 s, and, as seen in Fig. 3.2 of Chapter 3, the semilogarithmic plot of J(t) shows significant curvature over this period, even without any additions to the sample. Thus application of the same analysis to such a sample generally leads to a negative value of

$$\Delta J^- = j_1^-(t) - j_2^-(t).$$

For this reason proton flux was measured in samples with and without antibody under all the conditions tested, and the proton flux change resulting from the action of antibody was taken to be

$$\Delta J = \Delta J^+ - \Delta J^-.$$

The standard error in this quantity was determined from the standard errors in the extrapolations to time t_c of the four linear fits

involved.

d) Bundle frequency measurements.

The rotation frequency of the flagellar bundle of glycolyzing cells was determined using the apparatus described by Lowe et al. (1986) and in more detail in Graeme's thesis. Following Graeme's protocol, a suspension of swimming bacteria at a density of ca $5x10^8$ cells/ml was observed in a flow cell on the thermostatted stage of a Nikon S-Ke microscope, equipped with a Zeiss Optovar and a beam splitter to allow simultaneous video recording. The cells were imaged onto the cathode of a photomultiplier tube. The bundle of a swimming cell exerts radial forces on the cell body which cause the body to gyrate at the frequency at which the bundle rotates relative to the medium. These small amplitude vibrations of the cell body were transduced by spatial inhomogeneities of the photocathode and thus appeared in the photomultiplier's output signal. The signal was filtered by a double-pole low-pass and a single-pole high-pass stage with roll-off frequencies at 200 Hz and 72 Hz respectively, amplified, and analyzed in real time by Fast Fourier Transform on a PDP 11/34 computer. The program computes the power spectrum over the interval from 1 Hz to 256 Hz at all multiples of 1 Hz.

The cells were metabolizing in buffer B [KCl 8.5] with 0.01 M glucose added. Power spectra were determined at temperatures between 12°C and 24°C, and swimming motility was recorded on video tape simultaneously (Ikegami ITC-47 camera; Panasonic NV-8950 recorder). To facilitate analysis of the tape record for swimming speed and body roll frequency the camera was focused onto the bottom coverslip of the flow

cell, where cells swim mostly in the focal plane. Finally 10 μg/ml FCCP was added to the bacterial suspension, which caused all motility to cease. Power spectra were recorded from this suspension under the same conditions used previously for swimming cells. These spectra represent the signal from sources unrelated to swimming motility, such as Brownian motion of the cell bodies, detector shot noise, and amplifier noise. They were subtracted from the corresponding swimming cell spectra to yield the signal due to motility. Sometimes one of the spectra had to be scaled slightly with respect to the other, for example because the cell density in the focal plane was not the same during the two recordings. The scaling factor was chosen such as to match the power density at the high-frequency end of the spectrum, where cell motility makes no contribution. Fig. 4.2 shows two power spectra obtained from glycolyzing cells at 24°C, the lower one in presence of FCCP. The difference spectrum contains two peaks. A low-frequency peak extending from 1 Hz to about 30 Hz results from the counter-rotation of cell bodies as well as the shot noise due to images of swimming cells moving across the photocathode. The high-frequency peak, usually well separated from the first one, is due to gyration of the cell bodies driven by the bundle rotation. The mean frequency of this peak as well as its uncertainty were estimated by eye. This peak was fairly symmetric except at the lowest temperatures, where the power dropped off more sharply at the low-frequency end.

e) Observation of swimming and tethered cells.

Video records of artificially energized swimming and tethered cells were obtained with the optics described in (d) excepting the beam

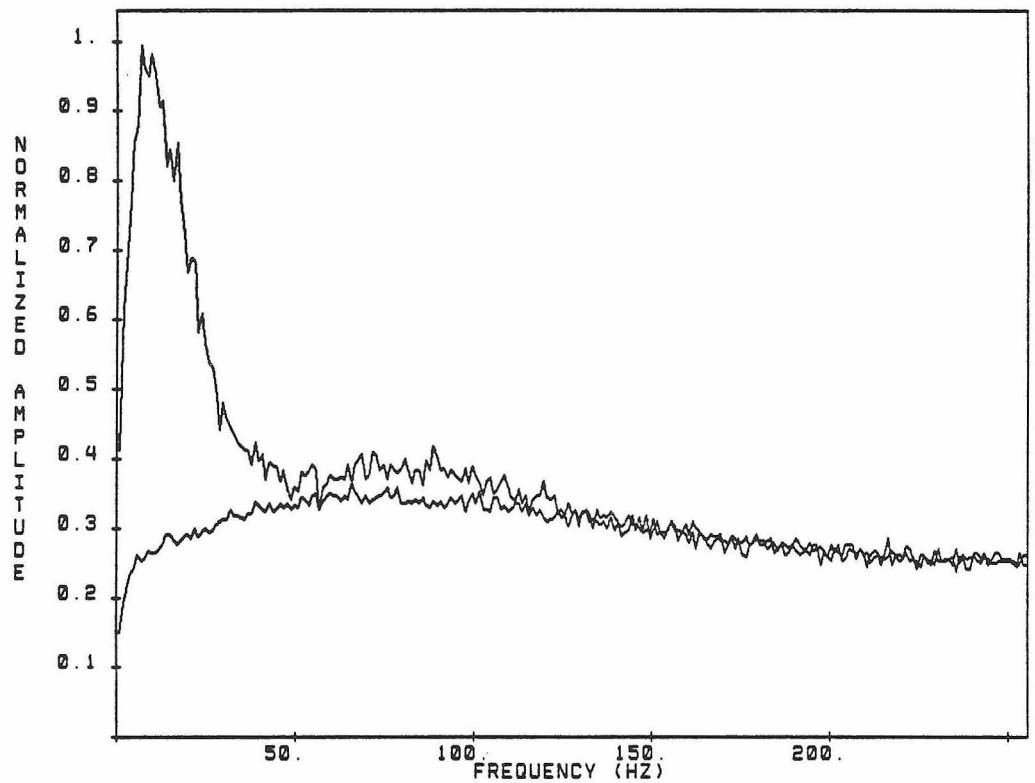

Fig. 4.2. Measurement of the rotation frequency of the flagellar bundle. Power spectra obtained from glycolyzing cells at 24°C. Upper curve: swimming cells. Lower curve: the same cells in presence of FCCP.

splitter, which was removed. Cells were energized by dilution from buffer C [KCl 8.5] into D [$MgCl_2$ 6.5] following the same procedure used for the flux measurements and described in part (c). Immediately following mixing the cell suspension was drawn into the flow cell. Both the dilution buffer and the flow cell were thermostatted. The polyethylene tubing inbetween was not, but I shortened it to a few cm in length. Observation of swimming cells was possible after 10 s, but not close to the bottom of the flow cell, because the medium there was not completely replaced by such a short flow. The swimming speed of these cells was measured by tracing their paths on the video monitor during a few seconds of play-back. Although some correction was possible for the path lengths of cells that did not swim perfectly parallel to the plane of focus, cells that swam closer to the vertical direction were excluded from this analysis. Body-roll frequencies were determined by counting the wobbles of the image of these cells over the same period of time. The mean and the standard error in the mean of both the swimming speed and the body roll frequency were computed for samples of 20 to 30 cells. Tethered cells were energized in exactly the same manner, but faster and longer flows were used to ensure that the medium was completely replaced close to the top coverslip (see also §3.3.f).

f) Flagellar staining.

My attempts at visualizing the flagella of our Streptococcus by electron microscopy or with the fuchsin stain described by Leifson (1951) failed, mainly because of excessive breakage of flagella during the drying process. I eventually used a wet-mount procedure that Howard learned about from Bruce Stocker. The complete protocol is given by

Heimbrook et al. (1986), and I will only summarize my version of this procedure. The stain was prepared just prior to use from two stock solutions which should be stored at 7°C: Stock I was obtained by adding 10 ml 5% phenol to 10 ml saturated $AlK(SO_4)_2 \cdot 12H_2O$ and dissolving 2 g tannic acid in the mixture. Stock II was a saturated solution of crystal violet in ethanol (ca. 12 g/ml). 10 parts of stock I were mixed with 1 part of stock II and drawn into a syringe. A microscope slide was wiped clean with 95% ethanol, rinsed with glass-distilled water, dipped into an aqueous solution of 10 μg/ml poly-L-lysine for a few seconds, rinsed again with water, and air dried. I placed a drop of bacterial suspension at a density of ca 10^8 cells/ml on the slide and covered it with a glass coverslip. After 10 minutes, during which the cell bodies settled onto the slide, a drop of stain was dispensed through a filter of 0.22 μm pore size onto one edge of the coverslip, from where it slowly flowed under the slip, becoming gradually more dilute as it mixed with the suspension medium. Stained flagella appeared a few minutes later, usually in the region of intermediate stain concentration. Due to the short-lived nature of the wet-mount the resolution of the filaments deteriorated with time, as more and more stain precipitated. It was therefore advantageous to take photographs for later analysis. I obtained my best exposures using phase contrast optics and Polaroid 665 positive/negative film.

A few more observations: The poly-L-lysine makes the cell bodies attach to the glass surface more efficiently except when the ionic strength of the medium is very low. I obtained good stains in 0.2 M KCl as well as in buffer C [KCl 8.5]. Staining directly in KTY growth medium did not work; there is plenty of other dirt in the suspension to

precipitate the dye. To ensure that the flagella are separated and do not stain together in one bundle, I either starved the cells thoroughly or pretreated them with 10 μg/ml FCCP. Fixing the cells in 20% formalin did not alter the results. I also saw nice stains when unsheared cells were allowed to settle onto glass coverslips coated with Prosil-28, as used in tethering experiments, but the sinusoidal shape of the filaments was lost under these conditions. Some flagellar breakage persists on the poly-L-lysine coated glass. Large shear forces occur due to the close proximity of coverslip and slide, illustrated in Fig. 4.3, and filaments, which adhere only lightly to the surface, are torn from the cell bodies. In those cases I saw regions of the slide where cells were completely shaved, while their flagella had gone off and landed an area downstream; I avoided taking pictures of such areas.

g) Calculation of torques.

I approximated the body of a swimming cell as a cylinder rotating at frequency of revolution f_B about an axis that intersects its symmetry axis at an angle γ and at a distance r from its center. The cylinder also translates along the rotation axis, which presumably corresponds roughly to the axis of the flagellar bundle. This translation does not affect the torque exerted by the fluid on the cylinder. By the methods of §2.2.a one computes this torque as

$$N = 2\pi f_B c_R$$

where

$$c_R = c_R^{\parallel} \cos^2\gamma + (c_R^{\perp} + c_T^{\perp} r^2) \sin^2\gamma.$$

For $\gamma = 90°$ one obtains the geometry of tethered cells, while Graeme estimated γ at about 22° in swimming cells by tracing their outline on

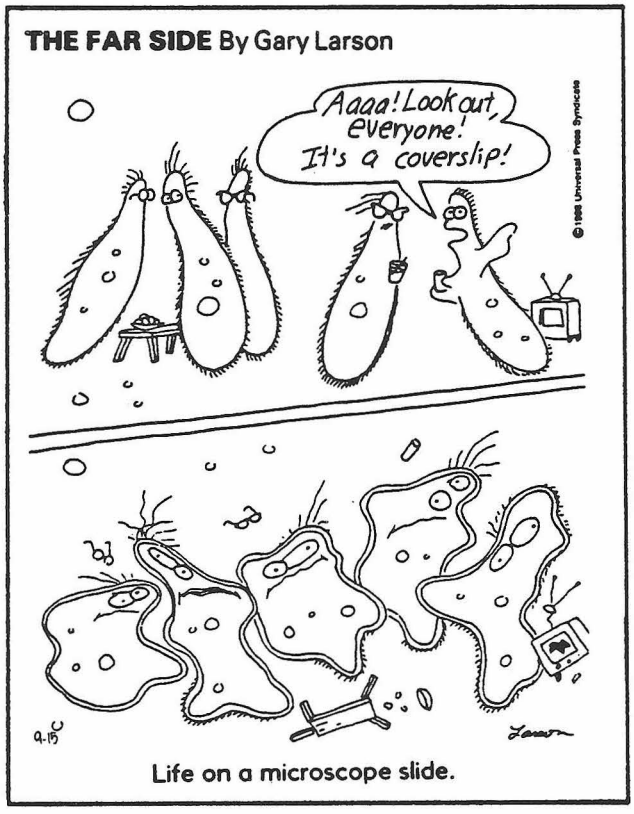

Fig. 4.3. The close proximity of coverslip and microscope slide may compromise the reliability of flagellar stains.

the video monitor over several body roll periods. The cell sizes were again determined from photomicrographs of cells tethered to a silanized glass coverslip. The spinning cells had a length of (3.04 ± 0.64) μm and a width of (1.36 ± 0.19) μm, where the uncertainty denotes the standard deviation in the sample. The corresponding averages over all cells attached to the slip were (3.27 ± 1.11) μm length and (1.27 ± 0.17) μm width. The latter sizes were taken to be characteristic dimensions of the average swimming cell. The distance between the rotation axis and the center of a spinning tethered cell, r, was determined from its length and the diameter of the bright disk it produced on a long-term photographic exposure and found to be (0.32 ± 0.27) μm. For swimming cells I estimated the distance r to be about 1/6 of the cell's length. All torques quoted in this chapter were calculated using these dimensions and the average body rotation rate in the respective sample.

The viscosities of H_2O and D_2O were taken from the Gmelin Handbook of Inorganic Chemistry (1963, 1964).

§4.3 EXPERIMENTAL CONDITIONS FOR ARTIFICIAL ENERGIZATION

In the following section I will outline my motivation for the choice of experimental conditions in measuring the proton flux coupled to flagellar rotation. I have taken this opportunity to catalogue a number of observations on flagellar motility, most of which I cannot explain. They are organized in groups concerning requirements for swimming, generation of a large artificial protonmotive force, Na^+/H^+ antiport, and the effects of choline, although all these topics are clearly interrelated. My own experiments are interspersed with the observations of others as well as pure speculation, and, since the guiding thread of understanding is mostly lacking, the presentation may seem somewhat haphazard.

a) Swimming motility of artificially energized cells.

Measurement of the proton flux coupled to motor rotation requires that cells swim vigorously for the following reasons. In order to detect the rotation-dependent portion of the flux on the background of much larger unrelated fluxes, it is advantageous to maximize the speed of the motor, hoping that this also maximizes the flow of translocated protons. The motors of glycolyzing cells spin fastest when the filaments join in a bundle, and the cells are swimming. Under those conditions the rotation rate is close to the highest speed observed when the motor is driving only a very small flagellar hook (Lowe et al. 1986). Graeme found that filaments of the tumbly Streptococcus mutant SM29 spin only about half as fast, presumably because the torque required to rotate an individual flagellum is much larger than when the

filaments are joined in a bundle (unpublished). Since rotation of the motor is to be stopped by cross-linking the flagella with antibody, the use of hook mutants or sheared cells to obtain high rotation speeds is not an option. Also knowledge of the motor's speed during the measurement is required to compute the stoichiometry of protons to revolutions. The only practical technique available for measuring large motor rotation rates, namely the optical detection of bundle frequencies from vibrations of the cell body, relies on coherent rotation of the filaments in a bundle. Finally, one can calculate the torque of the motor by observing the counter-rotation of the swimming cell's body, which allows an estimate of the efficiency of energy conversion.

A very large artificial protonmotive force is required to induce swimming in starved Streptococcus SM197. I monitored swimming motility during the experiment described in Fig. 3.4 of Chapter 3 and found that only 30% of the cells swim after a 1:100 dilution of external potassium, corresponding to a nominal Δp of -118 mV, and hardly any cells swim at a protonmotive force of -59 mV or less. Manson et al. (1977) saw a threshold Δp of -80 mV for initiation of swimming in Streptococcus wild-type strain V4051 with the chemoattractant L-leucine added to favor counterclockwise motor rotation. These thresholds are substantially larger than the minimum Δp required for rotation of tethered cells, which lies somewhere between -5 mV and -25 mV (Manson et al. 1980; Conley & Berg 1984; Khan et al. 1985). The threshold for swimming seems to be lower in metabolizing cells. Khan and Macnab (1980b) measured a threshold Δp of -30 mV to -50 mV for swimming in metabolizing cells of Bacillus subtilis that were partially deenergized using the uncoupler DNP. Shioi et al. (1980) obtained a threshold value of -30 mV by

reducing the membrane potential of metabolizing B. subtilis cells using valinomycin and large external potassium concentrations. They also determined the threshold for tethered cell rotation and found it to be very similar, between -25 mV and -40 mV. On the other hand, Matsuura et al. (1979) successfully starved B. subtilis and needed a protonmotive force of -100 mV to induce swimming. I can think of two effects that may contribute to this discrepancy. One is a possible hydrodynamical requirement for fast rotation of the individual flagellar filaments before they can efficiently join in a bundle. Once the bundle is formed and stabilized by the flow profile it generates (Anderson 1975), as is the case for metabolizing swimming cells, the protonmotive force may be reduced below the threshold for bundle formation without causing the bundle to disintegrate. Another, in my opinion very likely, possibility is that the artificially generated protonmotive force is lower than what we calculate it to be using the Nernst equation, as I will discuss below in more detail.

The generation of a large Δp during a flux measurement underlies several constraints. The potassium dilution ratio is limited because the stock cell suspension should not be kept much denser than 10^{10} to 10^{11} cells/ml, while a density of at least 10^8 to 10^9 cells/ml in the final sample is desirable for low-noise resolution of the proton uptake. The size of a pH-shift is constrained by the preference to avoid long-term exposure to non-physiological pH values above pH 9 and the fact that flagellar motility is impaired at a pH lower than pH 6 (Manson et al. 1977; Shioi et al. 1980). After the experiments described in the following paragraphs had led us to our final choice of buffers and ions in the starvation and energization media, Graeme performed an extensive

series of tests that became known as "vigorometry", a qualitative determination of how fast and how long cells swim under various conditions of artificial energization. The optimal method turned out to involve a pH-shift from pH 8.5 to pH 6.5 and a simultaneous 20- to 100-fold dilution of the external potassium after pretreatment of the cells with valinomycin.

b) Generating a large artificial protonmotive force.

Graeme and I invested much effort in finding ways to generate an artificial protonmotive force large enough to support fast and prolonged swimming. Most of my studies were done with tethered cells, because flagellar motility is most easily visualized this way and our major problem was not related to a difference between tethered and swimming cells. It became clear early on that the nominal value of the protonmotive force calculated from the shift in the external potassium concentration and the change in the external pH (see §1.2.d), Δp_{nom}, is not representative of the protonmotive force acting across the membrane, Δp. As discussed in Chapter 2, the saturation of the speed of tethered cells as a function of the nominal potassium diffusion potential and the comparatively high rotation rate of metabolizing cells suggests that the generation of an artificial membrane potential becomes inefficient at low external potassium concentrations. A similar saturation of the rotation speed is found when the nominal protonmotive force is composed primarily of a pH-gradient. Possible deleterious effects of low external K^+ concentration or low external pH on the motor itself do not seem to be responsible: when glycolyzing cells are subjected to the same procedure, they speed up.

There are other indications that the protonmotive force saturates at large values of Δp_{nom}. Hirota and Imae (1983) measured the protonmotive force across the membrane of an alkalophilic Bacillus as a function of the external potassium concentration, $[K^+]_e$, in presence of valinomycin and found that Δp was significantly lower than Δp_{nom} at $[K^+]_e$ below 1 mM. Shioi et al. (1980) saw similar deviations from the nominal Δp at low external potassium concentrations. Kashket and Wilson (1973) also obtained a lower artificial protonmotive force than expected from the Nernst equation and suggest that this may be caused by a partial barrier to ion diffusion between the cytoplasmic membrane and the bulk phase of the medium presented by the cell wall. There has been some debate about the extent to which protons pumped out of a bacterium or mitochondrion via the ATPase or an electron transport chain equilibrate with the bulk phase of the external medium (Kell 1979). For a metabolizing cell at steady state the net flow of any ionic species across the membrane vanishes. Measurements of the membrane potential or the pH-gradient, which often rely on the steady-state partitioning of some tracer substance, would therefore not be affected by any appreciable resistance to ionic flow between the conduction sites in the membrane and the bulk medium. In the case of artificially energized cells, however, there is net translocation of ions, H^+ flowing into and K^+ out of the cell, and any such permeability barrier would lower the protonmotive force acting across the membrane. The experiments described in Chapter 3, showing that addition of FCCP to the membrane dramatically increases the flux of protons in response to an artificial Δp, speak against any significant contribution of such a permeability barrier, unless one postulates that FCCP acts by circumventing it.

Another possibility is that the protonmotive force has dropped significantly from its initial value by the time tethered cell rotation rates are measured, which for technical reasons is about 20 s after energization. The calculations of Δp presented in Chapter 3 show that the protonmotive force may in fact decay appreciably over this period, due mainly to acidification of the cytoplasm. However, it is not clear why this effect should be more pronounced at high Δp_{nom}, since the initial rate of proton uptake is proportional to the potassium diffusion potential. The proton flux is more than twice as large in response to an equivalent pH-gradient, while no such difference is seen in the saturation of rotation rates. Another observation speaking against this interpretation is that tethered cell rotation rates increase slightly by 10% to 20% over the first minute following energization in a strong buffer. Fig. 3.9A of Chapter 3 does not show this effect, because the rise in the pH of the weakly buffered external medium accelerates the decay of Δp.

It appears that at this point the rotation rate of tethered cells is our best measure of the protonmotive force, while the nominal Δp is not a useful estimate at values much above -80 mV. The evidence for this is still somewhat circumstantial and a direct measurement of the protonmotive force in glycolyzing and artificially energized cells would be helpful towards understanding the origins of speed saturation at high Δp_{nom}.

c) Observations related to Na^+/H^+ antiport.

Until recently, most experiments on Streptococcus in our lab were performed using sodium phosphate as a buffering species. When the

external potassium concentration was reduced to generate a membrane potential, we generally added sodium chloride to keep the ionic strength constant. Shahid Khan found that tethered cells spin for a much shorter period of time when choline chloride is used to replace potassium chloride and suggested that this may be due to electroneutral exchange of sodium for protons across the membrane. I have presented proton flux measurements that point to the existence of such a mechanism in Chapter 3. Here I will summarize my observations on tethered cells that seem to be related to sodium/proton antiport.

Cells of SM197 starved in a buffer free of Na^+ and Li^+ (1 mM K_2HPO_4/KH_2PO_4, 0.1 mM EDTA/KOH, 0.2 M KCl, 0.2 M choline Cl, pH 7.5) rotated counterclockwise when the external choline Cl was replaced by NaCl or LiCl. They sped up gradually over 1 to 2 min and spun for longer than 10 min. The final speed increased when the external sodium concentration was raised, at least up to $[Na^+]_e$ = 0.1 M. The rotation stopped after addition of DNP or nigericin to the medium. Cells did not spin when the same experiment was performed at pH 8.5. After starvation in sodium-free medium these cells are likely to have a low internal sodium concentration. Addition of external sodium provides a driving force for Na^+/H^+ antiport, leading to extrusion of protons from the cytoplasm as shown in Chapter 3, Fig. 3.7A. Apparently Li^+ can replace Na^+ equivalently in this function. Gradually a proton concentration gradient builds up, which in turn drives the flagellar motor. The steady-state value of this pH-difference rises as the sodium driving force is increased. DNP or nigericin dissipate the proton chemical potential and thus stop rotation of the motor. This eliminates the exotic possibility that the motor may be directly driven by a sodium

gradient. At pH 8.5 the absolute H^+ concentration may be too low to allow efficient proton pumping.

Cells starved in a buffer containing sodium (1 mM K_2HPO_4/KH_2PO_4, 0.1 mM EDTA/KOH, 0.2 M KCl, 0.2 M NaCl, pH 7.5) rotated clockwise when the external NaCl was replaced by choline Cl. Again they sped up gradually and spun at a steady speed for over 6 min. These cells presumably contain a substantial amount of Na^+ after starvation. Even though metabolizing cells extrude sodium actively (Harold & Kakinuma 1984), the membrane has a significant passive conductance to Na^+ (Maloney 1977), such that the cessation of active transport during several hours of starvation allows for equilibration of internal and external sodium concentrations. Removal of external sodium drives the antiport in its presumed physiological direction, leading to uptake of protons (see Chapter 3, Fig. 3.7B). The cytoplasm gradually acidifies and the pH-gradient drives the flagellar motor.

Cells starved in a sodium-free buffer (1 mM K_2HPO_4/KH_2PO_4, 0.1 mM EDTA/KOH, 0.2 M KCl, pH 7.5) and energized by diluting the external potassium 20-fold with choline spun for about 10 min, slowing down gradually. If, after they had stopped, the external choline was replaced by Na^+ or Li^+, the cells started spinning, sped up over 5 min, and reached a final speed substantially higher than immediately after the initial energization. A possible interpretation is that the cells slow down and stop rotating in choline, because the flux of protons into the cell has acidified the cytoplasm, causing the decay of Δp. As outlined in Chapter 3 (Fig. 3.9C), the membrane potential at this point is not substantially lower than its initial value just after energization. Addition of external sodium drives the Na^+/H^+ antiport,

pumping protons out of the cell. The pH of the cytoplasm rises, and, since the membrane potential is still intact, an inwardly directed protonmotive force results. Since the external sodium concentration is large, proton exchange may even reverse the pH-gradient, leading to a Δp higher than the initial membrane potential after energization in choline.

Cells starved in a medium containing large amounts of external sodium (0.1 M Na_2HPO_4/NaH_2PO_4, 0.1 mM EDTA/KOH, 0.2 M KCl, pH 7.5) and energized by diluting the external potassium 20-fold with sodium spun for 15 min, slowing down gradually. In this case the sodium driving force is not very large. Nevertheless, the antiport seems to be working fast enough to avoid rapid acidification of the cytoplasm, by equilibrating the sodium and proton gradients. Thus the cells spin at about the same initial speed but for a substantially longer period of time than cells energized in absence of sodium.

When the starved cells in the above experiment were instead shifted to a sodium-free medium with a 20-fold dilution of potassium by choline, they spun slower and stopped after only 1 to 2 min. In this case the antiport is working to dissipate the Δp. An outwardly directed sodium driving force leads to uptake of protons, acidification of the cytoplasm, and rapid cessation of flagellar rotation.

When the same starved cells were energized by lowering the pH of the external buffer, they also slowed down rapidly and stopped after 1 to 2 min. The sodium driving force in this experiment is probably low and the Na^+/H^+ antiport tends to keep the pH-gradient small too. Protons rapidly flow into the cell through the exchanger, leading to a fast decay of Δp.

Cells starved in a sodium-free medium (1 mM K_2HPO_4/KH_2PO_4, 0.1 mM EDTA/KOH, 0.2 M KCl, pH 7.5) and energized by lowering the external pH rotated steadily for over 15 min. Again there is no sodium driving force, but now the absolute internal sodium concentration is too low to allow the exchanger to operate at any appreciable rate. As in the experiments at high pH, the antiport doesn't participate in ionic conduction.

The interpretation of the above observations in terms of sodium/proton antiport requires that this hypothetical exchange mechanism account for a large portion of the proton flux through the membrane of artificially energized cells when absolute proton and sodium concentrations are high. Since the presence of such a major conduction pathway could only hinder the detection of motor-related proton flux, and the cells can be energized efficiently in the absence of sodium, we preferred to omit sodium from all our media.

d) Observations regarding choline.

After sodium had been banned from the Streptococcus buffers, I decided to use only choline as the external cation to replace potassium, since it is generally assumed to be impermeant. This turned out to be a trap. In order to induce vigorous swimming in artificially energized cells of SM197 one needs to apply a potassium diffusion potential and a pH-gradient simultaneously. As it turns out, although tethered cells spin very well in response to a potassium dilution with choline or a pH-shift alone, rotation ceases within 1 or 2 min when both are applied simultaneously. This was a very surprising result, and I will summarize some of the related observations. Since I do not understand these

effects, the presentation of the results will not be followed by wise interpretations as in the preceding paragraphs.

Cells used in the following experiments were starved and tethered in a buffer containing 10 mM MES, 10 mM TAPS, 0.1 mM EDTA at pH 8.5 and either 0.2 M KCl or 0.2 M KCl + 0.2 M choline Cl as salts. Tetren was used as a chelator instead of EDTA in buffers containing Mg^{2+} or Ca^{2+}. Unless otherwise noted, the cells had also been treated with 2 μg/ml valinomycin for 2 min which was removed again from the external medium before energization. A potassium diffusion potential was generated by a shift to the same buffer containing 2 mM KCl and the remainder of the ionic strength provided by choline Cl, NaCl, or $MgCl_2$. A pH-gradient was usually imposed by shifting the external pH from 8.5 to 6.5.

After a dilution of potassium with choline or a pH-shift alone, these cells rotated for 10 to 15 min, as described in part (c). After a shift to choline Cl at low pH, however, they slowed down rapidly, and all cells stopped after 1 to 2 min. At this point choline could be replaced by sodium or magnesium, and the cells started spinning fast and steadily within one minute, only to stop once more when choline was again substituted for the other cations. The addition of 1 mM Ca^{2+} and 1 mM Mg^{2+}, ions involved in stabilizing the membrane, did not alter these observations. Even cells glycolyzing in starvation buffer with 10 mM glucose slowed down and stopped rapidly after a shift to choline Cl at low pH. This happened irrespective of whether these cells had been pretreated with valinomycin. When shifted to NaCl or $MgCl_2$ at low pH, glycolyzing cells sped up dramatically.

Cells starved in presence of 0.2 M KCl and 0.2 M choline Cl spun for a long time in response to a pH-shift alone, indicating that the

presence of choline at low pH by itself is not causing the rapid decay of motility. A dilution of the potassium with choline at low pH still caused rapid cessation of spinning in starved cells, but the effect on glycolyzing cells was less pronounced.

I found that the collapse of flagellar rotation in choline at low pH did not occur if the cells were first brought to low pH, allowed to spin for 1 min, and then shifted to choline. Under these conditions, speed and time course of tethered cell rotation were comparable to those seen in NaCl or $MgCl_2$. Cells energized in the reverse sequence, however, failed to spin any longer than after a simultaneous shift of potassium concentration and pH.

These experiments strongly suggest that choline is more than an inert, innocent bystander to membrane transport. In light of the effects on glycolyzing cells it seems that the external conditions of low potassium, high choline, and low pH directly affect the protonmotive force rather than blocking generation of an artificial Δp, say, by hindering transport of K^+ by valinomycin. Of course, a direct action on the motor cannot be excluded. In either case the effect is readily reversible when choline is removed from the medium. I have found few literature references to problems with choline, and I don't see them pointing in a very revealing direction.

The fishy smell emanating from jars of choline chloride suggests that they may contain impurities. One of the decomposition products of choline is trimethylamine (Collin 1957), which, as a weak base, could permeate the membrane in its uncharged form and thus serve as a proton conductor. However, these effects should be less pronounced at low pH, where most of the base is charged. Also, to efficiently clamp the

cytoplasmic pH to the external pH, the weak base concentration would have to be of the order of the cytoplasmic buffering capacity, ca 70 mM, which seems somewhat high for an impurity in 0.2 M choline Cl. Finally, I have seen that a pH-shift alone can support prolonged rotation in choline. Recently Kashket (1985a, 1985b) has reported that choline chloride interferes with the stimulation of the membrane potential by external potassium in K^+-depleted cells of E. coli at pH 8.15 and suggested that choline may prevent active uptake of K^+. It is not clear how this could cause the collapse of Δp in artificially energized cells, but maybe both observations are the result of a different, unknown effect of choline.

As a final result of all these experiments we picked Mg^{2+} for the external cation. After a shift to $MgCl_2$ at low pH cells spin fast initially and slow down gradually over about 10 min with a time course similar to that seen in NaCl. The initial proton flux under these conditions is relatively low, as reported in Chapter 3. Finally, Graeme determined that cells energized in this way swim fairly vigorously for a time period long enough to perform a measurement of the bundle frequency.

For the sake of completeness I should also explain the choice of buffering species. To simplify the interpretation of flux measurements it seemed preferable to eliminate as many membrane-permeating compounds as possible from the medium. S. lactis and other bacterial species are known to use membrane-bound anion exchangers that transport inorganic phosphate (Ambudkar et al. 1986). We therefore moved away from sodium phosphate as a buffering species and used large ions with sulfonate groups, to which biological membranes have a relatively low

permeability. The specific choice of dissociation constants is discussed in Chapter 3.

§4.4 RESULTS

a) Rotation-dependent proton flux.

When I first observed the flux timecourse shown in Fig. 4.1A, I suspected that my antibody stock contained potassium ions, thus reducing the potassium diffusion potential across the cell membrane on addition to the sample, which would cause the observed decrease in the proton flux. I therefore measured the K^+ concentration in 2 ml of buffer D [$MgCl_2$ 6.5] before and after addition of 50 μl of antibody stock. I used a K^+-electrode (Orion 93-19) and a sleeve junction reference electrode (Orion 90-01) filled with a slightly turbid solution of $AgNO_3$ in 0.067 M $MgCl_2$. On addition of the antibody the potassium concentration changed from $(3.74 \pm 0.05)\times10^{-4}$ M to $(3.67 \pm 0.10)\times10^{-4}$ M. Apparently the dialysis procedure had provided for complete exchange of potassium for magnesium in the antibody stock.

Another plausible explanation of the observed flux drop would be that the protein contained in the antibody stock solution significantly increases the buffering capacity of the cell suspension, thus leading to a slower change in the external pH, even though the membrane proton flux remains unchanged. I measured the external buffering capacity of a cell suspension in buffer D [$MgCl_2$ 6.5] before and after a 1:100 addition of antibody stock and found it to increase by at most 1% or 2%, clearly insufficient to explain a 20% drop in the rate of pH-change. The buffering capacity was reproducible to within about 3% in successive cell samples energized under identical conditions and showed no correlation with the presence or absence of antibody.

The drop in the rate of proton uptake could be due to the fact that

cells coagulate in tight clumps, thus limiting diffusive flux of protons through the weakly buffered medium to the cell surface. To test for this possibility I measured the antibody-dependent flux change in cells of the mutant V4058. Cells of this strain have the same size and shape as those of wild-type V4051 or the run-mutant SM197. They show many flagella, on average 7 per cell, but don't seem to rotate them: metabolizing cells are strictly non-motile, both in suspension and when tethered. The addition of 50 μl of flagellar antibody stock after energization agglutinates these cells into large clumps but changes the proton flux only by $\Delta J(V4058) = (-0.1 \pm 2.5)\times10^4$ H^+/cell/s. Under identical conditions cells of strain SM197 showed a flux change of $\Delta J(SM197) = (5.5 \pm 2.3)\times10^4$ H^+/cell/s. These measurements also eliminate the hypothesis that the antibody affects some other conductance in the membrane as well as all the suggestions forwarded in the preceding paragraphs.

Finally, a more direct indication for the involvement of flagellar motility comes from experiments in which cells of SM197 were pretreated with flagellar antibody. Cells that had been incubated with antibody in buffer C [KCl 8.5] and thus were already non-motile and agglutinated in clumps at the time of dilution showed a flux change of only $\Delta J(non\text{-}motile) = (0.8 \pm 3.6)\times10^4$ H^+/cell/s when 50 μl antibody was added to a 2 ml sample at 31 s after dilution. By contrast, addition of antibody to cells that had not been pretreated before dilution caused a flux change of $\Delta J(motile) = (4.9 \pm 3.2)\times10^4$ H^+/cell/s. In summary, these preliminary experiments convinced me that the flux drop was due to the inhibition of flagellar rotation, and I will therefore refer to it as the "rotation-dependent flux" or the "motor flux", where one must keep

in mind that only the fraction of the flow of protons through the motor which is coupled to rotation can be measured.

I then studied the dependence of the flux change on the concentration of antibody used. Fig. 4.4 shows the results of one such experiment, a plot of ΔJ^+ as a function of the volume of antibody stock added to a 2 ml sample at ca 32 s after dilution. As mentioned in §4.2.c, ΔJ^+ is negative when nothing is added to the sample, although the deviation from an exponential flux time course was relatively small in this experiment. The flux change increases with increasing amounts of antibody added and eventually saturates at about 5×10^4 H^+/cell/s. Although no swimming motility is observed at antibody concentrations as low as 10 μl stock per 2 ml suspension, it is possible that partial cross-linking of filaments inhibits formation of a bundle, while some filaments continue rotating. I routinely used 20 μl of stock in the following experiments, since the flux drop was clearly measurable at those concentrations, and I did not want to risk exhausting my limited supply of flagellar antibodies.

In order to deduce the total rotation-dependent flux from the flux drop seen on addition of finite volumes of antibody stock, a quantitative interpretation of the dependence of flux inhibition, ΔJ^+, on antibody concentration, [Ab], is useful. I assumed a simple dynamical model for the interaction between antibodies and the flagellar bundle: A cross-linked filament can break loose at a rate independent of the concentration of antibody. However, once it is spinning, the antibody molecules reattach at a rate proportional to the antibody concentration. Under these assumptions the flux drop is given by

$$\Delta J^+ = a + b \frac{[Ab]}{[Ab]+c}.$$

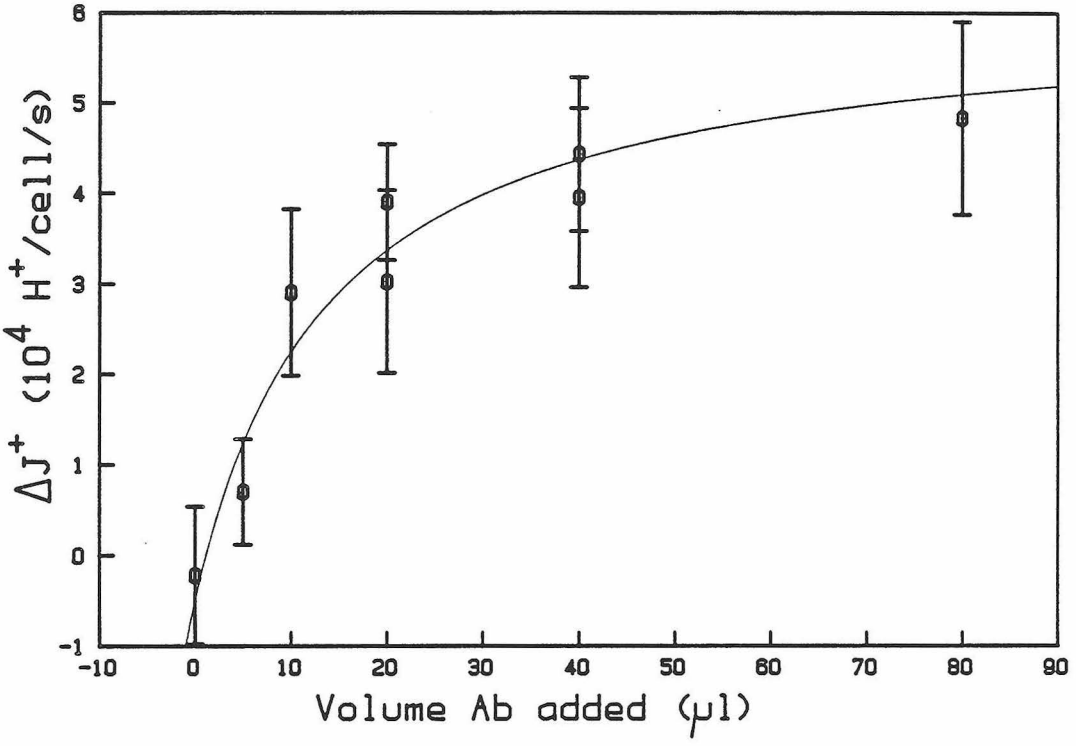

Fig. 4.4. The change in the proton flux, ΔJ^+, as a function of the volume of antibody stock added to the cell suspension.

The parameters a, b, and c were determined form a weighted least-squares fit, yielding the curve drawn through the data in Fig. 4.4. Half-maximal inhibition of the proton flux is obtained by adding 14 μl of antibody stock to a 2 ml suspension at a cell density of ca 10^9 cells/ml. I will use this curve to extrapolate from the antibody concentrations used during the experiment to the total rotation-dependent flux when computing stoichiometries in part (d). All the measurements of ΔJ quoted in the following paragraphs are uncorrected.

Fig. 4.5A shows both the total proton flux and the flux inhibited by addition of antibody to the sample as a function of time after energization. It is seen that the total flux decays much more rapidly than the fraction dependent on antibody, which changes only by 35% from 22 s to 48 s after dilution. Measurements at earlier times are not practical, because the large total flux inhibits the resolution of the rotation-dependent part. At times much later than 60 s swimming motility deteriorates, making interpretation of the measurements unreliable. For ease of later comparison the antibody-dependent flux is plotted again on a different scale in Fig. 4.6A.

The dependence of ΔJ on the temperature of the energization buffer is shown in Fig. 4.5B. Again, both the total flux at the time of antibody addition, 30 s after dilution, and the ensuing flux drop are plotted. The initial proton flux, J(0), measured in these same samples is plotted in Fig. 3.10A of Chapter 3. Even though J(0) increases dramatically with temperature, the proton flux decays more rapidly a high temperatures, and thus J(30s) is roughly independent of temperature. Consequently the resolution of ΔJ does not vary much with temperature either. The rotation-dependent flux is shown again on a

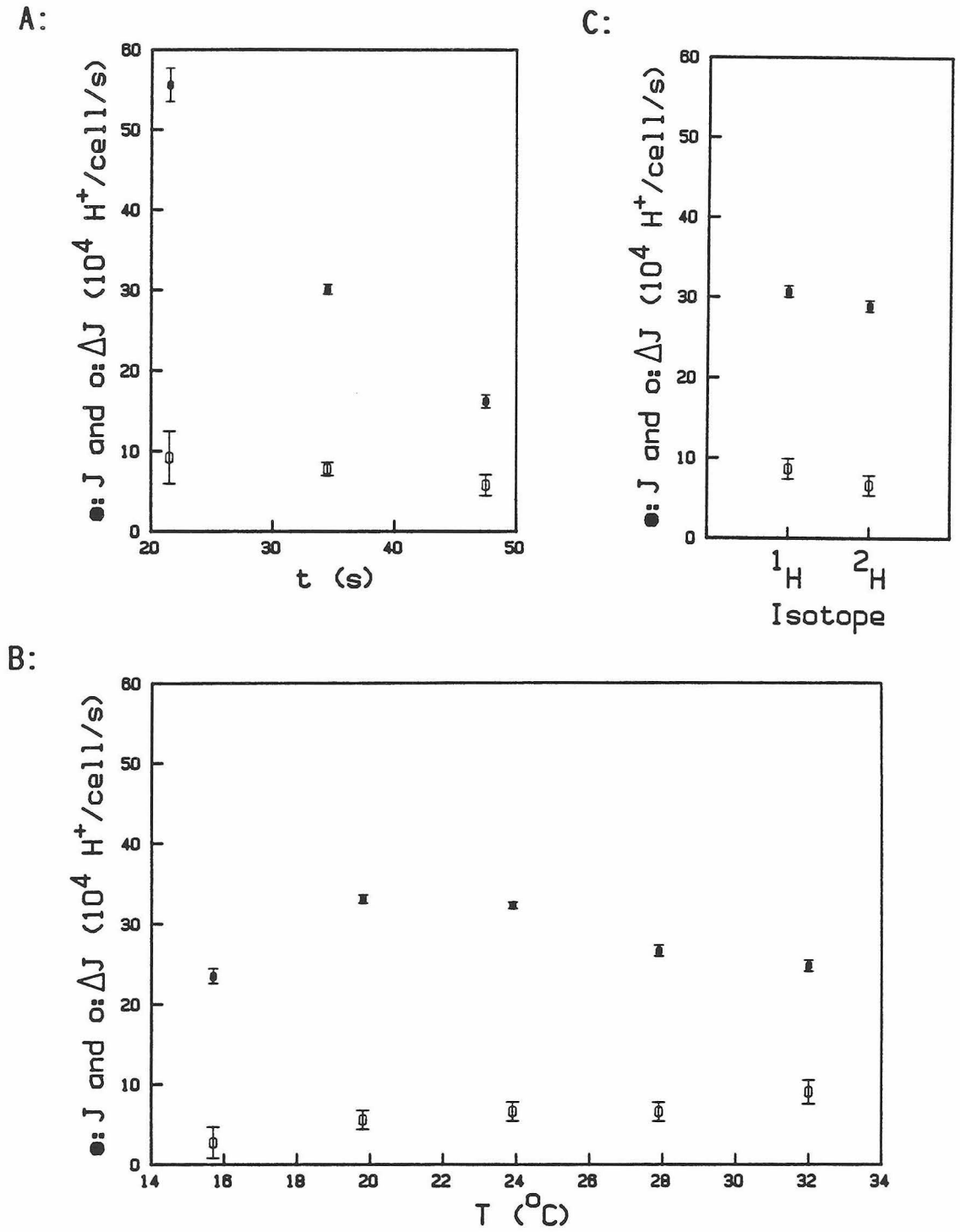

Fig. 4.5. Total proton flux (closed symbols) and rotation-dependent proton flux (open symbols) as a function of **A:** time after energization, **B:** temperature, and **C:** hydrogen isotope in the water.

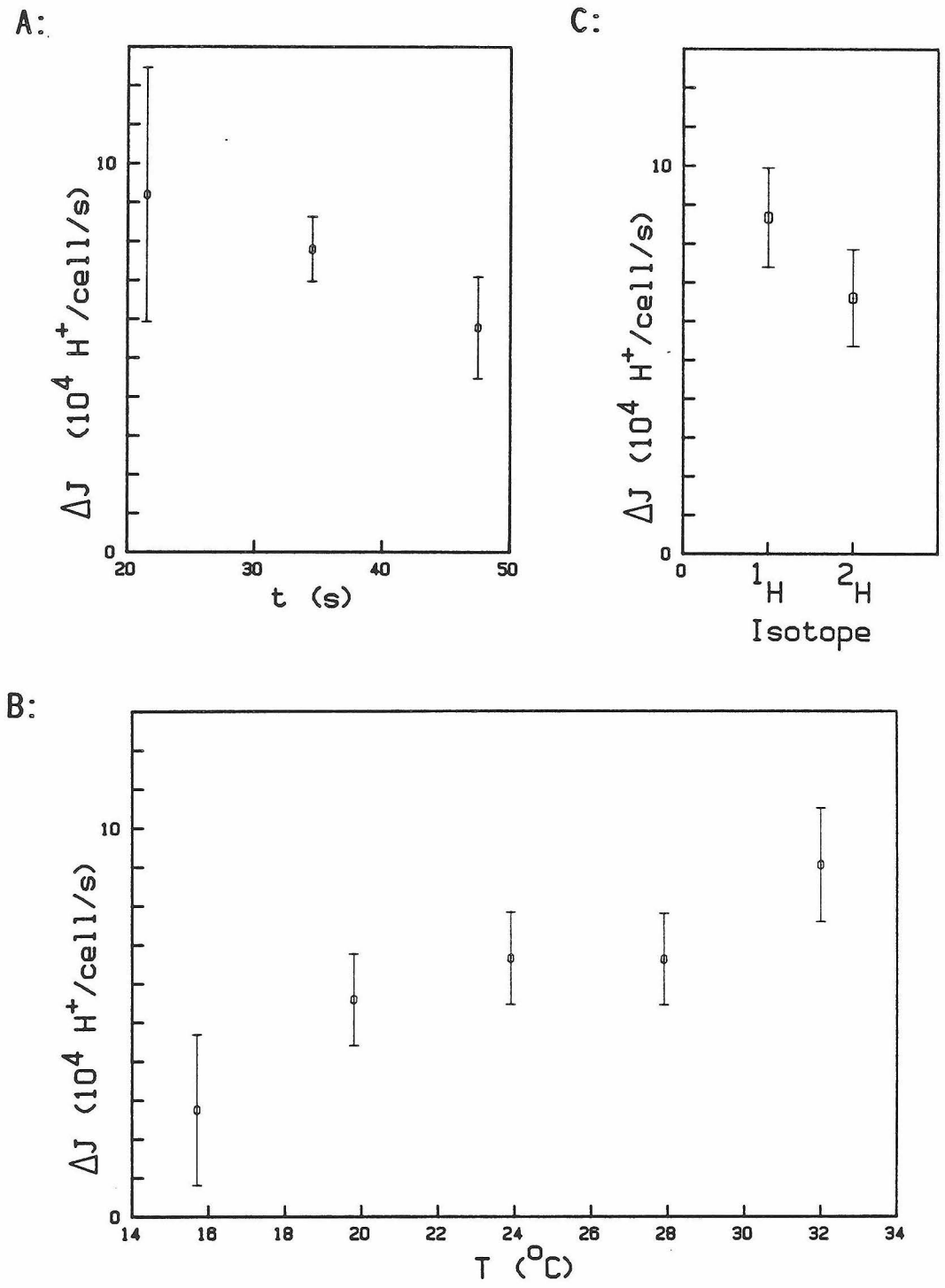

Fig. 4.6. Rotation-dependent proton flux as a function of **A:** time after energization, **B:** temperature, and **C:** hydrogen isotope in the water. Data replotted from Fig. 4.5.

different scale in Fig. 4.6B and increases by a factor of 3 as the temperature varies from 16°C to 32°C.

Fig. 4.5C shows a comparison of cells energized in H_2O and D_2O. As reported in Chapter 3, the initial flux is lower in D_2O than in H_2O but decays less rapidly. As a consequence the total flux at the time of antibody addition is virtually identical under the two conditions. The rotation-dependent flux is somewhat larger in H_2O, by a factor of 1.31 ± 0.24. It is plotted once more in Fig. 4.6C.

b) Motor speed.

Direct measurements of the bundle rotation frequency via the small vibration of the swimming cell body, as described in §4.2.d, are very tedious in the case of artificially energized cells. Since they swim less vigorously than energized cells, the signal due to bundle rotation is rather faint and can only be resolved after several hundred seconds of integration. But motility slows markedly over the first minute, and thus a single bundle frequency measurement requires the successive energization of up to 50 samples, each of which is analyzed over an interval of only a few seconds. In the resulting power spectrum the high frequency peak, corresponding to rotation of the bundle, often overlaps significantly with the much larger low frequency peak, making an interpretation of the spectrum more difficult. I therefore chose a different method to determine the rotation rate of motors in swimming cells.

This technique relies on the fact that the Reynolds number characterizing the fluid flow around a swimming bacterium is very small. Rotation of the helical flagellar bundle relative to the infinite medium

at the rotation rate f_F generates a thrust along the axis of the helix, which results in translation of the organism at velocity u relative to the medium. Also, since the external torque on the bacterium vanishes, the cell body must rotate in the direction opposite to the bundle at a rotation rate f_B. Intuitively it appears that the ratio of any two of the quantities f_F, u, and f_B depends only on the geometry of cell body and flagellar bundle but not on the absolute values of those quantities or the viscosity of the medium. Rigorously this can be seen as follows: When inertial forces are negligible compared to viscous forces, the Navier-Stokes equation for incompressible flow reduces to

$$\eta \, \Delta\vec{v} + \vec{\nabla}p = 0$$

where η is the dynamic viscosity of the medium, $\vec{v}$ is the velocity of the fluid relative to the lab frame, and p is the pressure, excluding the hydrostatic component. The boundary conditions are that $\vec{v}$ vanish at infinity and that $\vec{v}$ be equal to the velocity of the boundary at the surface of the bacterium. Consider the case where the bundle rotates in a medium of viscosity η_1 at a frequency f_1 relative to the body. Since the bundle has no symmetry axis, and the body in general does not rotate about its symmetry axis, the flow is unsteady, even in the rest frame of the bundle. Let the flow $\vec{v}_1(\vec{x},t)$ with pressure $p_1(\vec{x},t)$ be the solution corresponding to η_1 and f_1. The flow field does not depend on the viscosity since simply scaling the pressure provides a solution to the Navier-stokes equation: $\vec{v}(\vec{x},t) = \vec{v}_1(\vec{x},t)$ and $p(\vec{x},t) = (\eta/\eta_1)\, p_1(\vec{x},t)$ are the flow and pressure field corresponding to η and f_1. Similarly a solution for a different value of the motor frequency, f, is found by scaling the flow velocity and time dependence everywhere in the medium: $\vec{v}(\vec{x},t) = (f/f_1)\, \vec{v}_1(\vec{x},(f/f_1)t)$ and $p(\vec{x},t) = (f/f_1)\, p_1(\vec{x},(f/f_1)t)$ is the

solution corresponding to motor frequency f and viscosity η_1. Therefore the average translation velocity, u, as well as the average rotation frequency of the cell body relative to the lab frame, f_B, are proportional to the rotation rate of the bundle relative to the body, f.

Both u and f_B are readily measured for glycolyzing and artificially energized cells by tracing their paths on the video screen during playback of the recording and counting the number of wobbles of the cell body's image in a given period of time. I also determined the bundle frequency, f_F, in swimming metabolizing cells of the same cell stock from the vibration of the cell bodies. I then computed the resulting ratios f_F/u and f_F/f_B and, making the assumption that the geometry of swimming is the same in artificially energized and glycolyzing cells, I used these ratios to calculate the bundle frequency of artificially energized cells from their swimming speed or their body roll frequency.

To verify this critical assumption I measured u, f_B, and f_F for glycolyzing cells at temperatures between 12°C and 24°C. Over this temperature range the viscosity of water changes by about 36%. More importantly, the torque of the motor decreases significantly at lower temperatures, leading to a large decrease in the swimming speed and bundle frequency (Lowe et al. 1986). Fig. 4.7A shows a plot of the bundle frequency, f_F, as a function of temperature. Figs. 4.7B and 4.7C are plots of the ratios f_F/u and f_F/f_B respectively as a function of temperature. Even though the bundle frequency was lower by a factor of 3 at 12°C compared to 24°C, the swimming speed and body roll frequency varied proportionally over the entire range. Thus f_F/u and f_F/f_B were independent of temperature with mean values

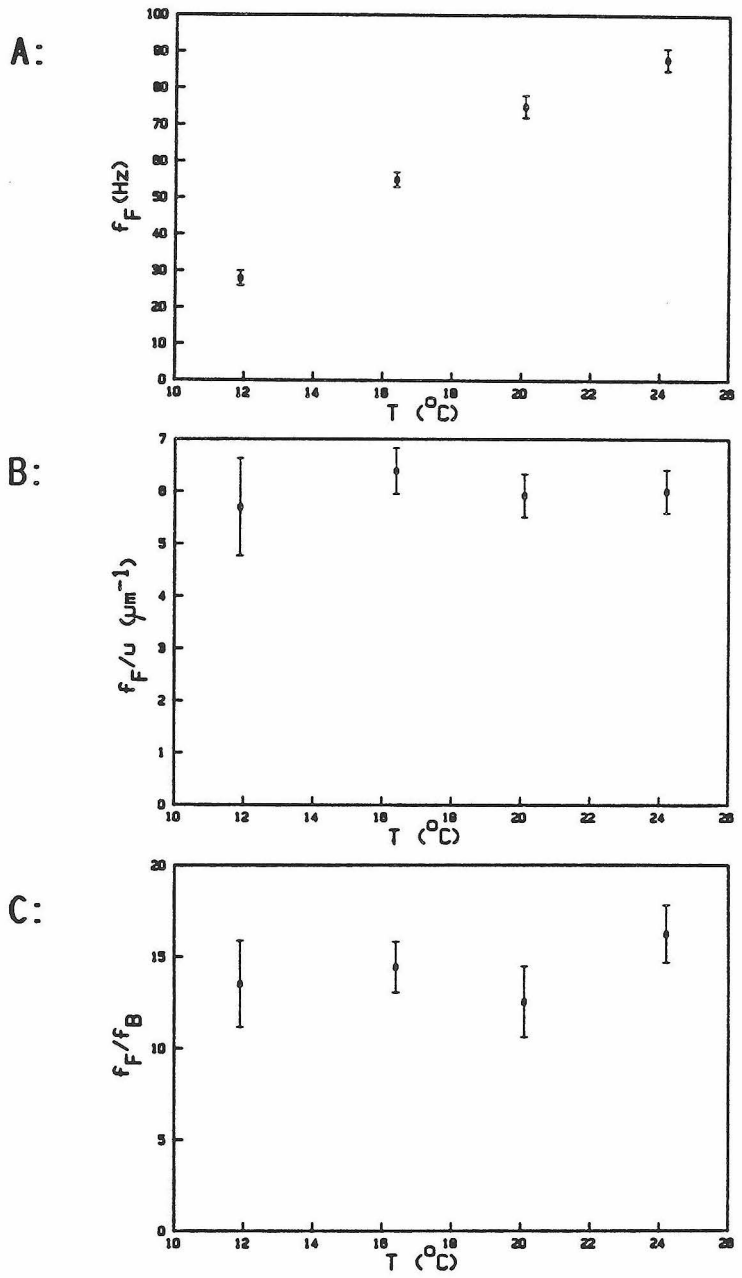

Fig. 4.7. Effects of temperature on the motility of glycolyzing swimming cells.

A: The flagellar bundle frequency as a function of temperature.

B: The ratio of flagellar bundle frequency to swimming speed as a function of temperature.

C: The ratio of flagellar bundle frequency to body roll frequency as a function of temperature.

$$\frac{f_F}{u} = (6.07 \pm 0.23)\ \mu m^{-1}$$

and

$$\frac{f_F}{f_B} = 14.48 \pm 0.85.$$

This result is reassuring since the swimming speed and body roll frequency seen at 12°C are comparable to those I measured on artificially energized cells. The uncertainties in the ratios f_F/u and f_F/f_B result mainly from the statistics in the population average of u and f_B. The swimming speed shows less variation over the population than the body roll frequency. I attribute this to the fact that variations in the size of the cell body affect its translational drag coefficient less than the rotational drag coefficient. For this reason I decided to use the swimming speed in deducing the bundle frequency of artificially energized cells. I still measured body roll frequencies in all samples since the motor frequency, $f^{(S)}$, is given by the sum of f_F and f_B.

Fig. 4.8A shows the motor frequency as a function of time after dilution. As explained in §4.2.e, these cells were artificially energized under the same conditions as for motor flux measurements. Therefore these are the speeds at which motors were spinning just before antibody was added in the samples shown in Fig. 4.6A.

The temperature dependence of the motor speed of swimming artificially energized cells is shown in Fig. 4.8B. The speeds were measured over the interval from 30 s to 35 s after dilution, corresponding to the 5 seconds following addition of antibody in the motor flux measurements of Fig. 4.6B. The speed depends approximately

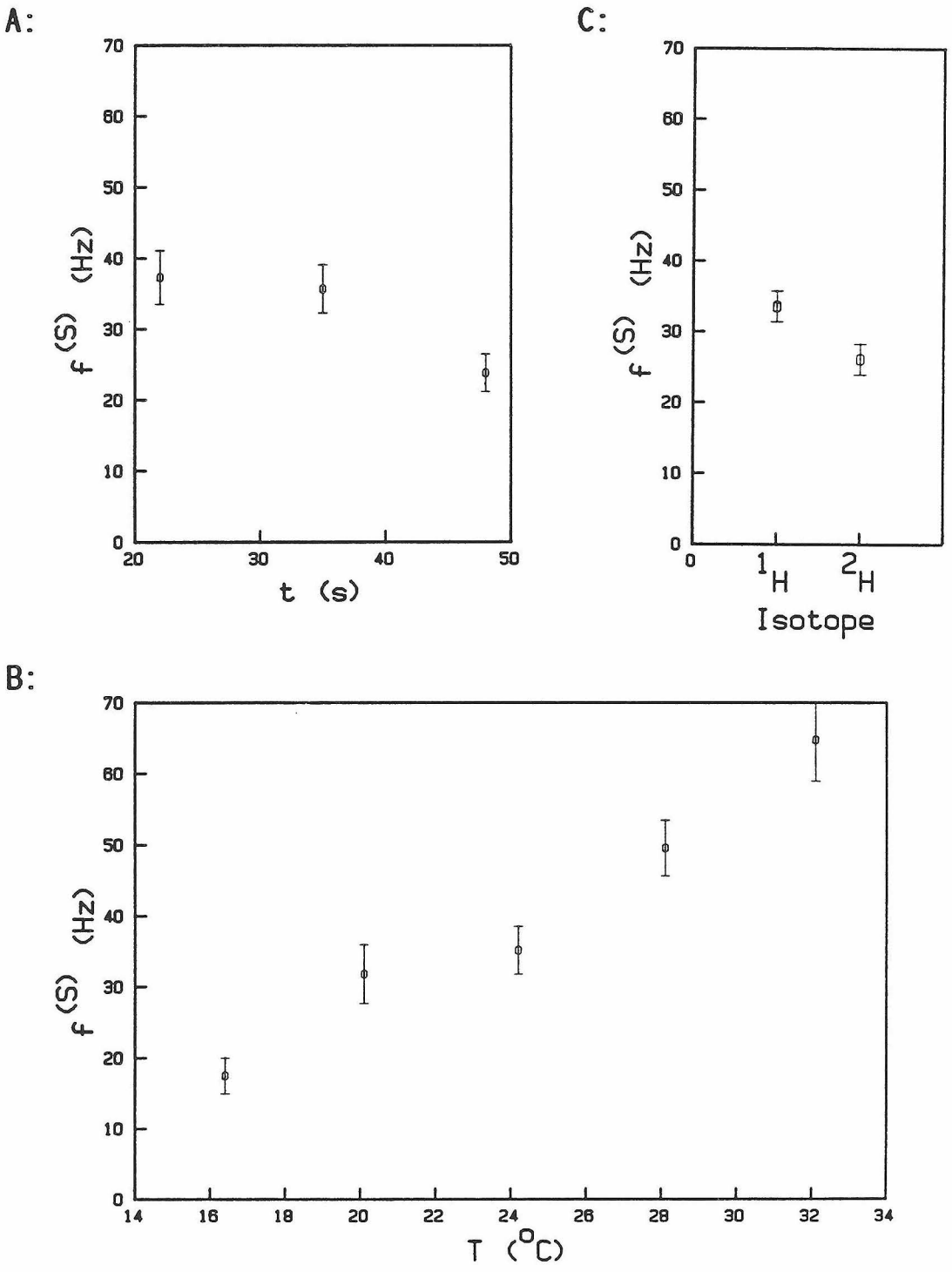

Fig. 4.8. The motor rotation rate in swimming artificially energized cells as a function of **A:** the time after energization, **B:** the temperature, and **C:** the hydrogen isotope in the medium.

linearly on temperature, increasing by a factor of about 3.5 from 16°C to 32°C.

Fig. 4.8C shows the effect on the motor speed of energizing cells in D_2O instead of H_2O. The motors spin faster in H_2O by a factor of 1.29 ± 0.14. Again the speed measurement coincides with the timing of antibody addition in Fig. 4.6C.

In analyzing these 12 samples of artificially energized cells I found an average ratio of swimming speed to body roll frequency of u/f_B = (3.36 ± 0.39) μm. This quantity did not correlate significantly with any of the external parameters tested. For glycolyzing cells, on the other hand, this ratio was equal to (2.53 ± 0.08) μm. The discrepancy may indicate that there are small differences in the swimming geometries of the average glycolyzing and artificially energized cell. In fact, the angle between the long axis and the direction of swimming seems to be larger on average in artificially energized cells than in glycolyzing cells. This sometimes leads to a more tumbly appearance of swimming. Again I would expect the effect of such a change on the body's rotational drag coefficient to be more pronounced than that on the drag coefficient for translation, which explains the larger value found for the ratio u/f_B. Since I used the swimming speed for the calculation of motor frequencies, I think that the results are not significantly in error.

During the swimming speed measurements, which were all performed on cells from the same concentrated suspension, an average of 19% of the cells were motile but not swimming. This fraction was remarkably independent of any of the parameters that I varied, that is time, temperature, and hydrogen isotope. I ignored these cells in my analysis

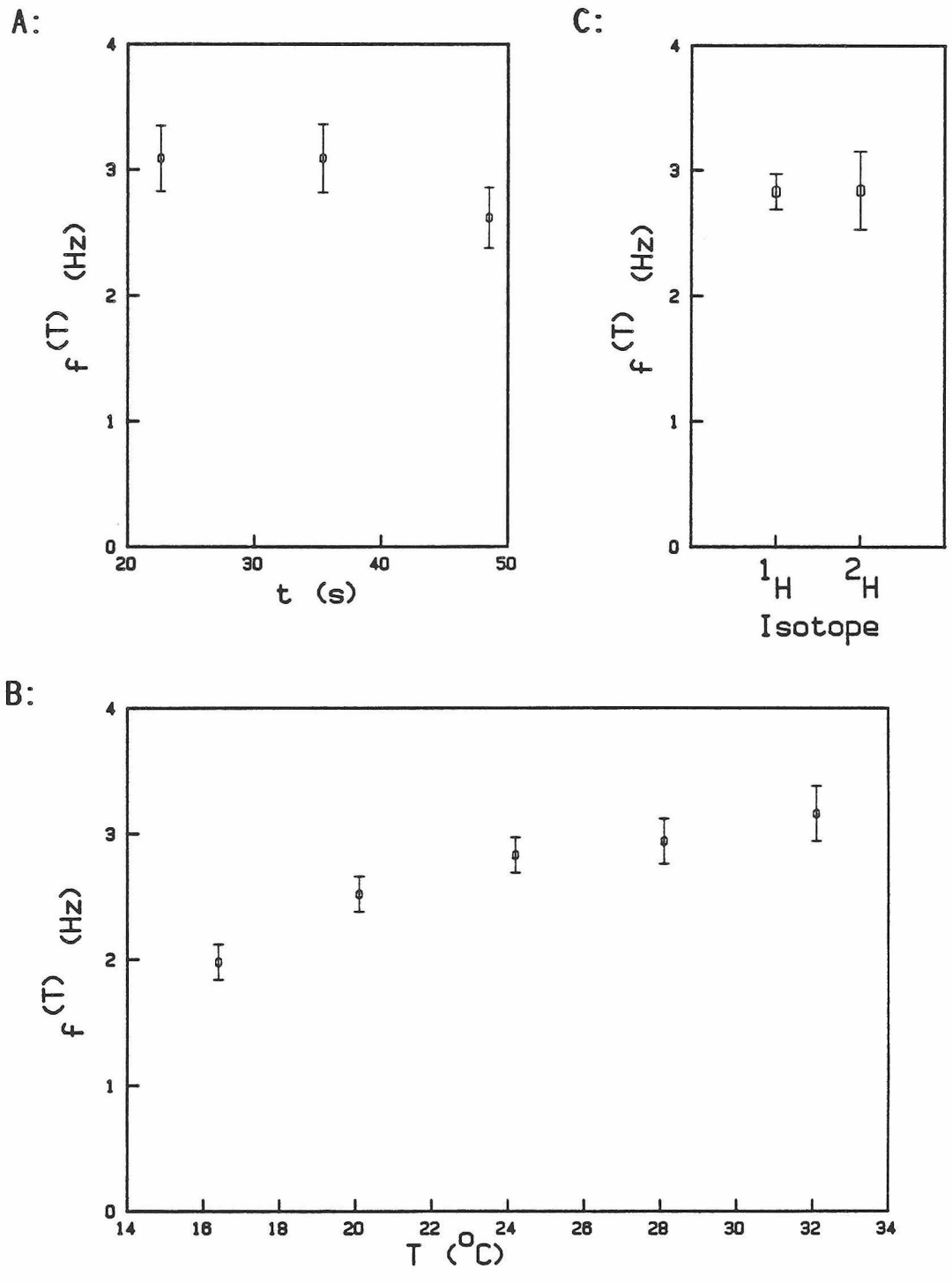

Fig. 4.9. The motor rotation rate in tethered artificially energized cells as a function of **A:** the time after energization, **B:** the temperature, and **C:** the hydrogen isotope in the medium.

of speeds and will try to correct for this in computing the stoichiometry.

I also measured the speed of the motor in tethered cells under conditions identical to those during measurements of motor flux or swimming speed. The rotation rate of the cell body was determined over the 5 s period following addition of antibody in the flux measurements. Fig. 4.9A shows the mean rotation rate $f^{(T)}$ as a function of time after energization and its standard error. A more extensive time course of the motor speed in this same experiment is shown in Fig. 3.9A of Chapter 3. The behavior of the mean rotation rate as a function of temperature is plotted in Fig. 4.9B. Each data point corresponds to a separate population of cells on a different coverslip. The temperature dependence of the motor speed is much less dramatic than at the high speeds of swimming cells. In fact, the rotation rate parallels the behavior of the fluidity of the medium, indicating that the torque generated by the motor is independent of temperature under these conditions. The mean rotation rate in H_2O is compared to the value found in D_2O in Fig. 4.9C. The data points in H_2O are those of Fig. 4.9B at 24°C. Unlike in swimming cells, the speeds are not significantly different.

c) Flagellation of SM197.

The method I used for staining flagella in a wet-mount preparation works quite reliably. With cells of the run-mutant SM197 it shows filaments of 3.2 μm wavelength, typically 1 to 3 wavelengths long. They appear to be flattened onto the glass surface but retain a sinusoidal shape with a peak-to-peak amplitude of 1.0 μm. For analysis of the

motor flux and the torque produced by the motor I was more interested in how many filaments there are on a cell. This number varies between 0 and 7 with about half of the cells showing 2 or 3 filaments. Fig. 4.10 shows the mean number of flagella per cell, F, as a function of growth time in a culture of SM197. Different stains of the same bacterial suspension often yield results that differ by much more than the uncertainty due to the population variance. These additional errors must be introduced by the staining technique, possibly through flagellar breakage, as discussed in §4.2.f. I prepared several stains of each of four bacterial suspensions used in flux experiments on different days. From each of the four sets I chose the stain that showed the largest number of filaments per cell. On average over the four cultures I found

$$F = (3.26 \pm 0.31) \text{ flagella/cell.}$$

The fraction of non-flagellate cells in these samples stains was 0.02. Even with this selection of stains I was worried that F might be severely underestimated. I therefore sent a culture of SM197 to Bob Macnab and asked him to inspect it under his high intensity dark-field microscope. With this instrument one can see the light scattered by single flagella of cells in suspension (Macnab 1976). Bob confirmed my observations on the distribution of the flagellar number as well as the average length of the filaments. Since this technique requires none of the mechanical abuse to which cells are subjected during staining, I am now confident that my estimate of the mean number of flagella per cell is not severely in error.

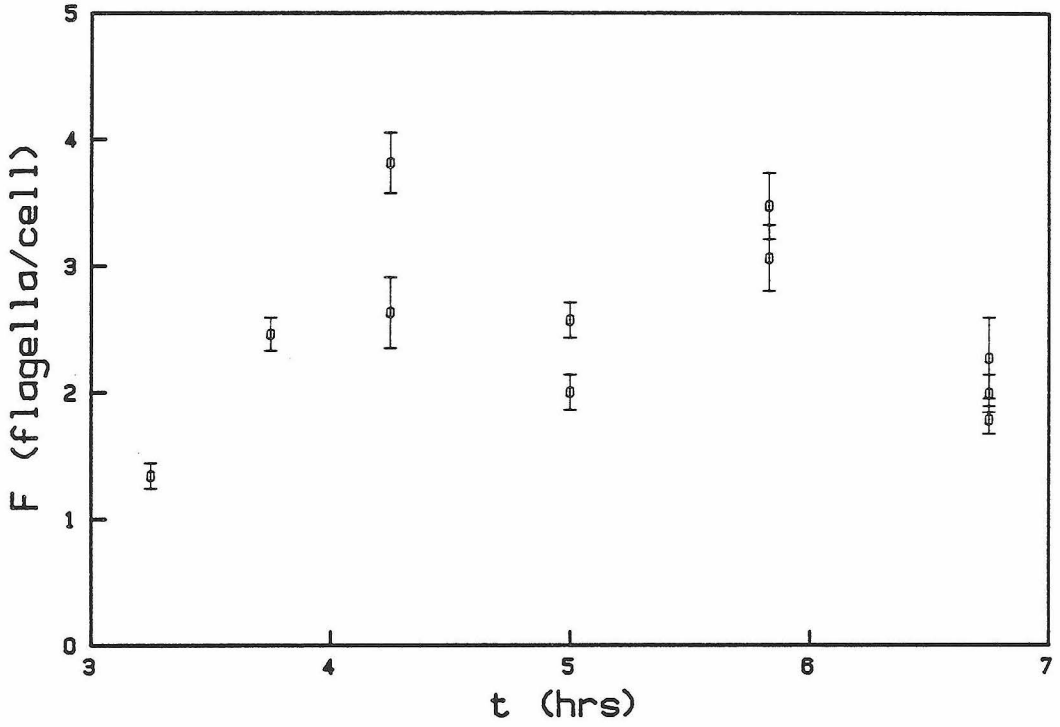

Fig. 4.10. The mean number of flagella on a cell of Streptococcus SM197 and its standard error as a function of the growth time. The samples contained on average 90 cells.

d) Stoichiometry.

For my purposes I will define the stoichiometry of the motor, S, as the ratio of the rotation-dependent proton flux to the motor speed. This definition does not take into account a possible component of the flux through the motor that persists when the motor is stalled. As mentioned earlier, the proton flux at stall cannot be measured by the techniques I used, and I will come back to this question in §4.5.

Before evaluating the stoichiometry I applied two corrections to the motor flux measurements. As discussed earlier, only part of the total rotation-dependent flux is inhibited by the amounts of antibody added to the cell samples. Using the numerical fit in Fig. 4.4 I extrapolated the observed flux drop to its value at infinite antibody concentration. The volume of antibody stock producing half-maximal inhibition was 14 μl, so the measurements of ΔJ obtained with 20 μl stock (time, temperature) were multiplied by (20+14)/20, those obtained with 40 μl antibody stock (H_2O/D_2O) were multiplied by (40+14)/40. I also wanted to take into account that only 81% of the cells are seen swimming after artificial energization. The fraction of non-flagellate cells in the stains that I considered representative was only 0.02; the fraction of cells with a single filament was 0.14. Cells of SM197 can swim with a single flagellum, since almost 100% of the cells in a glycolyzing suspension do. So it seems unlikely that the non-swimming cells in artificially energized samples are those with no or few flagella. Instead, I could imagine that those cells for some reason have a particularly low protonmotive force, below the threshold required for swimming. It is difficult to estimate the resulting effect on the rotation-dependent flux quantitatively. Presumably the rotation rate of

these flagella is low, both because of the lower Δp and because the filaments are dispersed and thus operate at larger torque. As I will show, the rotation-dependent flux is proportional to motor speed, so I expect these cells to contribute significantly less than the swimming cells to the measurement of ΔJ. Lacking any more information, I assumed that they don't participate at all in this measurement and therefore divided all values of ΔJ by 0.81. One should bear in mind that this approximation is likely to result in a high estimate of the stoichiometry and a low value for the efficiency calculated in part (e).

From the corrected value of the rotation-dependent flux, ΔJ^*, the motor speed, $f^{(S)}$, and the mean number of flagella per cell, F, one computes the stoichiometry

$$S = \frac{\Delta J^*}{f^{(S)} F}.$$

Figs. 4.11A, B, and C show this quantity as a function of time after energization, the temperature, and the hydrogen isotope respectively. In all three cases S does not depend on the parameter varied, even though both the motor speed and the motor flux change considerably. The mean values of the stoichiometry for these experiments are (1452 ± 171) H^+/revolution, (968 ± 99) H^+/revolution, and (1309 ± 166) H^+/revolution respectively. These values differ by more than the variation of S within each experiment, probably due to uncertainties introduced when one compares cells prepared from two different cultures. Largely unknown sources of variability affect almost all measurements, including those of total proton flux, to a comparable degree. A meaningful estimate of these quantities is usually obtained only after observing cells from several different cultures. The average value of the

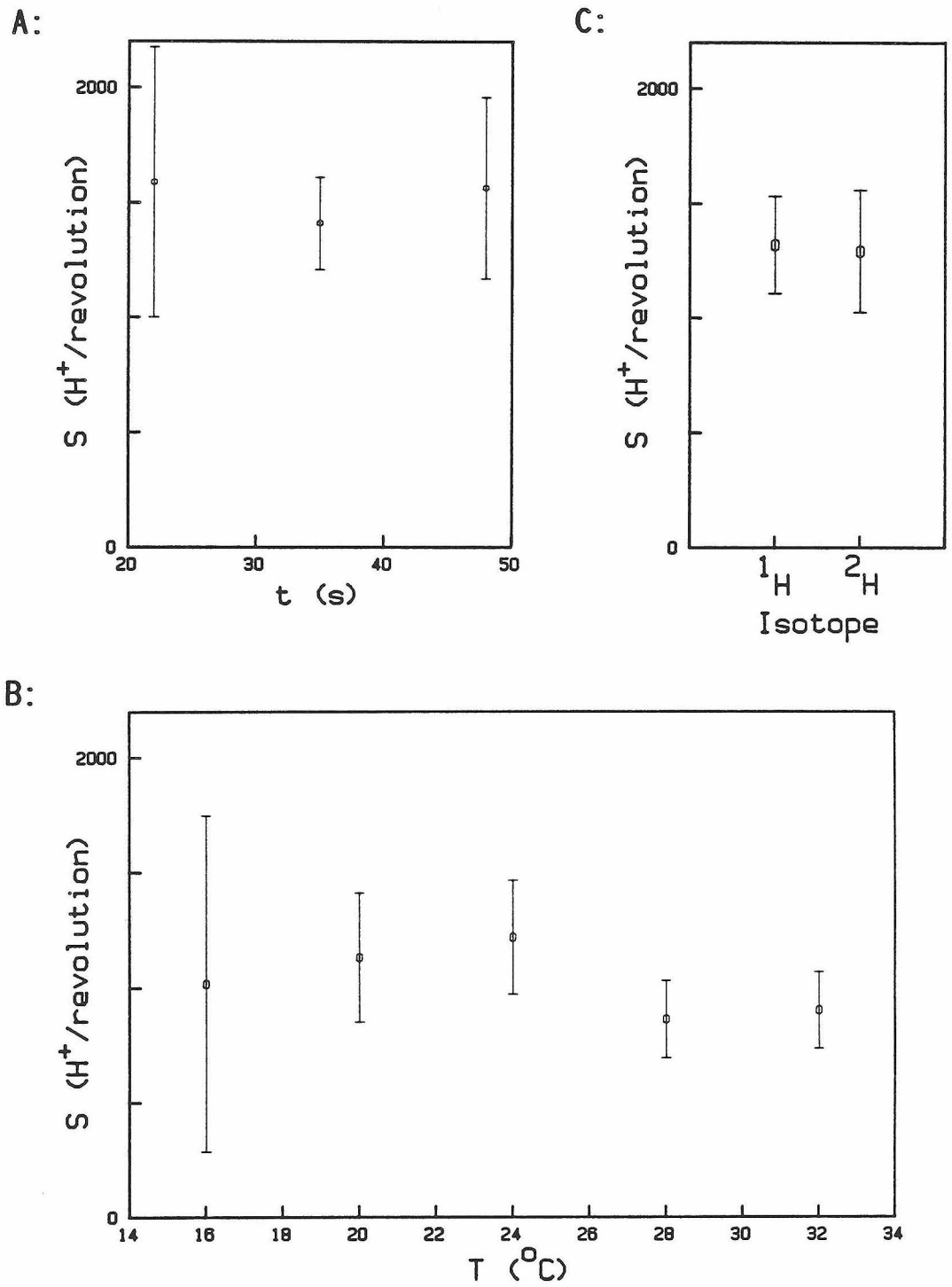

Fig. 4.11. The ratio of the rotation-dependent proton flux to the motor rotation rate as a function of **A:** the time after energization, **B:** the temperature, and **C:** the hydrogen isotope in the medium.

stoichiometry in the above three experiments is

$$S = (1136 \pm 146)\ H^+/\text{revolution}.$$

e) Torque.

During the experiments described in Lowe et al. (1986) Graeme measured the bundle frequency of glycolyzing SM197 cells swimming in media of different viscosities. We then computed the torque generated by the flagellar motor and found that it varies approximately linearly with speed. The torque seems to be largest at stall. The motors of tethered cells, spinning at a low speed of 5 Hz to 8 Hz, operate close to the stall torque, while in swimming cells the motors rotate at 90 Hz to 100 Hz but generate only 1/8 of that torque. These motors seem to be spinning close to the maximal speed attainable at zero torque.

From the measurements of motor speed and body roll frequency in swimming cells and the rotation rate of tethered cells I computed the torque at very low and very high speeds under artificially energized conditions. In both cases the torque was derived from the rotation rate of the cell body relative to the medium. I computed the frictional drag coefficient for this rotation by treating the cell body as a cylinder, as described in §4.2.g. In swimming cells this torque is due to the combined action of all motors whose filaments compose the bundle. In computing the torque generated by a single motor I assumed that all the filaments seen on a cell join in a single bundle, as suggested by the observations of Macnab (1976). I also neglected the possibility of frictional losses due to interactions within the bundle, an assumption I will justify later on. Under these conditions the average torque per motor in a swimming cell is

$$N^{(S)} = \frac{2\pi f_B \, c^{(S)}}{F}$$

where $c^{(S)}$ is the rotational drag coefficient of a swimming cell body, f_B is its roll frequency relative to the medium, and F is the mean number of flagella per cell.

For tethered cells the situation is more straightforward since only a single motor is driving the cell body, and its speed is observed directly. In this case the torque of the motor is

$$N^{(T)} = 2\pi f^{(T)} \, c^{(T)}$$

where $c^{(T)}$ is the rotational drag coefficient corresponding to the geometry of a tethered cell, and $f^{(T)}$ is its rate of rotation.

Figs. 4.12A, B, and C are graphs of motor torque as a function of motor speed under conditions where the speed changes with the time after energization, the temperature, and the hydrogen isotope respectively. For each set of external parameters these plots contain only two points: one for tethered cells, computed from the data in Fig. 4.9, the other one for swimming cells, computed from Fig. 4.8. As we had seen in glycolyzing cells (Lowe et al. 1986), the torque generated by the motor in a swimming, artificially energized cell is drastically smaller than at the low speeds of tethered cells. In discussing these quantities I will assume that the torque of a tethered cell is close to the stall torque, N_S, while the motor speed in a swimming cell is close to the maximum speed attainable under these conditions of energization, denoted by f_I. I will use the term "idle speed" for this value of the speed at zero torque. To avoid confusion I should note that the automotive concept of "idle" involves not only disengaging the clutch, and thus removing the load from the engine, but also throttling the flow of

gasoline. Our bacteria, on the other hand, leave their foot on the accelerator, even when the resistance to flagellar rotation is decreased.

In Fig. 4.12A the stall torque drops with time after energization, which is probably due to the decay of the protonmotive force. On the other hand, the idle speed also decreases. This suggests that f_I is at least partly limited by the protonmotive force. I will speculate on the implications of this in Chapter 5.

Fig. 4.12B shows that the stall torque does not vary with temperature. This suggests that the Δp is approximately independent of temperature. It also confirms the result of Khan and Berg (1983), who observed tethered SM197 at a lower Δp but over a wider range of temperature and saw no change in the torque. The idle speed, however, rises dramatically with increasing temperature, as seen in glycolyzing cells (Lowe et al. 1986). Clearly this is not a metabolic effect.

In Fig. 4.12C the stall torque increases by about 24%, while the idle speed decreases when protons are replaced by deuterons. The first result seems to contradict the observation of Khan and Berg (1983) that there is no isotope effect on the torque of the motor in SM197 when cells are energized with a potassium diffusion potential alone. However, given the fact that the protonmotive force under the conditions of energization that I used is clearly much lower than the value predicted by the Nernst equation, there is also considerable uncertainty about the equivalence of the Δp in H_2O and D_2O. Even though the Δp may be 24% larger in D_2O, the idle speed drops by 22%. I conclude that isotope effects play an important role in limiting the speed of the motor.

Fig. 4.12. The motor torque as a function of the motor rotation rate. Computed from the data of Fig. 4.9 (low speeds) and Fig. 4.8 (high speeds). Arrows indicate the sequence of parameters given below.
A: Dependence on the time after energization; t = 22 s ( ), 35 s ( ), and 48 s ( ).
B: Dependence on the temperature; T = 16°C ( ), 20°C ( ), 24°C ( ), 28°C ( ), and 32°C ( ).
C: Dependence on the hydrogen isotope in the water; ^{1}H ( ) and ^{2}H ( ).

A:

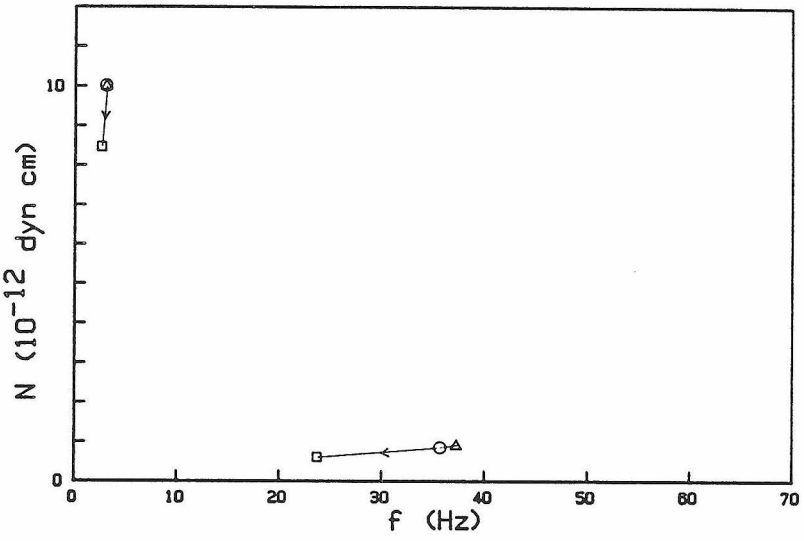
N (10^{-12} dyn cm)
10
0
0
10
20
30
40
50
60
70
f (Hz)

B:

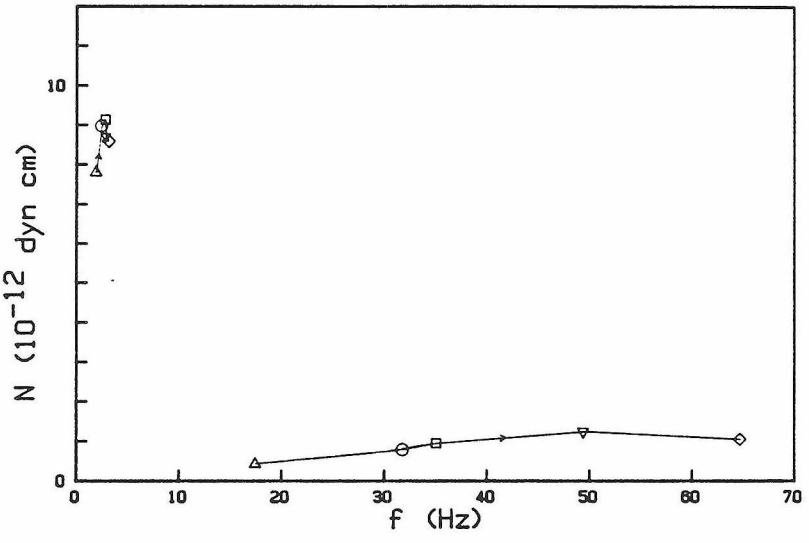
N (10^{-12} dyn cm)
10
0
0
10
20
30
40
50
60
70
f (Hz)

C:

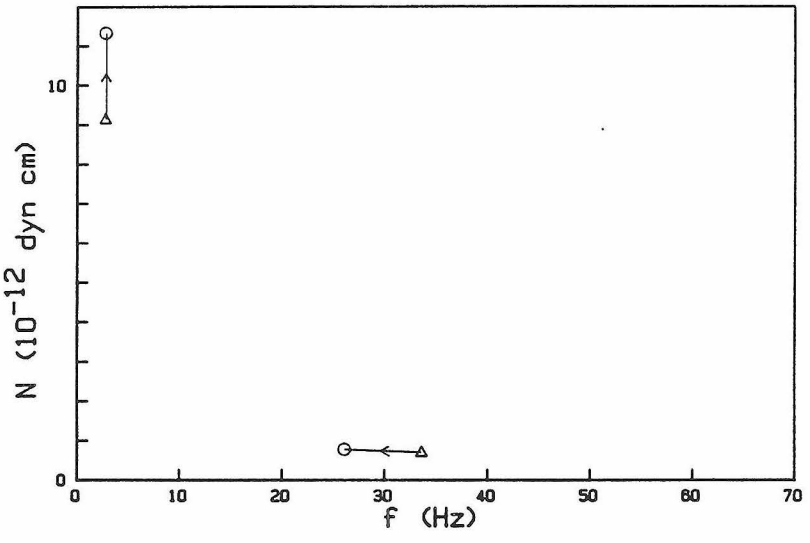
N (10^{-12} dyn cm)
10
0
0
10
20
30
40
50
60
70
f (Hz)

The linear decrease in the torque with increasing speed seen by Lowe et al. (1986) could be explained if the flagellar motor generated a torque independent of speed over the entire range, while friction forces within the bundle produced an opposing torque proportional to speed. Such forces could result from viscous shear in the fluid between filaments, which are rotating relative to each other, or from a direct mechanical interaction of the flagella. The strong dependence of the idle speed on the temperature and the hydrogen isotope effect argue against such an interpretation. Another indication that the torque generated by a single motor is not much larger than that deduced from its operation within the bundle is given by the fact that isolated flagellar hooks spin at essentially the same rate as flagellar bundles (Berg et al. 1982). The torque corresponding to this rotation is virtually zero on the scale of Fig. 4.12.

f) Efficiency.

In this context I will define the efficiency, ϵ, of the motor as the ratio of the mechanical power it generates to the electrochemical power dissipated by the portion of the proton flux coupled to rotation. Again this does not take into account any possible flow of protons through the stalled motor. With the previous definition of the stoichiometry, S, the efficiency is found as

$$\epsilon = \frac{N\ 2\pi f}{e\Delta p\ \Delta J^*} = \frac{N\ 2\pi}{e\Delta p\ S}.$$

Evaluation of the efficiency requires knowledge of the protonmotive force. As discussed in §4.3 of this Chapter, our best estimate for the Δp under these conditions of energization relies on the assumption that

the speed of tethered cells is strictly proportional to the protonmotive force. Tethered glycolyzing cells in buffer B [KCl 8.5] rotated at a mean rate 2.25 times as high as the rate seen 30 s after artificial energization in H_2O at 24°C. Assuming that the protonmotive force in glycolyzing cells is equal to the average value reported for S. lactis, -150 mV, I estimate the Δp of artificially energized cells to be -67 mV at the time of observation. Thus the efficiency of the motor in a swimming cell under those conditions is

$$\epsilon^{(S)} = 0.04.$$

The torque measured in swimming cells, $N^{(S)}$, increases with temperature, as seen in Fig. 4.12B. The tethered cell torque, $N^{(T)}$, on the other hand, does not vary with temperature, indicating that the protonmotive force remains unchanged. Therefore the efficiency increases with rising temperature.

In the course of these temperature experiments the stoichiometry, S, was found to be constant over a wide range of motor speeds from 17 Hz to 65 Hz. If S has the same value at the speeds of tethered cells, then the efficiency of flagellar rotation at low speed in H_2O at 24°C is

$$\epsilon^{(T)} = 0.5.$$

I was taught early on that no physical measurement is meaningful without an error analysis. This is the last and maybe most important experimental result quoted in this thesis and thus deserves particular attention in this respect. To good approximation the value of $\epsilon^{(T)}$ is affected by every single source of experimental error mentioned in this and all preceding chapters. I have tried to keep track of the resulting uncertainties in a consistent manner, but there are cases where even the uncertainty is largely unknown, for example in the numerical evaluation

of rotational drag coefficients or the value of the protonmotive force. I therefore cannot base my confidence in the above estimate on a rigorous treatment of error propagation. Fortunately the laws of physics restrict $\epsilon^{(T)}$ to values smaller than unity. Based on the work presented in this chapter I feel fairly certain that the efficiency of the flagellar motor at low speeds lies somewhere between 0.2 and 1.

§4.5 DISCUSSION

The experimental results presented in this chapter lead to the following two conclusions:

1. The stoichiometry of the rotation-dependent proton flux to the speed of the motor is remarkably constant under a variety of external conditions. These include changes in the protonmotive force with time after energization, variation of the temperature from 16°C to 32°C, and substitution of deuterons for protons in the medium. The motor speed at low loads varies greatly as these parameters are changed, but the rotation-dependent flux remains proportional to the rotation rate with approximately 1100 protons transferred per revolution.

2. The efficiency of the motor, computed as the ratio of mechanical power output to electrochemical power dissipated by the rotation-dependent proton flux, is of the order of a few percent at the rotation rates encountered in swimming cells. If the stoichiometry remains unchanged as the load on the motor is increased, this efficiency may be close to unity at the speeds of tethered cells.

The first result makes it tempting to postulate that the transfer of protons through the motor is tightly locked to the rotation of the flagellum by the mechanism of torque generation. In this case there would be no flow of protons when the motor is stalled, and the rotation-dependent flux I measured constitutes the entire flux of protons through the motor. As mentioned in §2.1, such a mechanism is by necessity reversible at low speeds: if the free energy drop of the protons moving through the motor were larger than the mechanical work performed, one could pump protons with an efficiency greater than one by rotating the

flagellum and driving the motor in reverse. Thus the high efficiency at low speeds that I observed experimentally is a direct consequence of the assumption of tight coupling.

The techniques by which I measured the motor-related flux cannot detect movement of protons through the stalled motor. Consequently my definitions of stoichiometry and efficiency have only considered the flux component which is coupled to rotation. Can one conceive a flagellar motor that shows a constant stoichiometry and high efficiency at low speeds, in which the proton flux is not tightly coupled to rotation? I will show that unit efficiency of the coupled flux at low speeds is a property of a much wider class of mechanisms, namely all mechanisms that show linear relationships between the two flows, the proton flux and the rotation rate, and their conjugate driving forces, the proton electrochemical potential and the external torque. The following analysis is motivated by the measurements reported in Lowe et al. (1986), which show that the relationship between motor speed and motor torque at constant protonmotive force is linear over the entire range of speeds accessible to the motor. It involves the same concepts used in Chapter 3 for the phenomenological discussion of ionic flows across the cytoplasmic membrane. Note, however, that this treatment does not account for the threshold effects observed at very low protonmotive force. The requirement for a small but finite Δp to initiate rotation and the fact that a deenergized motor does not exhibit rotational Brownian motion may result from static friction between the components of the motor and the cell wall (Khan et al. 1985). These interactions are probably not directly related to the process of torque generation in the motor itself.

In the language of thermodynamics the motor is a system whose state is described by two variables: the number of protons, n, that have passed through the motor since a given point in time and the angle traversed by the rotor since that time, θ. The corresponding flows are the proton flux, $J = dn/dt$, and the angular velocity of the rotor, $2\pi f = d\theta/dt$. Note that the symbols n and J previously represented the total movement of protons across the membrane but are restricted to flows through the motor in this discussion. The proton electrochemical potential, $-e\Delta p$, and the external torque, N, are the respective driving forces conjugate to J and $2\pi f$ respectively. (Strictly speaking the driving forces are the stated quantities divided by the absolute temperature, but the following treatment is not affected by omitting this factor.) Following the analysis presented in §3.2 one finds that the steady-state flows and forces are related linearly if the system operates close to thermodynamic equilibrium:

$$\begin{pmatrix} J_H \\ 2\pi f \end{pmatrix} = \begin{pmatrix} L_{11} & L_{12} \\ L_{21} & L_{22} \end{pmatrix} \begin{pmatrix} -e\Delta p \\ N \end{pmatrix}$$

with $L_{12} = L_{21}$ given by Onsager's reciprocal relations. Note that there may be other degrees of freedom internal to the motor, such that a complete thermodynamic description of its state requires more than two variables. Since the motor operates cyclically, no net flow of any such internal variables can occur during steady-state rotation. Thus the complete set of phenomenological equations is reduced to the two given above for J and $2\pi f$. One sees that this motor generates a stall torque of

$$(4.1) \qquad N_S = -(-e\Delta p)\,\frac{L_{21}}{L_{22}}$$

where the minus sign indicates that N is the torque applied to the motor externally and thus opposes rotation of the shaft. The idle speed, f_I, of the motor is obtained at N = 0:

$$(4.2) \qquad f_I = (-e\Delta p)\, L_{21}$$

The rotation-dependent flux, ΔJ, is given by the difference between the values of the total proton flux, J, when the motor rotates at speed f and when it is stalled:

$$J(f) = \left(L_{11} - \frac{L_{12}\, L_{21}}{L_{22}}\right) (-e\Delta p) + \frac{L_{12}}{L_{22}}\, 2\pi f$$

$$\Delta J = J(f) - J(0) = \frac{L_{12}}{L_{22}}\, 2\pi f$$

Thus the stoichiometry of the coupled flux is

$$S = \frac{\Delta J}{f} = \frac{L_{12}}{L_{22}}\, 2\pi$$

and its efficiency at low speeds is obtained as

$$\epsilon^{(T)} = \frac{(-N_S)\, 2\pi}{(-e\Delta p)\, S} = \frac{L_{21}}{L_{22}} \frac{L_{22}}{L_{12}} = 1$$

using the reciprocal relations. Therefore all linear mechanisms show unit efficiency of the coupled flux at low speeds.

The invariant stoichiometry, on the other hand, is not predicted implicitly. As the external conditions are varied, the point of thermodynamic equilibrium shifts, and thus the phenomenological coefficients L_{ik} change. For example, eqn. (4.2) shows that the coefficient L_{21} varies by up to a factor of 3 in the different experiments described in §4.4. To obtain constant stoichiometry, one must therefore postulate that L_{22} varies proportionally to L_{21}. An inspection of eqn. (4.1) shows that this feature is also required by the

experimental observation that the ratio of stall torque and protonmotive force is independent of the external conditions. But there is no a priori reason why a linear mechanism should have this property. The explicit requirement for proportionality between L_{21} and L_{22}, in addition to the requirement that the mechanism operates close to equilibrium even at large protonmotive force, makes the construction seem somewhat awkward compared to the simple assumption of tight coupling between proton flow and flagellar rotation.

I would like to compare our knowledge of flagellar motor physiology now to that after the experiments of Manson et al. (1980). At the time, it was known that the torque of the motor observed in tethered cells is proportional to the protonmotive force and independent of speed. This led to the suggestion that the number of protons carrying the motor through one revolution as well as the efficiency of energy conversion do not vary with the speed of the motor. Today we know that the speeds observed with tethered cells lie only in the lower 10% of the range accessible to the motor. The flux of protons coupled to rotation has been measured directly, and it was found that a fixed number of protons are linked to each revolution. The efficiency of the coupled flux has also been measured directly and is close to unity in tethered cells but decreases linearly with increasing speed. In spite of all these new results, the most simple and most stringent hypothesis, namely that of tight coupling between protons and revolutions, still explains all of the observations. If the motor is, in fact, tightly coupled, then very little additional information about the mechanism of torque generation can be obtained from the steady rotation of tethered cells (except, maybe, at very low temperature, see §2.4). Their speeds are so low that

the motor torque is virtually indistinguishable from the stall torque, which, as mentioned before, is simply determined by the second law of thermodynamics (eqn. (2.1)). To learn something about the physics of the motor mechanism one must therefore observe it at high speeds, far outside the reversible regime. The measurements of torque and proton flux in swimming cells reported here contain some of that information, which I will incorporate into an explicit model of the flagellar motor, presented in the following chapter.

CHAPTER FIVE. SOME THOUGHTS ON THE MECHANISM OF FLAGELLAR ROTATION

§5.1 INTRODUCTION

The detailed physical processes by which the flagellar motor generates torque are still unknown. However, there is a good deal of structural, genetic, and biochemical knowledge that should be taken as a basis from which to speculate about the function of this machine (see the General Introduction to this thesis for a summary and references). The number of different proteins composing the flagellar motor is well known, sometimes also their location within the structure, and, in a few cases, even their role in the mechanism. For example, the motA and motB proteins seem to be directly involved in the generation of torque, while the cheC and cheV gene products are probably essential components of the switch that determines the direction of flaellar rotation. However, these studies don't offer any indications how the various motor components achieve their function.

The search for biochemical inhibitors of flagellar rotation has not been very revealing. The motor mechanism poses few requirements on the composition of the aqueous medium surrounding it. As mentioned earlier, cells of E. coli swim happily in distilled water, and tethered envelopes of these cells spin even after their cytoplasm is replaced by a simple inorganic buffer (Eisenbach & Adler 1981). Copper and other heavy metal ions abolish swimming motility even at very low concentrations (Adler & Templeton 1967). Conley and Berg (1984) observed that imidazole reagents lowered the rotation rate of tethered artificially energized

Streptococcus cells without affecting the protonmotive force, which suggests a possible involvement of histidine side chains in the chemistry of torque generation.

In the absence of any strong direct clues regarding the molecular processes involved in torque generation, proponents of hypothetical motor mechanisms have generally drawn on a repertoire of design elements known to be used by other molecular machines: large water-filled ion channels, more specific proton conduction pathways along chains of hydrogen bonds, protein molecules with elastic linkages. These parts are then arranged in a geometry that respects the appearance of basal bodies under the electron microscope and ensures that the rotor turns when protons flow through the machine. Aside from a few exceptions, which can be eliminated by common sense, all these hypothetical mechanisms must be tested by comparing their predictions regarding function of the motor under various external conditions to the experimental observations. In this chapter I will first summarize our knowledge of the flagellar motor's function. Then I will explicitly construct a model of the flagellar motor which is based on the geometry chosen by Berg and Khan (1983) and whose predictions match the more recent measurements of the motor-related proton flux and the motor torque at high speeds. In doing so I hope to elucidate some of the special constraints imposed on this machine and to clarify a few misconceptions found in the literature. I will also discuss this particular model in relation to other proposed mechanisms and suggest some experimental approaches that may distinguish among them.

§5.2 FUNCTIONAL PROPERTIES OF THE MOTOR

The following is a list of empirical observations on flagellar rotation that any hypothetical mechanism of torque generation must account for. Most of this work was done on Streptococcus, but at this point there is no indication that the flagellar motors of other bacterial species are qualitatively different. The experiments of Manson et al. (1980) and those described in Chapter 2 have shown that the motor torque observed at the speeds of tethered cells is very close to the stall torque. I will therefore refer to torque measurements on tethered cells, whether rotating or not, as the "stall torque". Similarly, Lowe et al. (1986) found that the rotation rate of flagella in the bundles of swimming cells is almost equal to the maximal speed attainable at vanishing external torque. As in §4.4.e, I will call those rotation rates the "idle speed".

Some basic properties of flagellar rotation are:

a) The motor is driven directly by the electrochemical potential difference of protons or hydroxyl ions across the cytoplasmic membrane. In some species the motor is powered by the sodium electrochemical potential (see Chapter 3 for references).

b) The motor of a wild-type cell turns alternately clockwise and counterclockwise. The reversals are complete within about 10 ms, and no intermediate speed levels have been resolved. The motor rotates at approximately the same speed in either direction (Berg 1974, 1976). The length of the clockwise and counterclockwise intervals is modulated by the chemotaxis system, but reversals occur even in the absence of chemotactic signaling.

c) In Streptococcus mutants with an inoperative chemotactic switch the motor's rotation reverses when the sign of the protonmotive force is reversed (Khan & Berg 1983).

Other properties concern the relationship between the four quantities characterizing the steady-state operation of the motor: protonmotive force and proton flux at the input and rotor speed and torque at the output. These relationships vary when the external conditions, such as the temperature and the hydrogen isotope in the aqueous medium, are changed.

d) At a given temperature, hydrogen isotope, and a fixed protonmotive force, the torque generated by the motor drops with increasing rotor speed. For glycolyzing cells in H_2O at 22°C it appears to decrease linearly from a stall torque value of ca 2×10^{-11} dyn cm to zero at an idle speed of ca 100 Hz (Lowe et al. 1986, §4.4.e in this thesis).

e) At a given temperature and hydrogen isotope the stall torque is proportional to the nominal protonmotive force for $-\Delta p_{nom} \leq 80$ mV (Khan et al. 1985). A pH-gradient and an electrical membrane potential seem to be equally effective in this respect (Manson et al. 1980; Khan & Berg 1983; Conley & Berg 1984). The proportionality may hold over a wider range up to the protonmotive force of glycolyzing cells, but there is considerable uncertainty about the value of Δp in this regime, related to problems in generating large artificial membrane potentials (see §2.4.d). Khan and Berg (1983) have reported a significant difference between the speed of tethered Streptococcus after a pH-shift and after an equivalent potassium dilution. Their interpretation, namely that the discrepancy arises from a high internal potassium activity, appears to be wrong: the nominal protonmotive force is the same in both experiments

(see §1.2.d). The result therefore suggests that the chemical and electrical components of the protonmotive force are not equivalent in driving the motor, even at low Δp, and thus deserves further attention.

f) At a given temperature and hydrogen isotope the idle speed increases with the protonmotive force at least up to $-\Delta p_{nom}$ = 80 mV. This relationship has not been carefully studied (Khan & Macnab 1980b; Shioi et al. 1980; §4.4.e).

g) At a given protonmotive force the stall torque is independent of temperature and independent of the hydrogen isotope in the water (Khan & Berg 1983; §4.4.e).

h) At a given protonmotive force the idle speed increases markedly with temperature (Lowe et al. 1986 and references cited therein) and decreases when deuterons are driving the motor instead of protons (§4.4.e).

i) Under all the conditions investigated so far, which include those of (f) and (h) but not those of (d), the rotation-dependent proton flux is proportional to the speed of the rotor. Approximately 1100 hydrogen ions are coupled to one revolution of the rotor, and this number is independent of the temperature, the protonmotive force, and the hydrogen isotope (§4.4.d).

A few more observations concern fluctuations about the steady state rotation:

j) At zero protonmotive force the motor is locked into position by static interactions that do not permit rotational Brownian motion of the rotor. The motor stops in only 5 or 6 discrete angular positions (Khan et al. 1985; Chapter 1).

k) As the protonmotive force is gradually increased, the motor starts

rotating only when a threshold of 5 to 20 mV is crossed (Manson et al. 1980; Berg et al. 1982; Conley & Berg 1984). This behavior is not apparent when cells slow down as the artificial Δp is gradually decreased (Khan et al. 1985).

1) The body of a tethered cell which is rotating at a protonmotive force above threshold shows diffusive drift relative to the steady average rotation rate. Apparently the motor is free to execute rotational Brownian motion under the influence of a constant torque provided by the motor mechanism (Khan et al. 1985).

§5.3 AN EXPLICIT MODEL OF FLAGELLAR ROTATION

In this section I will present a hypothetical mechanism for torque generation. It relies and expands on the model presented by Berg and Khan (1983). I have chosen this particular arrangement of parts not because I regard it as the most viable of the proposed schemes, but because I am most familiar with it, and most of my calculations are expressed in this formalism. It is also very well suited for a gradual upgrading of the mechanism: I will start with the most basic version, containing a single degree of freedom in a process that tightly couples proton movement and rotor rotation. The predictions of this model directly contradict experimental observations on tethered cells, but the dilemma is resolved by the introduction of internal degrees of freedom, corresponding to the springs in the motor proposed by Berg and Khan. I will analyze the function of this mechanism at very high rotation rates. Comparison with the more recent experimental evidence in this regime suggests that the idle speed of the motor may be limited by proton conduction processes.

Throughout this discussion I will use explicit calculations only to illustrate behavior that can be predicted qualitatively from basic physical principles alone. I hope to avoid the excesses practiced on many pages of the Journal of Theoretical Biology, where a biological problem is often used merely as a pretext to exhibit the author's mathematical virtuosity. I have banned most of the algebra into the Appendix. The main purpose of this exercise is to acquire a feeling for the very special constraints imposed on this machine and to develop some criteria by which a hypothetical process of torque generation may be

evaluated and discussed without an explicit quantitative analysis of all its dynamic features. In this context I will compare the model developed here to mechanisms proposed by other authors.

a) The elementary coupling process.

Fig. 5.1 illustrates how the flow of protons is coupled to rotation of the rotor. The M-ring, which is attached to the rod, carries a set of proton-accepting sites spaced equidistantly on its periphery. As they are located within the membrane, these sites are not normally accessible to protons from the cytoplasmic or the external medium, unless they are aligned with one of the channels of a channnel complex. This latter device is attached rigidly to the S-ring and thus to the cell wall. It spans the entire membrane and lies in close proximity to the periphery of the M-ring. The side of the channel complex facing the M-ring contains two half-channels, running perpendicularly to the membrane, which are separated by the same distance as the proton binding sites on the M-ring. One of these channels, labeled (e), runs from the plane of the M-ring to the external face of the membrane; the other channel, labeled (i), runs from the plane of the M-ring to the cytoplasmic side. Thus, when a pair of adjacent proton-accepting sites is aligned with the two half-channels, one of the sites is in contact with the cytoplasmic proton bath, while the other one is connected to the external proton bath. Motion of the M-ring relative to the channel complex is constrained by the following two rules: A proton binding site moving past the central portion of the channel complex must be charged and thus occupied by a proton, while a binding site moving past either of the lateral portions of the channel complex and onward into

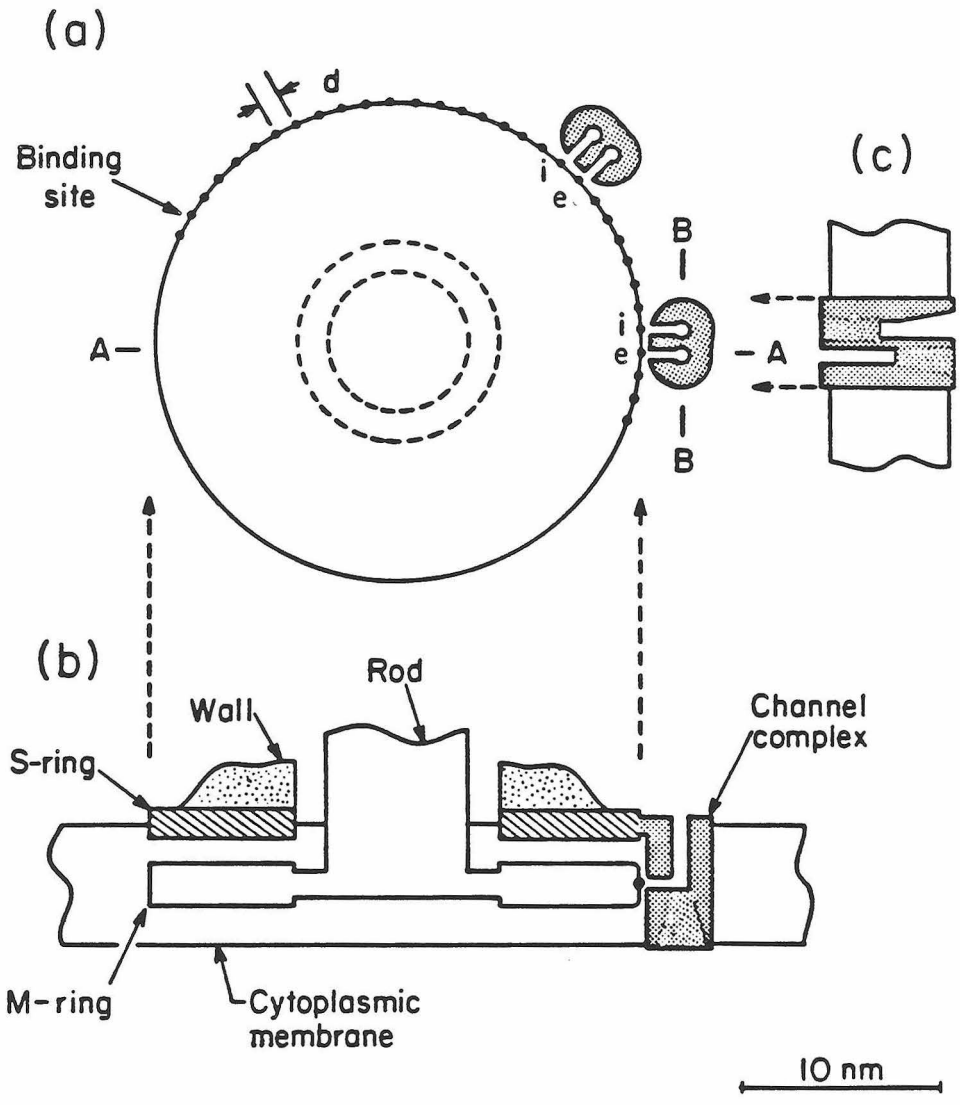

Fig. 5.1. Blueprint of the flagellar motor, as proposed by Berg and Khan. From Berg & Khan (1983), with permission.

the lipid environment of the membrane must be uncharged and therefore empty. These constraints could be implemented through electrostatic interactions between the local charge at the binding site and the surface of the channel complex. They are assumed to constitute the only interaction between the M-ring and the channel complex. Thus a proton can be transferred from the external medium to the cytoplasm only by the following path, illustrated in Fig. 5.2: It moves through the (e) channel and occupies an empty binding site on the M-ring (Fig. 5.2A); the M-ring then rotates in what shall be called the forward direction (Fig. 5.2B) until the proton is exposed to the (i) channel; finally it leaves the site and travels through the (i) channel into the cytoplasm (Fig. 5.2C). Similarly, movement of a proton from the cytoplasm into the external medium can only occur if the reverse sequence is executed, and the M-ring rotates backward. During steady rotation the number of protons transferred during each revolution is thus equal to the number of binding sites on the periphery of the M-ring.

How does this mechanism work dynamically? If the channel complex were not present, the M-ring together with everything attached to the shaft of the motor would undergo free rotational Brownian motion driven by the fluctuating forces from the surrounding medium. The channel complex and its interaction with the protonatable sites on the M-ring serve to constrain this random motion. If a protonmotive force is applied across the membrane, these constraints bias the Brownian motion in one direction, leading to net rotation of the rotor. Consider the situation where two binding sites are aligned with the channel as pictured in Fig. 5.2A. The rotor can move forward only when site (e) is occupied and site (i) is empty. It can move backward in the opposite

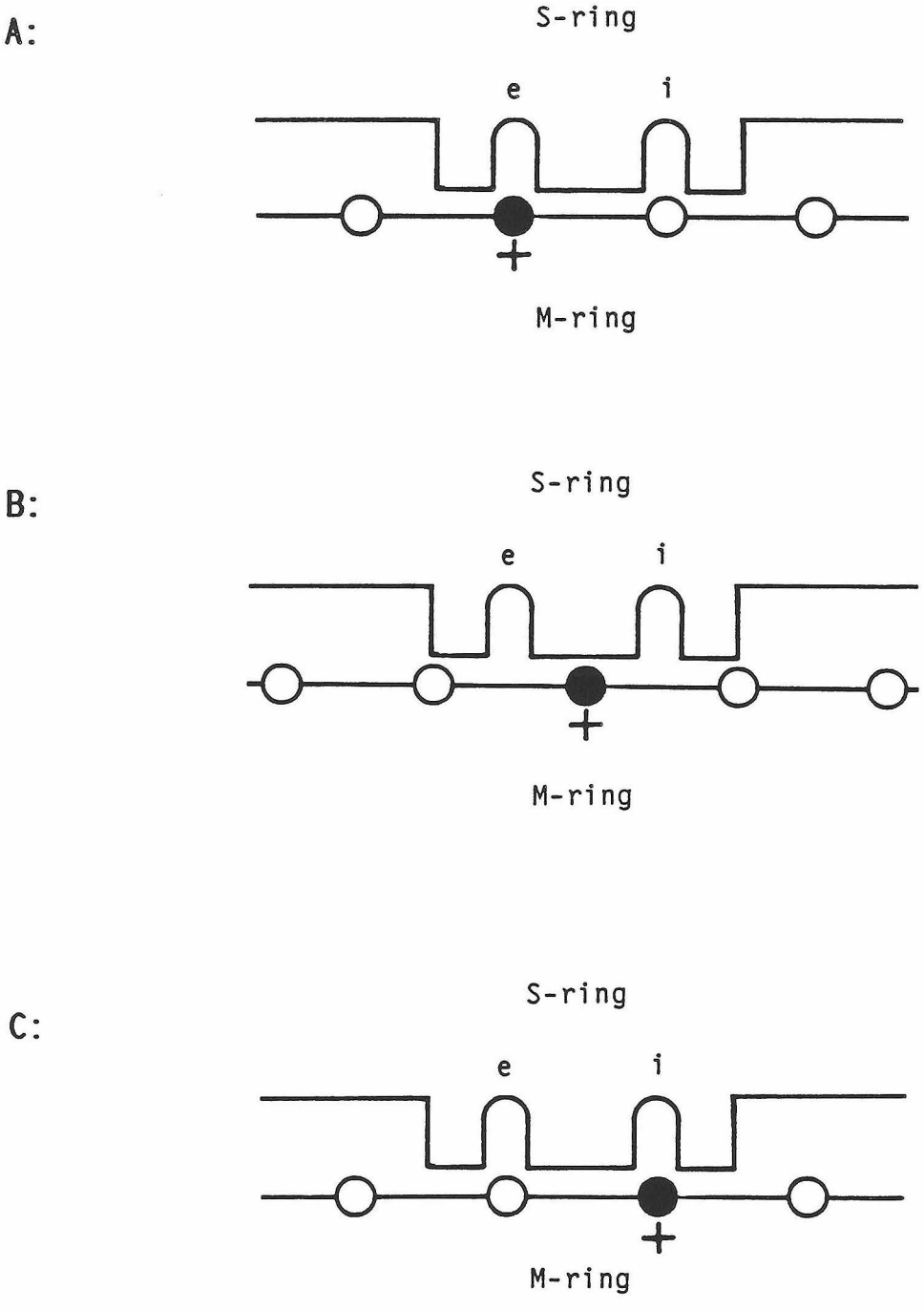

Fig. 5.2. Illustration of the coupling between movement of protons and rotation of the M-ring.

configuration with site (i) occupied and site (e) empty. If both sites are protonated or both sites are empty, the M-ring is locked in position. When a negative protonmotive force (the physiological direction) is imposed across the membrane, then the proton concentration at the (e) site will be larger than at the (i) site. Therefore the occupancy configuration required for forward motion is assumed more frequently than that which allows backward motion. When the M-ring eventually leaves the aligned position of Fig. 5.2A it is more likely displaced in the forward direction, as pictured in Fig. 5.2B, than in the backward direction. Eventually the binding sites find themselves aligned again with the two half-channels (Fig. 5.2C), their occupation probabilities equilibrate with the respective proton concentrations and the game starts over.

Feynman et al. (1963, Ch.46) discuss the physics of a similar device: the ratchet-and-pawl machine. A spring loaded pawl serves to bias the random Brownian motion of a ratchet wheel. Steady rotation of that device is only possible if one cools the pawl by transferring heat to a reservoir at lower temperature than the ratchet wheel. By contrast, the flagellar motor is not driven by thermal energy (contrary to frequent assertions in the literature; see, for example Macnab & Aizawa 1984), but by the entropic energy stored in the concentration difference between the two proton baths, or, if an electric field is applied across the membrane, by electrical potential energy. In the particular mechanism discussed here, the free energy of a proton is used to lift the pawl up every time a ratchet gear approaches from one side, and to keep it down when the ratchet wheel moves in the opposite direction. The latter description is somewhat reminiscent of Maxwell's

demon, but this particular member of the species obeys the law: it reduces the entropy of the rotor by biasing M-ring motion at the expense of a greater or equal increase in the entropy of the proton bath.

A few more assumptions are introduced in order to simplify calculations. No electric field is presumed to act in the plane of the M-ring. If the protonmotive force consists in part of a transmembrane electrical potential gradient, the proton concentrations in the (i) and (e) channels equilibrate with the local potential, which thus translates into a pH-difference of thermodynamically equivalent magnitude at the location of the (i) and (e) proton binding sites. Conduction of protons through these channels is assumed to be fast, such that removal of protons from the bottom of the (e) channel or addition to the top of the (i) channel during steady rotation does not perturb the proton gradients. The pH-difference between the (e) site and the (i) site thus corresponds to the full protonmotive force across the membrane, irrespective of the composition of the protonmotive force or the speed of the motor:

$$pH_e - pH_i = (pH_{ext} - pH_{int}) - \frac{e\psi_{ext} - e\psi_{int}}{kT \ln(10)}$$

where pH_{ext} and pH_{int} are the values of the pH in the external medium and the cytoplasm respectively, e is the electronic charge, and ψ is the electrical potential. The binding and unbinding of protons at the sites on the M-ring is also taken to be very rapid. Thus the time required for the occupancy of these sites to equilibrate with the respective proton baths after alignment with the (i) and (e) channels is so short that it has no effect on the rotation of the M-ring. Finally I will assume that the rotor executes free rotational Brownian motion when the

binding sites are not aligned with the channels. Interactions with the channel complex are restricted to the aligned configuration of Figs. 5.2A and 5.2C.

What qualitative features can one predict for the function of this mechanism? The bias in the forward direction and therefore the net speed of the rotor should increase with increasing protonmotive force. But the rotation rate cannot exceed a certain limit: even if the bias was perfect, such that the M-ring could only move in the forward direction whenever the sites are aligned with the channels, it would still require a finite time for diffusion of the M-ring to transport the protonated site from the (e) channel to the (i) channel. This time should be inversely proportional to the diffusion coefficient of the M-ring and everything attached to it. In fact, since the rotor executes Brownian motion at all times, this diffusion coefficient sets the time scale for the entire process, and the average rotation rate is expected to be proportional to the diffusion coefficient at all values of the protonmotive force.

A quantitative calculation of the speed proceeds as follows. The motion of the M-ring is equivalent to the one-dimensional diffusion of a particle, governed by

$$\frac{\partial}{\partial t}\, p(x,t) = \frac{\partial}{\partial x}\left\{D(x)\left[\frac{\partial}{\partial x}\, p(x,t) + \frac{1}{kT}\,\frac{\partial V}{\partial x}(x)\; p(x,t)\right]\right\}$$

where the particle's coordinate x corresponds to the angular position of the rotor, p(x,t) is the probability density function of the particle's position, D is its diffusion coefficient, assumed independent of x in this discussion, and V(x) is the potential energy of the particle at position x (see §5.5.a). No force acts on the particle, except at

discrete points, which are spaced equally at a distance d of each other. This distance corresponds to the separation of the m proton binding sites on the periphery of the M-ring, so $d = 2\pi/m$. When the particle finds itself at these positions, which I will call "ratchets", it has a different probability of moving in the positive x-direction, called forward, than in the opposite direction. The bias of these ratchets, χ, is defined as the ratio of the probability of moving forward to the probability of moving backward and depends only on the protonmotive force. It results from the constraints on the M-ring's motion relative to the channel complex when the protonatable sites lign up with the channels. Let H_e be the concentration of protons at the (e) site, H_i be their concentration at the (i) site, and K be the dissociation constant of these proton binding sites. Then the (e) site is occupied a fraction $H_e/(H_e+K)$ of the time, while the (i) site is occupied with probability $H_i/(H_i+K)$. Therefore the probability of finding the constraint for forward motion satisfied, A, and the probability with which backward motion is allowed, R, are given by

$$A = \frac{H_e}{H_e+K}\,\frac{K}{H_i+K}$$

$$R = \frac{K}{H_e+K}\,\frac{H_i}{H_i+K}$$

Their ratio is

$$\chi = \frac{A}{R} = \frac{H_e}{H_i} = e^{-e\Delta p/kT}$$

where the protonmotive force, Δp, is negative under the physiological conditions used to define "forward" and "backward". As shown in the Appendix (§5.5.c) the action of a ratchet with bias χ is described by a

discontinuous change in the potential V(x) at the position of the ratchet, x_r, of magnitude

$$[V(x_r)]^{+}_{-} = -kT \ln(\chi) = e\Delta p.$$

Note that the discontinuous step in the potential corresponds exactly to the change in free energy of the proton that passes through the motor when the rotor moves across the ratchet. The form of V(x) is illustrated in Fig. 5.3A.

We now start the particle off at x = 0, the site of one of the ratchets and ask with what probability, P, it will arrive at the next ratchet to the right, at x = +d, before encountering the ratchet on the left, at x = -d. We also want to know the time, τ, required, on average, to reach either of the adjoining ratchets. Once the particle arrives at +d or -d, the process starts over in the same fashion. Knowing P and τ, one can then compute the net rotation rate, f, of the M-ring. After a long time, t, it will have completed t/τ transitions between adjoining ratchets. Of these, a fraction P occurred in the positive x-direction. Therefore

$$f = \frac{P-(1-P)}{m\tau} = \frac{2P-1}{m\tau}$$

The probability, P, of capture at x = +d and the mean time to capture, τ are obtained by the techniques derived in the Appendix (see §5.5.c). One finds that

$$P = \frac{\chi}{1+\chi}$$

and

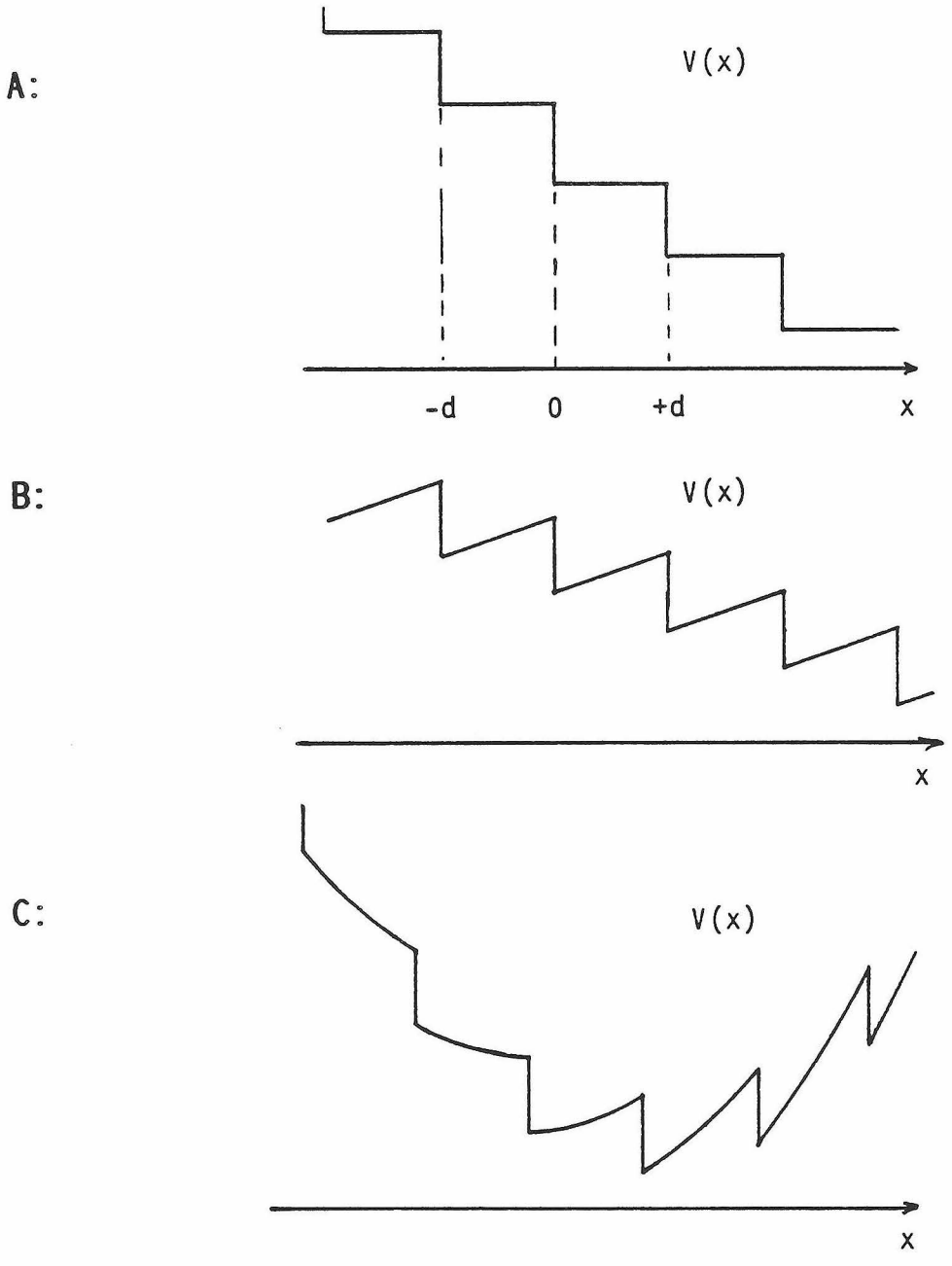

Fig. 5.3. The effects of "ratchets" on the diffusion of a particle. The equivalent potential, V(x), resulting from the action of a regularly spaced array of ratchets on

A: a free particle,

B: a particle under the influence of a constant force, and

C: a harmonically bound particle.

$$\tau = \frac{d^2}{2D} = \frac{2\pi^2}{m^2 D}$$

Therefore

$$(5.1) \qquad f = \frac{mD}{2\pi^2} \frac{\chi-1}{\chi+1} = \frac{mD}{2\pi^2} \tanh\left(\frac{-e\Delta p}{2kT}\right)$$

The predicted qualitative features are confirmed: The rotation rate is proportional to the rotor's diffusion coefficient, increases with Δp, but saturates at a maximal value of $Dm/2\pi^2$. At a given protonmotive force, what is the torque produced by the motor as a function of speed? The external torque, N, is measured as

$$N = 2\pi f c_{ext}$$

where c_{ext} is the rotational drag coefficient of the load attached to the M-ring external to the motor. The diffusion coefficient in eqn.(1) is given by

$$D = \frac{kT}{c_{int} + c_{ext}}$$

where c_{int} is the rotational drag coefficient due to friction within the motor. Thus

$$(5.2) \qquad N = kT \frac{m}{\pi} \tanh\left(\frac{-e\Delta p}{2kT}\right) - 2\pi f c_{int}$$

The external torque decreases from its stall value with increasing speed, because more and more of the free energy available per revolution is being dissipated by frictional forces within the motor. A surprising property is that even at low speeds the torque never exceeds the maximal value of kTm/π, irrespective of the protonmotive force. This early saturation of the stall torque with Δp is not observed experimentally (§5.2.e). More significantly though, this feature appears to contradict

my earlier assertion that any tightly coupled motor must operate reversibly as its speed approaches zero (see eqn. (2.1)). Here this seems to be valid only at very low protonmotive force, where

$$N \xrightarrow[f\to 0]{} kT\,\frac{m}{\pi}\,\tanh\left(\frac{-e\Delta p}{2kT}\right) \simeq \frac{m}{2\pi}\,(-e\Delta p)\ ,\ \text{if } -e\Delta p \ll kT$$

Before resolving this paradox I will discuss the rotation of the motor under a different type of load.

The torque, N, appearing in eqn. (5.2) is inferred from the drag forces associated with the rotor's net motion relative to the viscous medium. This drag results from the same fluctuations that drive the Brownian motion of the rotor in the first place. Could the motor in principle also operate against an externally applied torque? For example, one could imagine winding a string around the shaft of the motor, tying a fly to the end of the string, and lifting it off the floor by rotating the shaft. We now assume that there is no viscous drag external to the motor, so the Brownian motion of the rotor is determined by the diffusion coefficient $D = kT/c_{int}$. In addition to the interaction with the ratchets, the M-ring is subject to a constant torque at all angular positions. The potential V(x) thus rises linearly with x and changes discontinuously by $e\Delta p$ at each of the ratchets, as illustrated in Fig. 5.3B. The values of the capture probability, P, and the capture time, τ, in this potential are derived in the Appendix (§5.5.c), and one obtains an average rotation rate

$$(5.3) \qquad f = \frac{\frac{D}{m}\left(\frac{N}{kT}\right)^2}{\frac{2\pi N}{mkT} + \frac{(\chi-1)(\xi-1)}{(\chi-\xi)}}$$

where

$$\xi = e^{2\pi N/mkT}$$

The loss of symmetry relative to the case of vanishing external torque makes this expression somewhat less appealing. It has a simple form in the limit where both $2\pi N/m$ and $-e\Delta p$ are much larger than kT, which is discussed in the Appendix. As expected, eqn. (5.3) reduces to eqn. (5.1) when N = 0. Finally, one sees that the motor speed vanishes when $2\pi N/m = -e\Delta p$, and therefore the stall torque is

$$N_S = \frac{m}{2\pi}(-e\Delta p).$$

Clearly the motor now runs reversibly at very low speeds.

Why is this not true for rotation against purely viscous forces as described by eqn. (5.1)? The problem lies in the definition of "very low speeds", which should be clarified as meaning "very slow compared to the motor's internal processes". When we slow the motor down by applying an external torque, the internal processes are still going on at a fast rate determined by the diffusion coefficient D. The M-ring is happily stepping forward and backward, but the net rotation resulting from the difference between the rates of forward and backward motion is slow. If, on the other hand, we lower the rotation rate by increasing the viscous drag coefficient, we simultaneously decrease the diffusion coefficient, D, and thus the rate of the torque-generating processes by the same factor. The entire time-scale is simply extended, and the motor runs equally far from thermodynamic equilibrium, independent of the value of D.

b) Internal degrees of freedom.

The preceding analysis suggests a simple alteration by which the

motor can be made to drive large viscous loads more efficiently than in eqn. (5.2): one merely has to attach the rotor to the load rotating in the external medium with an elastic element instead of a rigid link. For example, if the shaft connecting the M-ring to the flagellum could sustain a certain amount of elastic twist, then the M-ring could move about at a fast rate determined by its low internal drag coefficient, c_{int}. It would twist up the spring, and from then on it could operate against a relatively steady external torque in the manner described by eqn. (5.3). The torque in the twisted shaft, in turn, would rotate the external load with large drag coefficient, c_{ext}.

Consider first the case where the external load is held fixed. The M-ring can still execute Brownian motion, but it now experiences two forces: the restoring force in the twisted shaft, with potential energy $V_s(x)$, and the force exerted by the ratchets, derived from the potential $V_r(x)$. The resulting potential $V(x) = V_s(x) + V_r(x)$ is plotted in Fig. 5.3C. Through the action of the ratchets the minimum of $V(x)$ is shifted away from $x=0$, the position where the spring is relaxed, to a new position, x_o, where the potential drop over one of the ratchets just balances the increase of the spring potential over the distance between ratchets:

$$\frac{2\pi}{m} \frac{\partial}{\partial x} V_s(x_o) \simeq -e\Delta p$$

At thermal equilibrium the M-ring is most likely to be found at that position. Therefore the average torque in the twisted shaft, which is equal to the stall torque required to hold the external load in place, is

$$(5.4) \qquad N_S = \frac{m}{2\pi}(-e\Delta p)$$

However, the position of the M-ring fluctuates to either side of its average position. The degree of these excursions is limited by the stiffness of the spring. At thermal equilibrium the probability of finding the M-ring in position x is proportional to $e^{-V(x)/kT}$ which is very small at locations where V(x) differs by more than kT from its minimum value at x_o. Therefore the root-mean-square deviation of x from the equilibrium position is approximately

$$\langle (x-x_o)^2 \rangle^{1/2} \simeq \left(\frac{kT}{\frac{\partial^2}{\partial x^2} V(x_o)} \right)^{1/2}$$

This provides a criterion for how weak the elastic shaft must be to make a difference compared to a rigid link when the external load is allowed to rotate. If the M-ring can move back and forth over several ratchets during the time it takes the load to rotate through the angular distance between two ratchets, then it will continue to operate in much the same way as at stall, keeping the twist in the shaft at about the same value. This requires that the width of its angular distribution at thermal equilibrium extend over more than one ratchet at a time,

$$\langle (x-x_o)^2 \rangle^{1/2} \geq \frac{2\pi}{m}$$

and therefore

$$\frac{\partial^2}{\partial x^2} V_s(x_o) \leq \left(\frac{m}{2\pi}\right)^2 kT$$

If the torque in the elastic shaft is proportional to the twist angle with torsional constant B, one obtains

(5.5) $$B \leq \left(\frac{m}{2\pi}\right)^2 kT$$

as a condition for the stiffness of the spring. A much stiffer shaft will not allow the M-ring to retain equilibrium with the protonmotive force, and thus the torque at low speeds will be limited as described by eqn.(5.2).

What happens when the frictional drag coefficient of the external load, c_{ext}, is gradually reduced, leading to faster and faster rotation? The M-ring must rotate relative to the ratchets on the S-ring at the same rate as the external load. But it can only do so if the external torque acting on it is smaller than the torque exerted by the ratchets. Therefore the elastic shaft will, on average, be less twisted than at stall. Since the torque in the spring doesn't change much when the M-ring moves forward or backward by a ratchet or two, the average rotation rate of the M-ring is well approximated by the rotation rate one would calculate if the external torque were equal to its time-average value and independent of position. Thus the relationship between torque and speed is given by eqn. (5.3). In the particular case of a viscous load one sets

$$N = 2\pi f c_{ext}$$

which turns eqn. (5.3) into an expression for the speed as a function of the external drag coefficient. The maximal rate of rotation at vanishing external torque is again given by

$$f_I = \frac{Dm}{2\pi^2}$$

where $D = kT/c_{int}$ is the rotational diffusion coefficient of the M-ring.

We know that the filament is, in fact, elastic. The Brownian

motion of de-energized tethered cells allows one to estimate the torsional constant of a short flagellar stub. In Streptococcus the average extent of this Brownian motion is $\Delta\theta = (kT/B)^{1/2} \simeq 6°$ (see §1.2.e), which would satisfy eqn. (5.5) if $m \geq 60$. Although this is not an unreasonable number of binding sites, it seems more satisfying to place the elastic element somewhere inside the motor. For example, tethered E. coli, particularly hook mutants, have much stiffer flagellar stubs but still don't show the rapid saturation of torque with Δp predicted by eqn. (5.2). An elegant solution is to attach the channel complex to the S-ring with an elastic connection, and thus let it move relative to the M-ring, which itself is connected rigidly to the external load. Not only does this provide the required spring, but it also increases the rates of the processes involved in torque generation. These are now determined by diffusive behavior of the channel complex, which is much smaller and more mobile than the M-ring. The resulting geometrical configuration is shown in Fig. 5.4. This is the model proposed by Berg and Khan (1983).

At first sight it seemed paradoxical that the inclusion of a simple spring in the motor should make it run more efficiently when driving large external loads. This effect illustrates the very special circumstances under which the flagellar motor operates, due mainly to the fact that thermal fluctuations are setting the time-scale on which things happen. The introduction of an internal degree of freedom in addition to the rotor angle allows the motor to adjust its operating point to the external load. This requirement for internal variables may be common to other molecular mechanisms.

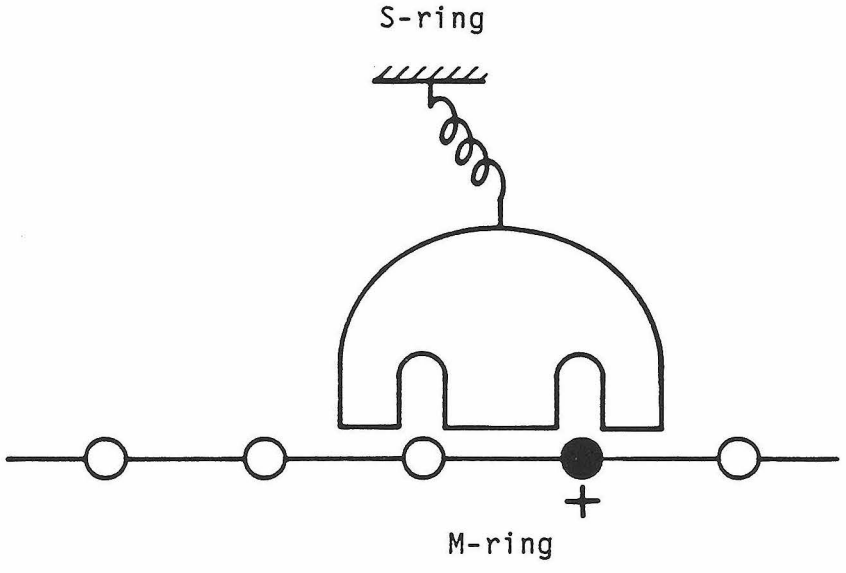

Fig. 5.4. The mobile channel complex in the model of Berg and Khan is elastically bound to the S-ring.

c) My physical picture of flagellar mechanics.

Before discussing the features of this mechanism at high speeds I would like to justify the prominent role of Brownian motion and diffusive effects in my analysis of the model. The flagellar motor operates at the boundary between two quite distinct physical descriptions of dynamical phenomena. On the one hand it causes motion of the flagellar filament or a tethered cell body through the aqueous medium. These processes occur on the scale of several micrometers and are safely described by the methods of continuum hydrodynamics. On this scale the molecular composition of the helical flagellum, the wall of the cell body, or the water surrounding it is of no importance. On the other hand, the active part of the machinery has a diameter of only 25 nanometers and consists of a small number of protein molecules, each of which may have its own specific role in the mechanism. Their motions range over distances comparable to the separation between the surrounding lipid chains. A description of these processes clearly must take the molecular nature of the components into account, and is therefore more likely to involve concepts of statistical mechanics.

One common property seems to characterize the motions of the motor's parts on all length scales: they are strongly damped. On the scale of the rotating cell body this feature is adequately expressed by the Reynolds number of the flow in the surrounding fluid, equal to about 10^{-5}. As noted by Berg (1974), viscous forces acting on the tethered bacterium are so large compared to inertial forces that the rotation would stop within a millionth of a revolution if the motor were suddenly disengaged and the cell body left to coast by its own inertia.

The interaction of the M-ring as a whole with its environment can

probably still be described in the framework of hydrodynamics. This structure is at least partially submerged in the cytoplasmic membrane and unlikely to be shielded completely from contact with lipid or water molecules. Since the size of the M-ring is still considerably larger than that of the solvent molecules, one may treat the surroundings of the rotor as a homogeneous medium of a certain bulk viscosity. Thus one can calculate the Reynolds number of a freely spinning rotor with no external load attached to it. Assuming that the dominant interactions are those with the lipid membrane, a medium of viscosity $\eta \simeq 1$ g/cm/s, one obtains

$$\mathrm{Re} = \frac{\rho \Omega a^2}{\eta} \simeq 10^{-9}$$

where $\rho \simeq 1$ g/cm^3 is a typical protein density, $\Omega \simeq 1000$ s^{-1} is the highest angular frequency of free hooks, and $a \simeq 10^{-6}$ cm is the radius of the M-ring. As a consequence, an M-ring left to coast freely will stop after about 10^{-9} of one revolution. In particular, this implies that a suggestion by Mitchell (1984), that the rotor may act as a flywheel whose inertia carries the motor through positions where it generates no torque, is unlikely to meet with great success. For similar reasons, the observation by Rosen (1974) that the angular momentum of a rotating hook is of the order of Planck's constant, is entirely irrelevant, although not without considerable value for amusement.

On the next smaller scale of individual protein molecules, for example the putative channel complex, the concepts of continuum hydrodynamics are no longer appropriate. The intramembrane particles seen in membrane freeze fractures, which may play the role of the

channel complex, have a diameter of 3 to 4 nm, only a few times larger than the lateral separation between lipid chains. Movement of these motor components over distances of the order of 1 nm, the separation between the putative proton binding sites on the M-ring, is presumably very strongly damped by collisions with the lipid molecules, but these interactions may be more structured than the friction associated with motion in a homogeneous viscous fluid.

Finally, small protein side groups and elastic linkages may move in an environment that is partially shielded from the surrounding lipid or aqueous solvent. On this scale damping may result primarily from interactions within the macromolecule which couple the movement along the one coordinate relevant for torque generation to the many other modes of the protein, thus dissipating the energy in that particular degree of freedom.

The dynamical behavior of proteins is often analyzed within the formalism of transition state theory. In that framework one assumes that the macromolecule exists only in a finite number of discrete conformational states, identified by deep minima of the free energy function in the configuration space of the system. Transitions among such states require that the system pass over a free energy barrier of height large compared to kT, termed the transition state. In Eyring's original formulation of the transition state theory (Eyring 1935) the dynamical evolution of the system is described in terms of undamped oscillations in the free energy well corresponding to the initial state. Under the influence of fluctuating thermal forces a small fraction of the oscillation periods result in a transition across the barrier into the neighboring well, that fraction being given by the Boltzmann factor.

Thus the rate of transitions is given by

$$k = \nu\, e^{-\Delta V/kT}$$

where ν is the oscillation frequency in the initial state, and ΔV is the free energy difference between the transition state and the initial state.

This picture is appropriate for chemical reactions in dilute gases, but, as indicated above, undamped oscillations on the scale of the movements within the flagellar motor are unlikely. However, the essential features of the transition state formalism are retained even when frictional forces are dominant. Under those conditions the system may be viewed as performing stochastic Brownian motion in its configuration space under the influence of a potential given by its free energy. If the barriers between neighboring states are large compared to kT, the system will still spend most of its time within the free energy wells, wandering across the well many times before it once makes a transition into another state. Under those conditions one finds that the rate of transitions has the same dependence as in Eyring's derivation, but ν is now given by the rate at which the system can diffuse across the initial well. This correspondence was first pointed out by Kramers (1940), and I have sketched a derivation in the Appendix (§5.5.b).

The approach of transition state theory relies on the critical assumption that motion of the system, in our case bending or stretching of protein components, is severely restricted by free energy barriers of considerable magnitude. Only under those conditions can one even speak of "states" in what is really a continuous space of the generalized coordinates that define the conformation of the protein. Although use

of this formalism is very prevalent in the literature, few authors take the time to justify the assumptions on which it is based. It is certainly attractive to reduce the complex dynamics in a continuous space to a conceptually simpler network of transitions among a finite set of discrete states. Conveniently, these transitions also occur at a constant rate, which reduces the time-dependent evolution of the system to a set of first-order differential equations with constant coefficients that can be solved by simple algebraic techniques. However, I feel that some loss of generality is involved in making these a priori assumptions. I therefore chose to describe the movement of proteins within the flagellar motor in terms of Brownian motion under the influence of a generalized potential. The concept of transitions among states is replaced by passage across given surfaces in the configuration space of the system. The calculation of the time required for Brownian motion to carry the system through regions between these surfaces is illustrated in the Appendix (§5.5.a). In the specific case where the potential acting on the system shows deep wells, one obtains the results of transition state theory.

Although the "ratchets" with their discontinuous step potential are certainly an idealization of what one could construct from the available natural materials, the discussion of the preceding sections shows that tight binding by deep potential wells between various elements of the motor is in no way essential for the generation of torque. The detailed form of the interactions among moving parts probably cannot be probed by the analysis of steady-state flagellar rotation rates alone. The measurements of the variance in the motor speed by Khan et al. (1985) suggest that motion of the rotor with respect to the stator is, in fact,

not restrained by deep potential wells. The angular position of spinning tethered cells shows a diffusive drift superposed on the steady rotation rate. The effective diffusion coefficient of this stochastic component is very close to the rotational diffusion coefficient of the cell body. If the rotor were strongly bound to the stator at certain angular positions, one would expect the diffusion coefficient to be reduced by the Boltzmann factor corresponding to those potential barriers. However, this observation does not preclude that small components, such as the postulated channel complexes, do bind strongly to the rotor, since they would have only a very small effect on the diffusive behavior of the rotor.

d) Rotation at high speeds.

In part (b) I have shown that the stall torque of the model mechanism pictured in Fig. 5.4 is directly proportional to the protonmotive force and independent of the temperature or the hydrogen isotope driving the motor. This conforms very nicely with the experimental observations, but it is merely a consequence of the fact that proton movement is tightly coupled to M-ring rotation, which makes the motor reversible at low speeds (see eqn. (2.1)). In order to distinguish among all the imaginable tightly coupled motor mechanisms one must therefore compare their function at high speeds, when they operate far from thermal equilibrium. A systematic experimental study of this domain has been possible only recently through Graeme's technique for measuring bundle rotation frequencies in swimming cells. At room temperature the flagella of glycolyzing Streptococcus spin at about 100 Hz, and these rotation rates appear to be close to the maximal

motor speed attainable at vanishing external torque. What idle speed does our model mechanism predict? Since the mobile element is now chosen to be the channel complex, the maximal rotation rate is limited by the time it takes the channel complex to diffuse across the distance between two adjacent proton binding sites on the M-ring:

$$f_I = \frac{2D_C m}{(2\pi a)^2}$$

where a is the radius of the M-ring, and D_C is the translational diffusion coefficient of the channel complex.

At this point one needs a good estimate for the number of binding sites, m. If a single channel complex is driving the motor, as assumed so far, then m is equal to the number of protons transferred during one revolution. Experimentally, the stoichiometry is found to be approximately 1100 protons/revolution, which is obviously somewhat too large for the number of binding sites on a ring of 70 nm circumference. However, there is strong evidence that the motor contains more than one torque generator. Block and Berg (1984) studied a strain of E. coli carrying a defective motB gene in the chromosome, whose flagellar motors did not rotate. Copies of the wild-type gene were then introduced into the cells on a plasmid under control of the lac promoter. Addition of an inducer to tethered cells initiated synthesis of the wild-type motB protein, which apparently was inserted into otherwise complete motors, since the cells started spinning within about 15 minutes of induction. Their speed increased in discrete steps of equal size over several minutes, and the final speed was on average 16 times higher than the speed after the first step. It appears likely that the motB gene codes for part of a torque generator, of which up to 16 copies can operate

independently in a single motor. Structurally these torque generators might well be identical to the intramembrane studs, of which 14 to 16 are seen surrounding flagellar insertion sites in freeze-fractured membranes of Aquaspirillum serpens. If the motor had 16 channel complexes, then 70 binding sites on the M-ring would be sufficient to explain the observed stoichiometry of proton flux to rotor rotation rate.

An estimate of the diffusion coefficient D_C is obtained from the size of the channel complexes and the viscosity of the lipid membrane in which they move. If 16 of them are assembled on the periphery of the M-ring, then they can be no more than 4 nm across. A sphere of 2 nm radius in a medium with the viscosity of olive oil, ca 1 g/cm/s, has a diffusion coefficient of about 10^{-8} cm^2/s. Measurements of protein mobilities in the cell membrane yield similar values: Rhodopsin, a transmembrane protein of molecular weight 38000, has a diffusion coefficient of $4x10^{-9}$ cm^2/s (Stryer 1981, p.224, p.897). Using this latter value for D_C, m = 70, and a = 11 nm, one finds an idle speed of

$$f_I \simeq 10^4 \text{ Hz}$$

This is about 100 times larger than the highest rotation rate observed in Streptococcus, which suggests that the mobility of the channel complex is not in any way limiting the speed of the motor. Under these conditions the stretch in the elastic linkage would always be in equilibrium with the bias of the ratchets and thus the proton concentrations at the (e) and (i) sites on the M-ring. So what causes the experimentally observed decrease in torque at increasing speed?

Berg and Khan (1983) estimate a maximum speed of 300 Hz from a

channel complex diffusion coefficient of 10^{-10} cm^2/s. Such a low value of D_C is not warranted by the action of viscous forces alone, but there could certainly be other effects restraining the mobility of the channel complex. For example, it may interact strongly with the M-ring or the S-ring, and if this interaction potential shows many deep wells, the effective diffusion coefficient might be considerably smaller. Additional friction could also result from motion internal to the protein when the elastic linkage to the S-ring is stretched and relaxed.

However, there are some indications that the maximal speed of the motor is not limited by the mobility of the channel complex. Experimentally one finds that the idle speed increases with protonmotive force even at values of $-e\Delta p$ much larger than kT (§5.2.e). But, as discussed in §5.3.a for diffusion of the M-ring (eqn. (5.1)), the drift rate of the channel complex in the absence of a restoring force in the spring saturates rapidly with increasing bias of the ratchets and depends only weakly on Δp when $-e\Delta p \gg kT$. Furthermore, the idle speed depends on whether protons or deuterons are driving the motor. To accomodate this in the model of Berg and Khan one would have to postulate that the potential resulting from interactions between M-ring and channel complex, which determines the effective diffusion coefficient, D_C, depends strongly on whether a proton or a deuteron is bound at the site on the M-ring.

I therefore suggest a different set of assumptions which identify proton conduction through the (e) and (i) channels as the process that limits the idle speed of the motor. In this model the mobility of the channel complex is assumed so high that it always keeps the torque on the rotor in equilibrium with the occupancy of the proton binding sites

at the periphery of the M-ring. But the proton concentrations at the (e) and (i) sites are not necessarily in equilibrium with those in the external medium and the cytoplasm. For the simplicity of the discussion I will assume that the (i) site is either very close to the cytoplasm or connected to it through a wide open pore, such that $H_i = H_{int}$ at all times, and only conduction through the (e) channel needs to be considered. For now, I will treat the case where the protonmotive force consists of a transmembrane pH-gradient alone. Then the total protonmotive force is

$$\Delta p = -\frac{kT}{e} \ln \frac{H_{ext}}{H_{int}}$$

of which

$$\Delta p_{diss} = -\frac{kT}{e} \ln \frac{H_{ext}}{H_e}$$

is dissipated in proton conduction through the (e) channel, and

$$\Delta p_{eff} = -\frac{kT}{e} \ln \frac{H_e}{H_{int}}$$

is available for torque generation. The latter process occurs reversibly, such that

$$N = \frac{nm}{2\pi} (-e\Delta p_{eff})$$

where n is the number of independent channel complexes (see eqn. (5.4)). The dissipation along the (e) channel, Δp_{diss}, vanishes at zero speed, when there is no proton current through the channel. It rises with increasing proton flow and matches the total protonmotive force at the idle speed.

If one defines the combined conductance, G, of all the (e) channels

in the motor by

$$J = G\ (-\Delta p_{diss})$$

where J denotes the total flux of protons through the motor, then the motor torque is given by

$$N = \frac{nm}{2\pi}\ (-e\Delta p - \frac{e}{G}\ J)$$

$$= \frac{S}{2\pi}\ (-e\Delta p - \frac{Se}{G}\ f)$$

where S = nm is the number of protons transferred per revolution. Thus the motor is completely defined by the stoichiometry S and the channel conductance G. The stoichiometry is a constant and measured at ca 1100 protons/revolution. The channel conductance, on the other hand may depend on all the external conditions: temperature, pH, and the hydrogen isotope. It can also depend on Δp_{diss}; the drop in the electrochemical potential across the channel may not be proportional to the proton current. What physical conduction mechanism would have the right properties to fit some of the experimental observations? A possible clue to the nature of this channel is given by the linear decrease of torque with speed in glycolyzing cells (§5.2.d). Under those experimental conditions the channel current apparently is directly proportional to the protonmotive force across the channel, Δp_{diss}, over a wide range from $-\Delta p_{diss} = 0$ at stall to $-\Delta p_{diss} = -\Delta p \simeq 6kT$ at the idle speed. If the protons were transferred in a water-filled pore and their movement determined by simple diffusion, one would expect their concentration gradient to be proportional to the proton current. But in the very special case where the diffusion coefficient of protons, D_H, is inversely proportional to the local proton concentration, c, one finds

that the proton current is instead determined by the gradient of the proton electrochemical potential. This holds even in presence of an electric field:

$$j = -D_H(c)\left(\frac{\partial c}{\partial x} + \frac{e}{kT}\frac{\partial \psi}{\partial x}\, c\right) = -\frac{D'_H}{c}\left(\frac{\partial c}{\partial x} + \frac{e}{kT}\frac{\partial \psi}{\partial x}\, c\right)$$

$$= -\frac{D'_H}{kT}\frac{\partial}{\partial x}(\mu_H + e\psi) = \frac{D'_H}{kT}\frac{\partial}{\partial x}(e\Delta p)$$

where j is the proton current density, μ_H is the proton chemical potential, and ψ is the electrical potential. Statistical mechanics predicts such a form of the diffusion coefficient if the protons are mainly scattered by other protons (see, for example, Feynman et al. 1963, Ch.43). While this may be expected in a dilute gas, it certainly is not the case in a water-filled channel. But a different conduction mechanism approximates these conditions more closely: proton transfer along ligand chains. Consider the behavior of protons jumping along a string of sites, for example, a linear array of hydrogen bonds, whose ends are in contact with two proton baths at different concentrations. Their motion can be described by a one-dimensional random walk. Since at most one proton can occupy each site at any time, the stepping rate of this random walk, and thus its effective diffusion coefficient, is lower in the regions of high proton concentration. As can be verified numerically, the dissociation constants of the sites along the chain may be chosen such that the current is approximately proportional to the Δp-drop across the chain for $-e\Delta p_{diss}$ ranging from 0 to 10 kT. I therefore suggest that hydrogen ions are transported through the channel complex along a chain of discrete ligand sites. The occurrence of such conduction mechanisms, termed "proton wires", in biological systems has

been postulated for some time, but remains somewhat speculative (see Nagle & Tristram-Nagle 1983 for a review). For example, hydrogen bonds in a β-pleated sheet structure could form a chain along which hydrogen ions travel much as they do in ice. The properties of the histidine side group make it a possible candidate for construction of such a channel.

How do the predictions of this mechanism compare with the known dynamical properties of the motor?

The stall torque is directly proportional to the electrochemical potential of the hydrogen ions. Although, so far, I have only discussed the case where the protonmotive force consists of a pH-gradient, protons can also be driven through the channel by an electric field, which makes transitions to a ligand site at lower electrical potential more frequent than to a higher potential. In the absence of a net proton current through the channel, the two ends of the ligand chain are again in thermal equilibrium with each other, so the full protonmotive force is applied at the channel complex binding sites. One can even relax the assumption made by Berg and Khan (1983) that no electric field acts between the bottom of the (e) channel and the top of the (i) channel: if the protonmotive force between these two locations consisted partly of an electrical field in the plane of the M-ring, the resulting force on the proton at the M-ring binding site between the two channels would simply add to the torque exerted on the M-ring through the action of the ratchets. Since the channel conductance is large enough to allow rotation rates of 100 Hz, the Δp-drop across the channel is very small at the speeds of tethered cells, and thus the motor torque under these conditions is not much lower than the stall torque. The properties (a),

(c), (e), and (g) of §5.2 are therefore confirmed.

Under all conditions the proton flux through the motor is directly proportional to its speed. To match observation (i) of §5.2 one must choose the product of the number of M-ring binding sites and the number of channel complexes as

$$mn = S = 1100.$$

When other external conditions are kept unchanged, the current through the channel increases with the protonmotive force applied between the two ends. One thus predicts that the idle speed of the motor should increase with Δp, property §5.2.f. If one assumes 16 independent (e) channels, then an idle speed of 100 Hz corresponds to a proton translocation rate in each ligand chain of

$$\frac{J}{n} = \frac{S\, f_I}{n} \simeq 7000\ H^+/s$$

which is within the range expected for the putative hydrogen-bonded chains. Also, at a given protonmotive force the Δp-drop across the channel increases with the motor rotation rate, leading to a decrease of the torque generated by the channel complex. Thus property §5.2.d is predicted correctly.

The transition of a proton between adjacent sites on the ligand chain may require a considerable activation energy. One would therefore predict the transition rates and thus the conductance of the (e) channel to increase as the temperature rises, which explains the observed increase of the idle speed. An Arrhenius plot of the idle speed measured by Lowe et al. (1986) as a function of temperature shows significant curvature, suggesting that no single activated chemical process is limiting the rotation rate. Conduction along a hydrogen-

bonded chain has this property, because many transitions with similar activation energies occur in series. The conductance should also be lower in D_2O since the transfer rates among neighboring sites depend largely on the vibration frequency of the hydrogen ion in the bond potential. Thus the dependence of the idle speed on the temperature and the hydrogen isotope (property §5.2.h) is an implicit feature of this model.

At vanishing protonmotive force the motor is locked (property §5.2.j), presumably due to static barriers, as postulated by Khan et al. (1985). This requires that the barrier potential, which might result from interactions with the cell wall, be much larger than kT. Nevertheless, the barriers may be crossed at a protonmotive force of much less than kT/e: If the barrier potential has a rotational symmetry of 6, and 1100 protons carry the M-ring through one revolution, then ca 100 protons are available to climb over the rising side of the barrier. At a Δp of only 5 mV the motor could thus overcome a barrier potential of 20kT, which explains the low threshold Δp for rotation (§5.2.k).

Once steady rotation is initiated, the static barriers seem to disappear, much as if grit had been dislodged from the motor bearings. Under these conditions the model explicitly assumes that the rotor executes free Brownian motion at all times, except during the brief periods when the binding sites on the M-ring align with the channel complex. One therefore predicts that a diffusive drift characterized by the diffusion coefficient of the external load should superpose on the steady average rotation rate (§5.2.l).

Läuger (1977) proposed a model of the flagellar motor with some of the same ingredients as the mechanism described here. In that version

protons flow from the external medium into the cytoplasm by entering the motor near the axis, moving in a radial direction between the faces of the M-ring and the S-ring towards the periphery, from where they are transferred to the internal medium. The opposing faces of the M-ring and the S-ring each carry several rows of proton ligand sites, which are arranged in a radial direction on one ring and slightly tilted with respect to that direction on the other ring. During their movement between the two rings protons are restricted to the intersections between two ligand rows, which offer them an energetically favorable environment compared to the hydrophobic membrane. As the rings rotate relative to each other, the intersection of two ligand rows moves in the radial direction. Thus the flow of protons is coupled to rotation of the motor, but the coupling appears to be quite rigid. This model seems to lack the internal degree of freedom required for efficient rotation against a viscous load. That defect could be fixed by putting the ligand rows of at least one ring onto somewhat elastic spokes. In fact, if these spokes are mobile enough to allow the proton to jump inward and outward among several sites without simultaneous rotation of the shaft, then Läuger's mechanism acquires most of the dynamical features of the model I have described here. The two might only be distinguished by their geometry.

Changes of the motor's direction of rotation during chemotaxis are assumed to be initiated by a reversal of the roles of the (i) and (e) channels within the channel complex. To allow for rapid and complete reversals, the switches in the individual channel complexes, represented by "gating particles" in the model of Berg and Khan (1983), must be highly correlated. Howard has suggested an alternative solution: the

periphery of the M-ring might carry two rings of proton binding sites, separated by a small distance perpendicularly to the membrane, such that only one ring is in contact with the (i) and (e) channels. The M-ring may flip into a different configuration that exposes the other ring to the channels. The proton binding sites on one ring are uncharged unless occupied by a proton, as assumed so far, while the sites on the other ring are negatively charged unless occupied by a proton. Thus the constraints on the motion of the M-ring relative to the channel complex reverse when the nature of the binding sites changes. This solution is more satisfactory, at least in principle, because the chemotactic signal acts on a single rigid structure instead of several entities that are explicitly assumed to be only loosely connected.

Finally, this model makes a notable prediction regarding the dependence of the idle speed on the absolute pH of the medium. The channel resistance is large at very high pH, because few protons are in the channel, and at very low pH, where too many protons are in the channel, blocking each other's motion. The idle speed should thus be largest for pH-values close to the pK of the sites in the conducting chain and decrease markedly at lower and higher values. Such an effect has actually been observed by Shioi et al. (1980). They measured the swimming speed of glycolyzing B. subtilis at various values of the external pH. Even though the protonmotive force varied only little, the swimming speed was maximal at pH 7 and dropped significantly below pH 6 and above pH 8. In this context it may be relevant that the histidine side chain, suspected to be involved in torque generation on the basis of the experiments of Conley and Berg (1984), is titrated near neutral pH. Maybe protons are transported through the channel complex along a

string of histidine residues.

§5.4 SUMMARY

a) The question of coupling.

Models of the flagellar motor and other energy converting enzymes, such as membrane pumps or ATPases, are often classified as belonging to either of two kingdoms: the tightly coupled or the loosely coupled mechanisms. It is important to note that these are not two disjoint classes. Rather, the tightly coupled machines form a subset of the loosely coupled mechanisms. The latter allow flow of the input variable, protons in the case of the flagellar motor, without simultaneous flow of the output variable, such as the revolutions of the flagellum. An engineer's analog of this type of mechanism is a transmission that contains a friction clutch. Tightly coupled machines permit only simultaneous flow of the two variables in a ratio that is strictly defined by the innards of the mechanism. A transmission containing only gear wheels satisfies this description. Clearly any loosely coupled machine can be transformed into a tightly coupled version by strengthening the constraints imposed on the relative slip between input and output flows. In a transmission this corresponds to locking the friction clutch.

Oosawa and Masai (1982) propose a model of the flagellar motor that allows slip between the movement of protons and flagellar rotation. In a later paper (Oosawa and Hayashi 1983) the transition to a tightly coupled mechanism is shown in detail. As expected, this version contains fewer free parameters than the original, more general scheme. However, Oosawa and Hayashi argue that a tightly coupled motor would show irregular motion at low protonmotive force, because fluctuations in

Δp or the flow of protons would translate directly into fluctuations of the rotor speed. Smooth rotation at low Δp, they conclude, is possible only via loose coupling.

Unfortunately their argument remains rather vague. The discussion centers on the steady-state values of the motor's torque and the proton flux, and the subject of fluctuations is never considered quantitatively. It is unclear that the motor's stochastic behavior with respect to thermal fluctuations is at all related to the degree of coupling, which merely describes the relationship of steady-state quantities. More likely, those properties are determined by the internal degrees of freedom. For example, in the mechanism presented here several protons can move into or out of the cell without concomitant motion of the rotor. The channel complex simply advances or retreats with respect to its equilibrium position. The extent of this slop is determined by the number of ratchets accessible to the channel complex in its thermal motion, assumed to be greater than one on the basis of the discussion in §5.3.b. In the long run, however, the discrepancy between the total angle traversed by the rotor and the total number of protons transferred is never larger than this slop, so the motor is still tightly coupled in its steady-state operation. Fluctuations in Δp can only affect the torque on the rotor if they persist long enough for the channel complex to move across several ratchets. With the assumptions about the mobility of the channel complex made in §5.3.d this time is of the order of a few μs. A similar critical time scale for thermal fluctuations appears in the model of Oosawa and Masai, given by the time required for transitions of their mobile protein linkage between the two sides of the membrane. The

stochastic studies of flagellar rotation by Khan et al. (1985), which showed that the rotor exhibits rotational Brownian motion superimposed on the steady rotation, imply that motion of the rotor is not restricted by the torque generating machinery during most of a flagellar revolution. This condition can be met irrespective of the degree of coupling in the motor mechanism.

To date there is no experimental evidence suggesting that slippage between proton movement and M-ring rotation occurs. More significantly, many of the features of flagellar rotation follow implicitly from the assumption of tight coupling. As mentioned repeatedly in this chapter, all the measured properties of the stall torque are consistent with reversible operation of the motor at low speeds, which itself is a consequence of the assumption of tight coupling. Furthermore, the ratio of the rotation-dependent proton flux to the rotor speed is invariant under all experimental conditions tested so far. It is also very close to the number of protons per revolution predicted from the value of the stall torque under the assuption of tight coupling. A less restrictive, loosely coupled mechanism with significant flow of protons through the stalled motor could account for all these properties only by ad hoc arrangement of many free parameters.

The assumption that flagellar rotation is, in fact, tightly coupled to the movement of protons through the motor should therefore serve as a working hypothesis for further investigations. It provides the simplest framework to accomodate all the known properties of the motor. It also makes several strong predictions which can be tested quite stringently.

b) Some suggestions for further work.

The tight coupling hypothesis could be tested further in two experimental regimes. One involves measurements of the torque generated at the speeds of tethered cells as a function of the protonmotive force, to determine whether the proportionality predicted by the reversible operation of the motor holds over a wider range. The main challenge lies in measuring an artificially generated protonmotive force reliably at values above 80 mV. As outlined in Chapter 3, the Δp may drop rapidly upon energization, which makes it essential to choose a fast probe. Voltage- and pH-dependent dyes might be useful; they could be calibrated with standard ionic exchange techniques under more steady conditions, maybe in partially deenergized metabolizing cells. Such direct measurements of Δp would be very valuable in deciding whether the apparent pH-dependence of the stall torque as well as its saturation at large nominal protonmotive force (see Chapter 2) actually reflect difficulties in generating an artificial membrane potential. If this were not so, the assumption of tight coupling would have to be abandoned. The apparent discrepancy between the effects of a pH-gradient and an electrical potential on the stall torque reported by Khan and Berg (1983) should be another incentive to verify the value of the artificial protonmotive force (see §5.2.e).

In the high-speed regime the measurements of rotation-dependent proton flux could be extended. In particular one could determine its dependence on the rotor speed by changing the medium viscosity. I expect such measurements to be affected by a smaller experimental error than those presented in Chapter 4, because the protonmotive force, the temperature, and the hydrogen isotope remain unchanged. Thus the flux

through channels unrelated to the motor, which constitutes the dominant portion of the total flux, should remain constant throughout the experiment. I have attempted to artificially energize cells in media with various concentrations of Ficoll, a highly branched sucrose polymer whose solutions are newtonian. The cells swim fine, but the resolution of the flux change on addition of antibody deteriorates. Lowe et al. (1986) found that a tenfold increase in viscosity is needed to slow the motor down by a factor of two, and under these conditions the mixing time in my stirred cell suspension was unacceptably long. Ficoll also has an appreciable buffering capacity at these concentrations, which makes it necessary to use higher cell densities. Being of a purely technical nature, these problems are likely to be solved. An incentive for doing so may lie in the observation that cells of strain V4051, which tumble upon artificial energization without forming a bundle, show only about half of the rotation-dependent flux seen in SM197. As mentioned earlier, the flagella of the mutant SM29, which tumbles incessantly even when glycolyzing, spin only half as fast as those of strain SM197.

Further investigation of the dependence of the motor's torque on its rotation rate could also be fruitful. So far, this relationship has only been described in glycolyzing Streptococcus at 22°C in H_2O. The extreme values, namely the stall torque and the idle speed have been measured under artificially energized conditions at various temperatures and in D_2O. A more detailed study under those conditions, changing the medium viscosity to vary the motor's speed, would yield more information on the behavior far from thermodynamic equilibrium. One might also test the predicted dependence of the motor's idle speed on the external pH in

Streptococcus. This could be done in glycolyzing cells and should be paired with a measurement of the protonmotive force. Another open question is whether a pH-gradient and an electrical membrane potential are equally effective in driving the motor at high speeds, where their equivalence is no longer guaranteed by thermodynamics. Could the results of such experiments still be modeled by assuming that proton conduction is limiting the motor's speed?

Not all questions will be answered by measuring steady-state averages of speed, torque, protonmotive force and proton flux alone. I think that the single piston E. coli engines under construction now will be very helpful in determining variations in the torque generating process during the course of a flagellar revolution. Since the averaging effect over many torque generators is avoided, these strains should allow a closer look at the interaction between M-ring and S-ring. There is some hope that studies of the stochastic behavior of these engines will offer more insight on the nature of protein movements within the mechanism. Are they best described by instantaneous transitions among discrete conformational states, or is a more general formalism, such as that of continuous Brownian motion, more appropriate? The flagellar motor may be uniquely suited for such investigations, since the immediate result of motions on the molecular scale is visible to the almost naked eye.

§5.5 APPENDIX

a) Properties of continuous diffusion derived from those of the discrete random walk.

A discrete random walk accurately approximates diffusion in a continuous variable if its character, namely the length of the steps and the rate at which they occur, changes appreciably only over distances of many steps (see, for example, Chandrasekhar 1943). In this limit random walks are often used to approximate diffusion problems in numerical applications. Here I will show that many of the properties of continuous diffusion follow from the nature of the discrete random walk. In particular, one can derive the time-dependent diffusion equation, the corresponding backward equation, the probability of capture at an absorbing barrier, the mean time to capture, as well as higher moments of the capture time distribution. All these results can be obtained by other methods (see, for example Gardiner 1983), but I feel that the following treatment makes them more intuitive from first principles. It will also be helpful in discussing the effects of "ratchets" in part (c).

Consider a one-dimensional discrete random walk with step size δ among sites on the real axis at $x = i\delta$ where i is integer. During a short time interval dt a particle at site i steps to site (i+1) with probability $k_i^+ dt$, and it steps to site (i-1) with probability $k_i^- dt$. Given that the particle started at site i' at time t', what is the probability $p_i(t)$ of finding it at site i at time t? Consider transitions from site i to the adjoining sites over the interval from t to t+dt. The particle will cross from site i to (i+1) with probability

$p_i(t)\ k_i^+\ dt$, and in the opposite direction with probability $p_{i+1}(t)\ k_{i+1}^-$ dt. The net transfer of probability from site i to (i+1) is given by $j_i(t)\ dt$, where

$$j_i(t) = p_i(t)\ k_i^+ - p_{i+1}(t)\ k_{i+1}^-$$

is the probability flux between sites i and (i+1) at time t. The time rate of decrease of the probability of finding the particle at site i must equal the total probability flux out of site i, so

$$\frac{\partial}{\partial t}\ p_i(t) = -(j_i(t) - j_{i-1}(t)) \tag{5.6a}$$

where $j_i(t)$ may be rewritten as

$$j_i(t) = -\left\{ \frac{k_{i+1}^- + k_i^+}{2}\ (p_{i+1}(t) - p_i(t)) + (k_{i+1}^- - k_i^+)\ \frac{p_{i+1}(t) + p_i(t)}{2} \right\}. \tag{5.6b}$$

This is the Fokker-Planck equation describing the time evolution of the random walk. Two types of boundary conditions are generally considered: at an absorbing site one demands that $p_i(t) = 0$, while the boundary condition at a reflecting site is $j_i(t) = 0$. In the limit of very small step size δ this random walk approximates a continuous diffusion process. If one defines a probability density $p(x,t)$ with $p(i\delta,t) = p_i(t)/\delta$ and a probability current $j(x,t)$ with $j(i\delta,t) = j_i(t)$, then equations (5.6a) and (5.6b) turn into differential equations

$$\frac{\partial}{\partial t}\ p(x,t) = -\frac{\partial}{\partial x}\ j(x,t) \tag{5.7a}$$

$$j(x,t) = -\ D(x)\ \frac{\partial}{\partial x}\ p(x,t) - C(x)\ p(x,t) \tag{5.7b}$$

where

$$D(x) = \lim_{\delta \to 0} \delta^2 \frac{k_i^+ + k_{i+1}^-}{2}$$

and

$$C(x) = \lim_{d \to 0} \delta \, (k_{i+1}^- - k_i^+).$$

Equations (5.7a) and (5.7b) describe time-dependent diffusion in a potential V(x) if one identifies D(x) with the diffusion coefficient and C(x)/D(x) with 1/kT ∂V(x)/∂x, such that

$$(5.8) \qquad \frac{\partial}{\partial t} p(x,t) = \frac{\partial}{\partial x} \left\{ D(x) \left[\frac{\partial}{\partial x} p(x,t) + \frac{1}{kT} \frac{\partial V(x)}{\partial x} p(x,t) \right] \right\}.$$

In analogy to the discrete version, the boundary conditions are that p(x,t) = 0 at an absorbing boundary and j(x,t) = 0 at a reflecting barrier.

Equation (5.8) could also have been obtained as follows: Fig. 5.5 shows a graph of the relevant transition probabilitiess in this process. Time increases downwards, and the various sites are displayed horizontally. The vertices of the graph correspond to various possible states of the particle; for example, a vertex in row t and column i denotes that the particle is at site i at time t. Each segment of the graph is labeled with the corresponding transition probability, namely the probability that a particle in the upper (earlier) state will reach the lower (later) state. Thus the probability of reaching a particular state (i,t) from the initial state (i',t') is given by the sum of the transition probabilities for each path leading from (i',t') to (i,t). The transition probability for each path is given by the product of the

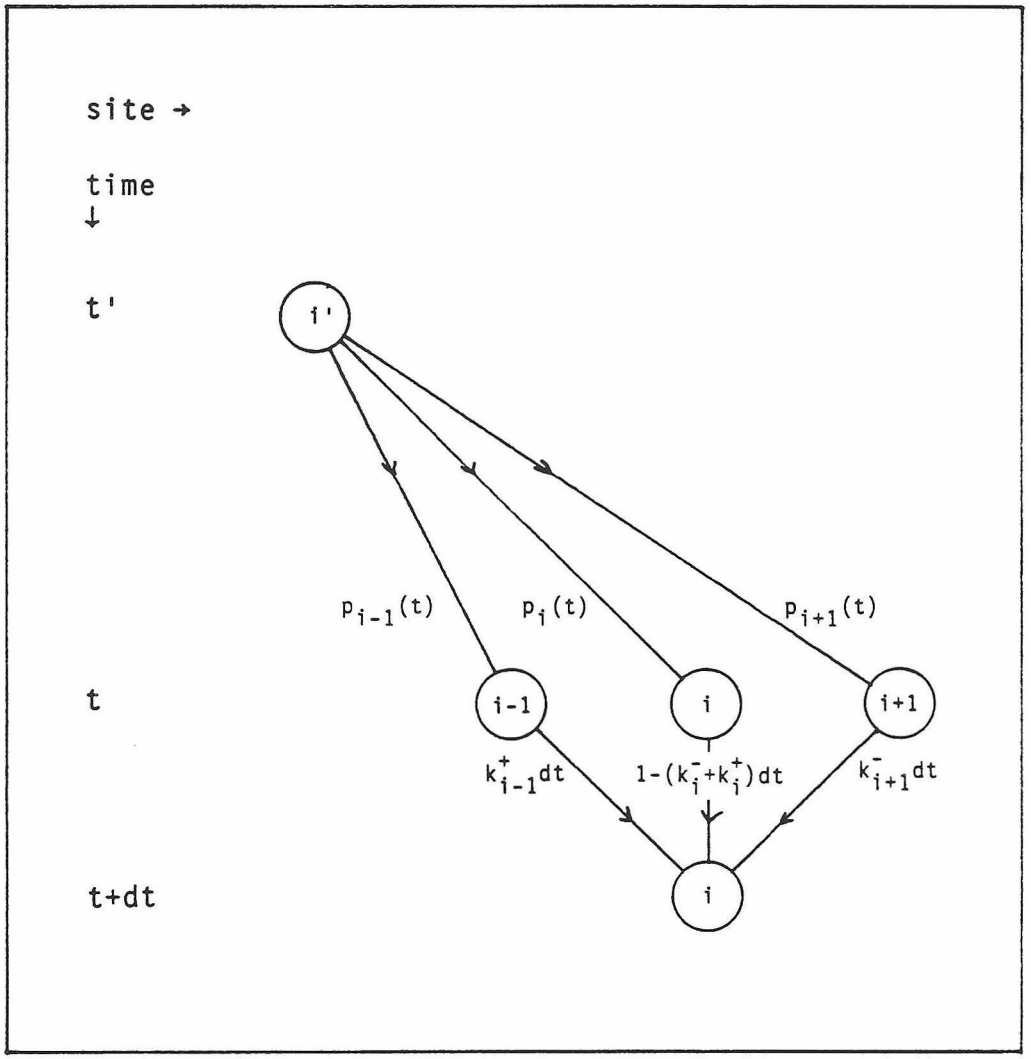

Fig. 5.5. Transition probabilities during a random walk, illustrating the derivation of the Fokker-Planck equation.

transition probabilities corresponding to each of its segments. Thus one finds

$$p_i(t+dt) = k^+_{i-1}dt\ p_{i-1}(t) + \{1-(k^-_i+k^+_i)dt\}\ p_i(t) + k^-_{i+1}dt\ p_{i+1}(t)$$

which turns into equation (5.8) after some rearrangement of terms and taking the appropriate limit at small δ.

A similar graph is useful in deriving the corresponding backward equation. Given that the particle is at site i at time t, we now want to know the probability $p_{i'}(t')$ that it started from site i' at time t'. One now has to consider what happened during the first short time interval of the walk. Fig. 5.6 shows a graph of the relevant transitions. Each segment between two states is labeled by the probability that the particle started in the upper state given that it reached the lower state. One finds $\bar{p}_{i'}(t'-dt)$ by summing the probabilities for each path leading backward from the final state (i,t) to this initial state. Thus one obtains

$$\bar{p}_{i'}(t'-dt) = k^-_{i'}dt\ \bar{p}_{i'-1}(t') + (1-(k^+_{i'-1}+k^-_{i'+1})dt)\ \bar{p}_{i'}(t') + \\ + k^+_{i'}dt\ \bar{p}_{i'+1}(t').$$

The boundary conditions on $\bar{p}_{i'}(t')$ are similar to those on $p_i(t)$: the probability that the particle originated from an absorbing site is zero, while the probability current

$$\bar{J}_{i'}(t') = \bar{p}_{i'+1}(t')\ k^+_{i'} - \bar{p}_{i'}(t')\ k^-_{i'+1}$$

vanishes at a reflecting boundary. In the limit of small step size δ the above equation turns into a differential equation for the

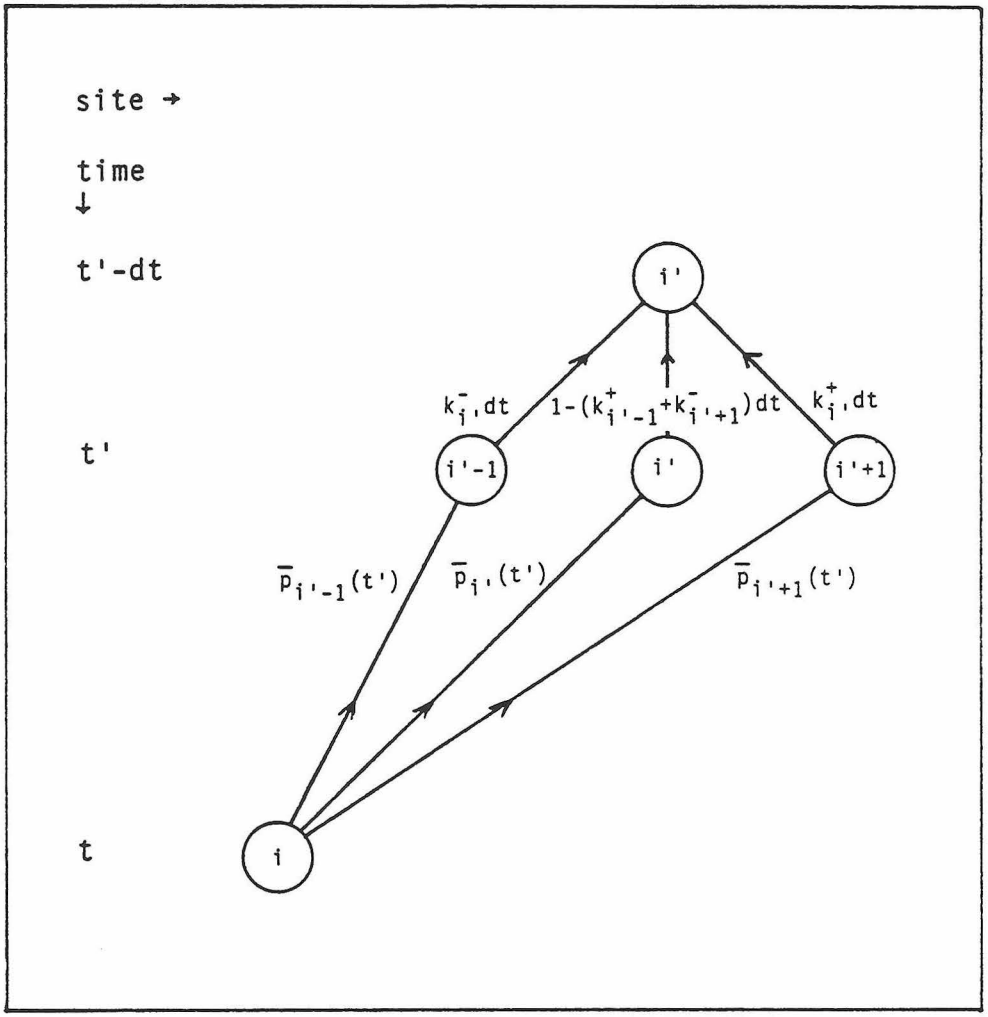

Fig. 5.6. Transition probabilities during a random walk, illustrating the derivation of the backward Fokker-Planck equation.

probability density $\bar{p}(x',t')$

$$\frac{\partial}{\partial t'}\bar{p}(x',t') = \frac{\partial}{\partial x'}\left\{D(x')\left[-\frac{\partial}{\partial x'}\bar{p}(x',t') + \frac{1}{kT}\frac{\partial V(x')}{\partial x'}\bar{p}(x',t')\right]\right\}$$

which is called the backward diffusion equation. Boundary conditions are that $\bar{p}(x',t') = 0$ at an absorbing barrier and

$$\bar{j}(x',t') = -D(x')\left[-\frac{\partial}{\partial x'}\bar{p}(x',t') + \frac{1}{kT}\frac{\partial V(x')}{\partial x'}\bar{p}(x',t')\right]$$

at a reflecting barrier.

Next I will consider capture probabilities. If the particle starts walking at site i, what is the probability, P_i, that it will reach site m ($m>i$) before site l ($l<i$). If sites m and l are absorbing, this is the probability that a particle released at i is absorbed at m. We now consider what happens during the first step of the random walk. That step takes the particle to (i+1) with probability $k_i^+/(k_i^-+k_i^+)$. From there it has a probability P_{i+1} of being captured at site m. A first step to (i-1) occurs with probability $k_i^-/(k_i^-+k_i^+)$, and from there the particle arrives at site m with probability P_{i-1}. Fig. 5.7 shows a graph of these transitions with their respective transition probabilities. One sees that

$$P_i = \frac{k_i^-}{k_i^-+k_i^+}P_{i-1} + \frac{k_i^+}{k_i^-+k_i^+}P_{i+1}$$

which can be rewritten as

$$\left[\frac{k_i^++k_{i+1}^-}{2}(P_{i+1}-P_i) - \frac{k_{i-1}^++k_i^-}{2}(P_i-P_{i-1})\right] - \\ - \frac{1}{2}\left[(k_{i+1}^--k_i^+)(P_{i+1}-P_i) + (k_i^--k_{i-1}^+)(P_i-P_{i-1})\right] = 0.$$

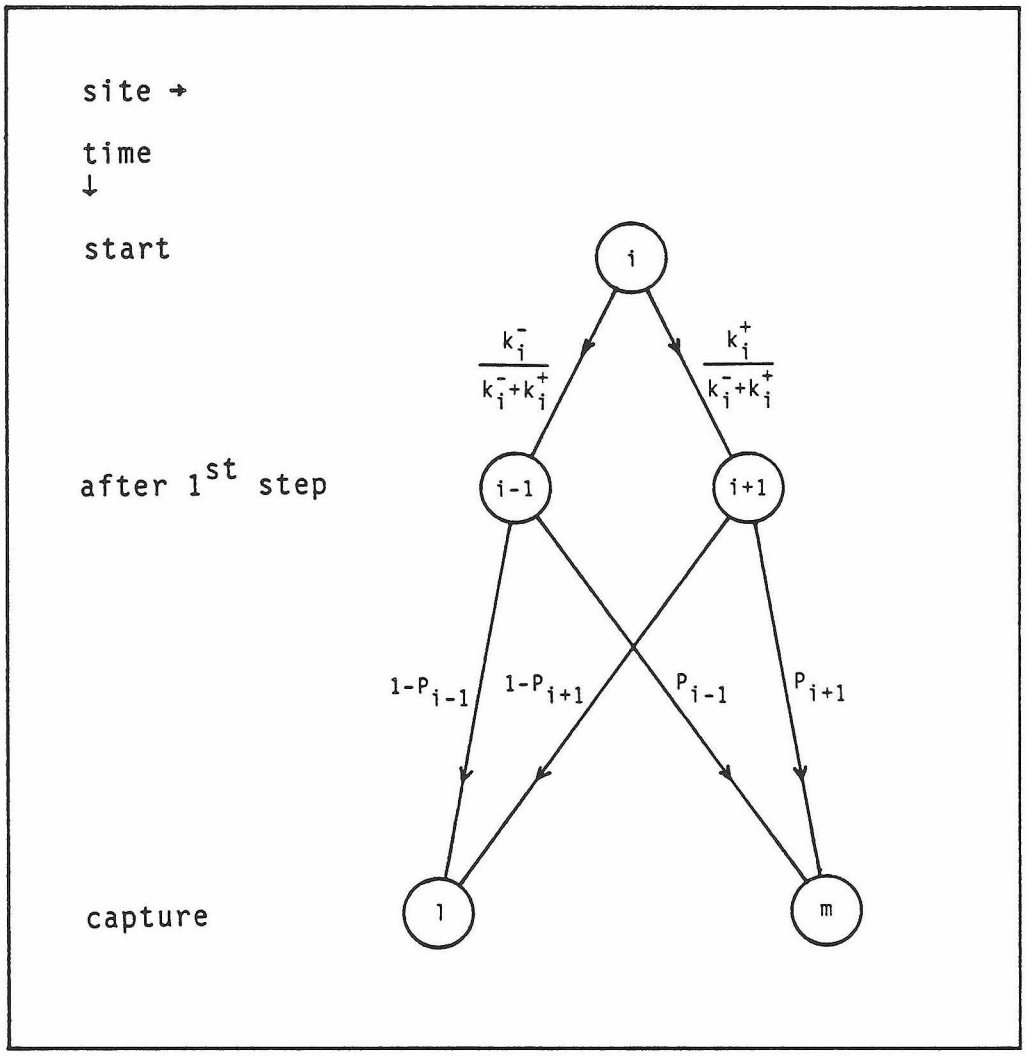

Fig. 5.7. Transition probabilities during a random walk, illustrating the calculation of capture probabilities and capture times.

In the limit of small δ one can again define the capture probability $P(x)$ as a function of the continuous variable x with $P(i\delta) = P_i$. The above equation then turns into a differential equation for $P(x)$

$$(5.9) \qquad \frac{\partial}{\partial x}\left[D(x)\,\frac{\partial}{\partial x}\,P(x)\right] - C(x)\,\frac{\partial}{\partial x}\,P(x) = 0.$$

Boundary conditions are that $P(x) = 1$ at the boundary whose capture probability is being considered, $P(x) = 0$ at all other absorbing boundaries, and $\partial P/\partial x = 0$ at reflecting barriers.

Given that the particle starts its random walk at site i and that it eventually gets captured at site m, what is the average duration $\langle t\rangle_i$ of its walk? The first step takes an average time of $1/(k_i^- + k_i^+)$. With probability $k_i^+/(k_i^- + k_i^+)$ the particle then finds itself at site (i+1), from where it takes an average time of $\langle t\rangle_{i+1}$ to reach m. If it had stepped to (i-1), an additional time of $\langle t\rangle_{i-1}$ would be required for capture. Thus the mean time to capture from site i is obtained by weighting the mean capture times for the two paths between the initial and the final state shown in Fig. 5.7 with their relative probabilities. Since the total probability of capture from site i is equal to P_i, one finds

$$\langle t\rangle_i = \frac{1}{P_i}\left(\frac{k_i^+}{k_i^- + k_i^+}\,P_{i+1}\left\langle t + \frac{1}{k_i^- + k_i^+}\right\rangle_{i+1} + \frac{k_i^-}{k_i^- + k_i^+}\,P_{i-1}\left\langle t + \frac{1}{k_i^- + k_i^+}\right\rangle_{i-1}\right)$$

which is equivalent to

$$(k_i^- + k_i^+)\,P_i\,\langle t\rangle_i = P_i + k_i^+\,P_{i+1}\,\langle t\rangle_{i+1} + k_i^-\,P_{i-1}\,\langle t\rangle_{i-1}.$$

In the limit of small step size δ one defines $\tau^{(1)}(x)$ as the mean capture time from x, and the above difference equation turns into

$$(5.10)\quad \frac{\partial}{\partial x}\left[D(x)\,\frac{\partial}{\partial x}\,[P(x)\,\tau^{(1)}(x)]\right] - \\ - C(x)\,\frac{\partial}{\partial x}\,[P(x)\,\tau^{(1)}(x)] + P(x) = 0$$

with $P(x)\tau^{(1)}(x) = 0$ at all absorbing boundaries, and $\partial/\partial x[P(x)\tau^{(1)}(x)] = 0$ at reflecting boundaries. If one is merely interested in the mean time to capture at any of the absorbing boundaries, irrespective of where the particle lands, then $P(x) = 1$ identically, which simplifies the equation considerably.

Finally, one can compute higher moments of the capture time distribution. Let $\langle t^{\nu}\rangle_i$ be the ν^{th} moment of the time to capture if the random walk starts at site i. Since the time required for the first step is not correlated with the time required for all others, one can write, in analogy to the case $\nu = 1$,

$$\langle t^{\nu}\rangle_i = \frac{1}{P_i}\left(\frac{k_i^+}{k_i^-+k_i^+}\,P_{i+1}\,\langle(t+\frac{1}{k_i^-+k_i^+})^{\nu}\rangle_{i+1} + \right. \\ \left. + \frac{k_i^-}{k_i^-+k_i^+}\,P_{i-1}\,\langle(t+\frac{1}{k_i^-+k_i^+})^{\nu}\rangle_{i-1}\right).$$

For small step size δ, the total time to capture is much longer than the first step, so

$$(t+\frac{1}{k_i^-+k_i^+})^{\nu} \simeq t^{\nu} + \nu\,t^{\nu-1}\,\frac{1}{k_i^-+k_i^+}$$

and thus

$$(k_i^- + k_i^+)\, P_i \langle t^\nu \rangle_i = k_i^+ P_{i+1} \langle t^\nu \rangle_{i+1} + k_i^- P_{i-1} \langle t^\nu \rangle_{i-1} +$$

$$+ \nu \left(\frac{k_i^+}{k_i^- + k_i^+} P_{i+1} \langle t^{\nu-1} \rangle_{i+1} + \right.$$

$$\left. + \frac{k_i^-}{k_i^- + k_i^+} P_{i-1} \langle t^{\nu-1} \rangle_{i-1} \right)$$

$$\simeq k_i^+ P_{i+1} \langle t^\nu \rangle_{i+1} + k_i^- P_{i-1} \langle t^\nu \rangle_{i-1} + \nu P_i \langle t^{\nu-1} \rangle_i .$$

In the continuous limit one defines $\tau^{(\nu)}(x)$ as the ν^{th} moment of the capture time. Its spatial dependence is governed by

$$(5.11) \quad \frac{\partial}{\partial x} \left[D(x) \frac{\partial}{\partial x} [P(x)\, \tau^{(\nu)}(x)] \right] - C(x) \frac{\partial}{\partial x} [P(x)\, \tau^{(\nu)}(x)] +$$

$$+ \nu\, P(x)\, \tau^{(\nu-1)}(x) = 0$$

with boundary conditions analogous to the case $\nu = 1$.

b) General solutions and calculation of the transition rate across a large barrier.

Equations (5.9), (5.10), and (5.11) for the capture probability and the capture time can be integrated directly. Consider diffusion of a particle with diffusion coefficient D(x) in a potential V(x) between two absorbing boundaries at x = a and x = b (b>a). Let P(x) denote the probability that a particle released at x is captured at b and $\tau^{(\nu)}(x)$ be the ν^{th} moment of the time to capture at b. Then

$$(5.12) \quad P(x) = \frac{\phi(x)}{\phi(b)}$$

$$(5.13) \qquad \tau^{(\nu)}(x) = \psi^{(\nu)}(b) - \frac{\phi^{(\nu)}(x)}{P(x)}$$

where

$$\phi(x) = \int_{x'=a}^{x} \frac{1}{D(x')} e^{V(x')/kT} \, dx'$$

and

$$\psi^{(\nu)}(x) = \int_{x'=a}^{x} \int_{x''=a}^{x'} \frac{1}{D(x')} e^{\frac{V(x')-V(x'')}{kT}} \nu \, P(x'') \, \tau^{(\nu-1)}(x'') dx'' dx'.$$

These equations allow an estimate of the time required to cross a large potential barrier by diffusion (see, for example, Gardiner 1983). Consider a potential consisting of two wells separated by a barrier of height large compared to kT, as shown in Fig. 5.8. We want to determine how long it takes for a particle that starts at point c in the left well to appear at b in the right well. The particle will wander back and forth many times in the left well before making the first transition, and thus one doesn't expect the transition rate to depend strongly on the choice of c and b, as long as they are both far from the top of the barrier. If the left bound, a, of the interval is chosen high up on the left wall of the potential, one sees that $P(c) \simeq 1$: the particle almost certainly crosses the barrier before arriving at a. Also, $\psi^{(\nu)}(c)$ is much smaller than $\psi^{(\nu)}(b)$ since the exponential in the integral is very large when $x' \simeq e$, the top of the barrier, and $x'' \simeq c$, the bottom of the well. To a first approximation one can expand the potential V(x) about these two extrema with a truncated Taylor series and then extend the integral over all values of x. Thus

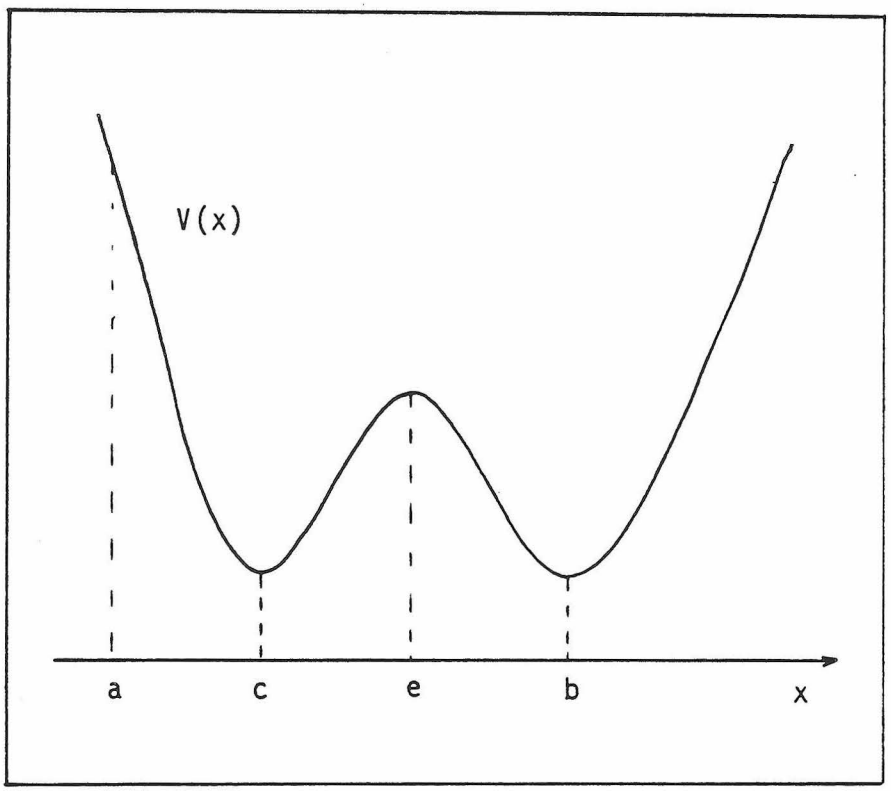

Fig. 5.8. Two potential wells separated by a barrier, illustrating the calculation of transition rates in the limit of transition state theory.

$$\psi^{(\nu)}(b) \simeq \int_{x'=-\infty}^{+\infty} \int_{x''=-\infty}^{+\infty} \frac{1}{D(x')} e^{\frac{\{V(e)-\epsilon/2(x-e)^2\}-\{V(c)+\gamma/2(x-c)^2\}}{kT}} \cdot \nu\, \tau^{(\nu-1)}(x'')\, dx''\, dx'$$

where $\gamma = \frac{\partial^2 V(c)}{\partial x^2}$ and $\epsilon = -\frac{\partial^2 V(e)}{\partial x^2}$.

In particular, the mean time to capture at b is

$$\tau^{(1)}(c) = \frac{1}{D(e)} \frac{2\pi kT}{\sqrt{\gamma\epsilon}} e^{\frac{V(e)-V(c)}{kT}}$$

and the higher moments are given by

$$\tau^{(\nu)}(c) = \nu\, \tau^{(\nu-1)}(c)\, \tau^{(1)}(c) = \nu!\, [\tau^{(1)}(c)]^{\nu}.$$

These can be recognized as the moments of an exponential distribution of capture times. Thus transitions from c to b occur at a constant rate per unit time

$$k = \frac{D(e)\sqrt{\gamma\epsilon}}{2\pi kT} e^{-\frac{V(e)-V(c)}{kT}}.$$

This result is very similar to that obtained from the formalism of transition-state rate theory, in which the motion of the particle in the wells is assumed to be essentially undamped. However, the frequency prefactor in the above expression is not a vibration frequency but determined by the times in which the particle can diffuse across distances of the order of the width of the well and the width of the barrier. This can be viewed as the rate at which it "attempts" to cross

the barrier. The exponential Boltzmann factor determines what fraction of these attempts is successful. For a large barrier that fraction is very small, and, since successive attempts at crossing the barrier are statistically independent, the transition rate is independent of the time spent in the left-hand well. This problem was first discussed by Kramers (1940), who derived an expression for the transition rate valid both in the underdamped and the overdamped regime (see also Chandrasekhar 1943).

c) Ratchets.

To understand the role of ratchets in continuous diffusion I will again discuss the discrete random walk and then take the limit of very small and fast steps. In the context of part (a) I will define a ratchet as a site r on the random walk coordinate with the property that a particle is always more likely to step from r to (r+1) than vice versa by a factor of

$$\chi = \frac{k_r^+}{k_{r+1}^-}$$

where χ is called the bias. If this property is maintained as the steps in the random walk get smaller and smaller, one eventually obtains the diffusion limit of a ratchet at position x_r. However, one finds that $C(x_r)$ diverges in this limit:

$$C(x_r) = \lim_{\delta\to 0} \delta\,(k_{r+1}^- - k_r^+) = \lim_{\delta\to 0} \frac{2}{\delta}\,\delta^2\,\frac{k_{r+1}^- + k_r^+}{2}\,\frac{1-\chi}{1+\chi}$$

$$= \lim_{\delta\to 0} \frac{2}{\delta}\,D(x_r)\,\frac{1-\chi}{1+\chi}.$$

But the integral of $C(x)$ across x_r is of the order of $\delta^2(k^-_{i+1}-k^+_r)$ and thus converges. This means that the potential $V(x) = \int C(x)/D(x)dx$ shows a finite discontinuity at $x = x_r$. The magnitude of this step can be found from a consideration of thermal equilibrium. When there is no flow across the ratchet, the ratio of the adjacent occupancy probabilities must be the inverse of the ratio of the stepping rate constants, $p_{r+1}\, k^-_{r+1} = p_r\, k^+_r$. In the continuous limit this applies for the probability densities, and thus

$$\chi = \frac{p(x_r)_+}{p(x_r)_-} = e^{-\frac{[V(x_r)]^+_-}{kT}}$$

where $p(x_r)_+$ is the limiting value of $p(x_r)$ approaching from $x > x_r$, $p(x_r)_-$ is the limit from $x < x_r$, and $[V(x_r)]^+_- = V(x_r)_+ - V(x_r)_-$. The effects of the ratchet on diffusion of the particle are therefore described by the effective potential

$$V_r = \begin{cases} 0 & , \text{ if } x < x_r \\ -kT \ln\chi & , \text{ if } x > x_r. \end{cases}$$

Formally, one could view such a ratchet as an intermediate between a reflecting boundary and an absorbing boundary. In particular, a ratchet with bias $\chi = 0$ looks like a reflecting boundary from $x < x_r$ and like an absorbing boundary from $x > x_r$, while the roles are reversed for $\chi = \infty$.

The ratchet potential adds to whatever other potential is affecting Brownian motion of the particle, and it thus becomes straightforward to calculate capture probabilities and capture times from equations (5.12) and (5.13). I will give the solution for the potential pictured in Fig. 5.3B. Ratchets of equal bias $\chi = \exp(-V_r/kT)$ are distributed equidistantly on the x-axis at the points $x_r = nd$. In addition, a

constant force, F, acts on the particle, whose diffusion coefficient, D, is assumed to be independent of x. We want to determine the average drift velocity of a particle in this potential. Focusing attention on the ratchet at the origin, let P be the probability that a particle released at the origin reaches the ratchet at +d before the one at -d, and let the mean time to capture at either x = +d or x = -d be denoted by τ. Then equations (5.12) and (5.13) lead to

$$P = \frac{e^{Fd/kT}}{e^{V_r/kT}+e^{Fd/kT}}$$

and

$$\tau = \frac{1}{D}\left(\frac{kT}{F}\right)^2 \frac{(e^{Fd/kT}-1)(e^{V_r/kT}-1) + \frac{Fd}{kT}(e^{Fd/kT}-e^{V_r/kT})}{e^{Fd/kT}+e^{V_r/kT}}.$$

The average drift velocity is given by

$$v = \frac{d}{\tau(0)}\{P-(1-P)\}$$

$$= \frac{D\left(\frac{F}{kT}\right)^2 d}{\frac{Fd}{kT} + (e^{Fd/kT}-1)(e^{V_r/kT}-1)/(e^{Fd/kT}-e^{V_r/kT})}.$$

In the limit where both Fd and V_r are much larger than kT this turns into

$$v \simeq d\ D\left(\frac{F}{kT}\right)^2 (e^{-V_r/kT}-e^{-Fd/kT}) \quad , \text{ if } \frac{V_r}{kT} \text{ and } \frac{Fd}{kT} \gg 1.$$

This functional form is predicted by the discussion in part (b): v/d is the difference between the transition rate from the well at the origin across the large barrier to the right, of height V_r, and the rate of transition across the large barrier on the left, of height Fd.

In the limit of vanishing field, F = 0, the capture probability and capture time are

$$P = \frac{\chi}{\chi+1} = \frac{e^{-V_r/kT}}{e^{-V_r/kT}+1}$$

$$\tau = \frac{d^2}{2D}$$

and the drift due to the bias in the ratchets becomes

$$v = \frac{2D}{d}\frac{\chi-1}{\chi+1} = \frac{2D}{d}\frac{e^{-V_r/kT}-1}{e^{-V_r/kT}+1} = \frac{2D}{d}\tanh\left(-\frac{V_r}{2kT}\right) \quad , \text{ if } F = 0.$$

The maximal drift velocity attainable is 2D/d, limited by the time it takes to diffuse across the distance between two ratchets. Note that τ does not depend on χ in this case. This is to be expected, since diffusion on the right side of the ratchet is symmetric to the conditions on the left side; the mean time to capture is unchanged even if the origin constitutes a reflective barrier, equivalent to a ratchet with infinite bias.

Finally, for χ=1 the ratchets vanish, and

$$v = \frac{DF}{kT} \quad , \text{ if } V_r = 0$$

which is recognized as the drift velocity of the particle in a constant field.

REFERENCES

Adler, J. and Templeton, B. (1967). The effect of environmental conditions on the motility of Escherichia coli. J. Gen. Microbiol. **46**, 175-184.

Aizawa, S.-I., Dean, G. E., Jones, C. I., Macnab, R. M., and Yamaguchi, S. (1985). Purification and characterization of the flagellar hook-basal body complex of Salmonella typhimurium. J. Bact. **161**, 836-849.

Ambudkar, S. V., Sonna, L. A., and Maloney, P. C. (1986). Variable stoichiometry of phosphate-linked anion exchange in Streptococcus lactis: Implications for the mechanism of sugar phosphate transport in bacteria. Proc. Natl. Acad. Sci. USA **83**, 280-284.

Anderson, R. A. (1975). Formation of the bacterial flagellar bundle. **In** "Swimming and Flying in Nature", eds. Wu, T.Y.T., Brokaw, C.J., and Brennen, C., vol.1, p.45-56. New York: Plenum.

Belyakova, T. N., Glagolev, A. N., and Skulachev, V. P. (1976). Electrochemical gradient of H^+ ions as a direct source of energy during bacterial locomotion. Biochemistry **41**, 1206-1210.

Berg, H. C. and Anderson, A. (1973). Bacteria swim by rotating their flagellar filaments. Nature **245**, 380-382.

Berg, H. C. (1974). Dynamic properties of bacterial flagellar motors. Nature **249**, 77-79.

Berg, H. C. (1975). Chemotaxis in bacteria. Ann. Rev. Biophys. Bioeng. **4**, 119-136.

Berg, H. C. (1976). Does the flagellar rotary motor step? **In** "Cell Motility", eds. Goldman, R., Pollard, T. and Rosenbaum, J., p.A47-A56. Cold Spring Harbor, New York: Cold Spring Harbor Laboratory.

Berg, H. C. and Purcell, E. M. (1977). Physics of chemoreception. Biophys. J. **20**, 193-219.

Berg, H. C., Manson, M. D., and Conley, M. P. (1982). Dynamics and energetics of flagellar rotation in bacteria. Symp. Soc. Exp. Biol. **35**, 1-35.

Berg, H. C. and Khan S. (1983). A model for the flagellar rotary motor. **In** "Mobility and Recognition in Cell Biology", eds. Sund, H. and Veeger, C., p.485-497. Berlin: de Gruyter.

Berg, H. C. and Block, S. M. (1984). A miniature flow cell designed for rapid exchange of media under high-power microscope objectives. J. Gen. Microbiol. **130**, 2915-2920.

Berg, H. C. (1985). Flagellar motility. **In** Roche Seminars on Bacteria, no.1. Hoffmann-LaRoche Inc.

Block, S. M., Segall, J. M., and Berg, H. C. (1983). Adaptation kinetics in bacterial chemotaxis. J. Bact. **154**, 312-323.

Block, S. M. and Berg, H. C. (1984). Successive incorporation of force-generating units in the bacterial motor. Nature **309**, 470-472.

Burchard, R. P. (1981). Gliding motility of prokaryotes: ultrastructure, physiology and genetics. Ann. Rev. Microbiol. **35**, 497-529.

Casimir H. (1945). On Onsager's principle of microscopic reversibility. Rev. Mod. Phys. **17**, 343-350.

Chandrasekhar, S. (1943). Stochastic problems in physics and astronomy. Rev. Mod. Phys. **15**, 1-89.

Cohn, D. E., Kaczorowski, G. J., and Kaback, H. R. (1981). Effect of the proton electrochemical gradient on maleimide inactivation of active transport in Escherichia coli membrane vesicles. Biochemistry **20**, 3308-3313.

Collin, R. L. (1957). Polymorphism and radiation decomposition of choline chloride. J. Am. Chem. Soc. **79**, 6086.

Conley, M. P. and Berg. H. C. (1984). Chemical modification of Streptococcus flagellar motors. J. Bact. **158**, 832-843.

Coulton J. W. and Murray, R. G. E. (1978). Cell envelope associations of Aquaspirillum serpens flagella. J. Bact. **136**, 1047-1049.

DePamphilis, M. L. and Adler, J. (1971a). Fine structure and isolation of the hook-basal body complex of flagella from Escherichia coli and Bacillus subtilis. J. Bact. **105**, 384-395.

DePamphilis, M. L. and Adler, J. (1971b). Attachment of flagellar basal bodies to the cell envelope: specific attachment to the outer lipopolysaccharide membrane and the cytoplasmic membrane. J. Bact. **105**, 396-407.

Dobell, C. (1960). "Antony van Leeuwenhoek and his 'little animals'", p.144. New York: Dover.

Eisenbach, M. and Adler, J. (1981). Bacterial cell envelopes with functional flagella. J. Biol. Chem. **256**, 8807-8814.

Eyring, H. (1935). The activated complex in chemical reactions. J. Chem. Phys. **3**, 107-115.

Feynman, R. P., Leighton, R. B., and Sands, M. (1963). "The Feynman Lectures on Physics", vol.1. Addison-Wesley Publishers.

Finkelstein, A. (1984). Water movement through membrane channels. Current Topics in Membranes and Transport **21**, 295-308.

Flagg, J. L. and Wilson, T. H. (1977). A protonmotive force is the source of energy for galactoside transport in energy depleted Escherichia coli. J. Membr. Biol. **31**, 233-255.

Fox, C. F. and Kennedy, E. P. (1965). Specific labeling and partial purification of the M protein, a component of the β-galactoside transport system of Escherichia coli. Proc. Nat. Acad. Sci. USA **54**, 891-899.

Gandour, R. D. and Schowen, R. L. (1978). "Transition States of Biochemical Processes", Ch.6. New York: Plenum Press.

Gardiner, C. W. (1983). "Handbook of Stochastic Methods". Springer.

Glagolev, A. N. and Skulachev, V. P. (1978). The proton pump is a molecular engine of motile bacteria. Nature **272**, 280-282.

Gmelin Handbook of Inorganic Chemistry (1963), ed.8, no.3, sect.5, p.1452. Verlag Chemie GmbH, Weinheim/Bergstr.

Gmelin Handbook of Inorganic Chemistry (1963), ed.8, no.3, sect.6, p.1929-1930. Verlag Chemie GmbH, Weinheim/Bergstr.

Happel, J. and Brenner, H. (1983). "Low Reynolds Number Hydrodynamics", Ch.5. Martinus Nijhoff Publ.

Harold, F. M. and Papineau, D. (1972). Cation transport and electrogenesis by Streptococcus faecalis. The membrane potential. J. Membr. Biol. **8**, 27-44.

Harold, F. M. and Altendorf, K. (1974). Cation transport in bacteria: K^+, Na^+, and H^+. Current Topics in Membranes and Transport **5**, 1-50.

Harold, F. M. and Kakinuma, Y. (1984). Primary and secondary transport of cations in bacteria. Annals New York Acad. Sci., **vol.456**, 375-383.

Hazelbauer, G. L. and Harayama, S. (1983). Sensory transduction in bacterial chemotaxis. Int. Rev. Cytol. **81**, 33-70.

Heefner, D. L. and Harold, F. M. (1980). ATP-linked sodium transport in Streptococcus faecalis I. The sodium circulation. J. Biol. Chem. **255**, 11396-11402.

Heimbrook, M. E., Wang, W. L. L., and Campbell, G. (1986). Abstracts of the Annual Meeting of the American Society for Microbiology, 1986, p.240. Washington, DC: American Society for Microbiology.

Hirota, N., Kitada, M., and Imae, Y. (1981). Flagellar motors of alkalophilic Bacillus are powered by an electrochemical potential gradient of Na^+. FEBS Letters **132**, 278-280.

Hirota, N. and Imae, Y. (1983). Na^+-driven flagellar motors of an alkalophilic Bacillus strain YN-1. J. Biol. Chem. **258**, 10577-10581.

Iino, T. (1977). Genetics of structure and function of bacterial flagella. Ann. Rev. Genet. **11**, 161-182.

Ishihara, A., Segall, J. E., Block, S. M., and Berg, H. C. (1983). Coordination of flagella on filamentous cells of Escherichia coli. J. Bact. **155**, 228-237.

Jeffery, G. B. (1915). On the steady rotation of a solid of revolution in a viscous fluid. Proc. Lond. Math. Soc. **14**, 327-338.

Kashket, E. R. and Wilson, T. H. (1973). Proton-coupled accumulation of galactoside in Streptococcus lactis 7962. Proc. Nat. Acad. Sci. USA **70**, 2866-2869.

Kashket, E. R. (1981). Proton motive force in growing Streptococcus lactis and Staphylococcus aureus under aerobic and anaerobic conditions. J. Bact. **146**, 369-376.

Kashket, E. R. (1985a). Effects of K^+ and Na^+ on the proton motive force of respiring Escherichia coli at alkaline pH. J. Bact. **163**, 423-429.

Kashket, E. R. (1985b). The proton motive force in bacteria: a critical assessment of methods. Ann. Rev. Microbiol. **39**, 219-242.

Kell, D. B. (1979). On the functional proton current pathway of electron transport phosphorylation. An electrodic view. Biochim. Biophys. Acta **549**, 55-99.

Khan, S. and Macnab, R. M. (1980a). The steady-state counterclockwise/clockwise ratio of bacterial flagellar motors is regulated by protonmotive force. J. Mol. Biol. **138**, 563-597.

Khan, S. and Macnab, R. M. (1980b). Proton chemical potential, proton electrical potential, and bacterial motility. J. Mol. Biol. **138**, 599-614.

Khan, S. and Berg, H. C. (1983). Isotope and thermal effects in chemiosmotic coupling to the flagellar motor of Streptococcus. Cell **32**, 913-919.

Khan, S., Meister, M., and Berg, H. C. (1985). Constraints on flagellar rotation. J. Mol. Biol. **184**, 645-656.

Khan, S., Walrond, J., and Reese, T. S. (1986). Identification of the flagellar motor by freeze fracture. Biophys. J. **49**, 415a.

Kihara, M. and Macnab, R. M. (1981). Cytoplasmic pH mediates pH taxis and weak-acid repellent taxis of bacteria. J. Bact. **105**, 384-395.

Kometani, T. and Kasai, M. (1978). Ionic permeability of sarcoplasmic reticulum vesicles measured by light scattering method. J. Membr. Biol. **41**, 295-308.

Kramers, H. A. (1940). Brownian motion in a field of force and the diffusion model of chemical reactions. Physica **7**, 285-304.

Krulwich, T. A. (1983). Na^+/H^+ antiporters. Biochim. Biophys. Acta **726**, 245-264.

Läuger, P. (1977). Ion transport and rotation of bacterial flagella. Nature **268**, 360-362.

Lanyi, J. K. (1979). The role of Na^+ in bacterial membrane transport. Biochim. Biophys. Acta **559**, 377-397.

Larsen, S. H., Adler, J., Gargus, J. J., and Hogg, R. W. (1974). Chemomechanical coupling without ATP: the source of energy for motility and chemotaxis in bacteria. Proc. Nat. Acad. Sci. USA **71**, 1239-1243.

Leifson, E. (1951). Staining, shape, and arrangement of bacterial flagella. J. Bact. **62**, 377-389.

Lowe, G., Meister, M., and Berg, H. C. (1986). Rapid rotation of flagellar bundles in swimming bacteria. Nature, in press.

Macnab, R. M. (1976). Examination of bacterial flagellation by dark-field microscopy. J. Clin. Microbiol. **4**, 258-265.

Macnab, R. M. (1978). Bacterial motility and chemotaxis: the molecular biology of a behavioral system. CRC Crit. Rev. Biochem. **5**, 291-341.

Macnab, R. M. and Aizawa, S.-I. (1984). Bacterial motility and the bacterial flagellar motor. Ann. Rev. Biophys. Bioeng. **13**, 51-83.

Maloney, P. C., Kashket, E. R. , and Wilson, T. H. (1974). A protonmotive force drives ATP synthesis in bacteria. Proc. Nat. Acad. Sci. USA **71**, 3896-3900.

Maloney, P. C. (1977). Obligatory coupling between proton entry and the synthesis of ATP in Streptococcus lactis. J. Bact. **132**, 564-575.

Maloney, P. C. (1978). Coupling between H^+-entry and ATP formation in Escherichia coli. Biochem. Biophys. Res. Comm. **83**, 1496-1501.

Maloney, P. C. (1979). Membrane H^+-conductance of Streptococcus lactis. J. Bact. **140**, 197-205.

Maloney, P. C. (1982). Coupling between H^+-entry and ATP synthesis in bacteria. Current Topics in Membranes and Transport **16**, 175-193.

Manson, M. D., Tedesco, P., Berg, H. C., Harold, F. M., and van der Drift, C. (1977). A protonmotive force drives bacterial flagella. Proc. Nat. Acad. Sci. USA **74**, 3060-3064.

Manson, M. D., Tedesco, P. M., and Berg, H. C. (1980). Energetics of flagellar rotation in bacteria. J. Mol. Biol. **138**, 541-561.

Matsuura, S., Shioi, J.-I., and Imae, Y. (1977). Motility in Bacillus subtilis driven by artificial Δp. FEBS Letters **82**, 187-190.

Matsuura, S., Shioi, J.-I., Imae, Y., and Iida, S. (1979). Characterization of the Bacillus subtilis motile system driven by an artificially created protonmotive force. J. Bact. **140**, 28-36.

Meixner, J. (1949). Thermodynamik und Relaxationserscheinungen. Z. Naturforschung **4a**, 594-600.

Miller, C. (1983). Reconstitution of ion channels in planar bilayer membranes: a five-year progress report. Com. Mol. Cell. Biophys. **1**, 413-428.

Miller, C. (1984). Ion channels in liposomes. Ann. Rev. Physiol. **46**, 549-558.

Mitchell, P. and Moyle, J. (1967). Acid-base titration across the membrane system of rat-liver mitochondria: catalysis by uncouplers. Biochem. J. **104**, 588-600.

Mitchell, P. (1984). Bacterial flagellar motors and osmoelectric molecular rotation by an axially transmembrane well and turnstile mechanism. FEBS **176**, 287-294.

Nagle, J. F. and Tristram-Nagle, S. (1983). Hydrogen bonded chain mechanisms for proton conduction and proton pumping. J. Membr. Biol. **74**, 1-14.

Onsager, L. (1931a). Reciprocal relations in irreversible processes I. Phys. Rev. **37**, 405-426.

Onsager, L. (1931b). Reciprocal relations in irreversible processes II. Phys. Rev. **38**, 2265-2279.

Oosawa, S. and Masai, J. (1982). Mechanism of flagellar motor rotation in bacteria. J. Phys. Soc. Japan **51**, 631-641.

Oosawa, F. and Hayashi, S. (1983). Coupling between flagellar motor rotation and proton flux in bacteria. J. Phys. Soc. Japan **52**, 4019-4028.

Parkinson, J. S. (1981). Genetics of bacterial chemotaxis. Symp. Soc. Gen. Microbiol. **31**, 265-290.

Parkinson, J. S. and Hazelbauer, G. L. (1983). Bacterial chemotaxis: molecular genetics of sensory transduction and chemotactic gene expression. **In** "Gene function in prokaryotes", p.293-318. Cold Spring Harbor Laboratory.

Perrin, F. (1934). Mouvement Brownien d'un ellipsoide (I). Dispersion dielectrique pour des molecules ellipsoidales. Le Journal de Physique et le Radium, Serie 7, Tome **5**, 497-511.

Perrin, F. (1936). Mouvement Brownien d'un ellipsoide (II). Rotation libre et depolarisation des fluorescences. Translation et diffusion de molecules ellipsoidales. Le Journal de Physique et le Radium, Serie 7, Tome **7**, 1-11.

Ravid, S. and Eisenbach, M. (1984). Minimal requirements for rotation of bacterial flagella. J. Bact. **158**, 1208-1210.

Reed, P. W. (1979). Ionophores. Meth. Enzymol. **55**, 435-454.

Reilly, C. N. and Vavoulis, A. (1959). Tetraethylenepentamine, a selective titrant for metal ions. Analyt. Chem. **31**, 243-248.

Repaske, D. R. and Adler, J. (1981). Change in intracellular pH of Escherichia coli mediates the chemotactic response to certain attractants and repellents. J. Bact. **145**, 1196-1208.

Rosen, G. (1974). Can the rotation of a bacterial flagellum appear quantized? Physics Letters **49A**, 395-396.

Sakmann, B. and Neher, E. (1984). Patch clamp techniques for studying ionic channels in excitable membranes. Ann. Rev. Physiol. **46**, 455-472.

Scholes, P. and Mitchell, P. (1970). Acid-base totration across the plasma membrane of M. denitrificans: factors affecting the effective proton conductance and the respiratory rate. Bioenergetics **1**, 61-72.

Shioi, J.-I., Matsuura, S., and Imae, Y. (1980). Quantitative measurements of protonmotive force and motility in Bacillus subtilis. J. Bact. **144**, 891-897.

Silverman, M. and Simon, M. I. (1972). Flagellar assembly mutants in Escherichia coli. J. Bact. **112**, 986-993.

Skulachev, V. P. (1975). Electric generators in coupling membranes: direct measurements of the electrogenic activity, molecular mechanisms and some specific functions. **In** "Enzymes, electron transport systems", Proceedings of the tenth FEBS meeting, p.225-238. Amsterdam: North-Holland Publishing Co.

Stryer, L. (1981). "Biochemistry", 2nd edition. San Francisco: W. H. Freeman.

Tanford, C. (1983). Mechanism of free energy coupling in active transport. Ann. Rev. Biochem. **52**, 379-409.

Tirado, M. M. and de la Torre, J. G. (1979). Translational friction coefficients of rigid, symmetric top macromolecules. Application to circular cylinders. J. Chem. Phys. **71**, 2581-2587.

Tirado, M. M. and de la Torre, J. G. (1980). Rotational dynamics of rigid, symmetric top macromolecules. Application to circular cylinders. J. Chem. Phys. **73**, 1986-1993.

de la Torre, J. G. and Bloomfield, V. A. (1981). Hydrodynamic properties of complex, rigid, biological macromolecules: theory and applications. Quart. Rev. Biophys. **14**, 81-139.

Wagenknecht, T., DeRosier, D., Shapiro, L., and Weissborn, A. (1981). Three-dimensional reconstruction of the flagellar hook from Caulobacter crescentus. J. Mol. Biol. **151**, 439-465.

Waterbury, J. B., Willey, J. M., Francks, D. G., Valois, F. W., and Watson, S. W. (1985). A cyanobacterium capable of swimming motility. Science **230**, 74-76.

Weibull, C. (1960). Movement. **In** "The Bacteria", Gunsalus, I.C. and Stanier, R.Y. eds., vol.1, p.153-205. New York: Academic.

Willecke, K., Gries, E., and Oehr, P. (1973). Coupled transport of citrate and magnesium in Bacillus subtilis. J. Biol. Chem. **248**, 807-814.